Royal Norwegian Council
for Scientific and Industrial Research
(NTNF)

NORSAR

NORSAR Scientific Report No. 1-91/92

Semiannual Technical Summary

1 April — 30 September 1991

Kjeller, November 1991

REPORT DOCUMENTATION PAGE

1a. REPORT SECURITY CLASSIFICATION UNCLASSIFIED	1b. RESTRICTIVE MARKINGS NOT APPLICABLE
2a. SECURITY CLASSIFICATION AUTHORITY NOT APPLICABLE	3. DISTRIBUTION / AVAILABILITY OF REPORT APPROVED FOR PUBLIC RELEASE DISTRIBUTION UNLIMITED
2b. DECLASSIFICATION / DOWNGRADING SCHEDULE NOT APPLICABLE	
4. PERFORMING ORGANIZATION REPORT NUMBER(S) Scientific Report 1-91/92	5. MONITORING ORGANIZATION REPORT NUMBER(S) Scientific Rep. 1-91/92
6a. NAME OF PERFORMING ORGANIZATION NTNF/NORSAR 6b. OFFICE SYMBOL (If applicable)	7a. NAME OF MONITORING ORGANIZATION HQ/AFTAC/TTR
6c. ADDRESS (City, State, and ZIP Code) Post Box 51 N-2007 Kjeller, Norway	7b. ADDRESS (City, State, and ZIP Code) Patrick AFB, FL 32925-6001
8a. NAME OF FUNDING / SPONSORING ORGANIZATION Defense Advanced Research Projects Agency 8b. OFFICE SYMBOL (If applicable) NMRO	9. PROCUREMENT INSTRUMENT IDENTIFICATION NUMBER Contract No. F08606-89-C-0005
8c. ADDRESS (City, State, and ZIP Code) 3701 N. Fairfax Dr. #717 Arlington, VA 22203-1714	10. SOURCE OF FUNDING NUMBERS PROGRAM ELEMENT NO. R&D; PROJECT NO. NORSAR Phase 3; TASK NO. SOW Task 5.0; WORK UNIT ACCESSION NO. Seq.no.003A2
11. TITLE (Include Security Classification) SEMIANNUAL TECHNICAL SUMMARY, 1 APRIL - 30 SEPTEMBER 1991 (UNCLASSIFIED)	
12. PERSONAL AUTHOR(S)	
13a. TYPE OF REPORT Scientific Summary 13b. TIME COVERED FROM 1 Apr TO 30 Sep 91	14. DATE OF REPORT (Year, Month, Day) Nov 1991 15. PAGE COUNT 145
16. SUPPLEMENTARY NOTATION NOT APPLICABLE	

17. COSATI CODES			18. SUBJECT TERMS (Continue on reverse if necessary and identify by block number)
FIELD	GROUP	SUB-GROUP	NORSAR, NORWEGIAN SEISMIC ARRAY
8	11		

19. ABSTRACT (Continue on reverse if necessary and identify by block number)

This Semiannual Technical Summary describes the operation, maintenance and research activities at the Norwegian Seismic Array (NORSAR), the Norwegian Regional Seismic Array (NORESS) and the Arctic Regional Seismic Array (ARCESS) for the period 1 April -- 30 September 1991. Statistics are also presented for additional seismic stations, which through cooperative agreements with institutions in the host countries provide continuous data to the NORSAR Data Processing Center (NPDC). These stations comprise the Finnish Experimental Seismic Array (FINESA), the German Experimental Seismic Array (GERESS), and two 3-component stations in Poland: Ksiaz and Stary Folwark.

(cont.)

20. DISTRIBUTION / AVAILABILITY OF ABSTRACT ☐ UNCLASSIFIED/UNLIMITED ☐ SAME AS RPT ☐ DTIC USERS	21. ABSTRACT SECURITY CLASSIFICATION
22a. NAME OF RESPONSIBLE INDIVIDUAL Ms. C. Finn	22b. TELEPHONE (Include Area Code) (407) 494-2251 22c. OFFICE SYMBOL AFTAC/TTR

DD FORM 1473, 84 MAR 83 APR edition may be used until exhausted. All other editions are obsolete

This Semiannual Report also presents statistics from operation of the Intelligent Monitoring System (IMS). The IMS has been operated in an experimental mode using NORESS and ARCESS data, and the performance has been very satisfactory. Preparations have been made for installing a new version of the IMS that accepts data from an arbitrary number of arrays and single 3-component stations.

The NORSAR Detection Processing system has been operated throughout the period with an average uptime of 99.3% as compared to 98.6% for the previous reporting period. A total of 2138 seismic events have been reported in the NORSAR monthly seismic bulletin. The performance of the continuous alarm system and the automatic bulletin transfer by telex to AFTAC has been satisfactory. A system for direct retrieval of NORSAR waveform data through an X.25 connection has been implemented, and has been tested successfully for acquiring such data by AFTAC. Processing of requests for full NORSAR/ NORESS data on magnetic tapes has progressed according to established schedules.

On-line detection processing and data recording at the NORSAR Data Processing Center (NDPC) of NORESS, ARCESS, FINESA and GERESS data have been conducted throughout the period. Data from the two stations in Poland have been recorded and processed in an experimental mode. Monthly processing statistics for the arrays as well as results of the IMS analysis for the reporting period are given.

There have been no modifications made to the NORSAR data acquisition system. The process of evaluating and testing technical options for refurbishment of the array is continuing.

Maintenance activities in the period comprise preventive/corrective maintenance in connection with all the NORSAR subarrays, NORESS and ARCESS. In addition, the maintenance center has been involved with occasional maintenance of equipment for FINESA and work in connection with the two stations in Poland. Other activities have involved testing of the NORSAR communications systems, and field studies at sites in Spitsbergen and the Kola Peninsula.

Summaries of seven scientific contributions are presented in Chapter 7 of this report.

In Section 7.1, the application of statistical parameter estimation theory to seismic holography algorithms is described. The theoretical framework for this application is developed, and the advantages of the statistical algorithms are analyzed by computer modelling experiments. Data from the six sensors of NORSAR subarray 01A for a Hindu Kush earthquake (22 February 1972, $m_b = 5.6$) have been used in this experiment together with simulated scattered waveforms. The statistical algorithm is found to be superior to the conventional seismic holography algorithm in this case, as it provides better resolution and suppresses "leakage" effects in the imaging process.

Section 7.2 describes a new maximum likelihood scheme for 3-component slowness estimation. This new technique incorporates the response of the crust beneath the receiver in the signal model. The paper presents examples of applications both for a single 3C station

and an array of four 3C stations, and demonstrates the utility of the method for slowness analysis of P-wave recordings. Plans are being made to extend the technique to analysis of SV and SH waves.

Section 7.3 follows up our previous studies on using adaptive statistically optimal algorithms for on-line event detection. It is found that regional P-phase detection at typical frequencies (2.5-4.5 Hz) requires noise adaptation for 8 azimuths and 2 velocities in order to achieve less than 3 dB worst case missteering loss. Preliminary results of applying a one-dimensional statistically optimal detector (ESTDET) are presented and compared with the traditional STA/LTA algorithm. The ESTDET method is found to be more sensitive, at a similar level of false alarm rates.

In section 7.4 we describe the current status and planned extensions of the regional array network in northern Europe. A new digital 3-component station in Apatity, USSR, is described, and preliminary analysis shows that it is very valuable for near-field studies of mining explosions in the Khibiny Massif. Noise surveys and plans for a small-aperture array at the Spitsbergen archipelago are described. This array is expected to become operational in 1992.

Section 7.5 presents an application of statistically optimal adaptive processing of array data in the context of separating interfering events. Besides the obvious importance of this application in detecting possible explosions in the coda of large earthquakes, it also serves to improve the capability of the "Threshold Monitoring" technique. This preliminary study indicates that with the appropriate modifications, the adaptive processing may significantly improve the detection threshold during event coda conditions.

In Section 7.6, a case study is presented on regional detection performance during the recently conducted GSETT-2 experiment. Using the bulletin of the Seismological Institute, University of Helsinki, as a reference, it is shown that the 90% detection threshold for Fennoscandia/NW Russia is close to 2.5 in terms of the duration magnitudes used in that bulletin. This shows that in a region with dense coverage of high quality arrays such as Fennoscandia, an excellent monitoring capability may be achieved. However, the extension of these results to different geological environments in other parts of the world is unproven.

Section 7.7 describes the contemporary seismicity of the NW part of the USSR. The paper is based on recordings from the regional station network operated by the Kola Science Centre since 1982. Selected seismic zones are described in some detail; the Kola-Finnmark zone, the Khibiny Massif, NE Archangelsk and a seismic zone in Novaya Zemlya. The Khibiny Massif zone is of particular interest, since it appears that a great increase of induced seismicity has taken place in recent years, following the increased mining activity in the area.

AFTAC Project Authorization	:	T/9141/B/PKP
ARPA Order No.	:	4138 AMD # 16
Program Code No.	:	0F10
Name of Contractor	:	Royal Norwegian Council for Scientific and Industrial Research (NTNF)
Effective Date of Contract	:	1 Oct 1988
Contract Expiration Date	:	30 Sep 1992
Project Manager	:	Frode Ringdal (06) 81 71 21
Title of Work	:	The Norwegian Seismic Array (NORSAR) Phase 3
Amount of Contract	:	$ 9,368,350
Contract Period Covered by Report	:	1 April -- 30 September 1991

This research was supported by the Advanced Research Projects Agency of the Department of Defense and was monitored by AFTAC, Patrick AFB, FL32925, under contract no. F08606-89-C-0005.

NORSAR Contribution No. 452

Table of Contents

1 Summary

This Semiannual Technical Summary describes the operation, maintenance and research activities at the Norwegian Seismic Array (NORSAR), the Norwegian Regional Seismic Array (NORESS) and the Arctic Regional Seismic Array (ARCESS) for the period 1 April -- 30 September 1991. Statistics are also presented for additional seismic stations, which through cooperative agreements with institutions in the host countries provide continuous data to the NORSAR Data Processing Center (NPDC). These stations comprise the Finnish Experimental Seismic Array (FINESA), the German Experimental Seismic Array (GERESS), and two 3-component stations in Poland: Ksiaz and Stary Folwark.

This Semiannual Report also presents statistics from operation of the Intelligent Monitoring System (IMS). The IMS has been operated in an experimental mode using NORESS and ARCESS data, and the performance has been very satisfactory. Preparations have been made for installing a new version of the IMS that accepts data from an arbitrary number of arrays and single 3-component stations.

The NORSAR Detection Processing system has been operated throughout the period with an average uptime of 99.3% as compared to 98.6% for the previous reporting period. A total of 2138 seismic events have been reported in the NORSAR monthly seismic bulletin. The performance of the continuous alarm system and the automatic bulletin transfer by telex to AFTAC has been satisfactory. A system for direct retrieval of NORSAR waveform data through an X.25 connection has been implemented, and has been tested successfully for acquiring such data by AFTAC. Processing of requests for full NORSAR/ NORESS data on magnetic tapes has progressed according to established schedules.

On-line detection processing and data recording at the NORSAR Data Processing Center (NDPC) of NORESS, ARCESS, FINESA and GERESS data have been conducted throughout the period. Data from the two stations in Poland have been recorded and processed in an experimental mode. Monthly processing statistics for the arrays as well as results of the IMS analysis for the reporting period are given.

There have been no modifications made to the NORSAR data acquisition system. The process of evaluating and testing technical options for refurbishment of the array is continuing.

Maintenance activities in the period comprise preventive/corrective maintenance in connection with all the NORSAR subarrays, NORESS and ARCESS. In addition, the maintenance center has been involved with occasional maintenance of equipment for FINESA and work in connection with the two stations in Poland. Other activities have involved testing of the NORSAR communications systems, and field studies at sites in Spitsbergen and the Kola Peninsula.

Summaries of seven scientific contributions are presented in Chapter 7 of this report.

In Section 7.1, the application of statistical parameter estimation theory to seismic holography algorithms is described. The theoretical framework for this application is devel-

oped, and the advantages of the statistical algorithms are analyzed by computer modelling experiments. Data from the six sensors of NORSAR subarray 01A for a Hindu Kush earthquake (22 February 1972, $m_b = 5.6$) have been used in this experiment together with simulated scattered waveforms. The statistical algorithm is found to be superior to the conventional seismic holography algorithm in this case, as it provides better resolution and suppresses "leakage" effects in the imaging process.

Section 7.2 describes a new maximum likelihood scheme for 3-component slowness estimation. This new technique incorporates the response of the crust beneath the receiver in the signal model. The paper presents examples of applications both for a single 3C station and an array of four 3C stations, and demonstrates the utility of the method for slowness analysis of P-wave recordings. Plans are being made to extend the technique to analysis of SV and SH waves.

Section 7.3 follows up our previous studies on using adaptive statistically optimal algorithms for on-line event detection. It is found that regional P-phase detection at typical frequencies (2.5-4.5 Hz) requires noise adaptation for 8 azimuths and 2 velocities in order to achieve less than 3 dB worst case missteering loss. Preliminary results of applying a one-dimensional statistically optimal detector (ESTDET) are presented and compared with the traditional STA/LTA algorithm. The ESTDET method is found to be more sensitive, at a similar level of false alarm rates.

In section 7.4 we describe the current status and planned extensions of the regional array network in northern Europe. A new digital 3-component station in Apatity, USSR, is described, and preliminary analysis shows that it is very valuable for near-field studies of mining explosions in the Khibiny Massif. Noise surveys and plans for a small-aperture array at the Spitsbergen archipelago are described. This array is expected to become operational in 1992.

Section 7.5 presents an application of statistically optimal adaptive processing of array data in the context of separating interfering events. Besides the obvious importance of this application in detecting possible explosions in the coda of large earthquakes, it also serves to improve the capability of the "Threshold Monitoring" technique. This preliminary study indicates that with the appropriate modifications, the adaptive processing may significantly improve the detection threshold during event coda conditions.

In Section 7.6, a case study is presented on regional detection performance during the recently conducted GSETT-2 experiment. Using the bulletin of the Seismological Institute, University of Helsinki, as a reference, it is shown that the 90% detection threshold for Fennoscandia/NW Russia is close to 2.5 in terms of the duration magnitudes used in that bulletin. This shows that in a region with dense coverage of high quality arrays such as Fennoscandia, an excellent monitoring capability may be achieved. However, the extension of these results to different geological environments in other parts of the world is unproven.

Section 7.7 describes the contemporary seismicity of the NW part of the USSR. The paper is based on recordings from the regional station network operated by the Kola Science

Centre since 1982. Selected seismic zones are described in some detail; the Kola-Finnmark zone, the Khibiny Massif, NE Archangelsk and a seismic zone in Novaya Zemlya. The Khibiny Massif zone is of particular interest, since it appears that a great increase of induced seismicity has taken place in recent years, following the increased mining activity in the area.

2 NORSAR Operation

2.1 Detection Processor (DP) operation

There have been 37 breaks in the otherwise continuous operation of the NORSAR online system within the current 6-month reporting interval. The uptime percentage for the period is 99.3% as compared to 98.6% for the previous period.

Fig. 2.1.1 and the accompanying Table 2.1.1 both show the daily DP downtime for the days between 1 April and 30 September 1991. The monthly recording times and percentages are given in Table 2.1.2.

The breaks can be grouped as follows:

a)	Hardware failure	8
b)	Stops related to program work or error	0
c)	Hardware maintenance stops	0
d)	Power jumps and breaks	0
e)	TOD error correction	0
f)	Communication lines	29

The total downtime for the period was 28 hours and 56 minutes. The mean-time-between-failures (MTBF) was 5.0 days, as compared to 4.1 for the previous period.

J. Torstveit

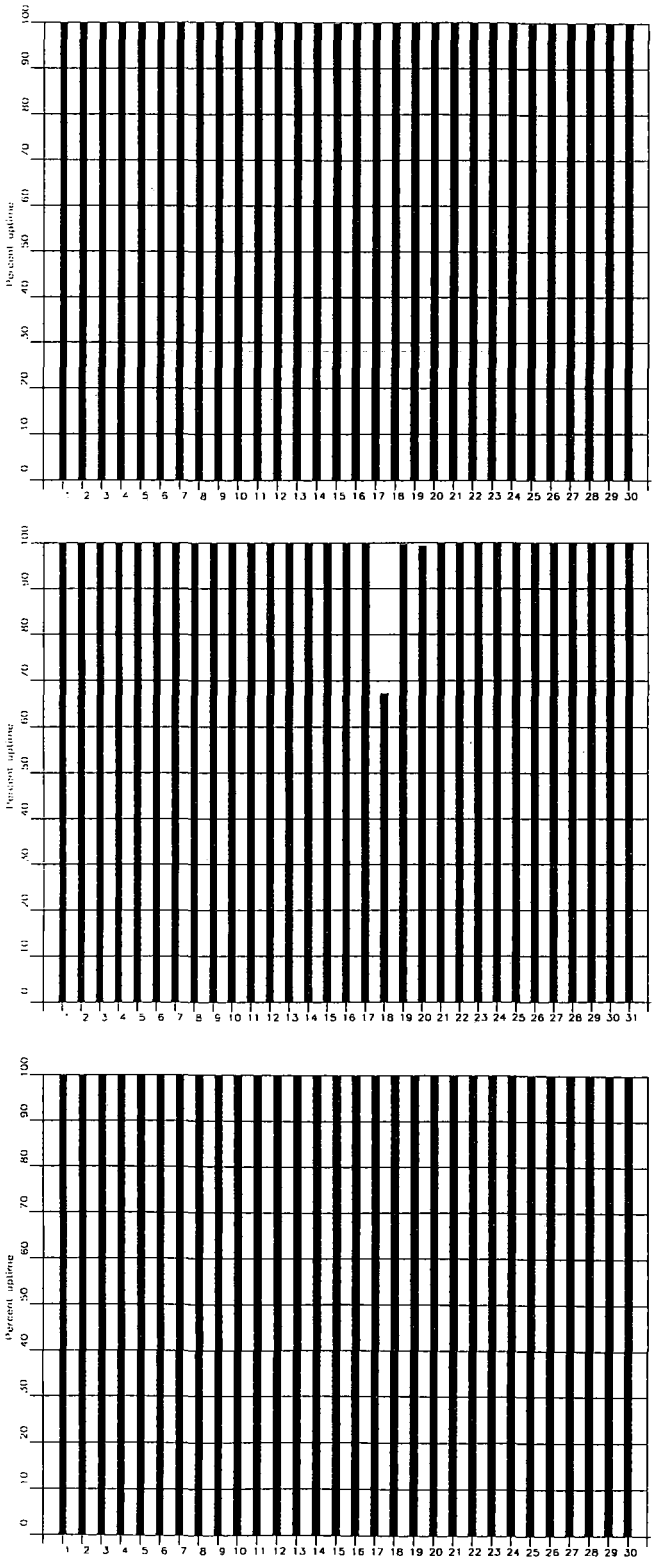

Fig. 2.1.1. Detection Processor uptime for April (top), May (middle) and June (bottom) 1991.

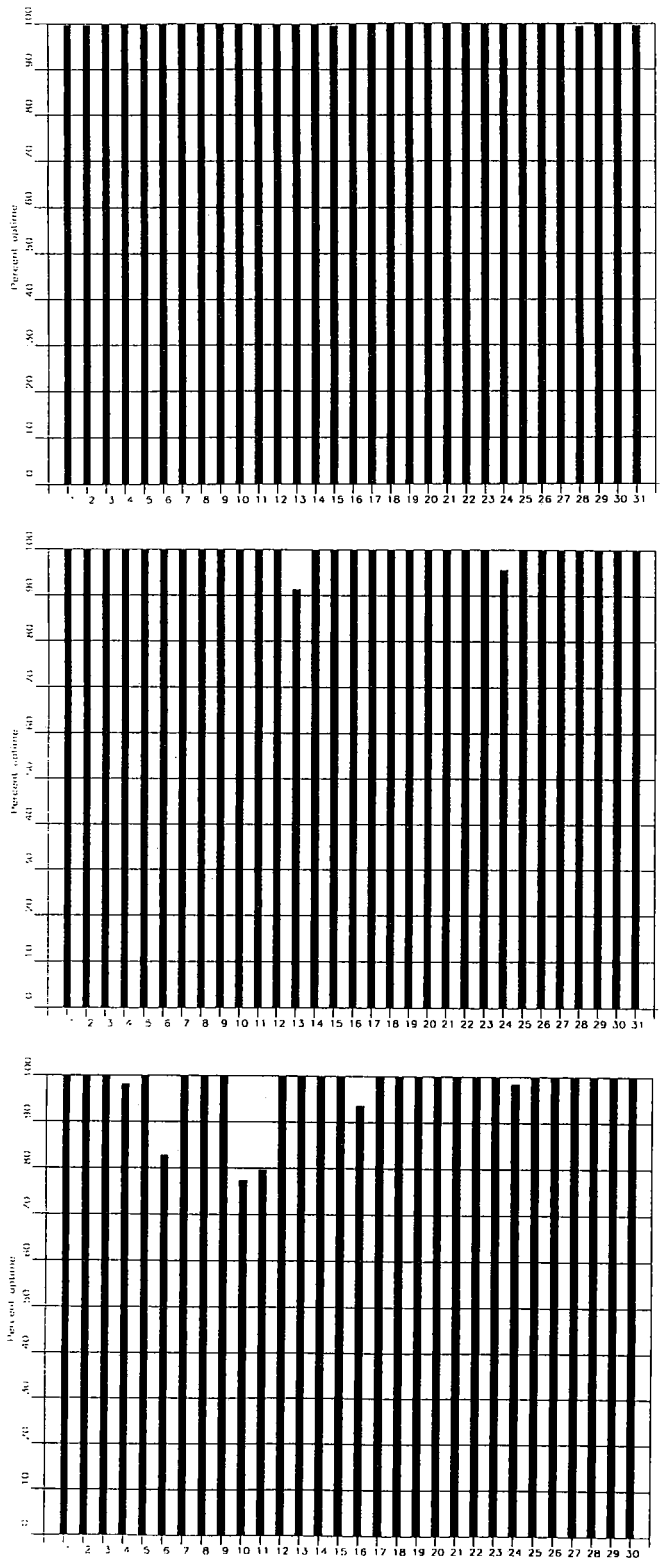

Fig. 2.1.1. Detection Processor uptime for July (top), August (middle) and September (bottom) 1991.

Date	Time	Cause
18 May	1220 - 1832	Hardware failure
18 May	1900 - 1932	Hardware failure
18 May	2038 - 2145	Hardware failure
13 Aug	1043 - 1248	Hardware failure
24 Aug	0704 - 0807	Hardware failure
04 Sep	0821 - 0848	Hardware failure
06 Sep	0952 - 1400	Hardware failure
10 Sep	1834 -	Line failure
11 Sep	- 0453	
16 Sep	0848 - 1021	Line failure
24 Sep	1916 - 1959	Hardware failure

Table 2.1.1. The major downtimes in the period 1 April -- 30 September 1991.

Month	DP Uptime Hours	DP Uptime %	No. of DP Breaks	No. of Days with Breaks	DP MTBF* (days)
Apr 91	719.83	99.98	5	3	5.0
May 91	735.85	98.90	6	4	4.4
Jun 91	719.73	99.967	7	7	3.7
Jul 91	743.50	99.93	11	7	2.6
Aug 91	740.87	99.58	2	2	10.3
Sep 91	703.28	97.66	6	6	4.2
		99.34	37	29	5.0

*Mean-time-between-failures = total uptime/no. of up intervals.

Table 2.1.2. Online system performance, 1April -- 30 September 1991.

2.2 Array communications

General

Table 2.2.1 reflects the performance of the communications system throughout the reporting period. The most common events which have affected the NORSAR array have been: damaged communications cable, NTA transmission system failure, synchronization problems, bad connections, attenuator fault, lightning and low line level.

Detailed Summary

April (weeks 14-17), 1-28.4.91

03C, 06C were affected (week 15), 03C by synchronization problems, and 06C probably by a short line outage. The other systems performed satisfactorily.

May (weeks 18-22), 29.4-2.6.91

Most systems were affected in May. It started with 06C (week 19) which lost synchronization, but after a Modcomp restart the system resumed operation. All systems were affected 18 May (week 20). Observations made indicated irregularities related to the NTA transmission systems.

Attempts to start the lines failed. 01A, 03C and 04C were then turned off (i.e., no command words transmitted to the subarrays). A Modcomp restart started the lines and resynchronized the remaining systems: 01B, 02B, 02C and 06C.

21 May (week 21) the three subarrays (01A, 03C and 04C) resumed operation after new attempts. 04C failed again the same day (21 May), and we were not able to restart the system.

23 May (week 21) the subarray was visited. Loop tests were run in B- and C-loop (local and digital). C-loop was accepted, but B-loop failed, which was reasonable since part of the 04C data path between Hamar and Berger Central now is on PCM equipment. Although the communications systems were inoperative before the test started, the C-loop functioned well when activated. An answer to this may be that activities in the CTV prior to the test reset the system.

31 May (week 22). Data from 01A were not accepted. The subarray was masked.

June (weeks 23-26), 3-30.6.91

We had synchronization problems regarding 02B, 02C and 03C (weeks 24, 25 and 26). Apparently, 02B and later 03C caused the trouble. We believe 02C lost synchronization in connection with the Modcomp's heavy engagement in trying to synchronize 02B.

13 June 02B was turned off here at NORSAR (i.e., isolated from the Modcomp I/F and the remainder of the 02B communications path).

27 June 02B was visited and tested in the B/C-loop, with the test equipment hooked up to the NDPC modem. The test did not reveal reduced system quality, and was therefore switched on again.

02C was turned off 14 June, and after a Modcomp restart, the system resumed operation. The 03C communications system was not quite reliable, as it was difficult to resynchronize after loss of synch. Also after a small TOD correction the system lost synch.

July (weeks 27-31), 1.7-4.8.91

Only two systems were affected this month: 01A and 03C. The latter was affected week 27 due to a defective attenuator located in Elverum. Week 29 we lost contact with 01A, caused by a defective communications cable in the 01A area. 03C again lost synch. week 30. A Modcomp restart resynchronized the system.

August (weeks 32-35), 5.8-1.9.91

Three systems were affected this period: 02B week 35 by a bad connection located in the NTA premises Lillestrøm; 02C by a broken communications cable weeks 32, 33 and 34 in the Mesnalia area; and 04C week 33, probably in connection with an NTA transmission equipment outage.

September (weeks 36-39), 2-29.9.91

In September all systems were affected, either individually or all simultaneously. 02B outage continued through week 35, and the subarray resumed operation 2 September. 01A was down between 6 and 9 September because of NTA cable work in the area. 01B was down a few hours on 6 September.

In connection with service on a 4381 disk 6 September, the system was taken down for approximately 1 hour. In that period no data acquisition took place.

10 September (after 3 p.m.) lines 1 and 3 (01A, 02B) stopped. During the period the Modcomp tried to resynch. 01A, 02B; the remaining subarrays lost synch also. 02B was probably the main cause of the outages, due to line degradation and loss of power in connection with lightning in the area.

11 September at 5 a.m. the Modcomp was restarted with 02B turned off (i.e., no transmissions of ICWs toward the subarray). An almost identical situation occurred a few hours later (after 8 a.m.). 01A and 01B stopped, followed by 03C. The remaining subarrays "went down" approximately 11 a.m. (02B was already down). Two Modcomp restarts were necessary in order to restore operation. 01B communications cable was seriously damaged by a grounding spear, and the communications path toward the subarray was therefore broken.

12 September approx. 0445 a.m. 03C resynchronized. 13 September 01B communications cable was repaired.

Finally, on 16 September 0845 a.m. we again lost data from all subarrays (02B was still down). According to NTA/Hamar the reason was an inoperative transmission path between Hamar and Lillestrøm. Three Modcomp restarts had to be carried out before all lines started (-02B), approximately 10 a.m. 19 September 02B restored after SLEM reset.

O.A. Hansen

Sub-Arrays	Apr (4) 1-28.4	May (5) 29.4-2.6	Jun (4) 3-30.6	Jul (5) 1.7-4.8	Aug (4) 5.8-1.9	Sep (4) 2.9-29.9	Average 1/2 year
01A	0.001	0.008 [2)]	0.0009	0.002 [12)]	0.001	0.44 [17)]	0.074
01B	0.001	0.063 [3)]	0.001	0.0007	0.0006	0.44 [18)]	0.084
02B	0.001	0.077 [4)]	0.0005 [9)]	0.025	0.033 [14)]	0.001 [19)]	0.023
02C	0.004	0.001 [5)]	0.001 [10)]	0.004	0.0005 [15)]	0.818	0.138
03C	0.002 [1)]	0.001 [6)]	0.003 [11)]	0.002 [13)]	0.003	0.497 [20)]	0.084
04C	0.0005	0.001 [7)]	0.006	0.002	0.0007 [16)]	0.818	0.138
06C	0.165	0.243 [8)]	0.001	0.001	0.001	0.818	0.205
Aver	0.025	0.055	0.002	0.005	0.005	0.547	0.106

Figures representing error rate (in per cent) followed by number 1), 2), etc., are related to legend below.,

Table 2.2.1. Communications performance. The numbers represent error rates in per cent based on total transmitted frames/week (1 April - 30 September 1991).

3),4),5),8),12)	Average 4 weeks
1),2),6),7),11),13),14),16),20)	Average 3 weeks
10),17),18)	Average 2 weeks
9),15),19)	Average 1 week

2.3 Event Detection operation

In Table 2.3.1 some monthly statistics of the Detection and Event Processor operation are given. The table lists the total number of detections (DPX) triggered by the on-line detector, the total number of detections processed by the automatic event processor (EPX) and the total number of events accepted after analyst review (teleseismic phases, core phases and total).

	Total DPX	Total EPX	Accepted Phases P-phases	Core Phases	Sum	Daily
Apr 91	10050	1316	337	51	388	12.9
May 91	8400	1050	270	48	318	10.3
Jun 91	7225	1213	412	51	463	15.4
Jul 91	8225	1336	313	70	383	12.4
Aug 91	9350	1275	259	82	341	11.0
Sep 91	9775	1123	200	45	245	8.2
			1791	347	2138	11.7

Table 2.3.1. Detection and Event Processor statistics, 1 April - 30 September 1991.

NORSAR Detections

The number of detections (phases) reported by the NORSAR detector during day 091 1991, through day 273 1991, was 52,231, giving an average of 289 detections per processed day (181 days processed). The distribution of these detections is given in Table 2.3.2.

B. Paulsen Gammelby
J. Fyen

NAO .DPX Hourly distribution of detections

Day	00	01	02	03	04	05	06	07	08	09	10	11	12	15	14	15	16	17	18	19	20	21	22	23	Sum	Date		
91	18	33	22	23	18	26	9	26	14	14	23	18	20	10	15	22	33	19	31	21	15	34	31	20	515	Apr 01	Monday	Annen
92	24	31	23	21	25	9	13	11	11	10	20	17	24	14	18	12	12	24	19	17	17	18	22	14	426	Apr 02	Tuesday	
93	16	16	20	24	16	15	9	14	4	10	9	18	14	15	11	13	10	7	13	10	13	18	12	23	330	Apr 03	Wednesday	
94	18	20	19	14	12	15	8	5	6	10	1	7	14	11	18	13	10	9	14	21	14	22	16	22	319	Apr 04	Thursday	
95	27	13	18	17	17	13	12	3	2	35	9	14	16	24	14	10	17	20	24	20	16	18	11	19	389	Apr 05	Friday	
96	15	27	25	24	23	21	17	10	17	15	20	19	9	11	14	11	14	17	23	22	24	24	30	22	454	Apr 06	Saturday	
97	30	37	31	24	19	30	17	21	17	22	25	17	21	17	17	16	15	19	20	25	17	23	27	26	533	Apr 07	Sunday	
98	24	22	16	19	6	8	2	6	7	7	7	12	16	13	10	13	13	16	9	23	24	22	28	20	343	Apr 08	Monday	
99	24	22	27	20	16	8	13	3	3	15	3	14	20	8	18	11	20	8	12	12	15	25	31	34	382	Apr 09	Tuesday	
100	25	24	20	28	20	8	8	15	34	10	11	24	7	13	7	10	8	6	13	16	14	20	20	12	373	Apr 10	Wednesday	
101	27	13	15	21	10	8	11	9	20	15	43	15	10	24	6	13	18	16	11	13	15	13	16	22	384	Apr 11	Thursday	
102	17	19	22	14	15	8	3	6	4	4	5	19	17	18	14	13	12	6	8	11	10	14	17	19	295	Apr 12	Friday	
103	15	29	12	20	12	9	7	19	15	29	10	25	3	17	21	21	9	15	21	18	15	15	17	17	391	Apr 13	Saturday	
104	14	17	13	21	11	13	13	8	12	3	5	7	6	4	9	14	12	9	20	36	21	29	17	12	326	Apr 14	Sunday	
105	15	23	19	20	9	8	5	5	3	4	19	5	1	18	3	11	7	7	9	11	5	7	8	10	232	Apr 15	Monday	
106	6	4	4	3	5	2	0	2	1	4	8	2	10	9	0	5	4	3	5	3	4	0	1	14	99	Apr 16	Tuesday	
107	10	15	15	22	19	12	6	6	6	12	6	9	23	17	16	10	10	16	9	15	10	12	16	13	305	Apr 17	Wednesday	
108	15	7	13	10	4	7	6	10	10	19	17	19	6	10	11	3	7	5	8	7	9	13	12	10	238	Apr 18	Thursday	
109	15	20	20	13	6	9	9	6	10	6	7	9	10	16	14	13	7	12	18	12	19	9	31	18	309	Apr 19	Friday	
110	22	17	17	12	14	8	11	6	8	6	14	6	5	12	16	6	4	11	19	5	11	12	11	12	265	Apr 20	Saturday	
111	25	32	25	14	19	26	26	25	21	10	13	13	16	13	16	22	19	17	21	17	16	22	19	24	471	Apr 21	Sunday	
112	22	29	24	15	9	9	5	3	12	4	6	25	14	12	5	9	8	9	9	23	7	14	37	23	333	Apr 22	Monday	
113	13	15	11	19	6	7	12	6	5	13	4	15	7	1	7	2	21	2	8	11	9	8	12	16	230	Apr 23	Tuesday	
114	25	25	22	20	9	18	1	6	3	11	32	11	21	13	8	16	10	8	11	15	18	23	21	16	363	Apr 24	Wednesday	
115	19	18	24	29	12	8	4	7	14	2	5	11	21	2	4	13	23	4	12	5	4	9	3	7	260	Apr 25	Thursday	
116	11	7	14	9	5	4	13	0	0	15	15	20	27	11	4	4	2	22	15	4	12	13	17	11	255	Apr 26	Friday	
117	16	12	3	10	3	9	1	25	4	6	9	8	6	5	4	15	14	8	23	14	16	11	12	8	242	Apr 27	Saturday	
118	16	11	13	26	19	24	13	7	6	2	4	5	1	5	4	11	3	1	5	5	10	13	13	4	221	Apr 28	Sunday	
119	24	17	14	7	8	4	5	2	0	40	58	39	13	25	12	18	16	17	49	32	32	30	20	20	502	Apr 29	Monday	
120	7	4	13	20	5	2	5	15	9	7	12	13	39	5	3	6	9	6	16	4	18	7	14	12	251	Apr 30	Tuesday	
121	16	9	23	27	20	21	6	27	3	3	8	9	2	5	11	13	13	21	11	14	14	17	20	20	333	May 01	Wednesday	Frste
122	28	30	25	17	8	3	2	10	3	16	12	3	10	10	8	13	8	6	8	11	14	23	16	15	299	May 02	Thursday	
123	11	26	30	18	14	10	16	12	11	9	5	14	7	8	2	4	2	5	8	8	26	13	10	22	291	May 03	Friday	
124	13	8	11	15	18	13	6	5	3	4	3	13	11	11	20	7	7	13	13	18	21	24	23	19	299	May 04	Saturday	
125	23	19	17	24	31	17	19	12	10	22	11	15	16	9	7	19	11	13	21	13	15	16	21	13	394	May 05	Sunday	
126	25	15	10	20	12	7	4	5	3	5	4	3	8	9	8	4	6	6	21	1	6	3	9	17	211	May 06	Monday	
127	7	9	12	14	12	1	0	17	4	3	4	9	23	8	14	5	4	0	9	8	5	9	10	7	194	May 07	Tuesday	
128	10	12	12	10	12	3	0	2	2	3	12	20	22	13	3	5	5	3	11	3	5	9	11	11	199	May 08	Wednesday	
129	8	22	7	14	0	0	1	12	11	11	11	20	13	8	13	11	10	16	13	16	20	16	16	11	280	May 09	Thursday	Kristi
130	13	24	12	17	16	16	8	4	1	7	6	5	5	22	7	14	4	8	12	8	26	20	16	13	284	May 10	Friday	
131	19	11	20	29	11	9	18	7	9	11	12	10	13	4	12	9	8	11	10	8	9	11	3	9	273	May 11	Saturday	
132	8	12	15	10	9	8	9	7	3	8	15	15	5	8	0	3	14	4	4	5	15	10	9	19	215	May 12	Sunday	
133	13	21	11	16	10	3	1	3	4	6	2	3	14	8	10	9	14	7	4	12	8	8	5	13	205	May 13	Monday	
134	18	10	6	16	10	5	5	8	6	14	8	6	10	12	22	13	10	8	11	16	15	11	21	14	275	May 14	Tuesday	
135	12	12	17	7	7	3	5	4	23	0	3	2	8	10	13	8	10	7	12	10	11	13	22	10	229	May 15	Wednesday	
136	18	19	29	17	8	10	9	7	5	3	2	13	9	5	13	16	9	8	7	12	22	18	18	15	292	May 16	Thursday	
137	12	13	22	21	12	13	13	8	9	5	41	18	14	6	15	1	2	7	3	7	5	12	10	0	269	May 17	Friday	Sytten
138	7	14	7	13	11	8	7	9	10	6	3	8	35	0	0	0	0	0	24	12	43	24	19	21	281	May 18	Saturday	
139	16	37	19	17	18	8	16	10	35	5	8	7	8	4	11	11	9	12	11	12	13	16	18	20	341	May 19	Sunday	Frste
140	13	16	14	11	20	16	13	15	18	20	17	13	7	13	12	16	13	16	18	6	16	15	11	13	342	May 20	Monday	Annen
141	20	18	14	23	14	7	3	5	7	6	8	21	4	6	10	9	6	19	14	20	7	9	9	9	268	May 21	Tuesday	
142	4	6	9	9	1	6	6	14	2	6	11	13	17	10	10	11	19	14	13	14	20	18	14	13	260	May 22	Wednesday	
143	11	16	16	16	13	9	9	7	6	5	5	15	15	20	6	4	9	7	19	21	3	11	16	12	271	May 23	Thursday	
144	14	8	13	13	6	1	7	9	12	9	6	9	20	12	4	15	8	3	9	13	2	29	15	7	244	May 24	Friday	
145	7	6	8	10	11	11	5	4	6	2	6	6	8	4	3	7	2	9	10	15	8	12	12	21	193	May 25	Saturday	
146	22	15	23	20	19	17	18	15	9	20	10	11	13	4	2	2	3	5	5	7	8	10	5	6	269	May 26	Sunday	

Table 2.3.2 (Page 1 of 4)

NAO .DPX Hourly distribution of detections

Day	00	01	02	03	04	05	06	07	08	09	10	11	12	13	14	15	16	17	18	19	20	21	22	23	Sum	Date
147	9	14	5	10	4	0	3	3	6	22	1	17	13	3	9	13	6	19	12	10	6	21	11	20	237	May 27 Monday
148	14	20	18	12	5	2	3	5	3	4	3	7	26	3	9	11	12	12	27	25	14	16	14	20	285	May 28 Tuesday
149	18	19	17	10	10	7	4	10	8	4	9	3	11	33	13	21	6	8	21	22	9	7	13	23	306	May 29 Wednesday
150	15	11	12	11	5	3	5	3	2	9	3	12	10	20	18	10	6	7	16	11	10	11	21	16	247	May 30 Thursday
151	16	26	18	15	10	19	3	5	2	7	26	11	6	8	10	16	11	17	12	8	19	13	17	20	315	May 31 Friday
152	29	24	23	18	17	19	12	15	17	21	10	15	7	10	6	6	18	16	15	15	22	24	20	25	404	Jun 01 Saturday
153	18	15	18	15	20	20	9	10	11	12	9	12	6	5	17	16	17	19	11	8	15	8	16	13	320	Jun 02 Sunday
154	9	13	23	20	7	7	3	1	10	5	11	6	6	10	9	10	1	13	7	14	19	16	15	20	255	Jun 03 Monday
155	18	20	22	13	17	5	4	4	7	4	18	10	7	14	2	9	19	7	16	10	11	14	11	22	284	Jun 04 Tuesday
156	15	19	22	11	9	2	7	7	9	21	8	20	23	4	10	4	5	9	8	9	7	13	8	11	261	Jun 05 Wednesday
157	9	13	21	14	2	8	5	4	17	4	0	9	30	11	3	8	12	3	8	4	10	14	13	9	231	Jun 06 Thursday
158	8	5	6	9	3	11	1	6	13	6	13	19	43	5	2	1	5	14	13	9	6	5	9	14	226	Jun 07 Friday
159	8	8	17	6	4	6	12	8	4	1	11	6	14	2	10	17	5	5	6	14	15	12	16	11	218	Jun 08 Saturday
160	7	4	5	16	7	8	11	5	27	6	8	16	5	14	8	11	15	12	10	13	27	11	18	14	278	Jun 09 Sunday
161	21	17	16	10	9	0	5	2	2	2	6	10	28	5	10	4	0	7	8	6	7	9	1	2	187	Jun 10 Monday
162	8	4	12	3	2	1	2	14	7	15	13	12	15	9	19	15	2	10	3	4	9	11	8	5	203	Jun 11 Tuesday
163	7	6	8	11	11	12	3	9	10	7	5	6	10	7	4	11	9	8	7	8	12	3	8	9	191	Jun 12 Wednesday
164	15	17	12	3	3	8	9	1	8	3	16	2	19	12	14	8	17	12	8	6	2	7	9	6	217	Jun 13 Thursday
165	6	10	26	3	5	6	13	15	5	11	8	8	25	10	20	4	3	15	7	10	11	8	12	8	249	Jun 14 Friday
166	9	48	14	8	16	8	9	19	23	42	38	37	35	33	29	9	9	28	7	5	19	19	12	15	491	Jun 15 Saturday
167	6	6	13	11	9	17	4	10	11	14	10	11	15	23	18	15	24	15	7	9	18	8	15	16	305	Jun 16 Sunday
168	14	8	8	20	12	4	0	3	2	2	9	6	3	14	5	15	13	8	4	4	9	17	6	12	198	Jun 17 Monday
169	7	8	18	7	2	6	3	0	14	8	3	15	19	10	8	9	12	8	23	7	9	12	7	20	235	Jun 18 Tuesday
170	19	9	11	10	10	6	6	7	9	11	12	15	9	8	15	13	8	2	3	7	9	8	11	9	227	Jun 19 Wednesday
171	8	11	8	8	3	27	17	12	16	8	6	15	22	3	5	7	0	17	2	7	4	5	6	3	220	Jun 20 Thursday
172	5	6	14	9	3	5	10	14	2	7	2	5	9	5	5	12	9	14	12	3	6	2	1	3	163	Jun 21 Friday
173	8	3	7	4	10	7	5	5	6	1	5	3	8	2	8	3	2	4	2	6	8	6	2	9	124	Jun 22 Saturday
174	14	6	13	2	9	3	3	3	10	4	10	14	2	6	2	2	6	5	7	5	4	36	9	19	194	Jun 23 Sunday
175	2	12	3	2	1	13	10	6	4	17	3	5	17	4	20	3	7	8	7	6	13	5	6	2	176	Jun 24 Monday
176	3	5	4	6	11	4	3	2	0	3	6	6	19	8	20	7	19	7	10	5	9	5	2	10	174	Jun 25 Tuesday
177	3	4	6	7	2	0	1	5	3	3	12	23	21	18	22	4	11	6	3	5	11	6	8	19	203	Jun 26 Wednesday
178	12	10	14	13	7	1	4	4	12	11	4	5	14	17	18	17	9	4	2	8	7	6	20	8	227	Jun 27 Thursday
179	12	10	9	8	6	3	0	2	5	2	7	12	13	11	14	8	7	10	9	13	4	7	9	19	200	Jun 28 Friday
180	17	11	16	8	20	18	9	10	23	10	24	11	15	5	4	14	12	13	14	10	20	16	12	11	323	Jun 29 Saturday
181	13	11	10	11	11	7	18	10	14	16	8	8	10	11	5	8	4	8	8	4	12	6	4	21	238	Jun 30 Sunday
182	14	9	10	3	8	3	12	10	2	9	6	18	9	24	13	32	10	6	0	2	5	4	8	19	236	Jul 01 Monday
183	8	14	5	8	11	13	11	6	3	11	14	18	8	9	12	8	5	9	1	6	9	22	7	8	226	Jul 02 Tuesday
184	6	7	14	8	10	0	5	7	21	29	0	11	10	8	26	17	4	6	5	11	11	4	6	6	232	Jul 03 Wednesday
185	8	11	10	1	4	1	25	7	5	15	18	36	16	11	9	7	18	4	10	8	8	10	7	11	260	Jul 04 Thursday
186	7	5	16	2	15	2	3	1	2	7	7	7	18	8	13	1	28	1	4	7	5	6	7	4	176	Jul 05 Friday
187	8	7	2	8	4	13	3	5	2	6	1	6	27	6	2	9	4	7	6	7	8	3	4	6	154	Jul 06 Saturday
188	1	4	8	10	9	17	0	6	1	6	12	13	0	2	3	1	3	7	6	2	0	0	5	2	118	Jul 07 Sunday
189	5	4	5	2	5	1	1	5	8	20	3	13	8	7	5	8	3	8	14	7	2	10	4	8	156	Jul 08 Monday
190	2	3	13	5	5	2	3	15	3	3	16	5	13	6	9	3	7	6	5	16	7	5	10	10	172	Jul 09 Tuesday
191	10	8	16	24	13	12	11	0	4	19	34	12	14	14	15	12	12	14	16	6	10	15	11	13	315	Jul 10 Wednesday
192	11	23	13	12	9	5	4	7	7	7	4	12	2	10	4	3	1	4	3	8	4	12	5	6	176	Jul 11 Thursday
193	10	15	12	8	9	12	1	2	3	9	24	38	8	7	3	9	7	16	15	13	5	9	25	16	276	Jul 12 Friday
194	14	25	12	19	11	7	17	7	7	5	4	7	16	6	5	9	3	14	18	18	28	20	10	21	303	Jul 13 Saturday
195	25	14	19	15	26	21	12	8	20	23	8	8	19	15	14	9	12	17	11	13	9	4	21	13	356	Jul 14 Sunday
196	14	9	6	9	5	8	5	0	0	1	13	5	20	6	8	3	10	11	5	16	5	6	5	4	174	Jul 15 Monday
197	7	12	8	10	3	6	16	10	6	7	8	12	25	13	8	18	3	9	15	6	17	11	14	6	250	Jul 16 Tuesday
198	14	14	17	15	18	11	3	3	8	7	16	6	6	16	10	5	6	17	10	6	16	17	24	19	284	Jul 17 Wednesday
199	22	32	27	23	8	5	7	5	10	4	15	16	21	3	14	17	8	8	2	9	11	18	13	5	303	Jul 18 Thursday
200	2	16	23	4	13	7	0	11	11	16	3	7	9	12	24	13	11	11	15	11	11	18	8	14	270	Jul 19 Friday
201	15	21	15	18	20	14	9	9	13	12	16	23	15	44	21	25	19	21	26	19	20	15	19	24	453	Jul 20 Saturday
202	15	23	22	31	23	34	22	21	20	16	21	14	28	18	29	21	18	27	19	13	16	23	27	25	526	Jul 21 Sunday

Table 2.3.2 (Page 2 of 4)

NAO .DPX Hourly distribution of detections

Day	00	01	02	03	04	05	06	07	08	09	10	11	12	13	14	15	16	17	18	19	20	21	22	23	Sum	Date
203	31	23	20	13	16	6	5	9	7	4	7	5	7	12	19	9	3	7	9	10	7	9	10	15	263	Jul 22 Monday
204	9	12	9	4	6	2	13	1	7	17	8	9	13	28	2	14	2	20	8	5	22	28	18	10	267	Jul 23 Tuesday
205	10	11	6	16	12	4	7	5	1	20	22	12	4	16	9	10	5	3	19	10	12	18	16	15	263	Jul 24 Wednesday
206	15	13	17	8	17	5	2	12	22	6	4	7	12	15	4	17	9	15	4	7	8	10	10	15	254	Jul 25 Thursday
207	6	5	5	11	13	5	4	7	6	7	9	15	22	12	9	14	9	5	9	4	5	7	14	4	207	Jul 26 Friday
208	4	11	8	5	8	10	7	3	5	8	12	12	13	15	26	7	16	15	16	16	12	17	20	19	285	Jul 27 Saturday
209	29	25	18	19	22	29	25	19	16	19	21	30	27	21	16	20	18	20	14	14	19	12	10	17	480	Jul 28 Sunday
210	22	21	21	18	9	0	0	1	7	1	11	1	31	6	5	10	9	8	12	7	20	11	11	4	246	Jul 29 Monday
211	6	12	15	8	9	5	5	10	15	6	10	13	7	22	17	15	5	7	10	20	11	9	15	9	261	Jul 30 Tuesday
212	12	13	5	23	18	4	6	4	12	6	6	18	26	11	4	19	7	14	19	18	4	9	15	13	286	Jul 31 Wednesday
213	6	24	28	10	6	3	1	4	3	3	1	5	18	13	10	9	9	3	20	11	9	9	22	7	234	Aug 01 Thursday
214	9	7	13	11	11	1	5	0	16	2	19	4	0	8	1	6	2	7	1	6	7	3	7	10	156	Aug 02 Friday
215	5	12	9	14	5	4	3	3	12	0	5	11	6	4	4	2	2	8	3	9	14	8	5	6	154	Aug 03 Saturday
216	6	6	22	9	9	1	6	12	1	11	6	10	31	14	11	8	11	5	14	14	12	21	9	4	253	Aug 04 Sunday
217	10	6	14	2	5	5	5	4	2	0	11	13	13	11	11	12	7	6	5	5	12	9	5	3	176	Aug 05 Monday
218	11	12	18	9	3	1	2	2	4	13	5	7	19	15	12	14	10	5	6	5	8	7	13	15	216	Aug 06 Tuesday
219	6	9	14	7	2	8	1	2	8	21	16	4	10	12	15	7	9	6	9	10	1	11	6	10	204	Aug 07 Wednesday
220	8	7	23	8	9	3	9	18	1	8	8	19	5	8	16	12	12	6	3	9	2	16	18	4	232	Aug 08 Thursday
221	8	8	15	9	5	7	20	17	6	6	7	6	12	12	11	20	13	11	18	20	22	25	26	23	327	Aug 09 Friday
222	15	24	29	25	21	18	13	17	21	14	10	20	13	17	17	26	28	18	26	20	23	26	21	18	480	Aug 10 Saturday
223	21	20	27	32	20	18	21	18	22	22	21	17	18	17	26	38	19	15	11	28	18	25	22	21	517	Aug 11 Sunday
224	20	26	29	20	18	13	7	18	14	17	16	11	15	20	21	9	12	10	15	12	4	16	10	21	374	Aug 12 Monday
225	17	19	13	8	14	5	4	3	5	21	12	0	5	11	8	8	16	15	17	4	11	23	14	15	268	Aug 13 Tuesday
226	14	16	15	9	8	2	0	11	6	14	3	9	11	11	16	18	8	18	15	22	14	12	12	13	277	Aug 14 Wednesday
227	22	16	16	35	11	13	12	5	10	3	16	38	6	38	17	14	6	21	11	13	13	21	15	22	394	Aug 15 Thursday
228	14	13	20	12	7	9	9	9	9	6	8	10	7	11	36	36	26	25	18	14	16	14	27	13	369	Aug 16 Friday
229	15	10	16	17	25	14	21	14	22	2	9	8	14	8	10	8	15	15	17	17	24	16	35	16	368	Aug 17 Saturday
230	25	15	30	22	17	25	28	26	23	18	20	31	19	28	25	19	26	23	21	16	23	18	19	17	534	Aug 18 Sunday
231	12	14	25	24	7	18	17	6	7	4	4	15	10	6	12	4	8	16	7	21	7	10	13	15	282	Aug 19 Monday
232	13	11	10	11	6	15	4	2	10	23	22	20	38	15	23	14	7	17	16	10	15	20	18	21	361	Aug 20 Tuesday
233	15	23	14	23	10	12	10	6	1	18	6	11	6	11	18	9	9	7	6	10	12	10	21	11	279	Aug 21 Wednesday
234	13	28	23	19	17	4	4	13	1	9	7	4	5	22	4	8	3	5	21	28	2	9	10	12	271	Aug 22 Thursday
235	12	16	9	14	19	5	6	9	5	15	3	7	6	4	6	8	13	11	9	14	20	10	18	16	255	Aug 23 Friday
236	22	19	15	24	16	19	10	0	17	16	15	33	9	7	13	8	14	23	14	14	14	10	19	14	365	Aug 24 Saturday
237	22	11	14	20	12	15	16	11	10	9	22	8	13	16	6	12	9	11	26	27	4	16	12	15	337	Aug 25 Sunday
238	13	12	10	9	5	0	8	2	2	9	10	13	8	17	4	10	1	5	8	4	7	17	15	14	203	Aug 26 Monday
239	18	14	17	12	6	2	1	1	6	15	5	8	13	11	4	9	10	21	17	18	16	20	16	17	277	Aug 27 Tuesday
240	22	21	10	12	14	6	1	3	3	12	8	4	16	7	16	11	14	5	15	17	8	21	25	17	288	Aug 28 Wednesday
241	14	13	11	12	12	13	5	7	10	7	22	5	14	17	6	25	12	13	23	28	9	15	16	15	324	Aug 29 Thursday
242	9	15	20	8	12	1	7	3	5	11	6	6	16	6	13	8	2	16	6	29	6	8	4	11	228	Aug 30 Friday
243	8	16	16	21	17	12	15	39	10	15	12	18	12	12	8	9	11	15	7	11	17	19	22	12	354	Aug 31 Saturday
244	22	18	19	19	10	20	21	10	15	8	14	15	6	11	7	12	10	8	15	17	11	15	24	22	349	Sep 01 Sunday
245	24	25	26	19	18	4	2	14	0	3	10	12	12	0	2	15	13	11	7	8	6	7	13	13	264	Sep 02 Monday
246	13	11	19	22	11	14	4	7	13	4	9	10	7	7	11	5	13	5	28	13	9	16	19	20	290	Sep 03 Tuesday
247	18	17	16	15	14	5	6	12	24	12	2	12	9	12	26	14	17	30	8	12	14	17	25	32	369	Sep 04 Wednesday
248	29	18	23	15	13	13	16	13	7	15	6	16	16	12	18	23	23	23	26	20	22	23	32	20	442	Sep 05 Thursday
249	21	25	24	23	19	10	10	16	21	12	0	0	0	0	27	16	13	13	20	9	28	19	28	9	363	Sep 06 Friday
250	17	13	15	21	26	15	13	15	9	9	13	7	12	9	20	10	13	14	12	19	23	13	17	24	359	Sep 07 Saturday
251	25	24	14	13	13	12	13	21	16	17	20	9	16	14	17	16	19	11	10	15	13	9	17	17	371	Sep 08 Sunday
252	31	9	20	11	8	18	5	7	6	0	2	4	6	7	3	11	11	4	15	12	11	14	15	14	244	Sep 09 Monday
253	14	15	14	14	18	6	6	13	5	4	6	9	12	21	17	36	19	12	5	0	0	0	0	0	246	Sep 10 Tuesday
254	0	0	0	0	10	24	8	11	7	15	32	24	13	22	8	15	15	12	7	9	17	14	15	22	300	Sep 11 Wednesday
255	22	20	17	14	18	9	6	4	7	4	0	8	18	10	4	13	4	3	6	3	16	9	11	20	246	Sep 12 Thursday
256	14	16	19	14	9	7	6	6	3	8	14	9	14	13	17	11	5	8	13	15	16	12	18	14	281	Sep 13 Friday
257	15	11	17	19	28	17	19	17	18	18	13	10	15	17	15	24	18	16	20	28	10	19	13	11	408	Sep 14 Saturday
258	26	12	14	18	21	19	19	14	19	16	21	14	17	12	22	10	15	19	7	14	24	11	17	22	403	Sep 15 Sunday

Table 2.3.2 (Page 3 of 4)

NAO .DPX Hourly distribution of detections

Day	00	01	02	03	04	05	06	07	08	09	10	11	12	13	14	15	16	17	18	19	20	21	22	23	Sum	Date
259	13	12	14	21	11	5	3	5	3	1	27	11	1	31	12	4	4	9	9	5	5	5	18	6	235	Sep 16 Monday
260	11	14	20	22	9	2	4	6	6	6	8	5	7	10	6	5	12	13	8	11	18	10	12	15	240	Sep 17 Tuesday
261	9	11	12	10	8	7	3	6	7	8	15	10	22	14	26	12	9	20	14	22	12	22	14	23	316	Sep 18 Wednesday
262	21	26	15	25	18	10	11	17	16	10	12	11	7	18	16	14	21	17	16	22	14	19	18	14	388	Sep 19 Thursday
263	16	15	20	15	11	11	7	8	4	7	6	0	0	0	0	0	0	0	0	0	0	0	0	0	120	Sep 20 Friday
264	0	0	0	0	0	0	0	0	0	0	0	0	0	0	0	0	0	0	0	0	0	0	0	0	0	Sep 21 Saturday
265	0	0	0	0	0	0	0	0	0	0	0	0	0	0	0	0	0	0	0	0	0	0	0	0	0	Sep 22 Sunday
266	14	15	15	18	20	7	4	14	6	13	8	13	11	16	16	19	19	22	12	16	12	21	13	23	347	Sep 23 Monday
267	17	15	34	21	21	16	14	8	10	21	18	22	19	26	16	16	19	18	12	18	16	8	14	12	411	Sep 24 Tuesday
268	8	16	12	26	11	14	3	23	10	12	12	13	14	21	19	21	8	14	11	8	16	25	19	14	350	Sep 25 Wednesday
269	16	21	12	13	11	4	4	11	3	11	3	21	24	28	9	6	4	12	12	8	17	8	17	8	283	Sep 26 Thursday
270	18	17	6	8	4	4	8	3	16	5	3	18	28	15	5	4	6	16	7	17	6	9	11	16	250	Sep 27 Friday
271	4	11	12	12	7	12	4	9	5	11	4	5	16	17	6	8	10	7	9	13	19	13	20	8	242	Sep 28 Saturday
272	22	17	11	21	19	14	20	13	16	8	7	9	4	7	10	7	12	9	13	15	13	20	16	15	318	Sep 29 Sunday
273	28	34	10	22	15	18	6	7	7	9	13	10	16	10	17	9	14	12	18	20	12	14	15	17	353	Sep 30 Monday
NAO	00	01	02	03	04	05	06	07	08	09	10	11	12	13	14	15	16	17	18	19	20	21	22	23		
Sum	2769	2612	1705	1586	1845	2218	2170	2057	2019	2202	2466	2539	2605	2802	2091	1453	1631	1993	2465	2089	1865	2187	2261	2601	52231	Total sum
181	14	15	15	14	12	9	8	9	9	10	11	12	14	12	12	11	10	11	12	12	12	14	14	14	289	Total average
126	14	15	15	13	10	7	6	7	7	9	10	12	14	12	11	11	10	10	11	11	11	13	14	13	268	Average workdays
55	15	16	16	17	15	15	12	13	13	12	13	13	13	11	12	12	12	13	14	14	16	16	16	15	333	Average weekends

Table 2.3.2. Daily and hourly distribution of NORSAR detections. For each day is shown number of detections within each hour of the day and number of detections for that day. The end statistics give total number of detections distributed for each hour and the total sum of detections during the period. The averages show number of processed days, hourly distribution and average per processed day.

3 Operation of regional arrays

3.1 Recording of NORESS data at NDPC, Kjeller

Table 3.1.1 lists the main outage times and reasons, and as can be seen the main reason for the outage is damage to the Hub caused by a thunderstorm.

The average recording time was 89.89% as compared to 99.2% during the previous reporting period.

Date	Time	Cause
07 Apr	2106 - 2138	Transmission line failure
13 May	2142 - 2158	Transmission line failure
05 Jun	0505 - 1055	Software work
05 Jun	1105 - 1127	Software work
18 Jun	1735-	HUB failure due to thunderstorm
25 Jun	- 1158	
15 Jul	1122 - 1254	Transmission line failure
15 Jul	1320 - 1346	Transmission line failure
26 Jul	2048 - 2052	Transmission line failure
27 Jul	0550 - 0605	Transmission line failure
31 Jul	2230 -	HUB failure
02 Aug	- 0720	
16 Aug	1445 -	HUB failure due to thunderstorm
26 Aug	- 1400	
28 Aug	0555 - 0559	Transmission line maintenance
28 Aug	0622 - 0626	Transmission line maintenance
28 Aug	0759 - 0825	Transmission line maintenance
28 Aug	0837 - 0856	Transmission line maintenance
10 Sep	1228 - 1245	Transmission line failure
17 Sep	0624 - 0632	Transmission line failure
18 Sep	1118 - 1126	Transmission line maintenance

Table 3.1.1. Interruptions in NORESS recordings at NDPC, 1 April - 30 September 1991.

Monthly uptimes for the NORESS on-line data recording task, taking into account all factors (field installations, transmission line, data center operation) affecting this task were as follows:

April	:	99.91
May	:	99.96
June	:	76.58
July	:	99.50
August	:	63.50
September	:	99.91

Fig. 3.1.1 shows the uptime for the data recording task, or equivalently, the availability of NORESS data in our tape archive, on a day-by-day basis, for the reporting period.

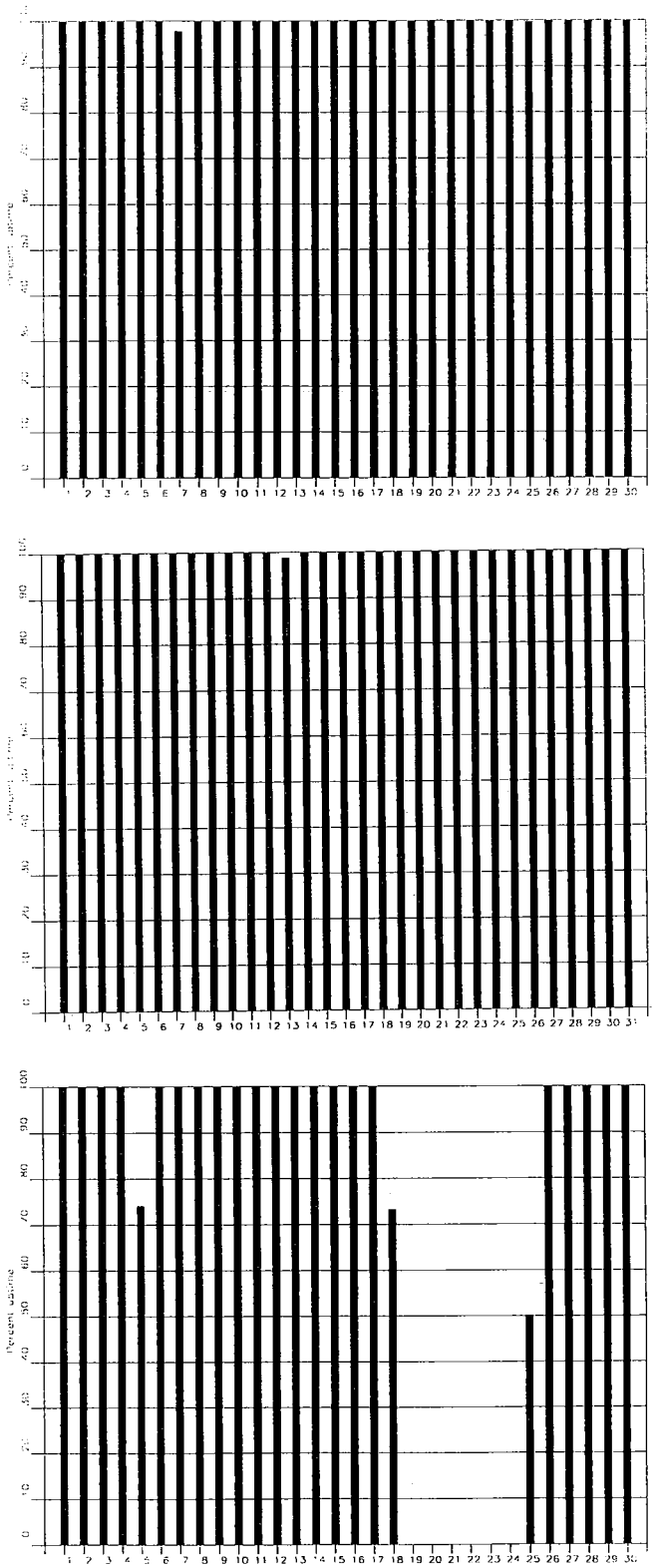

Fig. 3.1.1. NORESS data recording uptime for April (top), May (middle) and June (bottom) 1991.

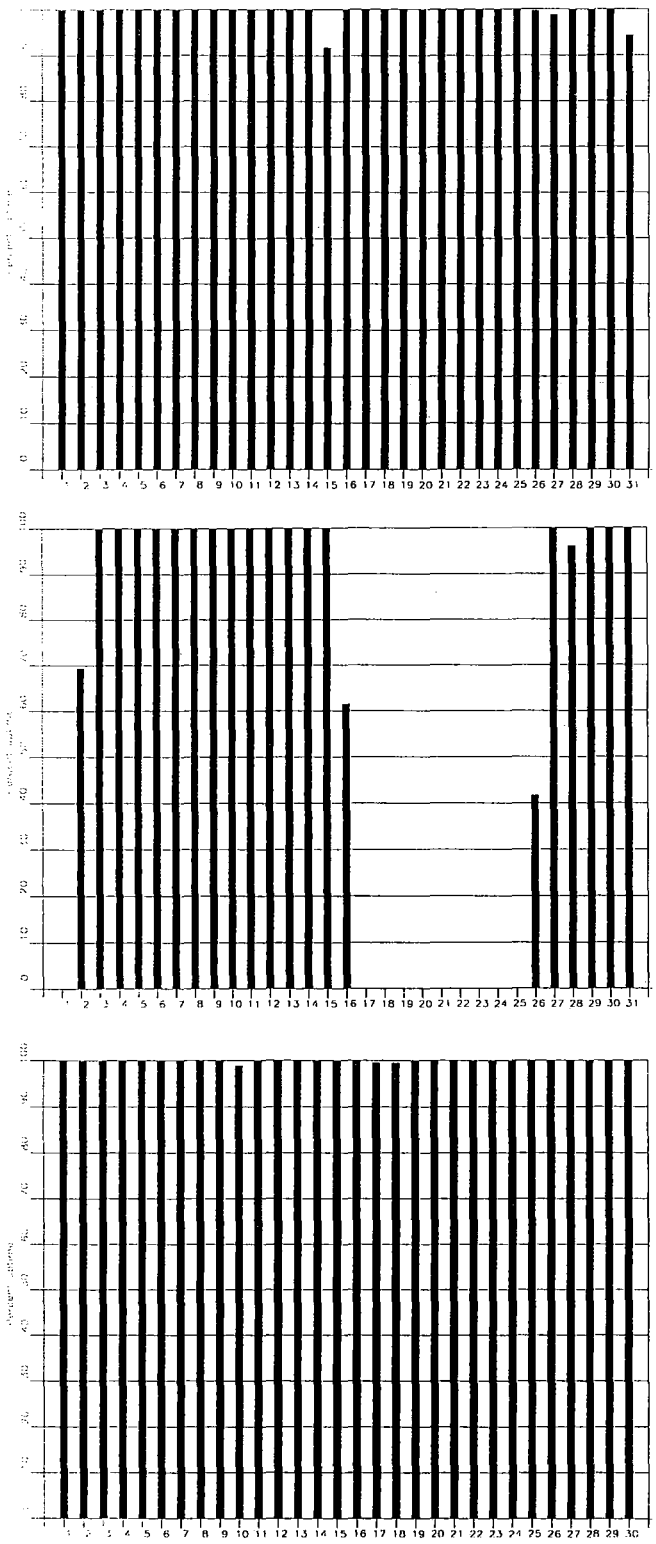

Fig. 3.1.1. (cont.) NORESS data recording uptime for July (top), August (middle) and September (bottom) 1991.

3.2 Recording of ARCESS data at NDPC, Kjeller

The main reasons causing most of the ARCESS outage in the period are: service on the satellite link, and hardware failure at NDPC.

The average recording time was 97.32% as compared to 98.4% for the previous reporting period..

Date	Time	Cause
03 Apr	0933 - 0946	Service on the antenna
04 Apr	1511 - 1544	Hardware failure NDPC
04 Apr	1612 - 1645	Hardware failure NDPC
04 Apr	1715 - 1745	Hardware failure NDPC
04 Apr	1810 - 1840	Hardware failure NDPC
04 Apr	1901 - 1911	Hardware failure NDPC
04 Apr	1924 -	Hardware failure NDPC
05 Apr	- 0555	
05 Apr	0620 - 0629	Hardware failure NDPC
05 Apr	0643 - 1019	Hardware failure NDPC
10 Apr	0807 - 0820	Service satellite link
10 Apr	0826 - 0838	Service satellite link
10 Apr	0856 - 1009	Service satellite link
10 Apr	1043 - 1140	Service satellite link
10 Apr	1359 - 1407	Service satellite link
11 Apr	0702 - 0717	Service satellite link
17 Apr	0132 - 1535	Power break HUB
22 Apr	2204 -	Software failure
23 Apr	- 1013	
01 Jun	0516 - 0534	Hardware failure
06 Jun	0735 - 0819	Hardware failure
17 Jun	0953 - 1626	Service HUB
17 Jun	1658 - 1709	Service HUB
17 Jun	1725 - 1759	Service HUB
17 Jun	2040 - 2102	Service HUB
18 Jun	0839 - 0904	Service HUB
18 Jun	1156 - 1313	Service HUB
19 Jun	0445 - 0453	Software service
19 Jun	0459 - 1200	Software service
18 Jul	1035 - 1043	Unknown
25 Jul	2037 - 2108	Unknown
26 Jul	0629 - 0757	Hardware service
26 Jul	0804 - 1226	Hardware service
12 Aug	1807 - 1830	Software failure

14 Aug	0625	- 0824	Service satellite link at HUB
14 Aug	0900	- 1134	Service satellite link at HUB
14 Aug	1146	- 1202	Service satellite link at HUB
15 Aug	0653	- 0702	Service satellite link at HUB
15 Aug	0858	- 0908	Service satellite link at HUB
16 Aug	0157	-	Satellite link failure
17 Aug		- 1217	
24 Aug	1916	- 1924	Satellite link failure
24 Aug	1931	- 1838	Satellite link failure
15 Sep	1321	- 2004	Power break HUB

Table 3.2.1. The main interruptions in ARCESS recordings at NDPC, 1 April - 30 September 1991.

Monthly uptimes for the ARCESS on-line data recording task, taking into account all factors (field installations, transmissions line, data center operation) affecting this task were as follows:

April	:	93.62%
May	:	99.99%
June	:	97.56%
July	:	99.12%
August	:	94.59%
September	:	99.06%

Fig. 3.2.1. shows the uptime for the data recording task, or equivalently, the availability of ARCESS data in our tape archive, on a day-by-day basis, for the reporting period.

J. Torstveit

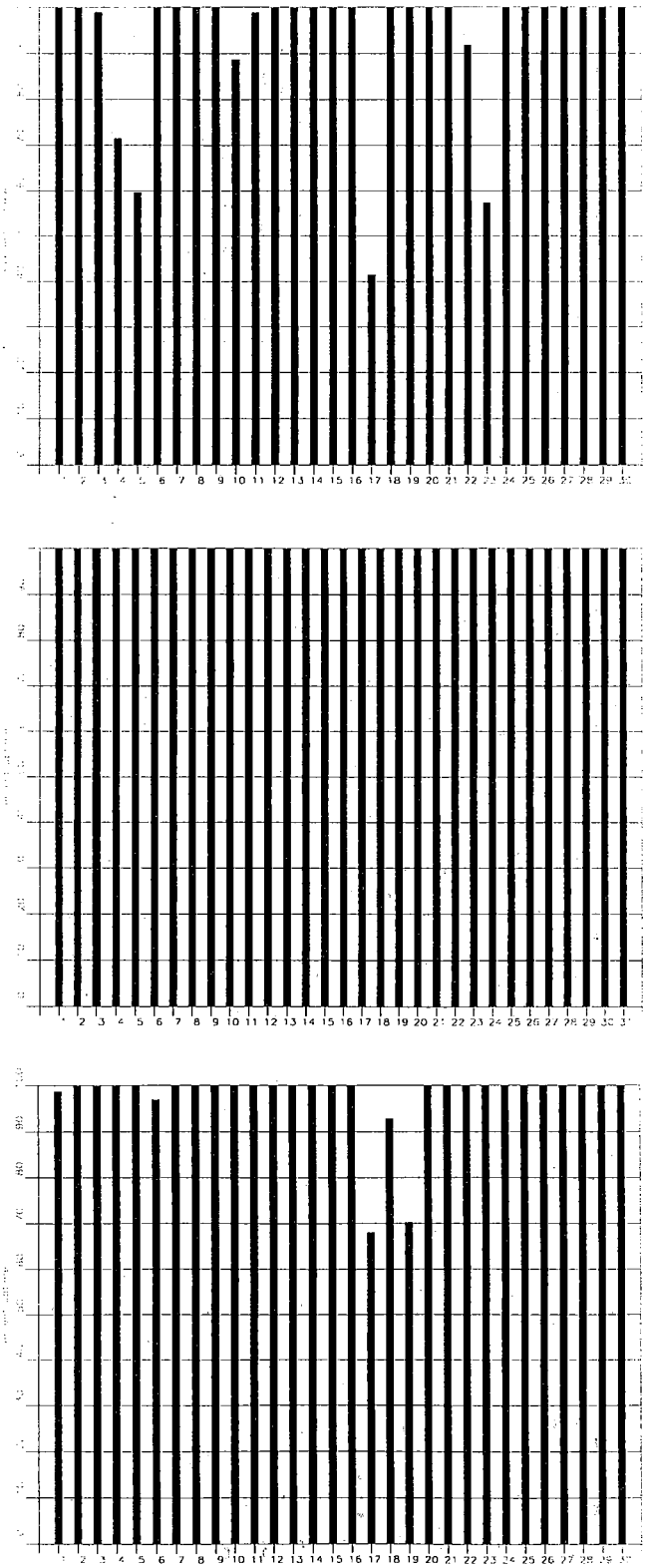

Fig. 3.2.1. ARCESS data recording uptime for April (top), May (middle) and June (bottom) 1991.

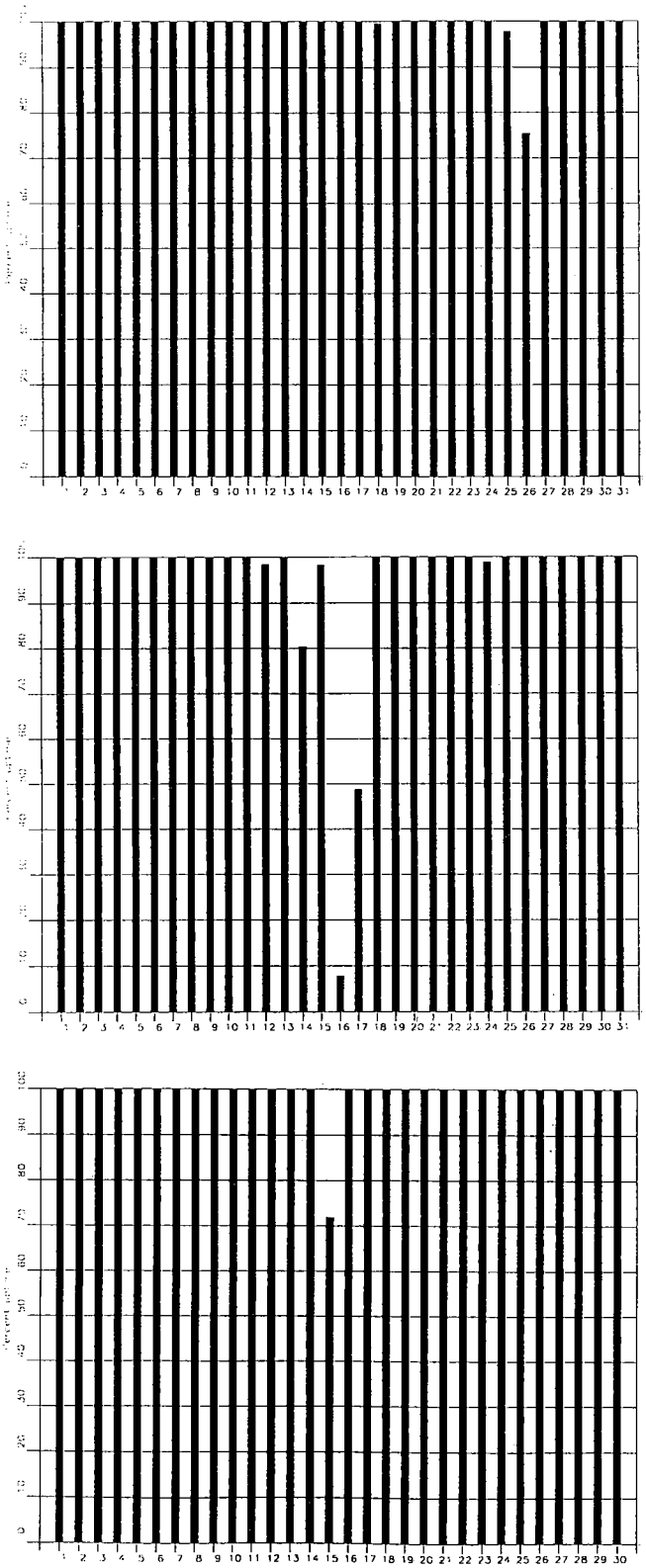

Fig. 3.2.1. ARCESS data recording uptime for July (top), August (middle) and September (bottom) 1991.

3.3 Recording of FINESA data at NDPC, Kjeller

The average recording time was 66.2% as compared to 98.9 for the previous period. As can be seen from Table 3.3.1 below, the main reason for the downtime is transmission line failure and HUB failure.

Date	Time		Cause
05 Apr	1030	- 1129	Transmission line failure
16 Apr	1149	- 1252	Service at HUB
27 Apr	1241	- 1407	Hardware failure NDPC
28 Apr	2015	- 2113	Hardware failure NDPC
03 May	0053	- 0556	Hardware failure NDPC
05 May	1515	- 1552	Hardware failure NDPC
06 May	0259	- 0356	Hardware failure NDPC
06 May	1031	- 1052	Hardware failure NDPC
07 May	1407	- 1502	Hardware failure NDPC
08 May	0756	- 0812	Hardware service NDPC
08 May	1046	- 1302	Hardware service NDPC
14 May	2047	- 2127	Transmission line failure
15 May	1509	-	Transmission line failure due to thunderstorm
17 May		- 0755	Transmission line failure due to thunderstorm
17 May	1355	-	Transmission line failure due to thunderstorm
20 May		- 1008	Transmission line failure due to thunderstorm
22 May	1249	-	Transmission line failure
23 May		- 1027	Transmission line failure
25 May	1140	-	Bad data due to numerous gaps
28 May		- 1110	Bad data due to numerous gaps
30 May	0841	- 1201	Software upgrade
03 Jun	0642	- 1308	Software upgrade
08 Jun	0319	- 0658	Transmission line failure
10 Jun	0941	-	Transmission line service
12 Jun		- 0900	Transmission line service
12 Jun	0900	-	Transmission line failure
26 Jun		- 0822	Transmission line failure
29 Jun	0001	-	Transmission line failure
17 Jul	-	0620	Transmission line failure
17 Jul	1618	-	Transmission line failure
18 Jul		- 0934	Transmission line failure
18 Jul	1033	-	Transmission line failure
22 Jul		- 0950	Transmission line failure
29 Jul	1100	- 1408	Transmission line failure
03 Aug	1625	-	Transmission line failure
05 Aug		- 1221	Transmission line failure

05 Aug	1316	-	Transmission line failure
06 Aug		- 0630	Transmission line failure
09 Aug	0452	- 0937	Transmission line failure
09 Aug	2243	-	Transmission line failure
12 Aug		- 1148	Transmission line failure
12 Aug	1439	-	Transmission line failure
16 Aug		- 0706	Transmission line failure
16 Aug	1048	-	Transmission line failure
22 Aug		- 0955	Transmission line failure
27 Aug	1908	- 1937	Transmission line failure
12 Sep	0912	- 1055	Transmission line test
13 Sep	0627	- 0853	Service HUB

Table 3.3.1. The main interruptions in FINESA recordings at NDPC, 1 April - 30 September 1991.

Monthly uptimes for the FINESA on-line data recording task, taking into account all factors (field installations, transmissions line, data center operation) affecting this task were as follows:

April	:	99.29%
May	:	75.64%
June	:	38.76%
July	:	32.09%
August	:	51.86%
September	:	99.39%

Fig. 3.4.1 shows the uptime for the data recording task, or equivalently, the availability of FINESA data in our tape archive, on a day-by-day basis, for the reporting period.

J. Torstveit

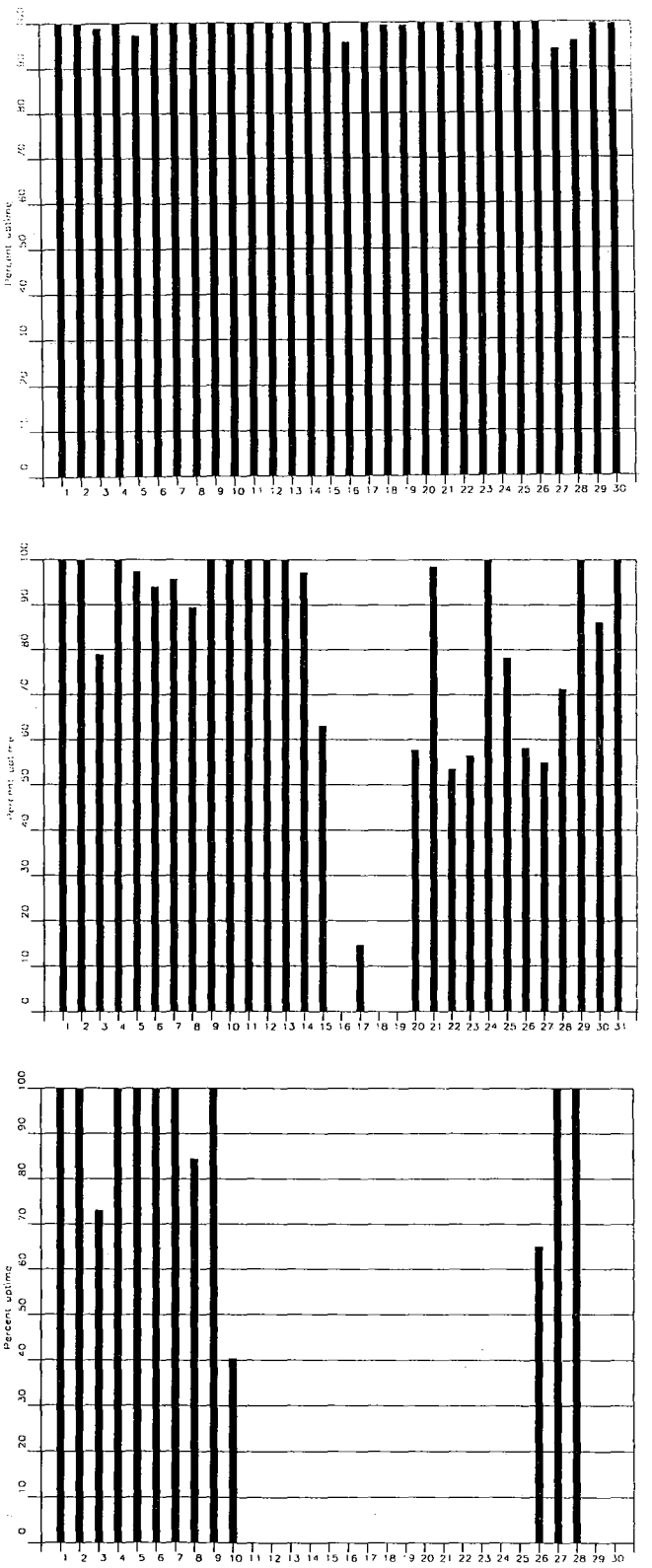

Fig. 3.3.1. FINESA data recording uptime forApril (top), May (middle) and June (bottom) 1991.

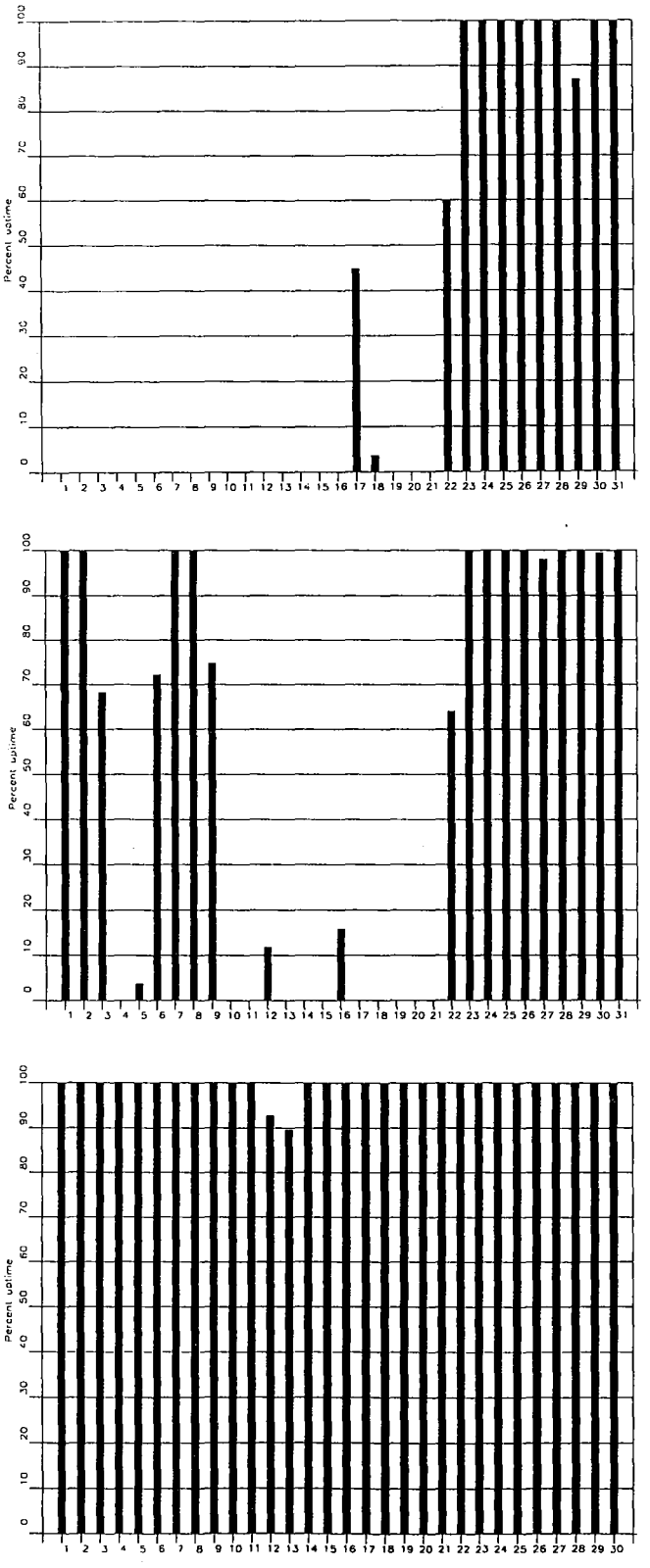

Fig. 3.3.1. (cont) FINESA data recording uptime for July (top), August (middle) and September (bottom) 1991.

3.4 Event detection operation

This section reports results from simple one-array automatic processing using signal processing recipes and 'ronap' recipes for the ep program (NORSAR Sci. Rep. No 2-88,89).

IMS results are reported in section 3.5.

NORESS detections

The number of detections (phases) reported during day 091 1991, through day 273 1991, was 31,966, giving an average of 193 detections per processed day (166 days processed).

Table 3.4.1 shows daily and hourly distribution of detections for NORESS.

Events automatically located by NORESS

During days 091 1991, through 273 1991, 2218 local and regional events were located by NORESS, based on automatic association of P- and S-type arrivals. This gives an average of 13.4 events per processed day (166 days processed). 63 % of these events are within 300 km, and 88 % of these events are within 1000 km.

ARCESS detections

The number of detections (phases) reported during day 091 1991, through day 273 1991, was 84,791, giving an average of 463 detections per processed day (183 days processed).

There were several periods during which local disturbances generated a great many detections at the ARCESS array. These are very near-field events that occur in particular when the temperature is below freezing and suddenly drops more than 10 degrees Celsius.

Table 3.4.2 shows daily and hourly distribution of detections for ARCESS.

Events automatically located by ARCESS

During days 091, 1991, through 273, 1991, 3999 local and regional events were located by ARCESS, based on automatic association of P- and S-type arrivals. This gives an average 21.9 events per processed day (183 days processed). 46 % of these events are within 300 km, and 86 % of these events are within 1000 km.

FINESA detections

The number of detections (phases) reported during day 091 1991, through day 273 1991, was 34,925, giving an average of 275 detections per processed day (127 days processed).

Table 3.4.3 shows daily and hourly distribution of detections for FINESA.

Events automatically located by FINESA

During days 091 1990, through 274 1991, 2095 local and regional events were located by FINESA, based on automatic association of P- and S-type arrivals. This gives an average of 16.5 events per processed day (127 days processed). 64 % of these events are within 300 km, and 86 % of these events are within 1000 km.

GERESS detections

The number of detections (phases) reported during day 091 1991, through day 274 1991, was 34,007, giving an average of 199 detections per processed day (171 days processed).

Table 3.4.4 shows daily and hourly distribution of detections for GERESS.

Events automatically located by GERESS

During days 091 1991, through 273 1991, 2783 local and regional events were located by GERESS, based on automatic association of P- and S-type arrivals. This gives an average of 16.3 events per processed day (171 days processed). 71 % of these events are within 300 km, and 89 % of these events are within 1000 km.

Poland detections

The number of detections (phases) reported by the station KSP during day 176 1991, through day 273 1991, was 38,143, giving an average of 397 detections per processed day (96 days processed).

The data transmitted from the station SFP were in general very unreliable throughout the reporting period, with lots of gaps, wrong gain and wrong time. It was not possible to process the data received from the SFP station during this period.

J. Fyen

NRS .FKX Hourly distribution of detections

Day	00	01	02	03	04	05	06	07	08	09	10	11	12	13	14	15	16	17	18	19	20	21	22	23	Sum	Date		
91	4	49	54	59	32	13	3	10	6	9	5	12	11	5	1	2	11	3	12	4	4	5	8	8	330	Apr 01	Monday	Annen
92	1	1	1	2	12	1	9	5	5	2	14	13	23	17	5	6	5	2	6	11	1	3	4	5	154	Apr 02	Tuesday	
93	3	0	1	4	2	7	0	5	6	13	8	5	10	16	6	6	6	1	5	0	15	1	2	3	125	Apr 03	Wednesday	
94	3	4	4	9	1	2	1	2	3	11	5	4	22	9	13	9	1	3	6	15	3	2	4	4	140	Apr 04	Thursday	
95	4	2	2	2	13	9	7	12	3	14	6	8	18	7	6	7	7	5	9	3	16	0	2	2	164	Apr 05	Friday	
96	3	1	2	2	3	6	7	6	3	0	4	5	1	4	4	3	2	3	1	4	4	1	1	3	73	Apr 06	Saturday	
97	0	2	5	0	1	2	1	1	10	8	2	1	4	5	4	4	3	3	8	7	3	2	8	5	89	Apr 07	Sunday	
98	4	4	2	0	3	2	1	3	5	6	3	5	18	6	3	5	3	4	9	10	3	3	5	9	116	Apr 08	Monday	
99	4	2	5	2	5	0	8	3	3	10	2	14	24	12	14	7	5	7	1	15	2	4	4	11	164	Apr 09	Tuesday	
100	4	11	4	5	2	4	3	11	20	7	11	24	10	5	2	1	2	0	4	1	23	6	1	15	176	Apr 10	Wednesday	
101	6	1	4	6	0	2	2	13	19	18	31	5	6	19	4	6	3	2	4	5	17	1	1	3	178	Apr 11	Thursday	
102	0	3	5	0	2	3	2	4	3	4	3	9	13	12	13	2	2	1	6	1	20	2	2	17	129	Apr 12	Friday	
103	14	27	30	33	25	29	25	28	29	27	27	26	22	23	24	34	24	38	31	48	44	34	42	47	731	Apr 13	Saturday	
104	37	31	41	28	36	31	29	30	32	29	26	30	21	31	32	28	39	29	36	46	45	42	38	41	808	Apr 14	Sunday	
105	31	36	42	16	17	2	6	3	4	8	14	6	4	11	2	4	8	3	7	10	2	2	12	13	263	Apr 15	Monday	
106	16	20	18	1	2	2	8	7	8	6	9	5	10	18	7	7	4	3	8	1	7	9	10	6	192	Apr 16	Tuesday	
107	9	7	9	7	2	5	1	5	6	6	5	8	19	13	4	1	7	7	4	2	13	0	3	11	154	Apr 17	Wednesday	
108	2	0	12	3	3	7	14	14	14	13	12	14	8	15	17	5	5	5	10	4	15	2	3	7	204	Apr 18	Thursday	
109	3	6	10	17	10	6	8	11	5	10	12	8	6	16	9	7	5	4	9	1	16	2	12	9	202	Apr 19	Friday	
110	13	15	11	11	7	4	10	4	8	4	3	4	5	3	11	7	7	4	5	3	1	4	3	3	150	Apr 20	Saturday	
111	17	16	15	23	5	7	13	8	7	13	6	6	11	6	0	2	4	12	2	6	2	8	8	8	205	Apr 21	Sunday	
112	4	9	5	7	3	8	17	18	11	11	24	14	15	17	9	9	4	7	12	11	12	1	32	13	273	Apr 22	Monday	
113	3	1	7	6	2	14	24	11	3	21	6	14	10	10	4	5	27	5	11	16	8	7	3	10	228	Apr 23	Tuesday	
114	7	5	6	2	0	13	2	14	3	5	16	13	19	6	14	6	8	3	8	18	4	4	7	10	193	Apr 24	Wednesday	
115	4	2	9	7	2	3	1	11	18	17	36	13	45	17	14	11	19	6	12	4	20	2	3	9	285	Apr 25	Thursday	
116	3	0	2	2	2	4	10	6	8	18	15	16	31	16	7	3	4	11	10	11	31	5	8	4	227	Apr 26	Friday	
117	13	4	3	4	3	11	3	16	4	3	5	11	8	4	5	13	10	6	7	2	9	2	1	2	149	Apr 27	Saturday	
118	4	1	3	6	2	10	3	5	3	3	6	4	6	4	7	7	1	1	1	6	4	5	2	9	103	Apr 28	Sunday	
119	7	3	6	2	4	6	19	10	0	27	24	26	13	30	12	18	10	8	19	20	18	11	11	7	311	Apr 29	Monday	
120	2	1	12	7	4	3	4	21	13	11	25	14	31	7	1	7	4	4	19	14	6	1	0	8	219	Apr 30	Tuesday	
121	3	3	7	10	7	12	4	11	2	7	3	0	2	5	7	2	6	7	0	6	4	0	5	9	122	May 01	Wednesday	Frste
122	6	11	6	3	7	2	0	11	0	8	5	0	6	12	11	10	7	3	4	7	12	3	7	13	154	May 02	Thursday	
123	3	3	19	4	5	5	5	16	19	6	5	10	3	16	2	5	2	3	10	2	10	1	3	25	182	May 03	Friday	
124	6	2	10	5	5	4	5	2	0	1	1	7	2	1	9	6	3	17	4	3	3	15	6	4	121	May 04	Saturday	
125	3	3	9	7	10	2	4	5	2	10	4	19	10	2	0	9	5	5	7	3	4	0	9	8	140	May 05	Sunday	
126	10	3	8	2	5	5	0	5	6	7	7	8	18	13	9	7	11	5	12	1	8	4	0	8	162	May 06	Monday	
127	7	3	5	7	11	6	0	12	4	8	3	15	22	17	9	1	4	2	2	12	3	1	1	9	164	May 07	Tuesday	
128	3	3	9	1	4	3	2	13	9	10	8	19	16	18	7	4	5	3	9	3	15	4	6	9	183	May 08	Wednesday	
129	1	7	11	3	2	2	5	7	9	11	3	6	6	8	3	2	4	2	0	2	4	4	1	3	106	May 09	Thursday	Kristi
130	4	4	2	4	9	5	2	3	2	6	3	8	4	11	6	8	0	3	12	1	20	1	2	15	135	May 10	Friday	
131	3	4	8	2	8	5	3	3	3	7	9	6	7	1	3	5	3	7	5	2	4	5	1	1	105	May 11	Saturday	
132	0	1	1	2	1	6	4	7	5	10	16	29	37	20	2	5	14	3	5	1	13	5	3	7	197	May 12	Sunday	
133	5	7	7	7	8	6	13	3	8	20	6	7	12	12	12	12	6	4	6	12	3	2	0	7	185	May 13	Monday	
134	21	14	23	14	9	8	6	12	4	12	8	13	13	14	18	14	5	8	8	16	14	14	17	13	298	May 14	Tuesday	
135	13	18	12	12	7	3	5	5	21	5	3	28	13	10	18	7	5	3	5	9	15	1	2	9	229	May 15	Wednesday	
136	4	1	9	3	4	3	4	10	2	13	9	24	19	5	7	11	3	6	5	4	23	0	2	10	181	May 16	Thursday	
137	6	2	17	6	1	7	2	3	11	8	20	12	13	10	6	4	4	7	9	8	5	8	4	2	175	May 17	Friday	Sytten
138	4	6	3	9	4	8	6	4	8	1	3	5	8	6	0	4	5	8	0	0	3	2	6	3	106	May 18	Saturday	
139	2	14	3	2	4	1	3	4	18	5	3	3	10	2	5	8	7	6	9	12	2	1	8	15	147	May 19	Sunday	Frste
140	9	9	7	3	8	2	3	6	8	6	10	3	8	3	11	4	6	0	6	6	2	7	0	5	132	May 20	Monday	Annen
141	5	11	3	1	1	5	2	2	8	14	19	12	12	8	11	5	5	14	4	6	3	2	3	5	161	May 21	Tuesday	
142	1	4	4	7	0	0	8	10	8	12	2	15	9	18	10	2	8	7	5	4	18	3	0	4	159	May 22	Wednesday	
143	2	3	0	1	5	3	5	7	6	4	16	7	19	8	2	4	7	7	4	7	20	2	4	1	144	May 23	Thursday	
144	1	0	7	2	2	4	7	15	14	7	22	19	17	18	2	10	7	2	7	8	18	14	2	9	214	May 24	Friday	
145	3	4	4	11	3	1	4	3	6	2	6	7	5	2	2	5	3	7	12	9	7	7	12	9	134	May 25	Saturday	
146	13	6	12	10	12	9	8	7	10	26	12	7	21	3	14	8	10	4	2	4	8	6	4	13	229	May 26	Sunday	

Table 3.4.1 (Page 1 of 4)

NRS .FKX Hourly distribution of detections

Day	00	01	02	03	04	05	06	07	08	09	10	11	12	13	14	15	16	17	18	19	20	21	22	23	Sum	Date
147	5	8	4	4	5	7	10	5	7	24	2	13	13	8	29	12	9	18	11	3	19	7	3	15	241	May 27 Monday
148	6	7	7	8	8	7	7	9	8	8	19	14	22	9	11	3	7	6	21	13	25	3	2	7	237	May 28 Tuesday
149	5	5	9	12	3	4	6	3	6	6	17	1	15	37	17	9	6	5	18	9	9	5	1	10	218	May 29 Wednesday
150	0	2	6	8	2	3	7	12	9	9	7	9	23	20	14	8	11	7	15	9	9	13	2	4	209	May 30 Thursday
151	9	4	3	2	2	8	4	4	6	17	17	11	28	13	9	9	6	6	6	6	4	8	1	2	185	May 31 Friday
152	5	3	6	0	1	5	4	6	11	7	6	5	6	9	1	2	4	3	3	6	3	0	5	0	101	Jun 01 Saturday
153	4	2	5	4	4	4	0	1	6	12	16	4	4	1	4	4	8	7	2	3	5	2	6	4	112	Jun 02 Sunday
154	3	8	1	15	4	7	6	14	9	4	15	5	19	19	7	11	13	14	9	12	4	3	7	12	221	Jun 03 Monday
155	2	2	2	5	8	10	0	17	9	15	15	22	23	27	3	10	12	3	13	11	6	4	4	2	225	Jun 04 Tuesday
156	8	2	4	6	4	0	0	0	0	0	0	0	0	0	7	4	2	33	17	22	2	3	5	2	121	Jun 05 Wednesday
157	0	2	8	5	8	8	13	9	10	14	4	13	40	26	16	10	15	11	12	10	5	12	2	6	259	Jun 06 Thursday
158	0	3	1	5	2	6	5	11	6	9	12	18	38	17	3	3	15	5	8	22	6	13	8	5	221	Jun 07 Friday
159	4	5	7	3	4	7	16	8	5	11	3	6	13	3	16	9	1	5	8	14	6	2	5	1	162	Jun 08 Saturday
160	1	4	3	9	12	8	20	0	16	1	32	14	3	8	3	12	15	15	5	6	9	3	6	3	208	Jun 09 Sunday
161	5	8	5	3	4	6	6	1	0	8	9	15	35	14	9	4	4	15	6	21	3	4	6	6	197	Jun 10 Monday
162	8	6	8	7	10	16	9	19	17	25	34	25	26	18	33	9	11	9	2	18	5	4	5	4	328	Jun 11 Tuesday
163	8	5	2	7	24	9	17	9	16	20	10	19	13	27	1	7	6	8	5	11	11	6	7	3	251	Jun 12 Wednesday
164	5	11	2	4	3	18	20	13	17	14	19	12	23	15	18	3	15	15	13	1	15	1	2	2	261	Jun 13 Thursday
165	0	1	3	7	3	12	16	18	7	35	23	6	21	11	4	7	5	11	11	2	16	2	2	0	223	Jun 14 Friday
166	0	17	9	3	10	2	5	7	5	15	16	21	8	7	16	3	9	14	4	6	9	7	6	8	207	Jun 15 Saturday
167	2	1	8	2	2	10	5	9	9	8	6	6	4	27	5	2	1	4	2	7	10	5	3	2	140	Jun 16 Sunday
168	2	0	4	17	5	26	4	24	18	8	9	8	11	22	22	14	15	19	6	11	10	13	1	0	269	Jun 17 Monday
169	1	3	13	15	3	12	13	2	11	19	3	27	34	23	9	8	10	8	0	0	0	0	0	0	214	Jun 18 Tuesday
170	0	0	0	0	0	0	0	0	0	0	0	0	0	0	0	0	0	0	0	0	0	0	0	0	0	Jun 19 Wednesday
171	0	0	0	0	0	0	0	0	0	0	0	0	0	0	0	0	0	0	0	0	0	0	0	0	0	Jun 20 Thursday
172	0	0	0	0	0	0	0	0	0	0	0	0	0	0	0	0	0	0	0	0	0	0	0	0	0	Jun 21 Friday
173	0	0	0	0	0	0	0	0	0	0	0	0	0	0	0	0	0	0	0	0	0	0	0	0	0	Jun 22 Saturday
174	0	0	0	0	0	0	0	0	0	0	0	0	0	0	0	0	0	0	0	0	0	0	0	0	0	Jun 23 Sunday
175	0	0	0	0	0	0	0	0	0	0	0	0	0	0	0	0	0	0	0	0	0	0	0	0	0	Jun 24 Monday
176	0	0	0	0	0	0	0	0	0	0	0	1	21	9	17	7	13	3	11	13	5	1	1	3	105	Jun 25 Tuesday
177	2	1	4	7	3	8	9	7	18	9	35	14	23	11	21	2	14	5	8	18	6	4	2	13	244	Jun 26 Wednesday
178	7	3	1	5	12	27	7	2	11	31	7	7	24	16	15	12	6	5	10	8	21	5	6	7	255	Jun 27 Thursday
179	8	6	4	0	7	1	17	4	8	19	22	10	16	23	16	8	9	4	3	21	6	8	1	9	230	Jun 28 Friday
180	4	4	3	4	6	0	8	5	5	5	10	4	7	3	5	7	1	4	4	6	8	3	1	5	112	Jun 29 Saturday
181	0	0	5	2	0	1	8	3	1	0	2	3	3	3	10	7	2	1	4	0	5	2	8	13	83	Jun 30 Sunday
182	4	2	1	9	5	6	3	7	3	17	23	20	9	16	7	4	7	16	8	9	6	10	9	10	211	Jul 01 Monday
183	7	15	18	17	13	9	8	6	5	18	18	16	14	16	18	4	10	19	8	12	8	10	4	5	278	Jul 02 Tuesday
184	7	7	7	10	13	3	15	2	8	24	7	26	20	10	18	17	4	5	5	22	5	1	2	10	248	Jul 03 Wednesday
185	9	9	7	5	2	4	18	4	12	22	22	24	45	35	10	6	13	17	9	13	5	5	3	2	301	Jul 04 Thursday
186	8	3	12	10	13	2	15	6	3	11	8	18	14	6	12	4	24	0	22	4	4	6	3	4	212	Jul 05 Friday
187	6	6	3	3	4	10	3	2	4	3	4	10	25	7	12	5	5	6	3	9	11	7	2	7	157	Jul 06 Saturday
188	4	3	4	4	2	13	2	8	6	10	11	6	1	2	6	1	2	9	2	3	3	0	4	0	106	Jul 07 Sunday
189	7	4	8	11	5	6	5	1	5	19	10	8	21	20	14	5	11	7	13	10	20	5	3	2	220	Jul 08 Monday
190	3	3	7	12	6	2	9	11	5	10	41	35	22	10	7	3	10	4	9	34	1	3	3	4	254	Jul 09 Tuesday
191	1	3	4	8	5	7	12	3	4	8	11	5	11	10	18	11	5	2	2	14	3	3	0	4	154	Jul 10 Wednesday
192	5	6	6	5	8	9	6	9	11	11	17	43	22	16	10	5	3	20	9	8	3	7	2	2	243	Jul 11 Thursday
193	2	6	3	5	7	11	10	13	16	13	24	31	10	10	5	9	16	13	5	22	4	4	10	4	253	Jul 12 Friday
194	4	11	3	10	4	1	6	2	3	7	0	9	9	7	3	6	4	10	4	9	6	6	4	0	128	Jul 13 Saturday
195	4	4	10	4	4	5	4	1	5	12	8	8	3	9	22	0	8	6	5	4	2	2	5	4	139	Jul 14 Sunday
196	5	3	5	12	6	18	8	3	1	10	14	0	0	6	5	8	6	13	11	19	2	9	1	4	169	Jul 15 Monday
197	0	0	2	10	5	4	13	6	3	14	12	22	12	11	8	17	10	3	12	12	4	2	4	1	187	Jul 16 Tuesday
198	3	3	7	8	5	5	10	9	6	14	11	16	14	10	6	9	5	5	6	8	10	3	1	6	180	Jul 17 Wednesday
199	7	0	4	8	7	9	17	2	3	11	18	12	23	17	9	11	12	8	13	22	12	8	7	10	250	Jul 18 Thursday
200	4	11	6	11	8	7	9	13	9	18	4	10	14	17	23	7	6	18	4	15	6	7	4	4	235	Jul 19 Friday
201	1	6	2	4	6	2	5	2	7	4	5	5	5	5	13	6	5	2	5	11	0	1	2	2	106	Jul 20 Saturday
202	2	6	9	3	4	8	0	3	11	3	4	8	8	6	11	8	3	8	8	9	7	8	4	6	147	Jul 21 Sunday

Table 3.4.1 (Page 2 of 4)

NRS .FKX Hourly distribution of detections

Day	00	01	02	03	04	05	06	07	08	09	10	11	12	13	14	15	16	17	18	19	20	21	22	23	Sum	Date
203	4	2	3	21	2	14	14	7	6	5	4	6	6	7	7	10	8	10	10	18	4	7	5	1	181	Jul 22 Monday
204	4	5	4	13	1	8	14	6	11	20	13	16	13	22	11	10	3	17	5	8	5	11	10	2	232	Jul 23 Tuesday
205	4	5	6	17	4	8	11	6	4	17	19	17	14	22	15	11	6	5	15	4	7	1	3	3	224	Jul 24 Wednesday
206	8	1	4	10	12	12	9	3	14	8	5	17	10	9	10	18	21	17	9	5	10	7	7	2	228	Jul 25 Thursday
207	8	4	4	3	1	11	14	6	15	18	15	24	17	21	7	6	14	19	17	20	1	3	3	3	254	Jul 26 Friday
208	3	2	4	2	3	7	8	2	3	5	5	4	9	9	13	7	10	8	9	3	5	4	5	3	133	Jul 27 Saturday
209	7	3	2	9	6	7	7	3	7	5	3	8	9	6	2	5	3	9	2	8	11	2	3	3	130	Jul 28 Sunday
210	6	3	9	9	11	10	5	3	11	13	9	2	22	10	20	7	9	13	11	14	9	3	9	8	226	Jul 29 Monday
211	3	9	5	12	14	14	7	9	5	13	19	14	14	23	14	8	5	17	5	4	3	5	4	3	229	Jul 30 Tuesday
212	0	2	3	9	8	1	6	11	14	13	8	16	18	30	2	13	8	11	14	10	6	4	2	0	209	Jul 31 Wednesday
213	0	0	0	0	0	0	0	0	0	0	0	0	0	0	0	0	0	0	0	0	0	0	0	0	0	Aug 01 Thursday
214	0	0	0	0	0	0	0	6	26	9	15	7	14	12	4	9	9	17	6	20	1	3	0	7	165	Aug 02 Friday
215	4	7	2	4	6	10	2	7	11	5	3	16	5	7	2	2	9	7	2	7	7	0	0	3	128	Aug 03 Saturday
216	2	1	3	2	6	0	6	9	5	5	5	6	16	3	6	8	2	12	9	5	6	6	4	2	129	Aug 04 Sunday
217	7	1	3	10	6	3	10	2	5	3	2	9	18	17	10	12	18	11	12	13	1	8	12	4	197	Aug 05 Monday
218	3	4	7	14	4	2	5	3	3	13	9	8	14	21	10	14	8	12	4	5	5	10	8	14	200	Aug 06 Tuesday
219	0	5	7	3	6	7	2	5	6	15	14	12	14	18	14	5	4	6	12	5	5	4	5	0	174	Aug 07 Wednesday
220	10	1	13	12	7	9	13	14	4	15	9	22	7	9	16	9	4	9	2	10	3	12	15	3	228	Aug 08 Thursday
221	0	3	5	3	2	1	19	12	5	6	8	5	11	15	7	11	6	11	6	13	6	12	18	3	188	Aug 09 Friday
222	5	5	4	9	3	6	7	7	0	4	7	3	5	4	9	7	8	6	6	6	4	4	1	5	125	Aug 10 Saturday
223	0	1	4	4	7	2	3	4	8	5	4	4	5	3	2	4	8	4	5	5	2	5	8	0	97	Aug 11 Sunday
224	4	2	3	10	1	7	4	7	10	9	12	10	15	17	19	15	7	14	6	15	3	3	0	3	196	Aug 12 Monday
225	0	1	6	13	1	4	7	5	11	14	9	5	18	12	11	13	15	8	8	15	5	2	5	3	191	Aug 13 Tuesday
226	3	6	1	11	2	3	11	6	10	11	4	18	12	17	7	9	1	5	11	23	7	4	1	5	188	Aug 14 Wednesday
227	6	3	4	17	7	8	14	11	1	8	18	24	9	30	7	8	5	9	10	8	5	3	6	6	227	Aug 15 Thursday
228	2	6	2	7	2	2	3	4	4	5	6	9	16	16	22	0	0	0	0	0	0	0	0	0	106	Aug 16 Friday
229	0	0	0	0	0	0	0	0	0	0	0	0	0	0	0	0	0	0	0	0	0	0	0	0	0	Aug 17 Saturday
230	0	0	0	0	0	0	0	0	0	0	0	0	0	0	0	0	0	0	0	0	0	0	0	0	0	Aug 18 Sunday
231	0	0	0	0	0	0	0	0	0	0	0	0	0	0	0	0	0	0	0	0	0	0	0	0	0	Aug 19 Monday
232	0	0	0	0	0	0	0	0	0	0	0	0	0	0	0	0	0	0	0	0	0	0	0	0	0	Aug 20 Tuesday
233	0	0	0	0	0	0	0	0	0	0	0	0	0	0	0	0	0	0	0	0	0	0	0	0	0	Aug 21 Wednesday
234	0	0	0	0	0	0	0	0	0	0	0	0	0	0	0	0	0	0	0	0	0	0	0	0	0	Aug 22 Thursday
235	0	0	0	0	0	0	0	0	0	0	0	0	0	0	0	0	0	0	0	0	0	0	0	0	0	Aug 23 Friday
236	0	0	0	0	0	0	0	0	0	0	0	0	0	0	0	0	0	0	0	0	0	0	0	0	0	Aug 24 Saturday
237	0	0	0	0	0	0	0	0	0	0	0	0	0	0	0	0	0	0	0	0	0	0	0	0	0	Aug 25 Sunday
238	0	0	0	0	0	0	0	0	0	0	0	0	0	0	0	0	0	0	0	0	0	0	0	0	0	Aug 26 Monday
239	0	0	0	0	0	0	0	0	0	0	0	0	0	20	7	10	9	12	4	11	7	2	2	5	89	Aug 27 Tuesday
240	1	7	5	8	1	3	6	5	2	20	10	16	24	11	17	9	18	7	4	6	18	4	5	1	208	Aug 28 Wednesday
241	2	3	0	9	1	6	13	8	6	9	26	17	11	17	7	15	3	3	6	1	15	4	1	2	185	Aug 29 Thursday
242	2	3	7	6	3	1	6	11	6	13	12	9	22	6	10	9	4	9	8	8	7	1	1	3	167	Aug 30 Friday
243	2	5	2	6	12	3	11	12	6	7	15	7	16	8	7	4	7	3	6	6	7	1	7	9	169	Aug 31 Saturday
244	3	16	7	11	3	4	12	6	7	6	12	4	4	4	5	8	7	1	4	7	2	3	6	1	143	Sep 01 Sunday
245	3	2	9	5	13	3	5	12	5	9	8	11	21	11	3	9	10	17	6	16	2	5	4	2	191	Sep 02 Monday
246	1	13	8	14	5	7	7	9	14	13	10	19	12	15	10	5	5	6	7	15	3	0	3	4	205	Sep 03 Tuesday
247	0	2	1	6	1	3	4	7	18	10	5	12	15	11	15	7	4	16	6	15	5	3	6	3	175	Sep 04 Wednesday
248	2	0	2	2	3	3	1	3	4	9	4	9	22	9	11	9	13	10	17	12	0	4	4	5	158	Sep 05 Thursday
249	7	2	4	1	1	1	4	2	11	8	4	9	9	6	10	17	8	11	3	8	2	7	6	3	144	Sep 06 Friday
250	4	3	3	5	11	7	9	3	4	6	10	7	11	5	11	1	4	2	7	3	6	2	7	8	139	Sep 07 Saturday
251	3	4	1	4	6	6	3	14	20	18	12	2	2	7	26	3	13	5	5	8	3	3	4	0	172	Sep 08 Sunday
252	5	6	8	10	4	7	7	4	1	3	4	5	5	9	10	6	7	19	9	22	5	7	14	4	181	Sep 09 Monday
253	3	1	1	14	4	3	5	9	0	4	4	8	11	11	4	23	9	4	5	16	4	4	3	2	152	Sep 10 Tuesday
254	5	0	6	4	4	2	4	6	2	6	8	12	9	11	1	10	9	6	11	3	5	0	2	0	126	Sep 11 Wednesday
255	8	1	6	6	2	3	6	6	5	3	5	8	26	8	8	15	5	5	14	5	17	5	4	1	172	Sep 12 Thursday
256	1	3	3	4	3	3	3	7	10	6	14	4	20	9	10	7	12	8	9	14	3	9	6	0	168	Sep 13 Friday
257	3	5	4	0	3	15	18	14	6	6	17	17	9	15	25	10	25	18	9	6	2	8	2	3	240	Sep 14 Saturday
258	7	1	7	1	8	8	19	13	18	8	25	23	6	12	10	11	6	9	10	3	4	2	0	6	217	Sep 15 Sunday

Table 3.4.1 (Page 3 of 4)

NRS .FKX Hourly distribution of detections

Day	00	01	02	03	04	05	06	07	08	09	10	11	12	13	14	15	16	17	18	19	20	21	22	23	Sum	Date
259	1	2	0	5	0	3	3	1	4	5	17	12	5	26	14	1	5	6	4	19	3	7	4	2	149	Sep 16 Monday
260	3	2	4	16	1	1	4	3	5	5	11	20	8	9	14	7	6	5	5	19	7	6	3	0	164	Sep 17 Tuesday
261	0	5	2	4	2	3	3	10	5	13	17	7	27	13	10	8	1	19	6	10	5	10	2	7	189	Sep 18 Wednesday
262	2	9	1	4	7	4	4	7	7	7	9	13	11	14	0	4	19	8	5	10	2	3	0	2	152	Sep 19 Thursday
263	2	0	3	3	2	2	4	2	3	10	11	5	12	6	5	12	3	3	6	27	3	3	3	5	135	Sep 20 Friday
264	2	2	4	0	5	13	17	87	74	44	9	10	24	7	9	18	9	9	9	8	11	5	10	8	394	Sep 21 Saturday
265	8	5	17	12	5	12	15	12	15	2	7	12	8	9	5	18	16	20	3	0	4	2	0	1	208	Sep 22 Sunday
266	3	3	0	8	3	1	2	8	4	9	4	10	21	11	17	39	57	30	33	18	2	4	5	3	295	Sep 23 Monday
267	4	0	3	6	9	8	4	1	3	12	10	11	19	19	2	10	7	8	12	19	5	0	7	4	183	Sep 24 Tuesday
268	4	1	4	1	4	4	2	16	9	17	7	12	15	25	18	15	22	18	9	5	1	4	1	4	218	Sep 25 Wednesday
269	2	2	3	13	5	4	9	6	4	13	10	24	23	21	5	5	17	15	13	16	12	3	6	4	235	Sep 26 Thursday
270	3	1	1	6	0	4	5	4	6	13	6	14	25	21	5	11	9	12	6	27	2	3	3	3	190	Sep 27 Friday
271	2	2	0	6	3	3	6	5	1	6	10	8	20	10	5	7	2	6	5	9	7	3	4	1	131	Sep 28 Saturday
272	3	2	4	2	9	6	5	8	6	8	4	15	6	10	2	3	8	8	3	3	5	7	1	6	134	Sep 29 Sunday
273	12	13	3	0	4	10	2	4	9	5	17	6	12	12	15	14	10	6	13	2	7	3	1	6	186	Sep 30 Monday
NRS	00	01	02	03	04	05	06	07	08	09	10	11	12	13	14	15	16	17	18	19	20	21	22	23		
Sum	766	852	1042	1175	907	1028	1200	1301	1335	1749	1792	1931	2376	2057	1598	1327	1359	1388	1312	1626	1287	793	804	961	31966	Total sum
166	5	5	6	7	5	6	7	8	8	11	11	12	14	12	10	8	8	8	8	10	8	5	5	6	193	Total average
115	4	4	6	7	5	6	7	8	8	11	12	13	17	15	10	8	9	9	9	11	8	5	4	6	200	Average workdays
51	5	7	8	7	7	7	7	8	9	8	9	9	9	7	8	7	7	8	6	7	7	5	6	6	175	Average weekends

Table 3.4.1. Daily and hourly distribution of NORESS detections. For each day is shown number of detections within each hour of the day and number of detections for that day. The end statistics give total number of detections distributed for each hour and the total sum of detections during the period. The averages show number of processed days, hourly distribution and average per processed day.

ARC .FKX Hourly distribution of detections

Day	00	01	02	03	04	05	06	07	08	09	10	11	12	13	14	15	16	17	18	19	20	21	22	23	Sum	Date		
91	8	5	8	7	22	15	5	14	13	12	7	10	20	13	16	15	4	9	22	13	18	21	26	8	311	Apr 01	Monday	Annen
92	12	18	27	20	22	23	15	23	38	58	33	34	42	40	35	22	16	30	20	24	17	26	21	11	627	Apr 02	Tuesday	
93	9	6	8	9	9	5	14	22	20	14	12	18	25	25	13	8	5	16	16	6	9	11	9	3	292	Apr 03	Wednesday	
94	3	6	4	8	14	10	1	16	20	32	22	43	25	16	15	2	0	16	6	1	0	0	0	0	260	Apr 04	Thursday	
95	0	0	0	0	0	0	6	0	0	0	9	21	36	23	16	10	17	16	19	10	4	15	20	6	228	Apr 05	Friday	
96	7	4	6	11	7	11	9	13	31	12	11	31	11	15	26	9	13	9	9	3	8	14	15	5	290	Apr 06	Saturday	
97	7	2	7	4	5	8	3	9	6	10	8	5	14	8	18	14	10	8	11	19	8	9	10	16	219	Apr 07	Sunday	
98	2	9	4	4	9	14	15	6	25	26	20	16	16	37	40	15	6	18	12	15	16	25	31	18	399	Apr 08	Monday	
99	7	24	15	0	6	13	14	13	17	30	26	13	32	18	14	6	7	4	5	8	17	13	18	5	325	Apr 09	Tuesday	
100	10	15	12	11	9	16	12	16	10	0	20	3	40	23	23	22	15	2	15	8	8	8	13	9	320	Apr 10	Wednesday	
101	4	2	4	9	4	20	12	9	31	18	46	9	20	34	18	14	4	12	11	11	7	8	20	15	342	Apr 11	Thursday	
102	4	7	6	3	9	10	5	17	19	13	19	29	19	42	34	13	8	8	12	9	2	6	15	4	313	Apr 12	Friday	
103	2	17	5	1	9	15	14	11	30	20	17	32	22	9	7	6	2	6	11	4	6	4	20	9	279	Apr 13	Saturday	
104	10	2	10	5	6	5	19	4	11	5	14	7	1	17	2	13	5	7	13	14	14	11	23	2	220	Apr 14	Sunday	
105	10	8	7	6	15	13	6	20	22	14	11	22	27	32	18	11	25	16	17	15	5	11	22	10	363	Apr 15	Monday	
106	4	4	6	9	8	8	7	16	13	7	19	18	8	13	12	10	9	4	8	4	5	3	18	7	220	Apr 16	Tuesday	
107	3	3	0	0	0	0	0	0	0	0	0	0	0	0	0	44	185	162	122	70	74	69	56	69	857	Apr 17	Wednesday	
108	67	83	78	68	28	24	22	21	16	23	25	30	20	35	12	14	30	96	110	118	129	108	131	104	1392	Apr 18	Thursday	
109	78	65	74	40	32	42	19	40	46	39	36	24	64	26	12	22	39	64	90	96	115	112	116	108	1399	Apr 19	Friday	
110	109	86	102	80	51	81	73	88	88	49	63	51	16	14	10	17	6	21	62	105	109	109	112	102	1604	Apr 20	Saturday	
111	127	133	125	102	67	79	119	123	113	83	52	51	23	17	12	13	10	13	41	71	92	103	120	120	1809	Apr 21	Sunday	
112	112	108	111	89	44	53	80	86	71	36	25	34	22	23	12	10	3	7	10	12	9	17	53	21	1048	Apr 22	Monday	
113	0	0	0	0	0	0	0	0	0	0	14	32	21	6	9	7	20	9	12	6	4	17	6	11	174	Apr 23	Tuesday	
114	16	30	40	25	1	29	9	17	13	18	23	25	33	24	17	15	35	7	14	24	32	60	76	89	672	Apr 24	Wednesday	
115	110	106	104	57	16	10	39	35	34	28	21	36	48	30	15	19	13	21	14	19	10	27	22	24	858	Apr 25	Thursday	
116	51	74	75	46	5	17	21	15	25	22	21	21	33	21	27	10	18	16	12	13	18	4	25	6	596	Apr 26	Friday	
117	19	37	47	7	3	14	14	12	8	16	17	17	17	17	4	9	18	8	15	5	14	10	12	9	349	Apr 27	Saturday	
118	5	9	2	5	12	16	9	7	29	6	6	13	5	11	9	6	6	11	28	12	10	21	23	15	276	Apr 28	Sunday	
119	8	5	8	12	15	30	11	17	32	41	50	42	26	25	20	15	21	13	47	22	26	19	29	27	561	Apr 29	Monday	
120	32	42	24	10	4	7	11	31	15	32	25	17	45	16	4	24	5	10	18	11	22	11	17	3	436	Apr 30	Tuesday	
121	3	3	3	13	10	11	9	12	17	5	2	12	5	7	10	5	7	12	5	8	7	11	12	12	201	May 01	Wednesday	Frste
122	8	23	14	5	7	15	8	29	15	22	12	21	14	26	31	18	9	19	7	24	2	5	27	25	386	May 02	Thursday	
123	8	4	14	9	8	10	14	17	13	18	14	20	11	21	23	10	21	31	11	4	15	14	16	9	335	May 03	Friday	
124	15	11	7	7	15	17	15	4	12	27	12	10	15	12	21	3	12	13	14	5	27	13	14	3	304	May 04	Saturday	
125	7	9	3	9	5	10	5	4	4	17	15	14	20	15	8	25	13	17	40	41	67	18	16	9	391	May 05	Sunday	
126	23	32	7	15	6	7	7	16	28	17	17	19	37	33	40	17	22	8	34	91	163	165	151	126	1081	May 06	Monday	
127	106	52	45	14	6	10	9	25	28	31	14	17	39	31	24	24	11	10	161	071	581	922	041	79	1352	May 07	Tuesday	
128	29	34	18	12	13	14	21	14	30	22	26	51	46	29	9	7	12	20	147	171	461	551	861	72	1230	May 08	Wednesday	
129	144	102	37	7	12	12	20	23	22	10	8	12	32	9	2	9	10	22	10	311	57	228	240	196	1355	May 09	Thursday	Kristi
130	78	65	35	8	3	31	11	19	18	13	27	21	20	31	13	7	0	7	10	2	13	2	13	6	453	May 10	Friday	
131	4	8	11	1	4	10	8	7	9	8	14	11	4	6	3	15	7	11	9	12	12	26	13	6	219	May 11	Saturday	
132	28	16	2	1	13	6	6	6	7	4	9	16	10	12	13	8	23	8	14	6	22	109	98	30	467	May 12	Sunday	
133	34	19	14	19	10	38	26	54	53	42	21	55	23	30	27	114	145	169	170	151	150	142	104	51	1661	May 13	Monday	
134	61	90	70	71	57	35	47	47	46	35	81	81	79	73	47	37	45	60	53	7	7	12	7	5	1153	May 14	Tuesday	
135	6	2	2	1	5	12	23	14	24	21	18	24	24	40	16	11	7	11	14	11	8	16	7	2	319	May 15	Wednesday	
136	2	3	6	13	7	10	11	13	32	28	20	44	34	25	12	54	21	8	17	16	22	12	14	4	428	May 16	Thursday	
137	0	27	14	5	14	4	13	24	26	12	23	19	21	18	8	5	2	9	5	4	12	21	16	5	307	May 17	Friday	Sytten
138	2	11	3	4	13	10	4	7	2	5	9	36	13	12	2	3	2	8	2	6	15	4	14	8	195	May 18	Saturday	
139	3	19	5	5	4	5	5	3	11	5	2	1	3	6	3	4	5	12	3	23	7	6	12	10	162	May 19	Sunday	Frste
140	7	13	7	3	18	6	12	5	19	5	15	16	19	18	3	5	20	10	8	4	7	30	18	3	271	May 20	Monday	Annen
141	2	6	2	0	8	8	12	12	20	11	9	29	21	26	3	20	4	12	18	13	5	10	15	18	284	May 21	Tuesday	
142	5	3	11	20	5	7	9	10	14	22	24	18	25	25	18	14	11	22	20	12	18	7	18	7	345	May 22	Wednesday	
143	5	13	5	1	5	11	11	16	15	17	16	17	18	20	11	12	14	14	9	30	18	15	21	3	317	May 23	Thursday	
144	1	8	9	14	16	16	14	18	22	21	26	18	47	21	16	23	15	21	25	10	5	25	22	8	421	May 24	Friday	
145	5	4	3	15	7	8	4	6	10	19	29	27	24	13	12	18	24	17	11	15	10	8	4	3	296	May 25	Saturday	
146	2	9	3	2	10	13	12	7	16	1	13	14	10	19	12	11	5	17	26	6	19	4	19	2	252	May 26	Sunday	

Table 3.4.2 (Page 1 of 4)

ARC .FKX Hourly distribution of detections

Day	00	01	02	03	04	05	06	07	08	09	10	11	12	13	14	15	16	17	18	19	20	21	22	23	Sum	Date
147	5	7	2	19	9	11	15	13	16	18	7	25	29	27	22	18	9	29	18	16	7	18	19	10	369	May 27 Monday
148	4	5	5	6	6	15	18	9	13	15	19	14	22	22	10	14	11	23	10	26	6	16	8	14	311	May 28 Tuesday
149	3	2	9	3	8	16	4	14	26	36	30	22	13	22	12	10	6	4	10	7	8	14	13	10	302	May 29 Wednesday
150	3	1	4	5	10	15	7	25	12	24	14	34	29	23	13	12	8	10	13	7	15	18	16	6	324	May 30 Thursday
151	14	22	5	7	3	16	18	14	27	40	42	23	52	27	15	9	9	11	24	5	10	10	18	8	429	May 31 Friday
152	6	1	6	11	6	10	6	10	10	28	21	27	25	13	18	9	21	40	43	11	32	29	17	10	410	Jun 01 Saturday
153	6	3	7	10	6	16	7	2	3	8	2	4	15	12	17	8	22	19	31	12	10	3	19	3	245	Jun 02 Sunday
154	3	6	1	11	9	19	11	14	24	28	25	20	12	14	7	16	4	14	16	15	7	11	16	5	308	Jun 03 Monday
155	4	2	4	2	9	12	5	15	19	24	20	36	22	28	35	39	39	26	22	19	20	18	15	20	455	Jun 04 Tuesday
156	4	7	9	5	4	18	11	11	26	26	19	24	31	17	17	25	17	13	18	3	11	17	17	2	352	Jun 05 Wednesday
157	7	2	7	16	3	12	7	17	26	28	30	21	24	20	23	28	28	20	15	16	15	18	22	9	414	Jun 06 Thursday
158	12	10	17	23	13	15	25	16	12	24	25	27	48	23	16	15	8	11	16	14	13	2	24	13	422	Jun 07 Friday
159	12	4	10	7	6	4	12	7	13	21	12	30	27	19	12	13	7	5	5	32	5	9	11	5	288	Jun 08 Saturday
160	2	6	2	7	2	16	17	6	30	10	12	17	3	11	11	11	19	14	13	10	20	3	8	11	261	Jun 09 Sunday
161	4	9	19	18	10	18	12	26	32	36	21	31	15	21	13	9	19	12	15	7	17	11	19	7	401	Jun 10 Monday
162	4	9	3	1	8	21	8	21	9	10	13	24	14	18	33	41	8	24	12	7	7	1	28	2	326	Jun 11 Tuesday
163	5	5	5	15	11	14	14	46	33	30	20	25	14	20	13	31	9	8	11	17	11	10	26	6	399	Jun 12 Wednesday
164	19	20	9	14	3	20	18	4	32	28	31	42	44	14	34	3	29	21	12	22	20	30	20	10	499	Jun 13 Thursday
165	4	18	9	9	14	19	23	72	23	43	30	14	55	32	23	22	13	16	19	11	12	7	19	8	515	Jun 14 Friday
166	6	28	11	6	8	7	15	6	16	26	30	29	27	31	22	7	7	15	5	16	13	6	17	10	364	Jun 15 Saturday
167	4	3	4	3	5	16	10	10	14	12	20	7	14	19	11	3	6	8	12	15	22	10	17	6	251	Jun 16 Sunday
168	6	6	18	20	9	11	5	17	27	59	0	0	0	0	0	0	7	6	14	36	14	15	24	4	298	Jun 17 Monday
169	2	7	3	12	5	5	14	12	25	21	18	35	0	17	14	20	25	27	20	24	10	18	27	18	379	Jun 18 Tuesday
170	19	6	12	11	11	0	0	0	0	0	0	0	15	41	15	16	6	17	12	2	31	17	23	11	265	Jun 19 Wednesday
171	10	32	28	16	20	45	41	21	54	60	64	59	33	59	37	28	26	15	25	29	28	17	16	11	774	Jun 20 Thursday
172	9	27	8	7	5	15	29	52	82	44	37	21	48	37	21	9	12	13	7	10	10	5	1	5	514	Jun 21 Friday
173	7	1	6	1	8	8	18	16	11	27	30	23	33	21	21	12	14	2	10	18	4	7	1	7	306	Jun 22 Saturday
174	7	4	14	9	20	13	8	22	17	29	17	8	6	16	17	8	14	10	6	2	7	28	14	15	311	Jun 23 Sunday
175	2	8	12	15	11	22	33	18	27	21	9	21	33	12	14	8	11	10	14	15	7	15	13	2	353	Jun 24 Monday
176	3	2	0	7	3	10	11	27	25	43	22	15	16	10	18	31	9	11	14	13	7	9	8	6	320	Jun 25 Tuesday
177	6	2	6	12	20	14	15	9	45	31	30	36	26	19	29	8	10	19	14	14	6	21	10	18	420	Jun 26 Wednesday
178	10	8	6	21	10	10	9	25	57	44	24	27	40	27	28	34	13	28	16	24	8	22	16	7	514	Jun 27 Thursday
179	10	8	19	12	14	18	14	19	29	37	34	30	32	55	26	15	11	8	9	14	11	10	12	7	454	Jun 28 Friday
180	10	9	6	17	7	13	3	8	23	22	27	29	22	26	28	9	17	9	9	23	20	8	5	10	360	Jun 29 Saturday
181	6	5	9	17	10	14	15	19	35	34	31	34	31	35	20	21	15	22	27	12	30	14	18	27	501	Jun 30 Sunday
182	15	12	12	4	8	11	18	30	41	21	21	25	39	35	30	22	24	22	23	15	16	9	13	16	482	Jul 01 Monday
183	23	4	4	10	13	23	29	37	39	45	48	50	32	36	31	23	17	10	21	19	18	26	13	9	580	Jul 02 Tuesday
184	15	8	0	15	16	36	33	57	46	44	47	27	19	18	20	15	14	10	9	8	10	27	18	14	526	Jul 03 Wednesday
185	11	6	11	9	5	37	27	38	36	26	41	29	27	16	30	19	17	6	14	32	20	20	15	17	509	Jul 04 Thursday
186	9	12	5	11	10	13	24	20	21	23	32	21	56	25	28	15	9	29	14	15	12	22	27	8	461	Jul 05 Friday
187	17	8	4	8	18	20	16	7	19	24	25	43	31	26	16	18	10	10	8	21	14	7	3	3	376	Jul 06 Saturday
188	14	3	7	3	11	13	6	15	26	19	23	14	18	20	14	7	5	6	9	16	7	7	3	11	277	Jul 07 Sunday
189	5	14	17	25	10	27	10	16	34	25	21	44	13	29	23	9	12	3	17	7	9	37	13	1	421	Jul 08 Monday
190	5	5	6	11	17	10	19	34	41	31	22	42	33	27	41	25	11	12	20	21	19	13	18	3	486	Jul 09 Tuesday
191	17	5	4	15	9	39	25	27	49	36	35	24	39	38	22	15	31	5	12	17	32	5	8	15	524	Jul 10 Wednesday
192	6	9	6	19	11	16	13	9	39	28	38	33	33	38	30	17	24	25	13	5	12	4	8	7	443	Jul 11 Thursday
193	4	18	15	5	11	32	20	36	31	47	59	44	45	50	31	22	43	12	15	23	10	7	21	15	616	Jul 12 Friday
194	11	16	2	19	13	6	14	6	12	26	19	17	15	6	16	26	5	17	13	6	5	12	1	3	286	Jul 13 Saturday
195	4	10	10	9	13	10	9	5	13	32	12	24	11	9	13	6	9	19	39	33	3	9	18	3	323	Jul 14 Sunday
196	26	28	2	13	12	23	11	18	16	18	17	12	12	29	6	8	30	14	30	23	8	22	25	1	404	Jul 15 Monday
197	4	2	0	17	5	8	29	41	14	26	31	33	24	22	7	10	12	2	14	18	10	13	10	7	359	Jul 16 Tuesday
198	15	13	6	3	15	24	21	39	28	26	36	42	36	21	36	18	16	10	12	10	7	12	11	1	458	Jul 17 Wednesday
199	22	5	11	18	13	18	24	35	60	38	36	22	39	64	38	21	33	21	28	9	14	7	14	25	615	Jul 18 Thursday
200	4	23	5	24	13	21	27	35	19	58	24	53	45	42	47	15	11	5	19	5	10	12	14	0	531	Jul 19 Friday
201	13	5	5	21	11	20	12	11	25	37	34	38	15	18	24	8	11	10	10	11	8	17	6	10	380	Jul 20 Saturday
202	12	14	15	10	10	16	18	20	30	31	32	21	29	18	21	20	10	6	22	10	8	6	13	24	416	Jul 21 Sunday

Table 3.4.2 (Page 2 of 4)

ARC .FKX Hourly distribution of detections

Day	00	01	02	03	04	05	06	07	08	09	10	11	12	13	14	15	16	17	18	19	20	21	22	23	Sum	Date		
203	17	3	16	9	17	16	17	16	44	42	32	35	29	40	38	9	5	28	9	10	24	18	9	10	493	Jul	22	Monday
204	10	3	9	24	4	18	24	47	26	33	32	45	47	43	31	23	17	12	12	15	7	20	21	13	536	Jul	23	Tuesday
205	4	2	2	20	15	14	20	22	38	44	37	35	34	51	36	25	22	19	17	10	24	2	13	6	512	Jul	24	Wednesday
206	1	1	8	4	17	17	6	28	28	31	12	36	25	40	26	27	22	6	12	13	2	3	7	11	383	Jul	25	Thursday
207	5	10	11	20	23	25	16	0	2	0	0	0	10	52	34	26	19	27	13	17	21	4	11	4	350	Jul	26	Friday
208	5	6	3	16	10	23	13	5	11	48	21	38	16	25	18	8	20	10	21	8	6	3	3	3	340	Jul	27	Saturday
209	15	5	3	22	6	20	31	15	33	39	10	36	27	33	12	12	11	5	24	11	9	0	7	10	396	Jul	28	Sunday
210	6	7	38	13	8	31	16	28	51	50	35	37	46	31	19	10	11	13	17	13	14	29	15	14	552	Jul	29	Monday
211	18	8	16	5	12	27	13	28	27	24	16	33	20	18	17	20	8	18	11	30	12	19	27	10	437	Jul	30	Tuesday
212	9	13	12	19	11	25	8	32	23	32	26	46	18	39	16	25	10	20	24	14	18	15	27	9	491	Jul	31	Wednesday
213	6	8	15	4	8	23	15	21	41	20	35	43	34	30	20	25	13	23	15	11	15	9	12	5	451	Aug	01	Thursday
214	8	15	5	11	14	10	12	41	51	36	66	33	37	34	33	28	38	34	22	29	19	32	14	8	630	Aug	02	Friday
215	12	11	6	9	12	14	3	46	37	29	36	42	28	18	22	27	8	7	15	12	9	11	15	11	440	Aug	03	Saturday
216	2	5	6	3	3	11	14	29	28	34	39	19	29	29	29	20	19	12	10	11	8	15	4	13	392	Aug	04	Sunday
217	7	11	24	6	22	23	17	28	49	49	35	40	35	29	30	21	5	21	20	20	5	21	14	1	533	Aug	05	Monday
218	8	3	16	4	2	20	14	22	39	41	39	29	26	33	27	31	21	17	26	18	26	21	27	16	526	Aug	06	Tuesday
219	4	8	10	18	19	22	33	37	35	30	38	43	59	51	30	39	25	26	17	5	13	13	21	6	602	Aug	07	Wednesday
220	5	12	28	5	9	40	26	27	43	37	35	62	22	40	26	24	29	24	21	14	41	22	21	8	621	Aug	08	Thursday
221	1	8	7	14	9	35	32	44	44	76	18	24	52	59	39	32	32	17	31	15	11	24	23	8	655	Aug	09	Friday
222	6	12	0	11	12	14	10	10	23	42	31	31	18	26	35	14	20	11	50	17	10	17	11	6	437	Aug	10	Saturday
223	6	5	1	6	13	20	2	13	9	12	23	25	8	9	26	20	2	9	7	18	9	16	4	2	265	Aug	11	Sunday
224	8	6	3	13	16	29	10	20	44	32	17	34	34	25	27	18	6	5	15	14	7	11	15	8	417	Aug	12	Monday
225	9	14	16	21	1	15	7	23	38	28	41	26	47	25	17	32	20	17	22	23	40	31	27	19	559	Aug	13	Tuesday
226	2	12	5	18	8	26	3	0	31	0	0	8	35	43	49	32	24	21	14	22	5	10	23	17	408	Aug	14	Wednesday
227	15	5	3	22	25	17	11	15	39	15	17	37	47	39	29	23	15	28	18	28	17	16	40	9	530	Aug	15	Thursday
228	6	6	0	0	0	0	0	0	0	0	0	0	0	0	0	0	0	0	0	0	0	0	0	0	12	Aug	16	Friday
229	0	0	0	0	0	0	0	0	0	0	0	0	0	0	3	18	17	6	17	16	22	13	19	8	139	Aug	17	Saturday
230	2	3	4	6	11	17	15	13	13	16	20	18	32	16	15	14	0	19	22	11	6	8	8	11	300	Aug	18	Sunday
231	13	1	10	12	17	34	12	12	28	46	30	21	27	24	22	25	4	25	14	10	14	8	18	13	440	Aug	19	Monday
232	2	2	8	3	14	20	15	47	23	49	19	25	16	19	16	24	3	21	26	23	40	16	18	2	451	Aug	20	Tuesday
233	3	17	9	10	8	30	7	32	35	29	38	37	40	60	48	17	12	13	14	28	5	21	16	11	540	Aug	21	Wednesday
234	19	7	2	6	16	17	14	22	14	25	13	27	31	34	23	29	39	29	21	19	8	20	9	8	452	Aug	22	Thursday
235	4	5	21	3	13	17	18	42	26	41	38	27	40	25	18	12	32	28	20	23	8	8	11	6	486	Aug	23	Friday
236	6	3	1	4	3	15	3	13	10	39	29	34	23	11	10	11	19	13	19	12	7	2	29	5	321	Aug	24	Saturday
237	9	2	2	7	10	17	9	7	15	7	17	8	16	17	7	10	12	12	6	27	12	15	16	15	275	Aug	25	Sunday
238	4	5	10	6	13	23	19	48	44	26	47	39	38	25	20	16	24	7	27	0	20	30	23	7	521	Aug	26	Monday
239	6	5	4	21	2	14	8	17	24	34	15	9	48	21	17	14	18	10	13	13	7	14	22	9	365	Aug	27	Tuesday
240	3	10	2	3	4	19	11	17	23	50	54	20	44	29	22	30	2	28	23	15	5	16	36	11	477	Aug	28	Wednesday
241	9	23	7	9	27	29	18	55	75	51	92	111	46	34	18	12	18	13	11	10	8	19	13	9	717	Aug	29	Thursday
242	3	11	9	10	3	22	21	52	18	27	32	8	25	19	2	10	2	9	8	4	12	3	11	4	325	Aug	30	Friday
243	6	5	7	8	4	12	13	19	22	17	35	19	16	10	25	11	27	3	15	7	9	12	11	14	327	Aug	31	Saturday
244	4	16	5	10	3	8	14	16	12	3	26	28	18	21	13	13	25	22	45	14	18	19	19	7	379	Sep	01	Sunday
245	4	2	15	5	21	19	55	45	45	39	112	74	24	16	8	13	9	14	16	12	16	13	27	11	615	Sep	02	Monday
246	10	11	17	8	3	55	39	64	38	31	31	31	25	21	29	37	15	20	26	19	5	26	29	11	601	Sep	03	Tuesday
247	7	11	15	17	20	21	28	29	26	22	25	19	36	20	19	19	6	37	19	5	8	10	17	8	444	Sep	04	Wednesday
248	8	9	9	3	13	84	37	61	31	24	33	27	40	11	18	31	14	6	29	6	5	9	17	2	527	Sep	05	Thursday
249	11	6	3	2	3	12	11	31	31	23	14	20	36	16	25	19	22	32	28	25	27	25	21	19	462	Sep	06	Friday
250	13	24	15	15	14	14	12	15	12	15	23	12	7	19	28	12	15	9	2	7	9	5	14	1	312	Sep	07	Saturday
251	0	7	6	3	6	8	8	11	2	17	8	2	21	17	23	13	17	23	28	24	5	10	17	1	277	Sep	08	Sunday
252	7	8	9	20	15	24	23	27	15	24	14	8	13	21	26	32	14	24	24	9	18	13	23	5	416	Sep	09	Monday
253	4	4	3	8	25	23	3	14	12	19	31	42	4	36	36	13	15	7	29	13	9	27	18	4	399	Sep	10	Tuesday
254	5	9	8	13	7	23	11	3	21	34	27	33	29	28	26	21	20	14	15	11	7	12	15	11	403	Sep	11	Wednesday
255	18	8	4	13	12	19	13	13	35	16	17	20	11	27	47	45	10	7	16	14	11	19	14	5	414	Sep	12	Thursday
256	8	6	8	15	14	19	16	30	20	35	35	33	40	27	15	20	19	9	9	7	12	19	18	3	437	Sep	13	Friday
257	3	4	8	7	7	14	10	26	28	26	25	22	3	17	15	7	5	10	20	14	4	20	13	5	313	Sep	14	Saturday
258	9	5	10	4	14	11	6	9	16	5	5	11	15	16	0	0	0	0	0	0	7	7	13	7	170	Sep	15	Sunday

Table 3.4.2 (Page 3 of 4)

ARC .FKX Hourly distribution of detections

Day	00	01	02	03	04	05	06	07	08	09	10	11	12	13	14	15	16	17	18	19	20	21	22	23	Sum	Date
259	7	1	8	28	16	23	6	13	45	37	35	32	31	18	27	16	11	8	13	8	6	22	16	6	433	Sep 16 Monday
260	7	2	20	6	8	22	10	28	24	29	29	25	8	30	33	24	9	11	12	21	14	13	17	30	432	Sep 17 Tuesday
261	14	12	10	6	10	42	5	23	24	27	24	28	46	22	11	23	24	19	6	10	1	22	11	6	426	Sep 18 Wednesday
262	2	16	17	7	10	19	5	30	25	19	18	29	32	35	34	46	25	17	7	12	3	14	13	5	440	Sep 19 Thursday
263	13	15	7	4	10	23	23	24	17	27	25	20	34	29	20	20	14	11	18	8	28	4	26	9	429	Sep 20 Friday
264	20	5	3	2	15	26	7	21	23	21	28	50	15	13	8	23	18	9	13	15	10	11	14	4	374	Sep 21 Saturday
265	9	2	13	5	1	19	7	1	9	16	19	12	9	33	6	7	9	20	9	22	24	6	24	12	294	Sep 22 Sunday
266	3	5	11	17	12	21	11	29	24	32	23	7	25	50	3	25	25	16	8	15	19	2	20	7	410	Sep 23 Monday
267	6	6	2	11	5	18	9	29	16	27	15	22	22	36	27	18	12	42	33	13	13	14	34	3	433	Sep 24 Tuesday
268	16	2	4	3	5	34	6	22	44	38	33	34	35	26	31	19	24	27	28	7	19	13	11	7	488	Sep 25 Wednesday
269	8	8	4	19	4	23	13	10	18	23	15	28	30	45	25	11	7	7	12	7	19	6	20	13	375	Sep 26 Thursday
270	16	4	5	5	15	26	16	24	27	22	35	32	21	21	26	18	9	7	22	26	7	7	29	12	432	Sep 27 Friday
271	14	1	2	12	10	21	13	13	26	38	26	28	21	24	15	8	9	42	16	28	16	16	27	5	431	Sep 28 Saturday
272	11	3	7	2	6	2	8	14	32	9	6	4	24	24	9	22	3	20	10	19	5	38	17	18	313	Sep 29 Sunday
273	21	25	9	11	19	10	19	26	36	27	30	31	23	37	19	32	13	11	16	13	27	23	20	6	504	Sep 30 Monday
ARC	00	01	02	03	04	05	06	07	08	09	10	11	12	13	14	15	16	17	18	19	20	21	22	23		
Sum	2551	2481	2279	2333	3365	2032	3974	2810	4767	4767	4835	4555	4577	4763	3234	3630	3176	2942	3282	3655	3920	3561	2863	4439	84791	Total sum
183	14	14	13	12	11	18	15	22	26	26	25	26	26	25	20	18	16	17	20	18	19	21	24	16	463	Total average
126	13	14	13	13	11	20	16	25	29	29	27	29	30	29	22	20	18	19	21	18	20	22	25	16	500	Average workdays
57	14	14	11	11	11	15	13	15	20	20	20	21	17	17	14	12	11	13	17	17	18	21	23	16	379	Average weekends

Table 3.4.2. Daily and hourly distribution of ARCESS detections. For each day is shown number of detections within each hour of the day and number of detections for that day. The end statistics give total number of detections distributed for each hour and the total sum of detections during the period. The averages show number of processed days, hourly distribution and average per processed day.

FIN .FKX Hourly distribution of detections

Day	00	01	02	03	04	05	06	07	08	09	10	11	12	13	14	15	16	17	18	19	20	21	22	23	Sum	Date		
91	69	15	15	9	10	8	2	3	5	7	9	16	12	0	3	5	4	5	9	3	12	9	24	68	322	Apr 01	Monday	Annen
92	105	61	28	9	5	2	8	8	7	12	12	19	17	6	6	4	4	2	10	4	8	9	11	6	363	Apr 02	Tuesday	
93	2	5	3	5	6	3	7	5	7	13	17	19	16	6	14	7	8	10	11	5	10	15	6	4	204	Apr 03	Wednesday	
94	8	7	8	9	2	3	8	7	11	20	19	22	29	12	3	6	9	9	10	7	4	11	7	7	238	Apr 04	Thursday	
95	11	9	6	6	23	6	7	7	10	28	47	70	21	7	4	6	12	3	2	1	2	4	3	4	299	Apr 05	Friday	
96	2	1	5	4	2	10	7	6	2	7	3	8	4	3	4	1	4	1	2	2	3	3	5	3	92	Apr 06	Saturday	
97	2	1	1	1	1	8	3	6	15	17	20	13	9	7	3	0	8	2	7	5	4	9	7	7	156	Apr 07	Sunday	
98	9	12	4	8	8	2	8	5	12	12	14	15	22	16	7	8	10	6	6	7	8	13	8	5	225	Apr 08	Monday	
99	9	4	9	4	9	3	13	5	6	14	11	13	28	3	6	6	7	3	7	2	2	9	7	7	187	Apr 09	Tuesday	
100	9	11	9	9	7	1	5	7	14	12	16	28	30	15	7	8	8	4	1	5	5	11	2	9	233	Apr 10	Wednesday	
101	8	10	4	8	5	4	5	9	13	25	39	19	19	11	12	13	4	8	17	9	10	8	12	5	277	Apr 11	Thursday	
102	9	12	8	6	6	6	8	6	8	18	32	26	36	13	15	14	5	3	5	4	5	5	2	5	257	Apr 12	Friday	
103	6	11	7	2	6	8	5	18	32	25	22	13	28	19	12	7	6	2	5	7	2	7	5	5	260	Apr 13	Saturday	
104	5	5	2	5	6	3	7	6	8	20	8	23	26	19	19	8	11	4	6	7	11	8	9	12	238	Apr 14	Sunday	
105	14	5	12	5	3	1	9	8	17	6	19	12	24	9	5	7	8	6	9	7	5	2	3	3	199	Apr 15	Monday	
106	3	5	7	7	2	7	17	7	0	17	27	34	8	14	9	13	7	2	7	4	4	7	8	3	219	Apr 16	Tuesday	
107	3	13	13	2	9	4	10	2	23	14	10	19	29	11	5	8	8	9	10	5	5	3	7	5	227	Apr 17	Wednesday	
108	6	8	7	5	2	15	16	7	10	15	26	18	17	13	21	7	7	12	17	10	4	5	8	15	271	Apr 18	Thursday	
109	7	28	23	29	10	20	10	9	13	24	20	12	27	5	6	13	13	8	11	4	10	6	16	4	328	Apr 19	Friday	
110	13	13	17	11	5	3	7	9	31	47	43	37	44	40	23	44	14	21	22	9	8	12	12	18	503	Apr 20	Saturday	
111	25	25	38	40	32	18	20	4	5	7	7	14	5	12	9	4	1	6	11	11	8	17	10	8	337	Apr 21	Sunday	
112	14	21	12	12	4	10	13	7	14	17	21	22	16	7	2	5	1	9	11	7	9	8	24	13	279	Apr 22	Monday	
113	11	12	10	18	9	5	4	3	10	24	17	28	20	9	9	9	9	8	7	7	3	10	3	5	250	Apr 23	Tuesday	
114	14	5	14	6	3	14	4	9	10	16	24	16	19	12	8	6	7	5	8	9	6	2	12	11	240	Apr 24	Wednesday	
115	5	7	8	10	4	3	6	9	22	9	19	17	33	15	12	12	7	6	8	6	7	9	2	11	247	Apr 25	Thursday	
116	12	10	4	3	6	5	18	7	6	17	23	27	30	8	6	8	4	7	3	7	3	3	12	2	231	Apr 26	Friday	
117	5	7	4	4	6	2	4	15	14	23	22	39	22	0	12	11	15	9	11	8	12	4	7	0	256	Apr 27	Saturday	
118	5	5	3	5	6	11	5	8	11	13	4	10	17	14	10	12	8	5	12	10	2	9	9	11	205	Apr 28	Sunday	
119	8	7	5	4	0	1	7	9	19	42	31	30	18	27	16	15	12	12	21	19	19	11	11	12	356	Apr 29	Monday	
120	8	15	14	9	7	6	11	13	19	21	37	19	42	15	22	14	12	10	12	7	11	6	2	2	334	Apr 30	Tuesday	
121	9	12	5	16	18	31	15	32	42	51	38	32	35	23	26	40	5	15	6	8	13	4	12	12	500	May 01	Wednesday	Frste
122	6	26	13	12	4	1	8	6	3	12	15	7	10	9	10	8	6	7	9	7	8	10	5	5	207	May 02	Thursday	
123	9	0	0	0	0	0	13	13	16	6	20	5	5	10	5	11	12	9	5	12	10	5	3	14	183	May 03	Friday	
124	13	8	11	3	9	4	8	3	3	3	7	5	8	8	10	8	6	4	5	6	7	9	8	4	160	May 04	Saturday	
125	1	3	1	3	7	7	3	3	4	22	8	30	17	10	9	7	17	14	20	8	7	10	12	14	237	May 05	Sunday	
126	21	10	16	0	11	10	8	22	25	29	23	21	29	33	16	8	10	5	12	4	6	5	11	8	343	May 06	Monday	
127	11	5	6	6	2	2	5	14	11	9	12	18	18	12	2	3	6	8	19	8	6	7	6	3	199	May 07	Tuesday	
128	6	7	15	7	2	4	7	13	24	16	8	0	0	14	9	5	7	1	13	9	8	4	8	6	193	May 08	Wednesday	
129	10	12	10	5	6	20	25	37	48	39	26	37	14	16	14	6	7	7	9	7	7	8	11	6	387	May 09	Thursday	Kristi
130	5	17	10	8	9	6	28	27	17	15	13	19	16	12	12	2	7	7	2	4	9	5	4	8	262	May 10	Friday	
131	5	10	8	3	17	15	11	19	57	69	58	63	47	43	35	29	14	13	11	4	5	1	1	1	539	May 11	Saturday	
132	0	3	2	4	0	4	8	6	3	10	19	20	17	19	8	11	11	8	8	12	6	7	5	9	200	May 12	Sunday	
133	11	7	6	9	6	2	5	1	10	22	14	18	21	13	2	7	8	2	5	7	6	6	4	5	197	May 13	Monday	
134	12	8	7	8	0	4	4	10	9	16	20	18	17	7	12	4	6	2	3	12	5	8	5	2	199	May 14	Tuesday	
135	4	5	10	2	9	1	8	6	22	8	15	17	19	11	10	2	0	0	0	0	0	0	0	0	149	May 15	Wednesday	
136	0	0	0	0	0	0	0	0	0	0	0	0	0	0	0	0	0	0	0	0	0	0	0	0	0	May 16	Thursday	
137	0	0	0	0	0	0	0	1	14	51	22	0	0	43	0	0	0	0	0	0	0	0	0	0	131	May 17	Friday	Sytten
138	0	0	0	0	0	0	0	0	0	0	0	0	0	0	0	0	0	0	0	0	0	0	0	0	0	May 18	Saturday	
139	0	0	0	0	0	0	0	0	0	0	0	0	0	0	0	0	0	0	0	0	0	0	0	0	0	May 19	Sunday	Frste
140	0	0	0	0	0	0	0	0	0	0	23	32	47	32	9	13	17	12	3	7	5	8	5	1	214	May 20	Monday	Annen
141	3	10	3	4	1	3	12	2	20	18	20	31	27	30	24	19	5	12	8	3	7	7	3	4	276	May 21	Tuesday	
142	7	8	12	4	4	1	7	5	13	15	12	18	14	0	0	0	0	0	0	0	0	0	0	0	120	May 22	Wednesday	
143	0	0	0	0	0	0	0	0	0	0	5	19	26	22	12	18	7	6	9	15	9	12	7	8	175	May 23	Thursday	
144	11	19	10	5	10	7	19	14	20	31	26	38	19	11	8	11	13	10	12	4	5	13	3	2	321	May 24	Friday	
145	1	6	7	7	8	2	5	2	7	6	7	32	0	0	0	0	0	0	0	0	0	0	0	0	90	May 25	Saturday	
146	0	0	0	0	0	0	0	0	0	0	0	0	0	0	0	0	0	0	0	0	0	0	0	0	0	May 26	Sunday	

Table 3.4.3 (Page 1 of 4)

FIN .FKX Hourly distribution of detections

Day	00	01	02	03	04	05	06	07	08	09	10	11	12	13	14	15	16	17	18	19	20	21	22	23	Sum	Date
147	0	0	0	0	0	0	0	0	0	0	0	0	0	0	0	0	0	0	0	0	0	0	0	0	0	May 27 Monday
148	0	0	0	0	0	0	0	0	0	0	0	18	18	12	17	11	13	8	12	5	10	10	12	8	154	May 28 Tuesday
149	5	12	7	4	6	8	15	5	10	16	12	20	26	19	12	8	3	3	6	12	14	7	7	9	246	May 29 Wednesday
150	14	12	15	2	4	15	9	9	8	0	0	0	31	19	11	8	8	5	9	3	7	10	5	10	214	May 30 Thursday
151	8	16	5	7	0	6	10	23	15	23	26	35	34	26	17	6	8	3	15	5	12	7	5	2	314	May 31 Friday
152	10	5	13	14	13	20	12	21	11	13	16	7	9	15	5	10	3	3	6	5	0	0	2	1	214	Jun 01 Saturday
153	1	2	7	2	2	14	7	11	17	3	11	7	6	16	15	7	14	25	18	12	2	9	6	3	217	Jun 02 Sunday
154	7	6	17	6	2	7	15	0	0	0	0	0	0	24	26	5	13	19	5	7	12	10	16	4	201	Jun 03 Monday
155	4	13	5	9	9	1	6	19	13	11	19	15	18	13	19	15	16	16	21	10	10	13	18	14	307	Jun 04 Tuesday
156	12	12	21	8	11	26	14	21	11	18	26	24	40	27	36	12	22	18	13	17	6	11	15	16	437	Jun 05 Wednesday
157	7	14	14	7	16	13	20	11	17	12	21	22	31	10	14	16	11	17	31	3	18	6	13	10	354	Jun 06 Thursday
158	6	9	14	7	1	17	19	12	13	16	17	29	25	3	7	6	24	19	9	5	11	4	5	9	287	Jun 07 Friday
159	5	2	6	0	0	0	0	4	4	4	10	8	5	13	8	7	5	6	1	0	6	4	4	4	106	Jun 08 Saturday
160	3	10	11	5	8	9	13	18	36	2	4	10	6	5	5	4	8	5	5	7	17	9	4	7	211	Jun 09 Sunday
161	6	12	10	6	5	2	18	18	10	4	0	0	0	0	0	0	0	0	0	0	0	0	0	0	91	Jun 10 Monday
162	0	0	0	0	0	0	0	0	0	0	0	0	0	0	0	0	0	0	0	0	0	0	0	0	0	Jun 11 Tuesday
163	0	0	0	0	0	0	0	0	0	0	0	0	0	0	0	0	0	0	0	0	0	0	0	0	0	Jun 12 Wednesday
164	0	0	0	0	0	0	0	0	0	0	0	0	0	0	0	0	0	0	0	0	0	0	0	0	0	Jun 13 Thursday
165	0	0	0	0	0	0	0	0	0	0	0	0	0	0	0	0	0	0	0	0	0	0	0	0	0	Jun 14 Friday
166	0	0	0	0	0	0	0	0	0	0	0	0	0	0	0	0	0	0	0	0	0	0	0	0	0	Jun 15 Saturday
167	0	0	0	0	0	0	0	0	0	0	0	0	0	0	0	0	0	0	0	0	0	0	0	0	0	Jun 16 Sunday
168	0	0	0	0	0	0	0	0	0	0	0	0	0	0	0	0	0	0	0	0	0	0	0	0	0	Jun 17 Monday
169	0	0	0	0	0	0	0	0	0	0	0	0	0	0	0	0	0	0	0	0	0	0	0	0	0	Jun 18 Tuesday
170	0	0	0	0	0	0	0	0	0	0	0	0	0	0	0	0	0	0	0	0	0	0	0	0	0	Jun 19 Wednesday
171	0	0	0	0	0	0	0	0	0	0	0	0	0	0	0	0	0	0	0	0	0	0	0	0	0	Jun 20 Thursday
172	0	0	0	0	0	0	0	0	0	0	0	0	0	0	0	0	0	0	0	0	0	0	0	0	0	Jun 21 Friday
173	0	0	0	0	0	0	0	0	0	0	0	0	0	0	0	0	0	0	0	0	0	0	0	0	0	Jun 22 Saturday
174	0	0	0	0	0	0	0	0	0	0	0	0	0	0	0	0	0	0	0	0	0	0	0	0	0	Jun 23 Sunday
175	0	0	0	0	0	0	0	0	0	0	0	0	0	0	0	0	0	0	0	0	0	0	0	0	0	Jun 24 Monday
176	0	0	0	0	0	0	0	0	0	0	0	0	0	0	0	0	0	0	0	0	0	0	0	0	0	Jun 25 Tuesday
177	0	0	0	0	0	0	0	0	7	19	32	30	21	33	14	20	22	16	13	11	9	6	11	15	279	Jun 26 Wednesday
178	6	5	16	2	4	4	13	12	24	34	33	25	36	26	24	28	17	7	3	13	9	11	16	8	376	Jun 27 Thursday
179	10	7	7	8	6	6	5	12	12	18	25	28	34	21	18	20	20	14	34	30	33	43	17	70	498	Jun 28 Friday
180	0	0	0	0	0	0	0	0	0	0	0	0	0	0	0	0	0	0	0	0	0	0	0	0	0	Jun 29 Saturday
181	0	0	0	0	0	0	0	0	0	0	0	0	0	0	0	0	0	0	0	0	0	0	0	0	0	Jun 30 Sunday
182	0	0	0	0	0	0	0	0	0	0	0	0	0	0	0	0	0	0	0	0	0	0	0	0	0	Jul 01 Monday
183	0	0	0	0	0	0	0	0	0	0	0	0	0	0	0	0	0	0	0	0	0	0	0	0	0	Jul 02 Tuesday
184	0	0	0	0	0	0	0	0	0	0	0	0	0	0	0	0	0	0	0	0	0	0	0	0	0	Jul 03 Wednesday
185	0	0	0	0	0	0	0	0	0	0	0	0	0	0	0	0	0	0	0	0	0	0	0	0	0	Jul 04 Thursday
186	0	0	0	0	0	0	0	0	0	0	0	0	0	0	0	0	0	0	0	0	0	0	0	0	0	Jul 05 Friday
187	0	0	0	0	0	0	0	0	0	0	0	0	0	0	0	0	0	0	0	0	0	0	0	0	0	Jul 06 Saturday
188	0	0	0	0	0	0	0	0	0	0	0	0	0	0	0	0	0	0	0	0	0	0	0	0	0	Jul 07 Sunday
189	0	0	0	0	0	0	0	0	0	0	0	0	0	0	0	0	0	0	0	0	0	0	0	0	0	Jul 08 Monday
190	0	0	0	0	0	0	0	0	0	0	0	0	0	0	0	0	0	0	0	0	0	0	0	0	0	Jul 09 Tuesday
191	0	0	0	0	0	0	0	0	0	0	0	0	0	0	0	0	0	0	0	0	0	0	0	0	0	Jul 10 Wednesday
192	0	0	0	0	0	0	0	0	0	0	0	0	0	0	0	0	0	0	0	0	0	0	0	0	0	Jul 11 Thursday
193	0	0	0	0	0	0	0	0	0	0	0	0	0	0	0	0	0	0	0	0	0	0	0	0	0	Jul 12 Friday
194	0	0	0	0	0	0	0	0	0	0	0	0	0	0	0	0	0	0	0	0	0	0	0	0	0	Jul 13 Saturday
195	0	0	0	0	0	0	0	0	0	0	0	0	0	0	0	0	0	0	0	0	0	0	0	0	0	Jul 14 Sunday
196	0	0	0	0	0	0	0	0	0	0	0	0	0	0	0	0	0	0	0	0	0	0	0	0	0	Jul 15 Monday
197	0	0	0	0	0	0	0	0	0	0	0	0	0	0	0	0	0	0	0	0	0	0	0	0	0	Jul 16 Tuesday
198	0	0	0	0	0	0	0	0	0	0	0	0	0	0	0	0	0	0	0	0	0	0	0	0	0	Jul 17 Wednesday
199	0	0	0	0	0	0	0	0	0	0	0	0	0	0	0	0	0	0	0	0	0	0	0	0	0	Jul 18 Thursday
200	0	0	0	0	0	0	0	0	0	0	0	0	0	0	0	0	0	0	0	0	0	0	0	0	0	Jul 19 Friday
201	0	0	0	0	0	0	0	0	0	0	0	0	0	0	0	0	0	0	0	0	0	0	0	0	0	Jul 20 Saturday
202	0	0	0	0	0	0	0	0	0	0	0	0	0	0	0	0	0	0	0	0	0	0	0	0	0	Jul 21 Sunday

Table 3.4.3 (Page 2 of 4)

FIN .FKX Hourly distribution of detections

Day	00	01	02	03	04	05	06	07	08	09	10	11	12	13	14	15	16	17	18	19	20	21	22	23	Sum	Date
203	0	0	0	0	0	0	0	0	0	0	41	14	0	0	0	0	0	0	0	0	0	0	0	0	55	Jul 22 Monday
204	9	13	14	5	2	8	3	9	8	18	26	11	28	21	12	7	3	6	7	5	8	12	7	13	255	Jul 23 Tuesday
205	10	2	7	9	2	1	6	3	14	19	18	20	20	24	15	15	12	9	7	10	9	6	4	6	248	Jul 24 Wednesday
206	6	1	9	1	3	1	4	7	15	18	12	16	12	106	55	70	7	4	4	6	9	32	21	5	424	Jul 25 Thursday
207	9	9	5	4	2	7	2	7	18	24	22	12	23	5	11	6	10	3	9	13	4	2	1	2	210	Jul 26 Friday
208	6	1	9	1	6	12	4	2	4	11	11	7	7	6	10	3	5	2	5	1	5	6	1	3	128	Jul 27 Saturday
209	8	3	6	4	4	4	7	6	11	2	11	12	5	1	1	4	6	9	6	7	15	11	6	7	156	Jul 28 Sunday
210	10	16	13	5	10	2	1	7	4	9	22	0	0	0	4	8	9	12	10	7	8	7	10	14	188	Jul 29 Monday
211	5	11	5	10	7	6	2	5	6	14	25	31	29	14	24	13	23	17	8	11	13	5	6	7	297	Jul 30 Tuesday
212	3	8	8	4	0	15	26	5	17	13	19	20	19	12	9	11	8	6	16	7	5	19	6	11	267	Jul 31 Wednesday
213	7	1	10	19	5	12	2	19	22	16	12	11	13	16	10	6	13	3	13	16	28	6	8	7	275	Aug 01 Thursday
214	11	4	11	7	11	23	24	20	32	23	33	16	13	4	3	13	9	9	4	15	7	5	7	11	315	Aug 02 Friday
215	4	7	5	10	7	7	7	6	7	19	3	23	13	31	26	26	3	0	0	0	0	0	0	0	204	Aug 03 Saturday
216	0	0	0	0	0	0	0	0	0	0	0	0	0	0	0	0	0	0	0	0	0	0	0	0	0	Aug 04 Sunday
217	0	0	0	0	0	0	0	0	0	0	0	0	36	10	0	0	0	0	0	0	0	0	0	0	46	Aug 05 Monday
218	0	0	0	0	0	0	9	9	20	41	62	47	46	43	27	14	8	6	5	7	7	14	15	12	392	Aug 06 Tuesday
219	8	9	9	6	11	14	5	9	18	42	66	13	20	15	14	8	6	5	5	7	12	13	13	14	342	Aug 07 Wednesday
220	9	3	15	10	9	9	5	7	12	14	12	28	19	16	16	5	9	5	9	6	15	16	27	15	291	Aug 08 Thursday
221	10	11	16	6	4	0	0	0	0	2	8	15	21	26	10	3	8	5	11	6	11	18	10	0	201	Aug 09 Friday
222	0	0	0	0	0	0	0	0	0	0	0	0	0	0	0	0	0	0	0	0	0	0	0	0	0	Aug 10 Saturday
223	0	0	0	0	0	0	0	0	0	0	0	0	0	0	0	0	0	0	0	0	0	0	0	0	0	Aug 11 Sunday
224	0	0	0	0	0	0	0	0	0	0	0	0	0	0	0	0	0	0	0	0	0	0	0	0	0	Aug 12 Monday
225	0	0	0	0	0	0	0	0	0	0	0	0	0	0	0	0	0	0	0	0	0	0	0	0	0	Aug 13 Tuesday
226	0	0	0	0	0	0	0	0	0	0	0	0	0	0	0	0	0	0	0	0	0	0	0	0	0	Aug 14 Wednesday
227	0	0	0	0	0	0	0	0	0	0	0	0	0	0	0	0	0	0	0	0	0	0	0	0	0	Aug 15 Thursday
228	0	0	0	0	0	0	0	0	0	0	0	0	0	0	0	0	0	0	0	0	0	0	0	0	0	Aug 16 Friday
229	0	0	0	0	0	0	0	0	0	0	0	0	0	0	0	0	0	0	0	0	0	0	0	0	0	Aug 17 Saturday
230	0	0	0	0	0	0	0	0	0	0	0	0	0	0	0	0	0	0	0	0	0	0	0	0	0	Aug 18 Sunday
231	0	0	0	0	0	0	0	0	0	0	0	0	0	0	0	0	0	0	0	0	0	0	0	0	0	Aug 19 Monday
232	0	0	0	0	0	0	0	0	0	0	0	0	0	0	0	0	0	0	0	0	0	0	0	0	0	Aug 20 Tuesday
233	0	0	0	0	0	0	0	0	0	0	0	0	0	0	0	0	0	0	0	0	0	0	0	0	0	Aug 21 Wednesday
234	0	0	0	0	0	0	0	0	0	0	0	0	37	25	7	8	11	20	14	18	8	15	9	18	190	Aug 22 Thursday
235	12	10	15	13	57	34	10	30	17	22	21	23	9	9	10	3	12	8	13	14	5	13	12	3	375	Aug 23 Friday
236	12	14	3	1	8	19	11	13	20	16	23	21	9	11	15	15	15	10	5	24	7	1	7	3	283	Aug 24 Saturday
237	3	2	3	6	1	10	9	21	13	16	13	18	8	8	14	15	9	16	13	18	18	23	25	15	297	Aug 25 Sunday
238	20	19	23	20	4	9	13	6	13	13	18	21	9	18	12	12	7	11	8	10	13	20	12	15	326	Aug 26 Monday
239	11	16	8	4	13	8	13	18	22	31	22	33	34	25	17	12	7	9	7	5	7	18	16	19	375	Aug 27 Tuesday
240	15	23	18	28	19	19	25	26	21	33	28	50	37	23	11	9	15	5	13	5	12	21	19	16	491	Aug 28 Wednesday
241	6	7	14	9	26	30	24	25	35	18	18	27	15	12	12	15	10	15	10	13	18	15	11	12	397	Aug 29 Thursday
242	12	17	25	6	5	9	7	13	20	19	18	17	28	18	14	8	11	10	5	13	4	3	9	4	295	Aug 30 Friday
243	1	4	4	6	14	24	41	43	27	24	16	17	17	21	11	11	12	6	9	4	7	5	7	10	341	Aug 31 Saturday
244	4	17	21	11	10	13	16	15	19	9	16	21	14	17	11	9	12	9	12	13	14	15	21	14	333	Sep 01 Sunday
245	6	12	10	14	5	5	9	11	5	23	19	23	45	34	12	17	8	6	12	13	11	16	25	17	358	Sep 02 Monday
246	5	13	23	17	14	7	6	14	36	42	28	48	37	24	22	18	18	14	28	41	29	25	12	18	539	Sep 03 Tuesday
247	50	40	23	12	22	16	30	27	26	31	22	35	24	26	15	20	11	6	6	14	26	17	11	17	527	Sep 04 Wednesday
248	11	7	42	58	12	26	29	8	10	20	22	11	16	14	11	18	5	7	14	9	6	4	10	10	380	Sep 05 Thursday
249	14	9	8	8	3	6	7	8	13	24	12	14	18	28	19	8	11	10	7	9	10	9	21	13	289	Sep 06 Friday
250	14	11	8	15	9	9	7	8	8	6	10	9	13	21	25	22	10	6	9	17	13	16	7	10	283	Sep 07 Saturday
251	15	9	8	5	8	5	6	18	23	20	33	29	21	18	21	7	7	10	14	7	14	15	8	5	326	Sep 08 Sunday
252	6	11	17	5	6	6	8	9	13	12	17	18	16	8	18	8	6	5	11	5	7	12	10	11	245	Sep 09 Monday
253	9	4	4	8	5	4	8	10	3	20	37	32	10	9	6	11	10	6	8	12	13	10	16	21	276	Sep 10 Tuesday
254	14	13	19	16	4	5	6	15	14	32	21	48	26	28	45	8	30	12	15	13	10	12	11	10	427	Sep 11 Wednesday
255	17	12	13	17	17	5	11	16	23	5	3	1	10	1	9	32	6	8	5	10	7	5	8	15	256	Sep 12 Thursday
256	9	10	20	4	7	3	4	0	0	11	26	27	22	20	33	34	31	12	17	11	26	14	8	8	357	Sep 13 Friday
257	2	13	7	8	7	9	12	10	5	9	5	9	8	10	10	7	4	4	15	15	14	11	10	5	209	Sep 14 Saturday
258	5	10	21	5	4	21	33	15	5	13	16	19	29	21	22	16	34	28	27	36	39	27	8	9	463	Sep 15 Sunday

Table 3.4.3 (Page 3 of 4)

FIN .FKX Hourly distribution of detections

Day	00	01	02	03	04	05	06	07	08	09	10	11	12	13	14	15	16	17	18	19	20	21	22	23	Sum	Date
259	13	10	14	8	5	11	10	7	18	16	15	28	27	25	9	17	2	7	12	7	7	19	14	8	309	Sep 16 Monday
260	11	11	23	7	7	4	3	4	5	15	25	23	13	10	9	11	7	2	5	2	15	6	14	9	241	Sep 17 Tuesday
261	8	6	12	4	0	5	2	7	12	11	28	20	24	15	10	9	3	5	3	6	3	11	10	17	231	Sep 18 Wednesday
262	7	11	19	4	7	3	2	8	9	24	9	16	17	7	14	3	10	4	6	4	3	11	1	3	202	Sep 19 Thursday
263	7	2	4	5	6	0	1	9	8	13	24	17	17	7	3	4	9	13	6	2	7	10	7	5	186	Sep 20 Friday
264	7	4	34	5	1	0	6	7	12	6	10	17	14	30	9	20	11	8	3	7	5	10	8	22	256	Sep 21 Saturday
265	10	4	23	11	2	13	23	8	19	10	16	9	2	2	10	5	8	40	38	31	11	18	37	33	383	Sep 22 Sunday
266	18	8	14	11	5	10	13	15	13	14	22	11	12	12	9	12	5	11	7	12	14	15	5	7	275	Sep 23 Monday
267	10	10	11	10	3	9	5	10	13	10	22	17	10	22	7	7	5	25	14	6	6	5	15	9	261	Sep 24 Tuesday
268	15	9	16	14	7	6	3	12	16	16	14	19	27	20	18	9	5	10	12	7	8	10	10	5	288	Sep 25 Wednesday
269	8	11	4	8	1	12	2	13	12	14	26	27	25	14	4	7	14	17	12	11	13	9	14	8	286	Sep 26 Thursday
270	8	6	16	11	13	10	12	9	12	18	20	15	23	21	13	16	15	12	13	18	15	14	8	28	346	Sep 27 Friday
271	27	22	23	37	19	23	33	24	26	35	18	13	13	4	3	4	0	1	0	1	8	1	2	1	338	Sep 28 Saturday
272	0	3	2	4	7	3	2	6	5	8	4	2	3	2	1	2	6	4	7	12	10	11	5	5	114	Sep 29 Sunday
273	14	15	8	6	5	7	3	3	6	8	16	22	12	14	1	8	8	2	7	4	7	5	7	6	194	Sep 30 Monday
FIN	00	01	02	03	04	05	06	07	08	09	10	11	12	13	14	15	16	17	18	19	20	21	22	23		
Sum	1221	1211	1355	1002	876	1021	1216	1320	1761	2181	2443	2565	2515	2037	1560	1383	1179	1055	1219	1101	1152	1214	1159	1179	34925	Total sum
127	10	10	11	8	7	8	10	10	14	17	19	20	20	16	12	11	9	8	10	9	9	10	9	9	275	Total average
90	10	10	11	8	7	7	9	10	13	17	20	21	22	16	12	11	9	8	10	8	9	10	9	9	275	Average workdays
37	8	8	9	7	7	10	10	12	15	17	16	18	15	15	12	11	9	9	9	9	9	9	8	9	262	Average weekends

Table 3.4.3. Daily and hourly distribution of FINESA detections. For each day is shown number of detections within each hour of the day and number of detections for that day. The end statistics give total number of detections distributed for each hour and the total sum of detections during the period. The averages show number of processed days, hourly distribution and average per processed day.

GER .FKX Hourly distribution of detections

Day	00	01	02	03	04	05	06	07	08	09	10	11	12	13	14	15	16	17	18	19	20	21	22	23	Sum	Date		
91	0	5	14	5	8	11	4	5	7	11	16	17	7	10	10	9	3	4	7	7	6	3	11	10	190	Apr 01	Monday	Annen
92	4	9	3	8	1	1	6	10	8	17	13	13	4	7	3	12	0	4	8	1	5	3	3	2	145	Apr 02	Tuesday	
93	2	7	10	9	4	2	2	7	6	15	13	8	3	10	4	11	8	4	9	2	5	7	7	1	156	Apr 03	Wednesday	
94	1	7	10	14	6	5	3	2	7	20	11	14	12	8	14	11	5	2	5	10	12	7	2	4	192	Apr 04	Thursday	
95	4	1	4	1	11	8	1	7	8	17	19	15	6	2	3	5	8	5	3	8	3	1	1	0	141	Apr 05	Friday	
96	2	2	6	1	5	3	4	3	1	10	1	7	4	8	7	3	0	2	4	3	1	2	2	5	86	Apr 06	Saturday	
97	1	2	2	2	7	6	4	4	15	16	18	5	3	6	3	2	1	2	0	0	0	5	1	5	110	Apr 07	Sunday	
98	7	3	0	0	5	0	3	12	4	16	15	9	8	10	11	4	5	5	5	6	10	7	4	12	161	Apr 08	Monday	
99	6	9	7	5	4	0	0	0	0	0	25	8	3	8	7	7	5	4	4	5	5	3	7	13	135	Apr 09	Tuesday	
100	4	11	4	2	2	0	6	12	12	15	8	20	11	15	15	3	2	13	2	4	8	4	3	3	179	Apr 10	Wednesday	
101	8	10	5	3	1	0	10	17	19	7	36	12	8	30	26	24	11	10	7	9	4	8	20	9	294	Apr 11	Thursday	
102	11	4	3	3	3	0	1	10	14	14	6	20	6	9	12	6	6	10	12	9	2	7	11	7	186	Apr 12	Friday	
103	7	8	6	4	1	5	3	3	10	7	20	11	5	10	19	8	10	7	3	7	10	17	10	9	200	Apr 13	Saturday	
104	5	6	6	3	2	2	7	4	12	6	10	10	8	24	12	34	13	1	3	14	9	5	23	11	230	Apr 14	Sunday	
105	11	9	5	5	0	6	3	6	6	17	18	20	8	18	10	19	20	5	3	7	5	9	6	5	221	Apr 15	Monday	
106	5	0	0	0	5	0	1	8	8	13	17	16	15	8	6	12	8	10	4	6	5	5	6	3	161	Apr 16	Tuesday	
107	2	8	3	5	1	3	4	4	10	13	20	19	12	8	6	7	8	5	7	8	6	6	1	4	170	Apr 17	Wednesday	
108	6	5	3	5	5	4	7	4	7	2	0	4	18	11	10	10	12	8	13	19	11	47	8	3	222	Apr 18	Thursday	
109	5	4	0	5	5	2	3	16	3	21	12	6	13	6	5	7	3	3	7	6	6	11	8	4	161	Apr 19	Friday	
110	5	8	6	8	2	0	6	9	6	14	9	4	13	13	9	12	28	1	4	6	2	7	6	3	181	Apr 20	Saturday	
111	10	5	6	3	3	4	5	6	17	12	21	9	3	7	15	2	2	2	5	6	6	5	4	6	164	Apr 21	Sunday	
112	5	7	6	3	0	0	3	11	13	19	7	20	13	6	17	10	7	5	16	5	1	12	34	14	234	Apr 22	Monday	
113	3	6	11	9	2	4	8	14	8	9	17	10	6	5	10	9	15	4	11	18	8	6	4	1	198	Apr 23	Tuesday	
114	14	10	7	9	4	6	2	5	7	20	20	19	14	10	3	7	1	4	2	14	7	14	7	2	208	Apr 24	Wednesday	
115	8	7	8	1	5	3	9	11	13	10	14	21	11	4	8	11	3	4	5	3	10	5	6	5	185	Apr 25	Thursday	
116	7	3	11	8	1	4	10	6	7	15	12	24	10	2	11	7	2	7	4	6	6	6	14	12	195	Apr 26	Friday	
117	5	9	6	9	5	8	2	15	5	8	1	8	5	2	0	9	3	2	11	10	14	6	2	9	154	Apr 27	Saturday	
118	5	10	5	6	3	10	0	5	6	1	0	0	0	0	0	0	3	7	7	8	3	6	7	8	100	Apr 28	Sunday	
119	10	10	8	8	3	3	2	7	8	47	29	19	12	17	12	8	9	12	18	11	18	17	8	8	304	Apr 29	Monday	
120	6	4	8	12	0	2	5	22	10	10	15	20	13	7	11	16	5	6	10	6	5	6	2	9	210	Apr 30	Tuesday	
121	6	5	8	13	10	5	1	12	3	6	6	7	4	4	8	10	2	7	5	2	7	6	4	9	150	May 01	Wednesday	Frste
122	8	12	16	3	1	5	3	7	12	13	14	20	9	3	3	8	8	11	11	4	1	2	17	10	201	May 02	Thursday	
123	4	11	16	8	5	6	7	10	13	9	14	16	13	11	4	8	4	5	8	7	21	10	13	19	242	May 03	Friday	
124	11	8	9	7	10	10	4	5	6	14	21	9	7	8	10	4	4	3	5	4	6	11	5	8	189	May 04	Saturday	
125	16	5	6	3	10	16	9	5	7	4	0	3	5	9	11	3	5	8	3	6	3	0	8	4	149	May 05	Sunday	
126	14	7	2	4	1	2	8	11	21	16	22	17	17	8	12	11	6	0	6	1	8	4	6	11	215	May 06	Monday	
127	6	8	1	12	5	1	4	25	13	17	20	19	24	18	4	5	7	3	3	5	4	2	5	2	213	May 07	Tuesday	
128	2	1	11	12	3	4	4	19	6	33	18	21	20	18	3	13	4	2	3	0	2	5	0	4	208	May 08	Wednesday	
129	0	6	0	4	0	1	0	4	1	4	2	4	4	6	14	0	6	6	7	5	2	1	3	3	83	May 09	Thursday	Kristi
130	4	9	1	3	2	9	2	10	8	16	10	21	19	14	2	6	7	6	12	3	16	5	2	6	193	May 10	Friday	
131	2	0	6	8	3	8	9	13	16	6	14	6	6	2	8	4	2	5	7	3	2	1	0	2	133	May 11	Saturday	
132	0	0	6	4	1	0	3	2	12	4	12	4	7	8	1	2	7	2	2	0	4	0	2	6	89	May 12	Sunday	
133	1	5	1	17	8	5	0	0	10	14	19	19	8	7	7	13	6	0	2	7	6	5	25	22	207	May 13	Monday	
134	24	27	18	7	17	42	1	0	0	0	0	0	0	0	0	0	0	0	0	0	0	0	0	0	136	May 14	Tuesday	
135	0	0	0	0	0	0	0	0	0	0	0	0	0	0	0	0	0	0	0	0	0	0	0	0	0	May 15	Wednesday	
136	0	0	0	0	0	0	0	5	9	10	24	16	5	10	11	12	14	5	1	4	0	1	1	4	132	May 16	Thursday	
137	2	0	6	5	0	0	15	13	16	15	10	18	10	7	9	9	10	9	1	3	5	5	3	3	174	May 17	Friday	Sytten
138	3	9	8	6	16	19	15	22	14	20	7	19	15	5	9	6	2	6	0	6	1	3	3	1	215	May 18	Saturday	
139	1	8	1	4	1	3	2	8	6	5	4	2	12	12	4	8	6	3	4	2	2	0	4	2	104	May 19	Sunday	Frste
140	4	0	1	0	2	1	8	7	15	11	13	25	9	9	17	11	12	8	5	5	2	6	0	10	181	May 20	Monday	Annen
141	2	5	3	6	4	14	6	28	16	18	8	30	8	14	10	5	5	6	2	2	0	4	1	11	208	May 21	Tuesday	
142	1	3	7	4	2	5	5	19	19	37	19	22	17	19	23	28	16	2	5	1	3	7	6	3	273	May 22	Wednesday	
143	3	2	1	5	0	12	8	25	14	28	28	30	18	23	20	13	8	13	7	10	1	1	2	0	272	May 23	Thursday	
144	4	0	5	5	2	3	9	15	11	23	20	20	12	9	1	5	7	0	5	2	2	14	1	2	177	May 24	Friday	
145	1	5	0	7	0	4	6	13	12	15	23	31	16	4	0	1	3	2	7	1	2	2	15	4	174	May 25	Saturday	
146	3	0	6	34	16	41	30	112	116	2	5	15	7	33	1	6	12	4	5	1	0	0	5	2	2	665	May 26	Sunday

Table 3.4.4 (Page 1 of 4)

GER .FKX Hourly distribution of detections

Day	00	01	02	03	04	05	06	07	08	09	10	11	12	13	14	15	16	17	18	19	20	21	22	23	Sum	Date
147	2	3	0	5	2	0	10	14	5	18	33	12	13	6	14	9	3	3	8	6	3	2	1	6	178	May 27 Monday
148	4	0	6	7	0	6	15	13	15	26	38	24	14	9	10	1	5	1	6	7	0	4	5	0	216	May 28 Tuesday
149	5	10	2	2	0	1	9	17	12	27	19	18	8	13	17	6	1	2	2	5	14	0	1	3	194	May 29 Wednesday
150	9	2	0	0	0	0	3	15	12	22	18	17	5	11	5	7	5	1	2	5	2	6	14	2	163	May 30 Thursday
151	6	5	7	1	2	8	7	6	17	15	20	13	9	12	14	5	2	3	4	0	3	1	6	0	166	May 31 Friday
152	3	3	4	0	2	6	4	13	13	14	9	19	12	8	10	5	5	5	3	1	1	2	0	7	149	Jun 01 Saturday
153	1	0	5	6	2	2	0	4	2	3	5	7	2	8	6	5	5	3	3	6	2	25	45	25	172	Jun 02 Sunday
154	85	39	5	7	28	37	14	19	1	10	25	26	21	7	21	15	6	6	2	6	6	3	1	7	397	Jun 03 Monday
155	3	3	4	2	1	1	5	14	9	12	18	28	13	16	11	8	4	6	0	4	6	1	6	3	178	Jun 04 Tuesday
156	4	6	6	3	7	4	10	9	7	9	9	25	21	15	12	17	4	2	5	0	6	4	3	0	188	Jun 05 Wednesday
157	3	1	8	2	0	2	6	17	16	35	30	16	15	9	13	12	5	2	6	4	8	6	6	2	224	Jun 06 Thursday
158	2	2	0	2	0	0	4	0	0	0	0	0	0	3	16	10	8	4	5	2	7	2	9	0	76	Jun 07 Friday
159	3	2	5	3	0	2	4	9	12	12	30	6	36	18	23	9	1	4	5	3	4	2	3	4	200	Jun 08 Saturday
160	6	1	2	2	2	5	9	5	15	19	5	24	23	17	15	0	0	0	0	0	0	0	0	0	150	Jun 09 Sunday
161	0	0	0	0	0	0	0	0	11	20	15	12	12	0	0	0	0	0	0	0	0	0	0	0	70	Jun 10 Monday
162	0	0	0	0	0	0	0	0	0	0	0	0	0	0	0	0	0	0	0	0	0	0	0	0	0	Jun 11 Tuesday
163	0	0	0	0	0	0	0	0	0	0	0	0	0	0	0	0	0	0	0	0	0	0	0	0	0	Jun 12 Wednesday
164	0	0	0	0	0	0	0	3	5	23	41	20	15	9	10	8	11	12	4	2	1	1	1	3	169	Jun 13 Thursday
165	3	5	12	1	7	3	9	6	7	13	14	17	18	9	9	5	6	2	3	6	4	1	3	0	163	Jun 14 Friday
166	3	19	8	8	5	4	10	6	7	9	23	18	16	14	20	10	6	11	8	2	14	8	2	5	236	Jun 15 Saturday
167	8	49	7	11	2	6	1	4	8	9	12	4	8	5	4	17	15	4	0	1	8	4	8	4	199	Jun 16 Sunday
168	5	0	3	4	3	3	4	10	7	15	10	19	17	5	11	4	1	5	0	4	0	12	3	7	152	Jun 17 Monday
169	7	9	9	8	2	5	3	5	6	19	10	23	7	9	13	9	4	4	12	0	3	1	8	6	182	Jun 18 Tuesday
170	2	0	2	5	0	6	6	11	18	19	13	37	19	9	2	11	10	3	0	5	10	3	3	7	201	Jun 19 Wednesday
171	0	8	1	1	1	8	0	6	10	51	11	35	22	10	6	8	5	0	0	0	0	0	0	0	183	Jun 20 Thursday
172	0	0	0	0	0	0	0	12	9	4	0	0	0	0	8	8	4	2	2	2	4	0	6	0	61	Jun 21 Friday
173	4	4	3	2	4	6	6	3	8	15	24	16	9	9	7	5	2	2	3	3	0	2	2	0	139	Jun 22 Saturday
174	3	2	1	2	3	3	0	1	5	3	14	13	9	20	2	6	4	0	2	1	1	18	9	11	133	Jun 23 Sunday
175	6	11	4	6	90	9	35	18	24	22	39	43	50	16	11	16	0	0	0	0	0	0	0	0	400	Jun 24 Monday
176	0	0	0	0	0	0	4	16	30	15	26	24	29	32	32	26	28	23	31	16	14	24	28	20	418	Jun 25 Tuesday
177	26	25	29	19	22	24	42	38	38	65	46	47	33	53	18	35	3	0	0	1	8	1	8	8	589	Jun 26 Wednesday
178	2	8	0	5	2	6	8	17	28	11	18	23	26	50	25	15	8	5	4	13	8	17	17	16	332	Jun 27 Thursday
179	23	11	23	26	27	30	31	33	18	25	38	22	25	35	14	18	25	10	8	1	2	5	4	5	459	Jun 28 Friday
180	6	4	2	18	6	9	9	18	24	27	14	31	19	22	25	6	7	4	3	5	1	1	6	1	268	Jun 29 Saturday
181	0	6	10	8	5	1	5	1	7	3	6	12	4	10	8	9	8	5	13	2	4	1	0	10	138	Jun 30 Sunday
182	5	1	5	2	2	4	15	14	24	30	33	37	23	25	22	13	2	7	1	0	1	1	3	4	274	Jul 01 Monday
183	1	7	4	5	11	4	16	18	8	23	24	27	23	20	15	7	4	2	5	1	4	9	1	6	245	Jul 02 Tuesday
184	5	3	4	4	4	7	9	19	11	32	16	33	5	15	10	6	4	10	3	2	5	4	1	5	217	Jul 03 Wednesday
185	5	8	6	2	5	5	16	9	18	17	21	11	7	12	19	0	1	14	2	6	7	2	3	4	200	Jul 04 Thursday
186	0	2	4	8	7	3	6	14	15	28	18	20	7	19	9	8	1	1	2	0	4	3	3	6	188	Jul 05 Friday
187	3	2	0	5	5	3	8	9	7	4	18	35	2	2	9	6	3	34	6	4	2	0	0	5	172	Jul 06 Saturday
188	2	5	1	4	5	1	5	4	0	4	11	44	4	8	4	1	1	5	1	2	1	0	1	8	122	Jul 07 Sunday
189	4	4	6	6	2	12	10	7	11	15	19	58	11	2	6	3	2	1	1	0	0	2	3	1	186	Jul 08 Monday
190	11	3	8	6	1	0	5	13	37	39	93	37	32	11	12	6	4	0	3	0	0	0	0	0	321	Jul 09 Tuesday
191	3	2	0	0	2	5	10	19	13	49	34	11	4	2	17	10	5	5	3	2	5	9	0	11	221	Jul 10 Wednesday
192	4	2	1	2	1	1	31	16	20	43	16	8	5	15	14	4	4	8	41	11	1	27	4	0	279	Jul 11 Thursday
193	2	4	3	8	2	5	13	16	14	17	11	0	7	2	10	10	6	2	1	8	2	8	3	0	154	Jul 12 Friday
194	31	61	176	135	71	18	11	30	42	50	86	68	56	52	40	10	5	55	44	6	1	1	3	0	1124	Jul 13 Saturday
195	4	7	4	4	0	2	1	2	24	18	7	13	13	11	23	7	21	3	5	2	14	7	1	2	195	Jul 14 Sunday
196	10	4	1	4	4	7	13	13	26	12	22	29	19	17	17	10	12	14	14	13	11	8	1	1	282	Jul 15 Monday
197	9	0	9	0	9	15	7	17	18	25	26	24	16	26	35	8	7	10	13	11	3	0	1	5	294	Jul 16 Tuesday
198	7	3	0	12	2	6	13	22	17	31	23	35	20	23	22	21	11	4	2	8	3	9	0	6	300	Jul 17 Wednesday
199	0	1	1	4	2	9	52	17	15	46	29	55	15	15	23	15	4	5	4	3	7	7	1	6	336	Jul 18 Thursday
200	12	14	15	5	3	8	10	23	10	6	20	29	5	13	3	11	9	6	2	6	1	4	4	4	223	Jul 19 Friday
201	2	3	0	6	0	7	0	0	6	3	16	11	10	17	2	4	0	2	3	3	1	5	2	0	103	Jul 20 Saturday
202	0	5	1	0	1	3	1	2	3	1	17	8	9	11	8	10	4	2	5	0	2	4	4	10	111	Jul 21 Sunday

Table 3.4.4 (Page 2 of 4)

GER .FKX Hourly distribution of detections

Day	00	01	02	03	04	05	06	07	08	09	10	11	12	13	14	15	16	17	18	19	20	21	22	23	Sum	Date
203	6	9	0	5	4	3	16	11	20	22	13	19	6	9	9	17	2	4	8	5	2	7	2	2	201	Jul 22 Monday
204	2	10	5	1	0	6	8	12	11	8	22	7	19	4	7	2	9	8	0	7	3	5	3	6	165	Jul 23 Tuesday
205	9	0	7	21	0	4	11	12	13	29	19	11	9	17	28	75	4	6	5	0	1	1	0	3	285	Jul 24 Wednesday
206	10	1	9	3	9	2	10	7	13	21	10	22	24	19	11	15	11	3	0	3	1	1	1	4	210	Jul 25 Thursday
207	3	1	2	1	0	4	8	19	8	48	17	18	6	4	12	8	6	0	1	2	0	1	0	6	175	Jul 26 Friday
208	2	3	0	3	0	2	1	3	1	2	6	17	3	1	9	3	4	0	2	1	0	2	0	2	67	Jul 27 Saturday
209	4	0	0	5	4	2	2	2	3	4	5	10	4	7	5	2	2	1	0	6	0	1	2	10	81	Jul 28 Sunday
210	5	2	4	1	0	1	8	12	7	25	16	21	12	3	11	9	3	2	6	1	4	5	0	1	159	Jul 29 Monday
211	1	2	1	2	4	3	1	13	2	16	20	11	17	10	2	7	8	2	1	6	0	3	9	0	141	Jul 30 Tuesday
212	5	0	3	3	5	6	9	19	17	0	0	0	0	0	0	0	0	0	0	0	0	0	0	0	67	Jul 31 Wednesday
213	0	0	0	0	0	0	0	0	0	0	0	0	0	0	0	0	0	0	0	0	0	0	0	0	0	Aug 01 Thursday
214	0	0	0	0	0	0	0	0	0	0	0	0	0	0	0	0	0	0	0	0	0	0	0	0	0	Aug 02 Friday
215	0	0	0	0	0	0	0	0	0	0	0	0	0	0	0	0	0	2	2	6	0	0	2	1	13	Aug 03 Saturday
216	0	3	0	4	0	1	1	5	9	10	15	2	8	13	28	5	3	3	1	7	1	6	0	2	127	Aug 04 Sunday
217	2	3	5	5	6	3	10	24	24	21	9	23	9	6	2	5	6	7	8	4	0	2	10	3	197	Aug 05 Monday
218	1	0	7	5	0	0	3	11	8	11	5	17	3	9	12	21	8	1	2	3	4	3	2	5	141	Aug 06 Tuesday
219	4	2	5	5	0	2	8	8	11	19	25	21	15	10	4	6	3	14	2	9	4	0	2	3	182	Aug 07 Wednesday
220	9	0	10	1	7	1	2	16	23	19	33	17	9	10	15	7	7	3	3	2	7	1	6	26	234	Aug 08 Thursday
221	3	1	1	3	2	1	4	8	10	29	13	13	7	8	2	1	2	2	3	3	6	3	4	6	135	Aug 09 Friday
222	1	0	3	1	0	10	9	6	4	12	6	2	4	4	3	3	3	3	3	5	4	11	3		103	Aug 10 Saturday
223	4	4	4	6	3	3	0	1	10	3	0	6	4	6	2	1	4	2	2	3	7	12	1	5	93	Aug 11 Sunday
224	2	0	6	5	2	11	9	9	10	3	9	10	18	12	5	6	9	7	0	7	1	2	6	3	152	Aug 12 Monday
225	2	0	3	3	0	7	4	7	2	11	22	23	4	14	11	1	12	2	5	4	0	1	5	0	143	Aug 13 Tuesday
226	2	4	3	2	4	0	6	15	9	17	22	19	4	12	13	2	3	3	4	10	9	5	3	7	178	Aug 14 Wednesday
227	9	11	3	2	6	10	4	4	9	9	10	23	9	28	3	2	4	3	3	8	2	2	1	5	170	Aug 15 Thursday
228	6	3	3	3	1	5	5	15	13	23	15	18	12	6	7	5	2	0	2	2	0	2	6	0	154	Aug 16 Friday
229	3	1	0	0	0	2	6	10	3	4	8	4	8	6	8	5	4	3	2	2	2	1	11	8	101	Aug 17 Saturday
230	1	9	3	4	1	0	0	0	11	3	7	9	9	6	10	7	3	1	1	11	1	0	5	7	109	Aug 18 Sunday
231	2	3	7	4	0	8	12	9	12	10	8	19	9	8	16	7	10	2	2	5	5	0	2	4	164	Aug 19 Monday
232	5	0	1	0	2	3	9	12	14	12	28	16	10	14	19	7	9	11	4	2	0	3	2	1	184	Aug 20 Tuesday
233	6	6	5	5	2	6	8	19	9	19	13	16	16	16	16	3	13	6	3	5	0	5	3	3	203	Aug 21 Wednesday
234	1	3	2	1	5	0	3	17	16	24	21	23	7	3	11	5	8	5	2	3	0	3	0	0	163	Aug 22 Thursday
235	1	1	2	2	2	3	3	13	0	20	16	34	7	6	7	2	2	6	3	0	4	1	6	0	141	Aug 23 Friday
236	10	2	0	4	5	2	9	3	11	12	6	10	5	7	6	8	2	8	2	4	2	1	9	1	129	Aug 24 Saturday
237	4	2	3	2	4	7	5	9	12	14	12	15	16	14	14	4	9	2	2	7	1	2	2	0	162	Aug 25 Sunday
238	2	0	4	2	0	2	7	7	15	27	13	13	4	9	19	7	5	3	6	2	4	9	6	8	174	Aug 26 Monday
239	5	2	0	2	3	0	5	11	15	36	23	19	7	15	12	8	14	13	10	4	4	0	6	10	224	Aug 27 Tuesday
240	9	7	5	4	7	5	9	17	17	17	17	13	9	8	3	7	7	8	3	3	2	4	2	5	188	Aug 28 Wednesday
241	2	4	1	2	0	7	1	11	14	25	17	19	6	16	13	11	9	6	2	3	0	7	0	1	177	Aug 29 Thursday
242	4	2	8	2	1	0	4	12	9	22	39	23	6	12	6	9	3	7	3	4	5	2	1	3	187	Aug 30 Friday
243	2	2	1	4	3	8	1	6	1	14	8	7	12	10	3	3	4	1	1	1	5	6	2	3	108	Aug 31 Saturday
244	2	6	2	5	1	1	2	6	15	11	10	5	15	12	16	9	2	2	3	0	1	4	5	2	137	Sep 01 Sunday
245	0	0	0	0	0	0	0	0	0	0	0	0	0	5	11	10	4	15	9	4	4	2	1	7	72	Sep 02 Monday
246	3	2	6	7	4	4	3	6	13	16	15	14	11	11	15	13	3	5	4	2	4	2	0	3	166	Sep 03 Tuesday
247	2	1	1	2	1	2	1	18	27	27	15	11	15	11	6	17	11	6	9	4	10	6	4	3	210	Sep 04 Wednesday
248	1	0	2	3	2	3	4	4	25	39	12	23	12	11	7	3	7	7	14	8	2	4	2	3	198	Sep 05 Thursday
249	4	3	3	2	3	5	7	23	11	22	16	11	4	14	11	3	10	5	4	4	7	4	2	6	184	Sep 06 Friday
250	7	0	1	2	0	8	10	20	2	3	1	8	7	0	13	4	4	1	7	4	2	2	4	2	112	Sep 07 Saturday
251	1	3	1	1	2	0	0	2	6	3	12	0	5	1	8	4	1	9	8	8	1	2	2	4	84	Sep 08 Sunday
252	6	3	4	4	1	9	3	10	13	11	20	26	12	12	9	1	0	0	0	0	0	4	4	4	156	Sep 09 Monday
253	0	1	4	9	6	3	4	18	19	26	23	21	16	24	12	7	8	5	4	9	1	2	7	1	230	Sep 10 Tuesday
254	3	1	5	3	8	2	2	11	22	37	24	24	5	11	19	12	6	0	3	6	3	2	4	2	215	Sep 11 Wednesday
255	3	2	3	4	2	3	0	11	7	27	9	24	9	23	20	4	1	1	4	13	2	3	3	3	181	Sep 12 Thursday
256	4	3	14	3	2	1	14	21	12	15	25	16	16	25	14	14	2	1	1	1	0	4	5	1	214	Sep 13 Friday
257	2	3	2	7	5	1	4	1	5	2	7	7	7	8	3	2	3	2	1	5	1	5	0	4	87	Sep 14 Saturday
258	4	4	6	2	5	1	7	4	6	3	15	24	13	12	43	38	9	16	7	0	0	0	0	0	0	1011 Sep 15 Sunday

Table 3.4.4 (Page 3 of 4)

GER .FKX Hourly distribution of detections

Day	00	01	02	03	04	05	06	07	08	09	10	11	12	13	14	15	16	17	18	19	20	21	22	23	Sum	Date
259	0	0	0	0	0	0	0	0	0	0	0	0	0	0	0	0	0	0	0	0	0	0	0	0	0	Sep 16 Monday
260	0	0	0	0	0	0	0	0	0	0	0	0	0	0	0	0	0	0	0	0	0	0	0	0	0	Sep 17 Tuesday
261	0	0	0	0	0	0	0	0	0	0	0	0	0	0	0	0	0	0	0	0	0	0	0	0	0	Sep 18 Wednesday
262	0	0	0	0	0	0	0	0	0	0	0	0	0	0	0	0	0	0	0	0	0	0	0	0	0	Sep 19 Thursday
263	0	0	0	0	0	0	0	0	0	0	0	0	0	0	0	0	0	0	0	0	0	0	0	0	0	Sep 20 Friday
264	0	0	0	0	0	0	0	0	0	0	0	0	0	0	0	0	0	0	0	0	0	0	0	0	0	Sep 21 Saturday
265	0	0	0	0	0	0	0	0	0	0	0	0	0	0	0	0	0	0	0	0	0	0	0	0	0	Sep 22 Sunday
266	0	0	0	0	0	0	0	0	0	0	7	36	11	9	12	5	10	6	1	1	10	4	3	4	119	Sep 23 Monday
267	0	4	5	5	3	8	2	8	18	13	16	32	10	15	7	12	5	1	14	3	1	1	8	2	193	Sep 24 Tuesday
268	5	4	3	1	3	3	7	15	30	26	26	25	16	9	16	7	3	1	5	2	4	2	2	7	222	Sep 25 Wednesday
269	6	6	4	2	1	1	3	11	20	27	29	28	25	38	17	7	6	4	2	2	14	3	6	10	272	Sep 26 Thursday
270	11	14	2	9	5	2	6	14	12	18	10	40	13	11	9	6	7	5	2	8	2	1	2	4	213	Sep 27 Friday
271	6	6	3	8	8	8	7	2	6	4	1	14	1	0	6	0	4	4	3	1	7	4	5	3	111	Sep 28 Saturday
272	3	2	0	2	8	2	2	3	5	7	5	3	3	6	3	3	1	1	3	4	4	6	1	1	78	Sep 29 Sunday
273	5	0	1	1	4	5	0	0	10	17	11	10	21	13	6	2	5	3	10	0	1	1	4	3	133	Sep 30 Monday
GER	00	01	02	03	04	05	06	07	08	09	10	11	12	13	14	15	16	17	18	19	20	21	22	23		
Sum	854	985	938	943	908	949	1209	1899	1958	2820	2835	3010	2097	2187	2213	1596	1001	851	846	764	694	805	819	826	34007	Total sum
171	5	6	5	6	5	6	7	11	11	16	17	18	12	13	13	9	6	5	5	4	4	5	5	5	199	Total average
116	6	5	5	5	4	5	7	12	13	20	19	20	12	12	11	9	6	5	5	5	4	5	5	5	204	Average workdays
55	4	8	7	7	8	7	7	9	9	9	12	12	12	13	16	9	5	5	4	4	3	4	5	5	183	Average weekends

Table 3.4.4. Daily and hourly distribution of GERESS detections. For each day is shown number of detections within each hour of the day and number of detections for that day. The end statistics give total number of detections distributed for each hour and the total sum of detections during the period. The averages show number of processed days, hourly distribution and average per processed day.

KSP .FKX Hourly distribution of detections

Day	00	01	02	03	04	05	06	07	08	09	10	11	12	13	14	15	16	17	18	19	20	21	22	23	Sum	Date	
91	0	0	0	0	0	0	0	0	0	0	0	0	0	0	0	0	0	0	0	0	0	0	0	0	0	Apr 01 Monday	Annen
92	0	0	0	0	0	0	0	0	0	0	0	0	0	0	0	0	0	0	0	0	0	0	0	0	0	Apr 02 Tuesday	
93	0	0	0	0	0	0	0	0	0	0	0	0	0	0	0	0	0	0	0	0	0	0	0	0	0	Apr 03 Wednesday	
94	0	0	0	0	0	0	0	0	0	0	0	0	0	0	0	0	0	0	0	0	0	0	0	0	0	Apr 04 Thursday	
95	0	0	0	0	0	0	0	0	0	0	0	0	0	0	0	0	0	0	0	0	0	0	0	0	0	Apr 05 Friday	
96	0	0	0	0	0	0	0	0	0	0	0	0	0	0	0	0	0	0	0	0	0	0	0	0	0	Apr 06 Saturday	
97	0	0	0	0	0	0	0	0	0	0	0	0	0	0	0	0	0	0	0	0	0	0	0	0	0	Apr 07 Sunday	
98	0	0	0	0	0	0	0	0	0	0	0	0	0	0	0	0	0	0	0	0	0	0	0	0	0	Apr 08 Monday	
99	0	0	0	0	0	0	0	0	0	0	0	0	0	0	0	0	0	0	0	0	0	0	0	0	0	Apr 09 Tuesday	
100	0	0	0	0	0	0	0	0	0	0	0	0	0	0	0	0	0	0	0	0	0	0	0	0	0	Apr 10 Wednesday	
101	0	0	0	0	0	0	0	0	0	0	0	0	0	0	0	0	0	0	0	0	0	0	0	0	0	Apr 11 Thursday	
102	0	0	0	0	0	0	0	0	0	0	0	0	0	0	0	0	0	0	0	0	0	0	0	0	0	Apr 12 Friday	
103	0	0	0	0	0	0	0	0	0	0	0	0	0	0	0	0	0	0	0	0	0	0	0	0	0	Apr 13 Saturday	
104	0	0	0	0	0	0	0	0	0	0	0	0	0	0	0	0	0	0	0	0	0	0	0	0	0	Apr 14 Sunday	
105	0	0	0	0	0	0	0	0	0	0	0	0	0	0	0	0	0	0	0	0	0	0	0	0	0	Apr 15 Monday	
106	0	0	0	0	0	0	0	0	0	0	0	0	0	0	0	0	0	0	0	0	0	0	0	0	0	Apr 16 Tuesday	
107	0	0	0	0	0	0	0	0	0	0	0	0	0	0	0	0	0	0	0	0	0	0	0	0	0	Apr 17 Wednesday	
108	0	0	0	0	0	0	0	0	0	0	0	0	0	0	0	0	0	0	0	0	0	0	0	0	0	Apr 18 Thursday	
109	0	0	0	0	0	0	0	0	0	0	0	0	0	0	0	0	0	0	0	0	0	0	0	0	0	Apr 19 Friday	
110	0	0	0	0	0	0	0	0	0	0	0	0	0	0	0	0	0	0	0	0	0	0	0	0	0	Apr 20 Saturday	
111	0	0	0	0	0	0	0	0	0	0	0	0	0	0	0	0	0	0	0	0	0	0	0	0	0	Apr 21 Sunday	
112	0	0	0	0	0	0	0	0	0	0	0	0	0	0	0	0	0	0	0	0	0	0	0	0	0	Apr 22 Monday	
113	0	0	0	0	0	0	0	0	0	0	0	0	0	0	0	0	0	0	0	0	0	0	0	0	0	Apr 23 Tuesday	
114	0	0	0	0	0	0	0	0	0	0	0	0	0	0	0	0	0	0	0	0	0	0	0	0	0	Apr 24 Wednesday	
115	0	0	0	0	0	0	0	0	0	0	0	0	0	0	0	0	0	0	0	0	0	0	0	0	0	Apr 25 Thursday	
116	0	0	0	0	0	0	0	0	0	0	0	0	0	0	0	0	0	0	0	0	0	0	0	0	0	Apr 26 Friday	
117	0	0	0	0	0	0	0	0	0	0	0	0	0	0	0	0	0	0	0	0	0	0	0	0	0	Apr 27 Saturday	
118	0	0	0	0	0	0	0	0	0	0	0	0	0	0	0	0	0	0	0	0	0	0	0	0	0	Apr 28 Sunday	
119	0	0	0	0	0	0	0	0	0	0	0	0	0	0	0	0	0	0	0	0	0	0	0	0	0	Apr 29 Monday	
120	0	0	0	0	0	0	0	0	0	0	0	0	0	0	0	0	0	0	0	0	0	0	0	0	0	Apr 30 Tuesday	
121	0	0	0	0	0	0	0	0	0	0	0	0	0	0	0	0	0	0	0	0	0	0	0	0	0	May 01 Wednesday	Frste
122	0	0	0	0	0	0	0	0	0	0	0	0	0	0	0	0	0	0	0	0	0	0	0	0	0	May 02 Thursday	
123	0	0	0	0	0	0	0	0	0	0	0	0	0	0	0	0	0	0	0	0	0	0	0	0	0	May 03 Friday	
124	0	0	0	0	0	0	0	0	0	0	0	0	0	0	0	0	0	0	0	0	0	0	0	0	0	May 04 Saturday	
125	0	0	0	0	0	0	0	0	0	0	0	0	0	0	0	0	0	0	0	0	0	0	0	0	0	May 05 Sunday	
126	0	0	0	0	0	0	0	0	0	0	0	0	0	0	0	0	0	0	0	0	0	0	0	0	0	May 06 Monday	
127	0	0	0	0	0	0	0	0	0	0	0	0	0	0	0	0	0	0	0	0	0	0	0	0	0	May 07 Tuesday	
128	0	0	0	0	0	0	0	0	0	0	0	0	0	0	0	0	0	0	0	0	0	0	0	0	0	May 08 Wednesday	
129	0	0	0	0	0	0	0	0	0	0	0	0	0	0	0	0	0	0	0	0	0	0	0	0	0	May 09 Thursday	Kristi
130	0	0	0	0	0	0	0	0	0	0	0	0	0	0	0	0	0	0	0	0	0	0	0	0	0	May 10 Friday	
131	0	0	0	0	0	0	0	0	0	0	0	0	0	0	0	0	0	0	0	0	0	0	0	0	0	May 11 Saturday	
132	0	0	0	0	0	0	0	0	0	0	0	0	0	0	0	0	0	0	0	0	0	0	0	0	0	May 12 Sunday	
133	0	0	0	0	0	0	0	0	0	0	0	0	0	0	0	0	0	0	0	0	0	0	0	0	0	May 13 Monday	
134	0	0	0	0	0	0	0	0	0	0	0	0	0	0	0	0	0	0	0	0	0	0	0	0	0	May 14 Tuesday	
135	0	0	0	0	0	0	0	0	0	0	0	0	0	0	0	0	0	0	0	0	0	0	0	0	0	May 15 Wednesday	
136	0	0	0	0	0	0	0	0	0	0	0	0	0	0	0	0	0	0	0	0	0	0	0	0	0	May 16 Thursday	
137	0	0	0	0	0	0	0	0	0	0	0	0	0	0	0	0	0	0	0	0	0	0	0	0	0	May 17 Friday	Sytten
138	0	0	0	0	0	0	0	0	0	0	0	0	0	0	0	0	0	0	0	0	0	0	0	0	0	May 18 Saturday	
139	0	0	0	0	0	0	0	0	0	0	0	0	0	0	0	0	0	0	0	0	0	0	0	0	0	May 19 Sunday	Frste
140	0	0	0	0	0	0	0	0	0	0	0	0	0	0	0	0	0	0	0	0	0	0	0	0	0	May 20 Monday	Annen
141	0	0	0	0	0	0	0	0	0	0	0	0	0	0	0	0	0	0	0	0	0	0	0	0	0	May 21 Tuesday	
142	0	0	0	0	0	0	0	0	0	0	0	0	0	0	0	0	0	0	0	0	0	0	0	0	0	May 22 Wednesday	
143	0	0	0	0	0	0	0	0	0	0	0	0	0	0	0	0	0	0	0	0	0	0	0	0	0	May 23 Thursday	
144	0	0	0	0	0	0	0	0	0	0	0	0	0	0	0	0	0	0	0	0	0	0	0	0	0	May 24 Friday	
145	0	0	0	0	0	0	0	0	0	0	0	0	0	0	0	0	0	0	0	0	0	0	0	0	0	May 25 Saturday	
146	0	0	0	0	0	0	0	0	0	0	0	0	0	0	0	0	0	0	0	0	0	0	0	0	0	May 26 Sunday	

Table 3.4.5 (Page 1 of 4)

KSP .FKX Hourly distribution of detections

Day	00	01	02	03	04	05	06	07	08	09	10	11	12	13	14	15	16	17	18	19	20	21	22	23	Sum	Date
147	0	0	0	0	0	0	0	0	0	0	0	0	0	0	0	0	0	0	0	0	0	0	0	0	0	May 27 Monday
148	0	0	0	0	0	0	0	0	0	0	0	0	0	0	0	0	0	0	0	0	0	0	0	0	0	May 28 Tuesday
149	0	0	0	0	0	0	0	0	0	0	0	0	0	0	0	0	0	0	0	0	0	0	0	0	0	May 29 Wednesday
150	0	0	0	0	0	0	0	0	0	0	0	0	0	0	0	0	0	0	0	0	0	0	0	0	0	May 30 Thursday
151	0	0	0	0	0	0	0	0	0	0	0	0	0	0	0	0	0	0	0	0	0	0	0	0	0	May 31 Friday
152	0	0	0	0	0	0	0	0	0	0	0	0	0	0	0	0	0	0	0	0	0	0	0	0	0	Jun 01 Saturday
153	0	0	0	0	0	0	0	0	0	0	0	0	0	0	0	0	0	0	0	0	0	0	0	0	0	Jun 02 Sunday
154	0	0	0	0	0	0	0	0	0	0	0	0	0	0	0	0	0	0	0	0	0	0	0	0	0	Jun 03 Monday
155	0	0	0	0	0	0	0	0	0	0	0	0	0	0	0	0	0	0	0	0	0	0	0	0	0	Jun 04 Tuesday
156	0	0	0	0	0	0	0	0	0	0	0	0	0	0	0	0	0	0	0	0	0	0	0	0	0	Jun 05 Wednesday
157	0	0	0	0	0	0	0	0	0	0	0	0	0	0	0	0	0	0	0	0	0	0	0	0	0	Jun 06 Thursday
158	0	0	0	0	0	0	0	0	0	0	0	0	0	0	0	0	0	0	0	0	0	0	0	0	0	Jun 07 Friday
159	0	0	0	0	0	0	0	0	0	0	0	0	0	0	0	0	0	0	0	0	0	0	0	0	0	Jun 08 Saturday
160	0	0	0	0	0	0	0	0	0	0	0	0	0	0	0	0	0	0	0	0	0	0	0	0	0	Jun 09 Sunday
161	0	0	0	0	0	0	0	0	0	0	0	0	0	0	0	0	0	0	0	0	0	0	0	0	0	Jun 10 Monday
162	0	0	0	0	0	0	0	0	0	0	0	0	0	0	0	0	0	0	0	0	0	0	0	0	0	Jun 11 Tuesday
163	0	0	0	0	0	0	0	0	0	0	0	0	0	0	0	0	0	0	0	0	0	0	0	0	0	Jun 12 Wednesday
164	0	0	0	0	0	0	0	0	0	0	0	0	0	0	0	0	0	0	0	0	0	0	0	0	0	Jun 13 Thursday
165	0	0	0	0	0	0	0	0	0	0	0	0	0	0	0	0	0	0	0	0	0	0	0	0	0	Jun 14 Friday
166	0	0	0	0	0	0	0	0	0	0	0	0	0	0	0	0	0	0	0	0	0	0	0	0	0	Jun 15 Saturday
167	0	0	0	0	0	0	0	0	0	0	0	0	0	0	0	0	0	0	0	0	0	0	0	0	0	Jun 16 Sunday
168	0	0	0	0	0	0	0	0	0	0	0	0	0	0	0	0	0	0	0	0	0	0	0	0	0	Jun 17 Monday
169	0	0	0	0	0	0	0	0	0	0	0	0	0	0	0	0	0	0	0	0	0	0	0	0	0	Jun 18 Tuesday
170	0	0	0	0	0	0	0	0	0	0	0	0	0	0	0	0	0	0	0	0	0	0	0	0	0	Jun 19 Wednesday
171	0	0	0	0	0	0	0	0	0	0	0	0	0	0	0	0	0	0	0	0	0	0	0	0	0	Jun 20 Thursday
172	0	0	0	0	0	0	0	0	0	0	0	0	0	0	0	0	0	0	0	0	0	0	0	0	0	Jun 21 Friday
173	0	0	0	0	0	0	0	0	0	0	0	0	0	0	0	0	0	0	0	0	0	0	0	0	0	Jun 22 Saturday
174	0	0	0	0	0	0	0	0	0	0	0	0	0	0	0	0	0	0	0	0	0	0	0	0	0	Jun 23 Sunday
175	0	0	0	0	0	0	0	0	0	0	0	0	0	0	0	0	0	0	0	0	0	0	0	0	0	Jun 24 Monday
176	6	15	10	19	16	22	9	22	15	4	7	12	8	10	8	2	11	16	18	14	21	21	23	15	324	Jun 25 Tuesday
177	7	13	18	25	16	13	12	9	11	9	10	16	8	18	10	11	2	7	3	20	22	17	13	6	296	Jun 26 Wednesday
178	17	17	20	18	20	12	7	9	16	16	22	9	26	18	16	25	20	13	17	12	28	7	18	3	386	Jun 27 Thursday
179	16	8	19	25	13	19	12	13	11	17	1	8	5	8	13	10	11	4	7	16	20	8	27	7	298	Jun 28 Friday
180	15	9	15	28	12	10	6	17	12	21	10	24	21	15	26	18	34	30	24	25	27	15	13	12	439	Jun 29 Saturday
181	22	25	23	32	26	30	24	24	37	15	18	23	23	18	13	15	18	18	28	30	25	28	14	22	551	Jun 30 Sunday
182	19	22	28	22	12	20	11	16	4	0	0	0	0	0	0	0	0	0	0	0	0	0	0	0	154	Jul 01 Monday
183	0	0	0	0	0	0	0	0	0	0	0	0	0	0	0	0	0	0	0	0	0	0	0	0	0	Jul 02 Tuesday
184	0	0	0	0	0	0	0	0	0	0	0	0	0	0	0	0	0	0	0	0	0	0	0	0	0	Jul 03 Wednesday
185	0	0	0	0	0	0	0	0	0	0	20	8	15	8	7	8	4	2	10	14	17	19	12	6	150	Jul 04 Thursday
186	27	9	13	25	19	4	1	17	15	10	5	12	13	7	5	7	9	14	10	18	30	16	24	16	326	Jul 05 Friday
187	5	9	17	30	20	22	18	43	29	21	23	21	55	27	31	29	29	21	28	28	38	24	26	22	616	Jul 06 Saturday
188	18	32	32	24	12	43	25	41	25	20	21	32	13	13	18	17	12	12	28	20	23	14	19	13	527	Jul 07 Sunday
189	19	16	18	27	16	14	2	16	5	15	4	10	14	14	6	9	8	6	17	31	22	17	16	8	330	Jul 08 Monday
190	12	17	13	28	12	13	7	6	8	14	2	24	14	2	11	7	9	3	15	16	29	30	10	9	311	Jul 09 Tuesday
191	2	21	9	30	16	7	9	14	16	6	11	18	9	9	9	10	18	16	12	24	19	16	15	17	333	Jul 10 Wednesday
192	36	13	22	17	14	8	7	18	16	18	8	17	14	14	14	8	6	8	2	11	16	14	7	7	315	Jul 11 Thursday
193	27	22	19	30	20	7	7	16	14	12	23	23	12	25	16	7	11	22	17	13	18	18	18	17	414	Jul 12 Friday
194	11	14	14	35	155	13	9	22	21	21	27	30	23	27	17	22	19	25	21	28	23	18	22	13	630	Jul 13 Saturday
195	23	26	20	37	26	21	19	25	25	22	20	14	10	17	28	19	20	24	15	17	37	20	30	16	531	Jul 14 Sunday
196	7	18	11	27	12	16	10	11	9	9	15	13	23	22	28	23	26	17	22	32	37	19	63	2	472	Jul 15 Monday
197	10	13	14	23	21	15	16	14	17	13	15	14	13	20	10	11	22	20	17	21	28	13	17	10	387	Jul 16 Tuesday
198	17	16	11	21	17	10	9	12	30	16	9	35	13	14	19	18	17	14	15	21	21	21	19	7	402	Jul 17 Wednesday
199	7	13	19	22	18	17	23	16	10	18	9	27	24	14	18	8	20	11	17	29	40	22	12	10	424	Jul 18 Thursday
200	27	20	20	22	13	22	7	16	15	9	13	13	20	23	12	15	17	20	18	17	27	35	17	16	434	Jul 19 Friday
201	18	19	13	33	23	20	13	19	19	21	19	24	22	21	34	24	14	14	22	23	30	19	20	3	487	Jul 20 Saturday
202	15	23	20	28	18	27	41	22	33	20	22	16	18	13	14	19	27	21	21	19	22	24	21	11	515	Jul 21 Sunday

Table 3.4.5 (Page 2 of 4)

KSP .FKX Hourly distribution of detections

Day	00	01	02	03	04	05	06	07	08	09	10	11	12	13	14	15	16	17	18	19	20	21	22	23	Sum	Date
203	7	16	15	32	22	23	18	17	32	20	10	14	26	10	20	15	13	10	11	27	23	21	17	8	427	Jul 22 Monday
204	5	15	17	22	18	13	10	15	23	16	15	25	25	18	16	17	24	13	19	30	24	13	17	14	424	Jul 23 Tuesday
205	19	22	14	25	16	22	13	18	13	21	30	18	22	20	18	21	29	23	21	17	36	22	26	32	518	Jul 24 Wednesday
206	7	21	20	29	27	13	10	18	14	10	15	20	21	13	21	33	14	28	11	17	31	23	13	15	444	Jul 25 Thursday
207	22	10	20	26	23	16	17	15	15	19	27	15	27	15	19	12	19	18	14	29	29	11	19	5	442	Jul 26 Friday
208	20	27	7	25	16	17	11	9	8	29	9	19	15	24	23	12	18	16	21	15	23	16	27	6	413	Jul 27 Saturday
209	22	20	16	26	18	23	38	26	28	35	25	20	10	11	18	17	13	30	14	17	27	14	19	15	502	Jul 28 Sunday
210	13	17	20	24	35	25	25	29	22	31	21	46	28	18	18	26	19	14	15	24	33	21	45	17	586	Jul 29 Monday
211	4	16	9	25	21	11	13	27	16	19	20	25	25	14	23	18	27	10	9	41	35	17	19	14	458	Jul 30 Tuesday
212	5	20	14	23	15	9	14	28	20	14	5	33	23	19	27	19	22	13	22	22	15	22	21	11	436	Jul 31 Wednesday
213	17	30	10	32	17	16	23	13	14	12	14	22	31	23	10	17	14	13	21	22	20	22	15	11	439	Aug 01 Thursday
214	31	12	10	24	14	18	11	14	15	14	14	20	29	17	15	26	20	20	16	33	27	31	14	21	466	Aug 02 Friday
215	10	13	15	31	15	28	22	23	22	16	22	19	13	15	12	19	21	13	12	19	23	23	14	22	442	Aug 03 Saturday
216	26	31	22	28	13	16	22	18	24	13	27	15	13	10	12	9	18	7	15	31	28	15	20	9	442	Aug 04 Sunday
217	9	17	17	22	13	22	26	9	25	9	8	21	15	17	21	13	16	11	9	18	18	19	22	27	404	Aug 05 Monday
218	8	11	16	29	24	16	16	24	13	8	11	17	23	13	17	35	19	20	17	20	22	17	19	7	422	Aug 06 Tuesday
219	8	23	12	22	21	21	13	18	39	18	16	25	19	12	15	20	20	16	17	16	29	13	15	9	437	Aug 07 Wednesday
220	12	20	14	33	13	12	13	13	13	15	13	19	18	18	19	31	33	20	18	25	29	19	22	16	458	Aug 08 Thursday
221	9	22	26	23	19	18	3	14	25	24	18	15	24	16	16	9	17	9	16	14	21	16	23	7	404	Aug 09 Friday
222	10	15	23	23	19	17	11	26	29	17	9	22	20	19	26	15	19	11	25	25	23	31	29	12	476	Aug 10 Saturday
223	5	28	27	30	17	34	43	21	35	17	17	22	18	14	28	24	26	15	28	27	25	25	29	18	573	Aug 11 Sunday
224	7	10	8	20	8	19	6	3	9	3	8	8	21	13	11	11	18	10	12	19	25	18	20	6	293	Aug 12 Monday
225	8	11	8	26	11	13	9	5	3	9	5	15	13	13	9	8	19	14	12	19	23	18	10	15	296	Aug 13 Tuesday
226	15	22	11	18	6	0	4	10	13	7	11	10	18	24	18	17	13	8	18	53	37	24	8	20	385	Aug 14 Wednesday
227	2	31	15	43	23	36	42	15	17	15	12	18	18	32	11	10	25	21	21	28	33	14	20	8	510	Aug 15 Thursday
228	27	0	17	30	10	6	12	12	26	10	26	24	34	24	17	7	25	19	11	22	19	19	14	30	441	Aug 16 Friday
229	11	21	14	17	2	11	12	16	11	23	5	34	6	5	11	11	19	19	14	24	26	27	28	11	378	Aug 17 Saturday
230	4	28	22	34	13	27	27	20	37	16	9	13	7	9	23	10	26	21	23	28	23	28	14	6	468	Aug 18 Sunday
231	2	25	11	19	14	13	22	21	14	31	9	33	15	11	10	9	13	10	8	15	19	18	14	16	372	Aug 19 Monday
232	7	13	13	18	10	12	11	23	51	16	26	30	19	7	8	7	9	7	1	19	12	14	15	19	367	Aug 20 Tuesday
233	11	13	13	22	9	4	2	4	7	8	11	11	19	19	13	20	16	12	7	29	20	31	18	19	338	Aug 21 Wednesday
234	34	21	15	26	6	2	5	5	9	15	11	6	18	13	9	11	9	8	4	17	19	19	18	8	308	Aug 22 Thursday
235	11	6	10	21	9	8	5	6	15	9	12	19	28	16	13	15	9	8	11	38	25	22	15	7	338	Aug 23 Friday
236	25	19	16	19	12	21	23	15	22	15	7	25	20	16	20	20	32	19	27	26	30	23	28	13	493	Aug 24 Saturday
237	15	20	16	31	20	37	41	47	28	13	15	27	15	17	16	18	12	24	29	21	25	31	16	6	540	Aug 25 Sunday
238	5	20	15	30	9	12	3	8	8	6	4	8	11	7	10	10	4	36	15	14	19	20	14	11	299	Aug 26 Monday
239	8	20	20	21	7	1	7	3	7	6	5	21	9	13	9	6	6	3	7	19	28	16	14	9	265	Aug 27 Tuesday
240	10	19	18	17	11	9	11	14	22	11	10	12	17	3	6	14	7	3	5	20	29	20	42	10	340	Aug 28 Wednesday
241	12	11	17	28	5	10	12	10	8	21	12	17	8	11	5	7	5	5	13	9	24	15	26	5	296	Aug 29 Thursday
242	25	19	17	15	3	3	6	10	6	9	13	25	10	8	12	16	16	7	7	31	28	21	12	36	355	Aug 30 Friday
243	11	17	22	26	9	15	16	27	21	22	24	26	9	6	20	13	19	19	30	16	24	24	38	8	462	Aug 31 Saturday
244	6	20	18	29	15	37	33	21	22	24	17	14	18	9	13	11	20	11	15	15	34	21	22	10	455	Sep 01 Sunday
245	10	18	27	26	10	11	3	8	4	3	5	10	10	9	8	11	11	4	5	6	19	20	21	14	273	Sep 02 Monday
246	28	23	34	14	7	5	10	3	9	13	14	18	14	8	13	22	28	4	2	17	21	27	25	5	364	Sep 03 Tuesday
247	8	24	13	14	8	8	11	3	11	11	7	16	19	13	19	14	13	10	8	27	16	6	17	19	315	Sep 04 Wednesday
248	11	22	11	24	15	8	9	10	9	12	7	27	14	7	7	20	5	1	2	15	21	16	14	13	300	Sep 05 Thursday
249	26	16	7	15	3	1	8	19	9	21	9	11	18	19	24	6	21	14	13	14	18	11	13	7	323	Sep 06 Friday
250	11	9	14	18	3	18	3	8	6	8	2	13	13	31	26	19	25	19	17	23	20	20	18	11	355	Sep 07 Saturday
251	20	21	18	25	27	25	20	40	33	45	21	30	26	23	28	21	27	14	21	24	26	20	17	6	578	Sep 08 Sunday
252	16	15	22	29	9	18	9	13	11	15	12	12	7	8	5	3	15	3	13	10	18	22	21	11	317	Sep 09 Monday
253	10	13	6	19	5	8	0	22	14	16	16	25	14	19	9	14	7	7	10	11	12	33	37	9	336	Sep 10 Tuesday
254	13	29	27	16	6	5	8	13	9	19	11	17	14	6	5	6	12	5	15	18	22	18	13	5	312	Sep 11 Wednesday
255	9	18	16	31	12	17	4	7	8	15	11	17	27	4	9	9	11	6	12	23	37	33	28	15	379	Sep 12 Thursday
256	36	11	27	28	12	16	7	13	9	12	8	14	14	14	12	14	9	4	9	13	18	30	30	25	385	Sep 13 Friday
257	38	19	16	24	10	3	2	6	11	8	8	8	10	7	9	15	22	16	18	23	26	37	41	24*	401	Sep 14 Saturday
258	18	22	20	25	33	37	23	17	21	16	11	11	12	16	17	19	12	22	25	30	29	13	44	20	513	Sep 15 Sunday

Table 3.4.5 (Page 3 of 4)

KSP .FKX Hourly distribution of detections

Day	00	01	02	03	04	05	06	07	08	09	10	11	12	13	14	15	16	17	18	19	20	21	22	23	Sum	Date
259	26	38	28	34	11	19	5	8	13	17	13	22	7	8	10	15	9	5	11	41	22	25	40	20	447	Sep 16 Monday
260	25	8	17	19	9	8	11	17	9	22	8	16	14	11	4	7	6	7	17	25	23	20	19	4	326	Sep 17 Tuesday
261	17	13	11	19	6	6	9	7	8	8	18	22	20	18	13	8	6	8	13	40	19	24	28	13	354	Sep 18 Wednesday
262	14	18	21	17	22	5	5	5	12	7	13	18	8	10	9	16	9	6	25	28	28	22	15	11	344	Sep 19 Thursday
263	27	17	18	23	4	9	4	12	5	25	7	21	23	3	11	10	13	15	8	32	21	15	31	13	367	Sep 20 Friday
264	9	14	9	25	12	12	23	14	15	8	8	15	7	12	18	17	12	18	27	42	34	17	14	13	395	Sep 21 Saturday
265	31	11	15	37	10	27	23	19	13	7	12	20	11	15	12	7	16	14	11	22	46	29	12	14	434	Sep 22 Sunday
266	6	10	7	13	8	12	7	6	13	10	6	20	10	6	14	7	12	6	8	16	19	13	14	6	249	Sep 23 Monday
267	17	8	8	21	6	1	3	2	13	6	6	13	11	17	9	12	23	10	6	3	25	33	14	7	274	Sep 24 Tuesday
268	0	15	16	20	8	15	6	8	17	17	11	11	6	13	3	7	34	6	9	6	8	4	8	6	254	Sep 25 Wednesday
269	8	8	8	7	1	1	6	7	7	7	16	21	23	24	11	9	21	3	7	10	11	25	8	14	263	Sep 26 Thursday
270	21	12	6	19	6	8	22	17	14	20	17	25	18	14	6	9	17	13	10	19	20	13	9	6	341	Sep 27 Friday
271	6	13	22	25	19	9	13	9	18	7	8	11	8	12	15	10	23	15	23	17	29	21	13	9	355	Sep 28 Saturday
272	5	8	14	21	39	19	24	5	21	11	6	12	13	11	6	15	14	11	10	11	6	10	10	22	324	Sep 29 Sunday
273	11	17	11	15	27	5	9	6	8	14	3	6	13	15	16	10	20	17	6	14	19	16	17	20	315	Sep 30 Monday
KSP	00	01	02	03	04	05	06	07	08	09	10	11	12	13	14	15	16	17	18	19	20	21	22	23		
Sum	1399	1667	1562	2329	1515	1436	1280	1461	1573	1423	1237	1785	1612	1374	1401	1364	1590	1266	1418	2062	2328	1916	1932	1213	38143	Total sum
96	15	17	16	24	16	15	13	15	16	15	13	19	17	14	15	14	17	13	15	21	24	20	20	13	397	Total average
68	14	16	15	23	13	12	10	13	14	13	12	18	17	14	13	13	15	11	12	21	23	19	19	12	361	Average workdays
28	15	19	18	27	22	22	21	21	22	18	15	20	16	15	19	17	20	18	21	23	27	22	22	13	475	Average weekends

Table 3.4.5. Daily and hourly distribution of KSP detections. For each day is shown number of detections within each hour of the day and number of detections for that day. The end statistics give total number of detections distributed for each hour and the total sum of detections during the period. The averages show number of processed days, hourly distribution and average per processed day.

3.5 IMS operation

The Intelligent Monitoring System (IMS) was installed at NORSAR in December 1989 and was operated at NORSAR from 1 January 1990 for automatic processing of data from ARCESS and NORESS. A new version of IMS that accepts data from an arbitrary number of arrays and single 3-component stations has now been developed by SAIC, and has been operated at the Center for Seismic Studies (CSS) in Rosslyn, VA, since March 1991. This new version will be installed at NORSAR in October 1991. In anticipation of the new version of IMS, the operation at NORSAR of the first IMS version was discontinued on 30 June 1991. During July 1991, NORSAR personnel received a training course at the CSS for operation of IMS Version 2 and are well prepared for taking over the responsibility for the daily operation of IMS in October this year.

The statistics in the following reflect IMS operation at NORSAR during April to June 1991. In general, our routine operation of IMS during this period progressed well, and the system proved to be very powerful and flexible. The well-developed automatic processing combined with very versatile interactive tools has kept the analyst workload at a low level, and in fact only one analyst was required to handle the regular processing at any time.

Table 3.5.1 presents an overview of IMS event processor downtimes. Table 3.5.2 gives a summary of phase detections and processed regional events by IMS. From top to bottom, the table gives the total number of detections by the IMS, the number of detections that are associated with events declared, the number of detections that are not associated with any events, the number of regional events declared by the IMS, the number of such events rejected by the analyst, the number of events accepted by the analyst, the number of events accepted by the analyst without any changes, and finally the number of events accepted after some sort of modifications by the analyst. This last category is divided into two classes: Events where phases (not detected by the IMS) have been added by the analyst and events for which the phase assignments by the IMS have been changed or one or more phase detections have been removed.

From initial review of the IMS bulletin, it is clear that the final output is of very high quality from a seismological point of view. The IMS was used extensively for the reporting of regional events during the GSETT-2 test, conducted by the Geneva Group of Scientific Experts during 22 April - 2 June 1991.

B.Kr. Hokland
U. Baadshaug
S. Mykkeltveit

1991 Apr 14 19:30:00.000 - 1991 Apr 14 24:00:00.000
1991 Apr 17 15:30:00.000 - 1991 Apr 18 02:00:00.000
1991 Apr 18 17:00:00.000 - 1991 Apr 19 07:00:00.000
1991 Apr 19 19:00:00.000 - 1991 Apr 20 05:00:00.000
1991 Apr 20 18:00:00.000 - 1991 Apr 22 24:00:00.000
1991 Apr 26 17:00:00.000 - 1991 Apr 27 05:30:00.000

Table 3.5.1. IMS event processor (pipeline) downtimes.

	Apr 91	May 91	Jun 91	Total
Phase detections	16714	17063	16565	50342
-Associated phases	2849	2656	2392	7897
-Unassociated phases	13865	14407	14173	42445
Events automatically declared by IMS	1080	1183	973	3236
-Rejected events	197	286	176	659
-Accepted events	883	897	797	2577
Unchanged events	296	227	229	752
Modified events	587	670	568	1825
Phases added	67	49	69	185
Phases changed or removed	520	621	499	1640

Table 3.5.2. IMS phase detections and event summary.

4 Improvements and Modifications

4.1 NORSAR

NORSAR data acquisition

No modification has been made to the NORSAR data acquisition system. There is an increasing problem with loss of data.

NORSAR detection processing

The NORSAR detection processor has been running satisfactorily on the IBM during this reporting period.

Detection statistics are given in section 2.

NORSAR event processing

There are no changes in the routine processing of NORSAR events, using the IBM system.

NORSAR refurbishment

The process of evaluating and testing technical options for refurbishment of NORSAR has continued. A contract starting 1 Oct 1991 that will provide funding for such a refurbishment has now been signed. Technical progress will be reported in forthcoming Semiannual Technical Summaries.

4.2 Regional arrays and 3-component stations

Detection processing

The routine detection processing of the arrays is running satisfactorily on each of the array's SUN-3/280 acquisition systems. The same program is used for NORSAR, NORESS, ARCESS, FINESA, GERESS, KSP, SFP but with different recipes. The beam table for NORESS and ARCESS is found in NORSAR Sci. Rep. No. 1-89/90. The beam table for FINESA and GERESS is found in NORSAR Sci. Rep. No. 1-90/91.

Detection statistics are given in section 3.

Event processing. Phase estimation

This process will do F-K and polarization analysis for each detection to identify phase velocity, azimuth and type of phase, and the results are put into the ORACLE detection data base for use by IMS. Data for the three-component Polish stations have been made available for IMS.

Plot and epicenter determination

A description of single array event processing is found in NORSAR Sci. Rep. No. 2-88/89, and NORSAR Sci. Rep. 2-89/90.

J. Fyen

5 Maintenance Activities

5.1 Activities in the field and at the Maintenance Center

This section summarizes the activities in the field, at the Maintenance Center (NMC) Hamar, and NDPC activities related to monitoring and control of NORSAR, NORESS and ARCESS. Activities at other field sites are also listed..

Activities involve preventive and corrective maintenance, modification of equipment, for example, in connection with interfacing to the new NORSAT B satellite station (P.W. Larsen, ARCESS, August 1991).

NORSAR

This array was visited in May, June, July, August and September 1991. As in previous periods, activities related to this array have been diverse, involving: preventive and corrective maintenance such as line and communications tests, modem repair, SLEM test, adjustment of mass position (MP) and free period (FP) LP instruments, adjustment of channel gain and DC offset for all SP/LP channels, replacement of LP seismometer Remote Centering Devices (RCDs), cable splicing, RA-5 amplifier adjustments and replacements, replacement of main fuses after lightning, replacement of protection cards, replacement of discrete output card.

NORESS

The NORESS array was visited in June and August 1991 in connection with Hub unit replacement after serious damage by lightning, and repair of Hub I/F card which did not send synch. pulses to remote sites.

ARCESS

This array was visited in April, May, June, July, August and September -- in connection with activities such as: UPS failure after power outage, replacements of fiber optical receiver/transmitter at sites A2 and A3, modifications of all seismometer vaults, cleaning of fiber optical connectors, modification of "white box" to achieve correct I/F to the new NORSAT B satellite station, adjustment of fiber optical link to A2 and D6, removal of the old NORSAT B0 telemetry rack from the Hub.

FINESA

FINESA was visited in April, July and September in connection with field maintenance, replacement of RA-5 amplifier, and replacement of cable to remote sites after lightning.

Poland, Ksiaz/Stary Folwark

Problems which had been present ever since installation of the station were partially solved during a visit in April, and the communication link tested.

Subarray/ Area	Task	Date
Poland/Ksiaz/ Stary Folwark	Representatives from Teledyne Geotech, NTA satellite department and NORSAR solved problems which had been present ever since the installation of the stations. During communications tests, both NTA/Lillestrøm and NORSAR were engaged.	13-20 Apr
ARCESS	Local representative restored the operation after UPS failure	17 Apr
FINESA	NMC (Ø. Løken) carried out field maintenance	15,16,17 Apr
NDPC	Daily check of all arrays, i.e., NORSAR, NORESS, ARCESS, FINESA, GERESS and Poland (KSP,SFP). NORSAR SP/LP instruments calibrated every week. Free Period (FP) and Mass Position (MP) have been measured and adjusted when outside tolerances.	April
NORSAR 04C	Communications test. Replaced AHS-card in CTV modem	23 May
ARCESS	Replaced fiber optical receiver/transmitter at sites A2 and A3.	14,15,16 May
NDPC	Daily check of all arrays, i.e., NORSAR, NORESS, ARCESS, FINESA, GERESS and Poland (KSP,SFP). NORSAR SP/LP instruments calibrated every week. Free Period (FP) and Mass Position (MP) have been measured and adjusted when outside tolerances.	May

Table 5.1. Activities in the field and the NORSAR Maintenance Center, including NDPC activities related to NORSAR, NORESS, ARCESS, FINESA, GERESS and Poland (KSP, SFP) arrays, 1 April - 30 Sepember 1991.

Subarray/ Area	Task	Date
NORSAR 02B	Line and SLEM tests carried out	27 June
ARCESS	All seismometer vaults modified	10-21 June
NORESS	Hub unit replaced after serious damage by lightning	18-25 June
Apatity, USSR	Installed a Nanometrics data acquisition system unit and a 3-component S13 station	10-15 June
NDPC	Daily check of all arrays, i.e., NORSAR, NORESS, ARCESS, FINESA, GERESS and Poland (KSP,SFP). NORSAR SP/LP instruments calibrated every week. Free Period (FP) and Mass Position (MP) have been measured and adjusted when outside tolerances.	June
NORSAR 01A	Main fuses replaced after lightning. Comm. line quality tested. Adjusted MP/FP all LP instruments. Adjusted channel gain and DC offset all SP/LP channels	16 July
01B	Replaced MP and RP Remote Centering Devices (RCDs) NS LP seismometer. Adjusted all MP/FP RCDs. Adjusted channel gain all SP/LP channels	2 July
02B	Replaced MP/FP RCDs EW seismometer. Replaced discrete output card (X1). Adjusted MP/FP RCDs all LP instruments	19 July 15 July
02C	Adjusted MP/FP RCDs all LP instruments. Adjusted channel gain and DC offset all SP/LP channels	18 July
03C	Line check B/C-loop	1 July

Table 5.1 (cont.)

Subarray/ Area	Task	Date
04C	Adjusted MP/FP RCDs all LP instruments. Adjusted channel gain and DC offset all SP/LP channels	1 July
06C	Replaced protection card SP03. Adjusted MP/FP all LP seismometers. Adjusted channel gain and DC offset all SP/LP channels	17 July
ARCESS	Replaced fiber optical transmitters D4 Channel connectors fiber optical cables A3	25-26 July
FINESA	Replaced all RA-5 amplifiers	9,10,11 July
NDPC	Daily check of all arrays has been carried out weeks 27, 28 and 29, i.e., NORSAR, NORESS, ARCESS, FINESA, GERESS and Poland (KSP, SFP). The actual weeks NORSAR LP instruments were calibrated, Free Period (FP) and Mass Position (MP) were measured and adjusted (those outside specifications).	July
NORSAR		
01B	Adjusted RA-5 amplifier SP02	19 Aug
02C	Comm. check in cooperation with NTA/Lillestrøm	19 Aug
02B	Remote Centering Devices (RCDs) MP/FP all LP seismometers replaced	21-22 Aug
06C	Adjusted RA-5 amplifier SP02. RA-5 amplifier SP05 replaced.	23 Aug
NORESS	Hub I/F card repaired as it did not send synch pulses to the remote sites.	2 Aug
	Lightning caused array outage and deterioration of equipment throughout the entire array, such as: Hub, remote sites, TOD (clock), terminals (2), converter and modems.	16 Aug

Table 5.2 (cont.)

Subarray/ Area	Task	Date
	Array resumed operation, but sites A1, C2, D2 and D8 were still inoperative.	27 Aug
	All sites performed satisfactorily, but A1 was still inoperative due to lack of spare parts for the CPU.	30 Aug
ARCESS	"White box" modified during the stay. Afterwards successfully interfaced to the new NORSAT B satellite station.	13-16 Aug
Svalbard	Site survey and measurements carried out in order to find a suitable location for the planned miniarray in the Longyearbyen area.	19-21 Aug
NDPC	Daily check of all arrays has been carried out, i.e., NORSAR, NORESS, ARCESS, FINESA, GERESS, and Poland (KSP, SFP). Every week the NORSAR SP/LP instruments were calibrated. Free Period (FP) Mass Position (MP) were measured and adjusted (those outside specifications).	August
NORSAR 01B	Replaced RA-5 amplifier SP02 vault. Cable spliced SP04. Adjusted FP/MP all LP instruments	23,25 Sep
ARCESS	Adjusted fiber optical links for sites A2 andD6. Removed all NORSAT B0 telemetry racks from Hub	14-16 Sep
FINESA	Replaced cables to remote sites after lightning, for sites A2, B1, B2, B3, B6, C1, C4, C5 and C6.	10-13 Sep
NDPC	Daily check of all arrays has been carried out, i.e., NORSAR, NORESS, ARCESS, FINESA, GERESS, and Poland (KSP, SFP). Every week the NORSAR SP/LP instruments were calibrated. Free Period (FP) Mass Position (MP) were measured and adjusted (those outside specifications.	September

Table 5.1 (cont.)

5.2 Array status

As of 30 September 1991 the following NORSAR channels deviated from tolerances:

01A 01	8 Hz filter
02	8 Hz filter
04	30 dB attenuation

O.A. Hansen

6 Documentation Developed

Kværna, T. and D.J. Doornbos, Scattering of regional Pn by Moho Topography, *Geophys. Res. Lett.*, Vol. 18, 1273-1276, 1991.

Kværna, T. and F. Ringdal, Integrated array and 3-component processing using a seismic "microarray", submitted to *Bull. Seism. Soc. Am.*.

Lokshtanov, D.E., B.O. Ruud and E.S. Husebye: The crustal transfer function in seismic 3-component slowness estimation, submitted to *Geophys. Res. Lett.*

Ringdal, F., P.D. Marshall and R.W. Alewine: Seismic yield determination of Soviet underground nuclear explosions at the Shagan River test site, submitted to *Geophys. J. Int.*

Semiannual Tech. Summary, 1 Oct 90 - 31 Mar 91, NORSAR Sci. Rep. 2-90/91, Kjeller, Norway.

7 Summary of Technical Reports / Papers Published

7.1 Statistical optimization of seismic holography algorithms for array data processing

In this paper we describe the application of statistical parameter estimation theory to the problem of locating weak seismic radiation sources in the lithosphere. The radiation may have two origins. The first is scattering generated by an earthquake or other type of source. These scattered seismic waves are to be extracted from the background primary waves. The other origin is a weak seismic emission in the medium. The problem of mapping of a weak seismic radiation source's spatial distribution on the basis of seismic array data processing is called seismic holography.

Theory

The seismic field $\xi(t, \vec{\rho})$ measured on the surface may be given as the sum of the "signal" field, produced by the source, located in the medium at point $\dot{r}$, and the residual field $\eta(t, \vec{\rho})$:

$$\xi(t, \vec{\rho}) = \int_{-\infty}^{+\infty} \mu s(t-\tau)\, G(\tau, \dot{r}, \vec{\rho})\, d\tau + \eta(t, \vec{\rho}) \tag{1}$$

where $\vec{\rho}$ is the point on the surface, $\mu s(t)$ is a scalar waveform generated by the source at point $\dot{r}$, $G(t, \dot{r}, \vec{\rho})$ is the Green function of the medium, and μ is a scaling factor. According to eq. (1), the multidimensional time series $\dot{x}_t = (\xi(t/f_s, \vec{\rho}_1), \ldots, \xi(t/f_s, \vec{\rho}_m))$ ($\dot{x}_t$ is a column vector) recorded by one-component array sensors has the following structure

$$\dot{x}_t = \sum_{\tau=0}^{\infty} \mu s_{t-\tau} \dot{h}_\tau(\dot{r}) + \vec{\eta}_t = \mu s_t^* \dot{h}_t(\dot{r}) + \vec{\eta}_t, \qquad (t \in \overline{1, N}) \tag{2}$$

where $s_t = s(t/f_s)$, $\dot{h}_\tau(\dot{r}) = G(\tau, \dot{r}, \vec{\rho}_i), i \in \overline{1, m}$ is a column vector of the medium's impulse response for the seismic wave propagating from the source at point $\dot{r}$ to the sensors at points $\vec{\rho}_i$; $\vec{\eta}_t$ is the "noise" time series, generated by other sources located away from point $\dot{r}$; f_s is the sampling rate and * denotes convolution. In the case of scattering, η_t contains strong components generated by the primary wave, and may therefore influence the estimation of scattered wave power.

In most cases there is no a priori information about the source waveform and the "noise" field features. So from a statistical point of view it is reasonable to assume the scalar process s_t and the vector process $\vec{\eta}_t$ to be realizations of Gaussian stationary time series with zero mean and power spectral densities $\phi(\lambda)$ and $\mathbf{F}(\lambda)$, respectively. Under the additional assumption that s_t and $\vec{\eta}_t$ are statistically independent, the matrix spectral density of the time series $\dot{x}_t$ becomes:

$$\mathbf{F}_x(\lambda,\theta) = \theta\phi(\lambda)\vec{h}_r(\lambda)\,\vec{h}_r^{\,*}(\lambda) + \mathbf{F}_\eta(\lambda), \quad \lambda \in [0, 2\pi]$$
$$\theta = \mu^2$$
$$\int_0^{2\pi} \phi(\lambda)\,d\lambda = 1 \tag{3}$$

where

$$\vec{h}_r(\lambda) = \sum_{t=0}^{\infty} \vec{h}_t(\vec{r})\,e^{i\lambda t}$$

is the vector response of the propagation paths from point r to the array sensors; θ is the power of the seismic source at point $\vec{r}$ and $\lambda = 2\pi f/f_s$ is a normalized frequency.

For simple reference models, $\vec{h}_r(\lambda)$ may be computed by solving the "direct" seismic problem. With reference model of the medium, we mean the model which determines the main features of the seismic wave propagation without accounting for the inhomogeneities which are to be detected by the analysis of the scattered waves. This means that in equation (2), we ignore the effect of secondary scattering of the seismic waves caused by the inhomogeneities.

Equations (2) and (3) allow consideration of the problem of locating seismic scatterers as the statistical problem of source power θ estimation, which is successively solved for each point of the "scanned" medium area (Troitsky *et al*, 1980). Under the assumption that the power spectra $\phi(\lambda)$ and $\mathbf{F}(\lambda)$ are known, statistically optimal algorithms may be proposed for this estimation problem. But in practice these assumptions are never fulfilled and these algorithms must be modified to make them efficient also when we do not have full information about statistical features of the observations.

Statistically optimal algorithms for estimation of the seismic source power θ may be developed using the maximum likelihood method (in its asymptotical modification). Using the Bartlett formula (Bartlett, 1951) for inversion of the matrix in equation (3), we obtain:

$$\mathbf{F}_x^{-1} = \mathbf{F}_\eta^{-1} - \mathbf{F}_\eta^{-1}\vec{h}\vec{h}^{*}\,\mathbf{F}_\eta^{-1}\,\frac{\theta\phi}{1+\vec{h}^{*}\,\mathbf{F}^{-1}\vec{h}} \tag{4}$$

For the maximum likelihood estimate $\hat{\theta}_N$ of the power of a seismic source, located at point $\vec{r}$, Kushnir (1989) shows that the following equation holds:

$$\sum_{j=1}^{N} \frac{\phi_j V_j^2}{1+\hat{\theta}_N\phi_j V_j}\left[\left(\frac{|Z_j|^2}{V_j^2} - \frac{1}{V_j}\right) - \hat{\theta}_N\phi_j\right] = 0 \tag{5}$$

where $\phi_j = \phi(\lambda_j)$, $Z_j = \vec{h}_r^{\dagger}(\lambda_j)\mathbf{F}_\eta^{-1}(\lambda_j)\vec{X}_j$, $V_j = V(\lambda_j)$, $V(\lambda) = \vec{h}_r^{\dagger}(\lambda)\mathbf{F}_\eta^{-1}(\lambda)\vec{h}_r(\lambda)$, $\vec{X}_j = (1/(\sqrt{N}))\sum_{j=1}^{N}\vec{x}_t e^{i\lambda_j t}$. $\lambda_j = 2\pi j/N$, N is the number of observations, and $\dagger$ denotes the Hermitian conjugation.

Equation (5) must in general be solved by numerical methods, but in some practically important cases the solution may be written in "closed" form. Namely, if the source power is much less than the "noise" power, then from (5) the following approximate solution may be obtained (Kushnir, 1989):

$$\tilde{\theta}_N = \frac{\sum_{j=1}^{N}\phi_j V_j\left(\frac{|Z_j|^2}{V_j^2} - \frac{1}{V_j}\right)}{\sum_{j=1}^{N}\phi_j^2 V_j^2} \tag{6}$$

This is a consistent and asymptotically normal estimate, but it has larger variance than the exact solution of equation (5).

Estimates based on solving equation (5) do not provide answers to the problem of mapping of scattered seismic radiation sources formulated in the introduction, because such estimates assume that the power spectrum $\mathbf{F}_\eta(\lambda)$ of the "noise" and source waveform power spectrum $\phi(\lambda)$ are known. It can be shown that the information about $\mathbf{F}_\eta(\lambda)$ is very important because $\mathbf{F}_\eta(\lambda)$ determines the statistical properties of all power θ estimators. When $\mathbf{F}_\eta(\lambda)$ is unknown, it is reasonable to use the adaptive approach. In that case, $\mathbf{F}_\eta(\lambda)$ in equations (5) and (6) is substituted by $\tilde{\mathbf{F}}_\eta(\lambda)$ derived from the observations themselves. But in the first of the problems outlined in the introduction, it is impossible to consistently estimate $\mathbf{F}_\eta(\lambda)$ from observations. Often the same is true for the second problem. Substituting for $\mathbf{F}_\eta(\lambda)$ in the expressions (5) and (6), any consistent estimate $\tilde{\mathbf{F}}_x(\lambda)$ of the matrix power spectrum of the observations $\vec{x}_t$ yields, values $\hat{\theta}_N$ and $\tilde{\theta}_N$ approaching zero in probability. In other words, adaptation of the estimates in expressions (5) and (6) is impossible.

Nevertheless, the solution of the problem under the assumption of full *a priori* information about the observations' statistical features is useful. It allows us to find the important statistic, which is contained in all statistically optimal algorithms for array data processing. This statistic is the output of the optimal group filter (OGF):

$$y_t = \vec{r}_t^{\,*}\vec{x}_t \qquad Y_j = \vec{R}(\lambda_j)\vec{x}_j \qquad t, j \in \overline{1, N}$$

where

$$\vec{R}(\lambda_j) = \frac{\vec{Z}_j}{V_j} = \frac{\vec{h}^{\,\dagger}(\lambda_j)\,\mathbf{F}_\eta^{-1}(\lambda_j)}{\vec{h}^{\,\dagger}(\lambda_j)\,\mathbf{F}_\eta^{-1}(\lambda_j)\,\vec{h}(\lambda_j)} \tag{7}$$

$$\vec{r}_t = (1/(2\pi)) \int_0^{2\pi} \vec{R}(\lambda)\, e^{i\lambda t} d\lambda$$

If the input time series $\vec{x}_t$ fits the observational model (2), (3), then it is easy to show that the filter $\vec{R}(\lambda)$ minimizes the mean square value of the output noise component provided the signal component is undistorted. The remarkable feature of the filter $\vec{R}(\lambda)$ is that replacement in the expression (7) of the unknown spectral matrix $\mathbf{F}_\eta(\lambda)$ of the noise by the spectral matrix $\mathbf{F}_x(\lambda)$ of the observations, does not change its output: it keeps the signal undistorted and minimizes the noise component power. The new filter

$$\vec{K}(\lambda) = \frac{\vec{h}^{\,\dagger}(\lambda)\,\mathbf{F}_x^{-1}(\lambda)}{\vec{h}^{\,\dagger}(\lambda)\,\mathbf{F}_x^{-1}(\lambda)\,\vec{h}(\lambda)} \tag{8}$$

is equivalent to the filter given by equation (7). This can be shown using Bartlett's formula (4). Due to this property, each statistic, depending only on the output of OGF, has the adaptive feature. This means that in this statistic we may substitute instead of the unknown noise matrix power spectrum $\mathbf{F}_\eta(\lambda)$ any consistent estimate $\tilde{\mathbf{F}}_X(\lambda)$ of the matrix power spectrum of the observations $\vec{x}_t$, thus providing the adaptive (AOGF) filter $\hat{K}(\lambda)$.

Let us now consider some practically interesting modifications of OGF $\vec{R}(\lambda)$. In the case when the noise field mainly consists of coherent primary waves, generated by a seismic source, the matrix spectrum $\mathbf{F}_\eta(\lambda)$ may be written in the form:

$$\mathbf{F}_\eta(\lambda) = \varepsilon \mathbf{F}_g(\lambda) + \psi(\lambda)\,\vec{q}(\lambda)\;\vec{q}^{\,\dagger}(\lambda) \tag{9}$$

where $\mathbf{F}_g(\lambda)$ is the matrix power spectrum of the "diffuse noise" component, ε is a scaling factor, $\psi(\lambda)$ is the scalar power spectrum of the primary waveform, and $\vec{q}(\lambda) = (q_e(\lambda), 1 \in \overline{1,m})$ is the frequency response of the medium for the primary wave paths from the source to the array sensors. Using the Bartlett formula (4) it is easy to show that for the matrix spectrum (9), OGF $\vec{R}(\lambda)$ has the form:

$$\vec{R}(\lambda) = \vec{R}_o(\lambda) + \vec{o}_\lambda(\varepsilon), \qquad \vec{R}_o(\lambda) = \frac{\vec{h}^{\dagger}(\lambda)\,\mathbf{B}(\lambda)}{\vec{h}^{\dagger}(\lambda)\,\mathbf{B}(\lambda)\,\vec{h}(\lambda)} \tag{10}$$

where

$$\mathbf{B}(\lambda) = \left(I - \frac{\vec{q}(\lambda)\;\vec{q}^{\,\dagger}(\lambda)}{|\vec{q}(\lambda)^2|}\right), \qquad \|\vec{o}_\lambda(\varepsilon)\| \to 0 \quad \text{if } \varepsilon \to 0$$

I is the identity matrix.

$\|\vec{f}(\lambda)\|$ is the norm of the vector function $\vec{f}$. So if the "diffuse" components of the noise and signal fields are weak and hence the matrices $\mathbf{F}_\eta^{-1}(\lambda)$ and $\mathbf{F}_x^{-1}(\lambda)$ are close to singular, it is reasonable to use the stable form of OGF with frequency response $\vec{R}_o(\lambda)$.

In the opposite particular case, when the noise field is purely "diffuse", i.e., it may be modeled as white noise, the matrix power spectrum $\mathbf{F}_\eta(\lambda) = \sigma^2(\lambda)\mathbf{I}$ and

$$\vec{R}(\lambda) = \frac{\vec{h}^{\,\dagger}(\lambda)}{|\vec{h}(\lambda)|^2} = \vec{\Gamma}(\lambda) \tag{11}$$

The undistorted group filter $\vec{\Gamma}(\lambda)$ is the mathematical expression for the conventional algorithm of seismic holography (Troitsky, et al, 1980), comprising the "focusing of rays" radiated from a given point $\vec{r}$ of the scanned medium area. It compensates for the phase and amplitude distortions of the array records caused by the wave propagation from the source to the array sensors.

Let us consider the dispersion $\delta_N^2 = \frac{1}{N}\sum_{t=1}^{N} y_t^2$ of the group filter $\vec{R}_o(\lambda)$ output $y_t, t \in \overline{1,N}$. In case the input $\vec{x}_t$ has a matrix power spectrum described by the formulas (3) and (9), the property of the matrix $\mathbf{B}(\lambda)$: $\mathbf{B}(\lambda)\vec{q}(\lambda) \equiv 0$ yields:

$$P - \lim_{N\to\infty} \delta_N^2 = \theta + \beta_\varepsilon \tag{12}$$

where $\beta_\varepsilon \to 0$ if $\varepsilon \to 0$. So if the "diffuse" noise (caused, particularly, by scatterers located away from point $\vec{r}$) is small enough, the statistic δ_N^2 provides a consistent estimate of the scattered wave source power, thus suppressing the array noise generated by the primary wave. The OGF $K(\lambda)$ (8) has the same important feature. And, finally, it is clear that the relation (12) is valid for the adaptive filter $\vec{K}(\lambda)$.

Thus, in the case of coherent noise, the problem of consistent estimation of the seismic wave power radiated from point $\vec{r}$ can be solved rather effectively by using OGF $\vec{R}_0(\lambda)$ or AOGF $\hat{K}(\lambda)$.

At the same time, the conventional holographic group filter $\vec{\Gamma}(\lambda)$ cannot suppress the coherent noise and does not provide a consistent estimator of the seismic wave power radiated from point $\vec{r}$.This is so because the dispersion of the holographic filter $\vec{\Gamma}(\lambda)$ output (when the input $\vec{x}_t$ matrix power spectrum is defined by (3) and (9)) does not tend to the seismic wave power radiated from the point $\vec{r}$ when the "diffuse" noise component decreases.

Results of simulation

The benefits of using the optimal statistical algorithms for mapping of scattered wave sources have been analyzed by computer modeling. The records of a Hindu Kush earthquake on 22 February 1972 with magnitude 5.6 recorded by NORSAR have been used in this modeling. To check the algorithm's capability to process data recorded at arrays with

a small number of sensors and a small aperture, the six sensors of the central NORSAR subarray 01A have been chosen. The location of these sensors are shown in Fig. 7.1.1, and a record of the Hindu Kush earthquake is shown in Fig. 7.1.2.

The numerical experiments consisted of processing data from the six sensors of the central NORSAR subarray 01A. The data were composed as a sum of primary and scattered waves. As primary waves we have tested two cases: 1) observed array records of the Hindu Kush earthquake; 2) A plane P-wave with an apparent velocity and azimuth corresponding to that of the Hindu Kush earthquake. The modelling of this plane wave was done to check how the deviation from a plane wavefront affects the quality of the seismic holography algorithms. The scattered wave was simulated as a P-wave radiated from a point source located in a homogeneous medium 4 km beneath the NORSAR central subarray. The source waveform s_t of the simulated scattered wave was synthesized as a sample function of the stationary Gaussian random process with power spectrum estimated using the Hindu Kush earthquake P-wave record.

In Figs. 7.1.3-7.1.5 the results from processing four different data sets are depicted. The array data sets were the following:

a. The simulated plane wave from the Hindu Kush direction

b. The sum of a) and the simulated scattered wave from the point source beneath NORSAR

c. The original Hindu Kush earthquake records

d. The sum of c) and the simulated scattered wave from the point source beneath NORSAR.

The power of the scattered wave was equal to that of the primary wave.

In each of the four experiments the array signals were processed by the following algorithms: a) the conventional algorithm of seismic holography based on the filter $\vec{\Gamma}(\lambda)$ (11); b) the statistical algorithm based on the adaptive group optimal filter $\vec{K}(\lambda)$ (8) with the power spectral density inverse matrix $\mathbf{F}_x^{-1}(\lambda)$ estimated by the multidimensional autoregressive modeling of the observations $\dot{x}_t$; c) the statistical algorithm based on the undistorted group filter $\vec{R}_o(\lambda)$ (10), in which the vector $\dot{q}(\lambda)$ was chosen in correspondence with the plane wave with the azimuth and apparent velocity of the Hindu Kush earthquake P-wave.

The data processing procedure consisted of scanning, with steps of 0.8 km an 8 x 8 km plane parallel to the surface containing the scattered wave source in the central point. For each point scanned, the medium frequency response vector $\vec{h}_r(\lambda)$ was computed under the assumption of medium homogeneity. By this, the adjustment of the group filters for the extraction of the scattered wave radiated from the given point was provided. Then the filter output signals and their dispersion estimates were computed. As was pointed out, the dispersion of the outputs of all filters under investigation may be used as the estimates of the scattered wave power radiated from the given point. These estimates are biased because of primary wave power "leakage", and these biases have different values for the different filters.

The number of samples of the input vector time series $\hat{x}_t$ was as a rule equal to 128 in these experiments, and corresponded to the Hindu Kush earthquake P-wave record length. The matrix power spectrum $\mathbf{F}_x(\lambda)$ of the observations $\hat{x}_t$ used for the undistorting group filter adaptation was estimated by multivariate AR-modeling of order 5.

In Figs. 7.1.3-7.1.5 the scattered radiation power maps are depicted. They are calculated as the results of the numerical experiments described, with the conventional holographic filter (11) (Fig. 7.1.3), with the adaptive optimal group filter (7) (Fig. 7.1.4), and with the "spatial rejecting" filter (10) which uses the a priori information concerning the propagation direction of the primary wave (Fig. 7.1.5).

In these figures, the maps with label (a) are the results for the single simulated primary wave processing, with label (b) the results for the sum of the simulated primary wave and the simulated scattered wave processing, with label (c) the results for the Hindu Kush earthquake P-wave processing, and with label (d), the results for the sum of the Hindu Kush earthquake P-wave and simulated scattered wave processing.

Comparison of the maps in Fig. 7.1.3 shows that the conventional algorithm of seismic holography applied to processing of data from arrays with a small aperture and small number of sensors does not provide detection of the scattered wave. This may be explained by the effect of the primary wave power "leakage", practically evenly strong for all points of the scanned area. At the same time, as it is seen from Figs. 7.1.4 and 7.1.5, the statistical seismic holography algorithms provide strong peaks in the power maps, the maxima of which coincide with the point of the scattered wave source location. The explanation may be that the mentioned algorithms are capable of suppressing "leakage" by the mutual compensation of primary wave components at the different array sensors. The adaptive and "a priori" algorithms demonstrate the same ability for the suppression of the primary wave "leakage" and location of the scattered wave source, while in the case of detection of the scattered wave on the background of the Hindu Kush earthquake, the adaptive optimal group filter (Fig. 7.1.4d) has appeared more effective than the "a priori" filter (Fig. 7.1.5d). The advantage of the optimal group filter over an "a priori" filter in this experiment may be explained by the deviations of the Hindu Kush earthquake signal from a plane wave. This deviation significantly reduces the performance of the filter $\hat{R}_o(\lambda)$ (10). At the same time, for the adaptive filter $\hat{K}(\lambda)$ no assumptions are needed about the primary wave front shape, which makes it more flexible and effective.

A.F. Kushnir, E.A. Gulko, MITPAN, Moscow

References

Bartlett, M.S. (1951): An inverse matrix adjustment arising in discriminant analysis, *Ann. Math. Stat.*, Vol 22, No 1.

Kushnir, A.F. (1989): Parametric methods of geophysical time series statistical analysis. Dr. of Science Dissertation Thesis, Inst. of Physics of the Earth, USSR Academy of Sciences, Moscow.

Troitsky, P.N., E.S. Husebye and A.V. Nikolaev (1980): Nature, vol. 5, no. 284, 618-623.

Voievodin, V.V., and U.D. Kuznetsov (1984): Matrices and computational problems, M: Nauka, 318 pp (in Russian).

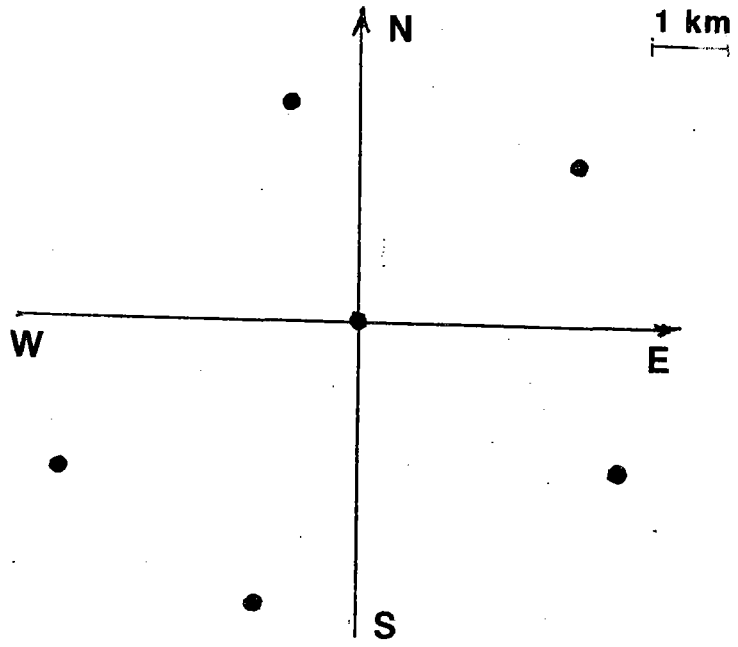

Fig. 7.1.1. NORSAR central subarray (01A) geometry.

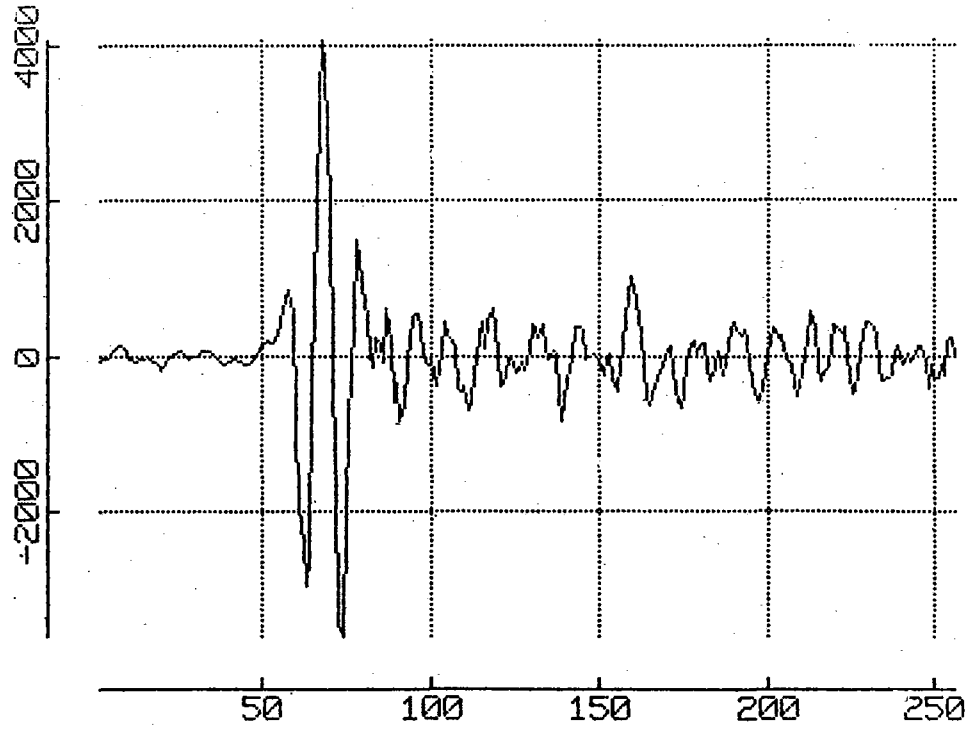

Fig. 7.1.2. Hindu Kush earthquake recordings at subarray 01A.

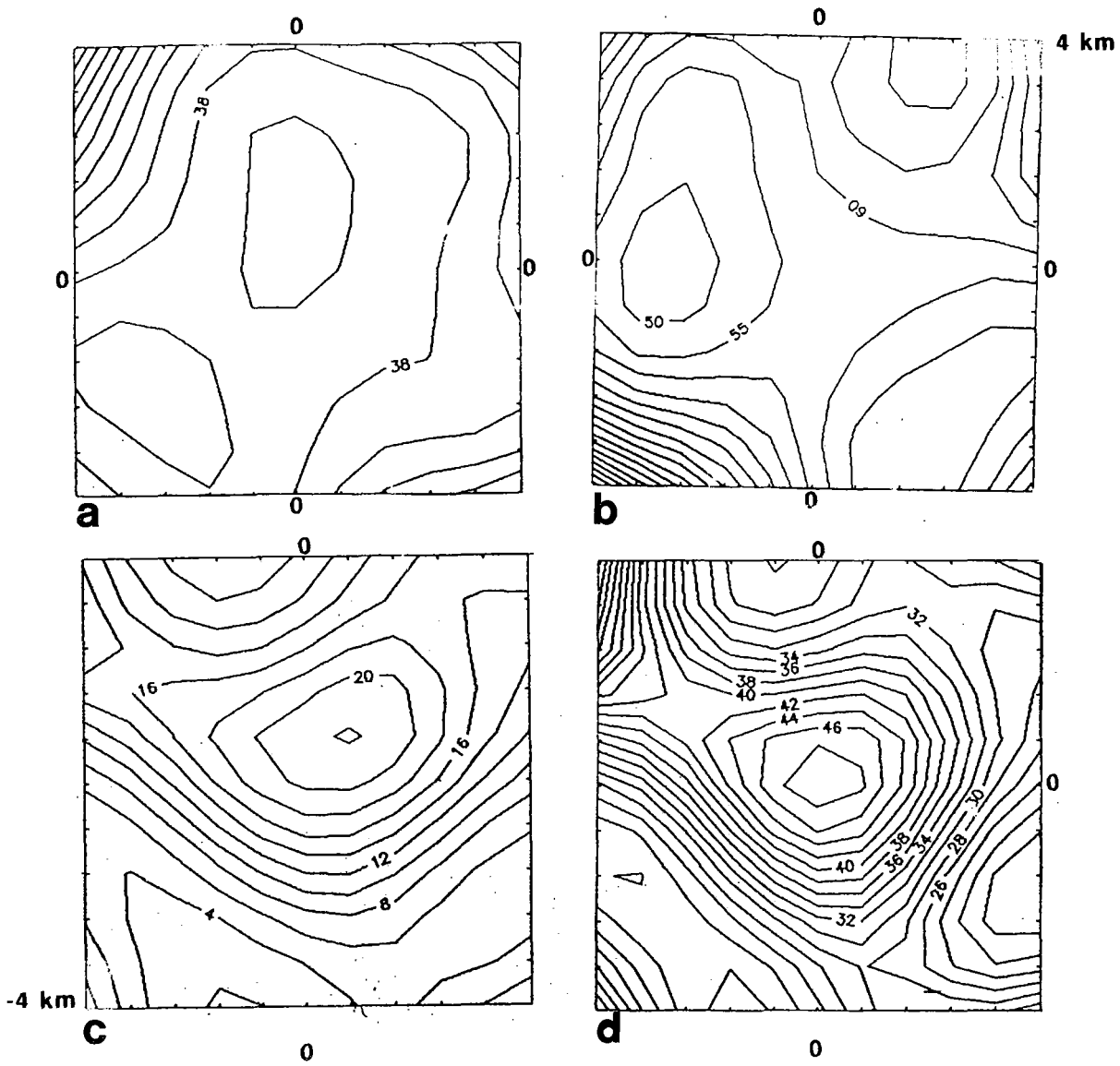

Fig. 7.1.3. Array data processing using conventional holographic group filter. (a) Simulated plane wave from earthquake; (b) simulated earthquake plane wave + simulated scattered wave; (c) P-wave of the Hindu Kush earthquake; (d) Hindu Kush earthquake P-wave + simulated scattered wave. The contour levels reflect the estimated power of waves arriving from different points of the scanned plane. The power estimates are *not* normalized, hence only relative values within each map should be considered.

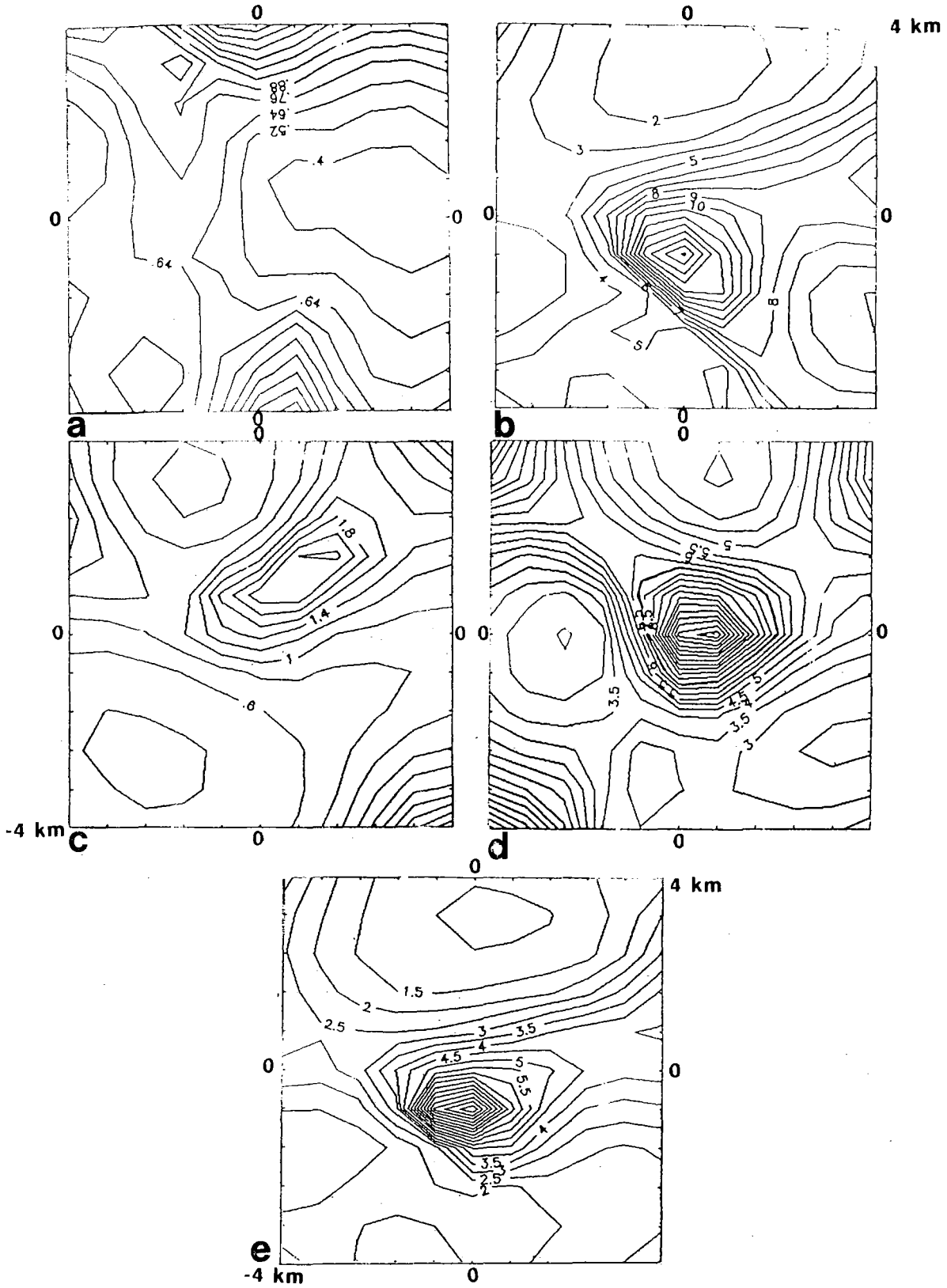

Fig. 7.1.4. Array data processing using adaptive optimal group filter: (a) Simulated plane wave from earthquake; (b) Simulated earthquake plane wave + simulated scattered wave; (c) P-wave of the Hindu Kush earthquake; (d) Hindu Kush earthquake P-wave + simulated scattered wave; (e) the same as (b) but for N=1024, p=10.

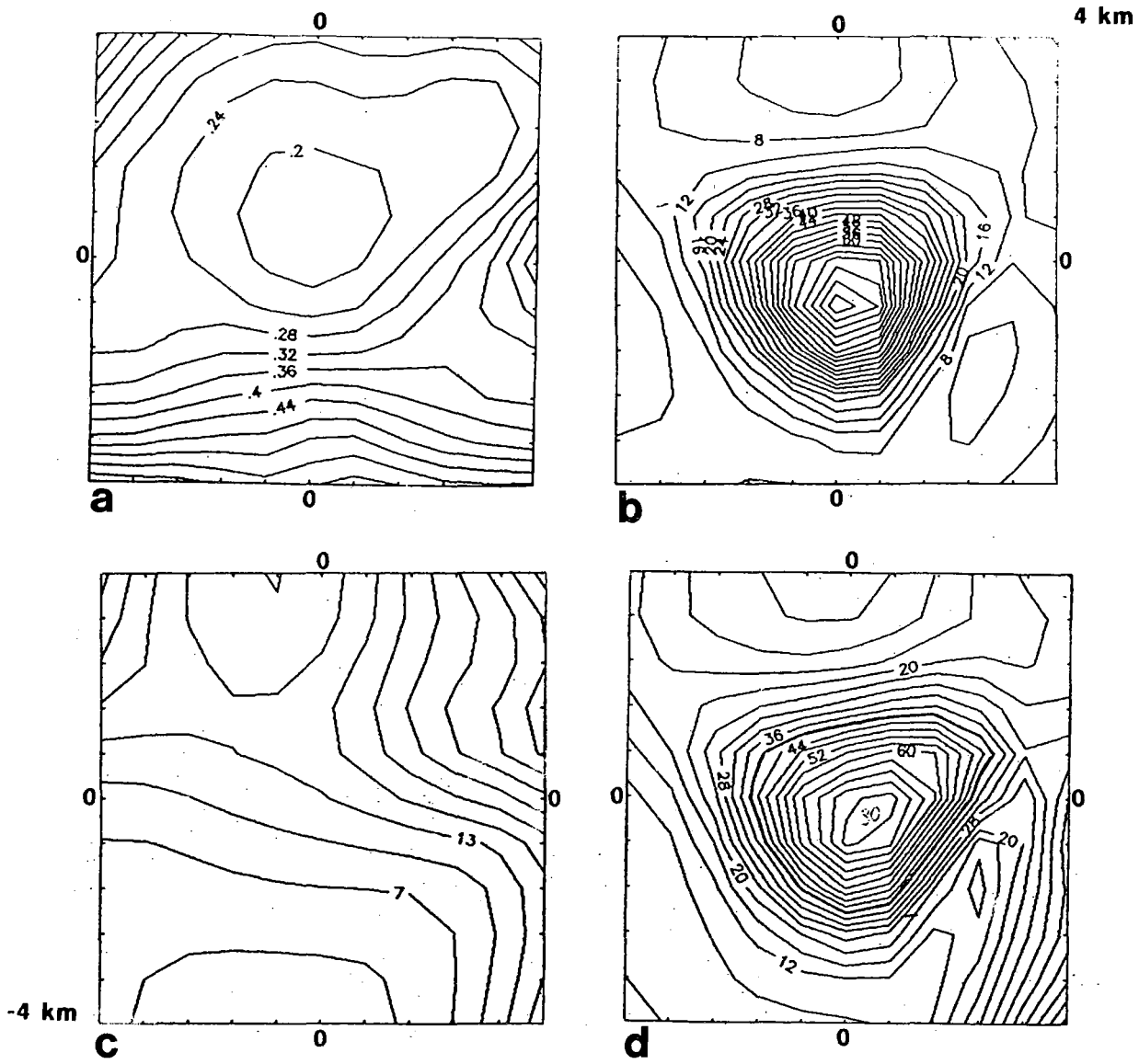

Fig. 7.1.5. Array data processing using spatial rejecting filter: (a) Simulated plane wave from earthquake; (b) Simulated earthquake plane wave + simulated scattered wave; (c) P-wave of the Hindu Kush earthquake; (d) Hindu Kush earthquake P-wave + simulated scattered wave.

7.2 A new ML scheme for 3-component slowness estimation which incorporates the crustal transfer function

Background

Efforts to exploit the wavefield information contained in the records of 3-component (3C) seismometers, say in terms of polarization characteristics, slowness vectors and other types of signal attributes, have until recently been less successful in the high frequency band 1-100 Hz. This problem has to a large extent been overcome by introducing flexible particle motion models in combination with effective maximum likelihood (ML) schemes for signal parameter estimation from 3C recordings (Christoffersson et al, 1988; Roberts et al, 1989; and Roberts and Christoffersson, 1990). Their techniques allow us to produce quite precise automatic preliminary bulletins for single 3C (digital) stations (Ruud and Husebye, 1991). A potential flaw in the above and similar techniques is that the response of the crust beneath the receiver is not incorporated in the signal model. However, recently Kennett (1991) suggested a new approach for decomposing the 3C seismograms of P, SV and SH waves incident onto the free surface by assuming that the slowness vector and the layered crustal structure beneath the station are known. A similar method can in principle be used for solving the inverse problem, and this is the subject dealt with here.

Method

The problem is that of estimating the azimuth φ and horizontal slowness p of the plane P-wave incident onto the layered structure below the free surface. In mathematical form, the model of our 3C recordings can be written as:

$$\bar{u}(\omega) = f(\omega_j)\,\bar{h}(\omega_j, \bar{s}, \bar{m}) + \bar{n}(\omega_j) \qquad (1)$$

where $\bar{u}(\omega_j) = [u_N, u_E, u_Z]^T$ is the vector of discrete Fourier amplitudes at angular frequency ω_j for the individual recording components (NS, EW, Z) calculated for a time window containing the signal; $f(\omega_j)$ is the product of the incoming signal amplitude and the seismometer frequency response; $\bar{h}(\omega_j, \bar{s}, \bar{m}) = (h_N, h_E, h_Z)^T$ is the crustal transfer function for an incoming P-wave at frequency $f(\omega_j)$ for slowness vector $\bar{s}(\varphi, p)$, and the presumed known crustal structure given by the model vector $\bar{m}$; $\bar{n}(\omega_j) = (n_N, n_E, n_Z)^T$ is the noise vector and T means transposed. Assuming the noise is Gaussian and uncorrelated at different frequencies, then $E(\bar{n}_k, \bar{n}_j^{\,*}) = \delta_{kj} C_j$ where E is mathematical expectation, the asterisk * implies Hermitian conjugation and δ_{jk} is the Kronecker delta symbol. With the above assumption it can be shown that the maximum likelihood (ML) functional will be

$$L = 1/2 \sum_j \ln(\det C_j) - 1/2 \sum_j (\bar{u}_j - f_j\bar{h}_j)^* C_j^{-1} (\bar{u}_j - f_j\bar{h}_j) \qquad (2)$$

where the summation is over N discrete frequencies in the selected signal bandwidth. L depends not only on the useful (informational) unknown parameters φ and p of the slowness vector, but also on the unknown regressor parameters $f(\omega_j)$. The ML estimates derived by maximization of the L functional (2) with respect to all unknown parameters will for a constant number of nuisance parameters $f(\omega_j)$ but an increasing sample size be

asymptotically optimal estimates of the useful slowness vector parameters (Kushnir and Lokshtanov, 1988).

Presuming $\bar{s}(\varphi,p)$ is fixed, $\bar{m}$ is known a priori and that the noise is orthogonal between components and with equal power at all components and frequencies, i.e., $C_j = \sigma^2 I$ (I is the identity matrix), the maximum of L with respect to f_j is achieved at the points

$$f_j = \bar{h}_j^* \bar{u}_j / \bar{h}_j^* \bar{h}_j \tag{3}$$

By substituting the f_j here into (2) we have that the ML estimates of the informational parameters can be obtained by minimizing the following functional

$$\Theta(\varphi,p) = \sum_j \left\| \bar{u}_j - \bar{h}_j (\bar{h}_j^* \bar{u}_j) / \bar{h}_j^* \bar{h}_j \right\|^2 \tag{4}$$

Now the functional (4) depends only on the observations $\bar{u}_j$ and the informational parameters φ, p.

By using normalized transfer functions in the formula (4), i.e., $\bar{g}_j = \bar{h}_j / (\bar{h}_j^* \bar{h}_j)^{1/2}$ we obtain

$$\Theta(\varphi,p) = \sum_j [\bar{u}_j^* \bar{u}_j - (\bar{g}_j^* \bar{u}_j)^* (\bar{g}_j^* \bar{u}_j)] \tag{5}$$

Thus minimizing (4) is equivalent to maximizing the sum of squares of projections of our observational vectors $\bar{u}_j$ onto the theoretical directions determined by the model vectors $\bar{g}_j$.

The ratio of the projected to the observed energy in the selected frequency band

$$QL = \sum_j [(\bar{g}_j^* \bar{u}_j)^* (\bar{g}_j^* \bar{u}_j)] / \sum_j (\bar{u}_j^* \bar{u}) \tag{6}$$

can be used as a quality measure of our estimation. For example, if we have pure signal, $\bar{n}_j = 0$ for all j in eq. (1), then QL will be equal to 1. When $\bar{n}_j$ increases, QL will decrease.

The above slowness estimation technique is described in detail in a paper by Lokshtanov et al (1991), which also includes its extension to an array of M 3C stations presuming $\bar{s}_i$ and $\bar{n}_i$ to be identical.

Results -- velocity analysis of NORESS events

For the frequency band of interest for our analysis (1-15 Hz) the most important part of the crust would be the upper 5 km as conversion and/or reflections from deeper layers will be separated in time from the primary phase. To our knowledge the only available information on vertical velocity structures in this part of the crust comes from a study of Lokshtanov et al (1991), where upper crust velocity models were found by inversion of short period Rayleigh wave fundamental mode phase velocity measurements from NORSAR subarrays. Their results suggest an upper low velocity layer about 1 km thick or alternatively a two-layer model over a half space. Model parameters are given in Table 7.2.1

together with those for uniform velocity halfspace model. For comparison all three models have been used in the analysis of the event examples, and in the result presentation below they are referred to as the halfspace, one-layer and two-layer models.

Analysis procedure: The analysis was performed both for the central single 3C station and for the array of four 3C stations. After azimuth was determined, the maximum of the quality parameter QL and the corresponding apparent velocity was found by searching over a predefined slowness interval. The results are presented for a sliding time window with 20% cosine tapering and with an updating interval of 1/10 of the window length. The reference time for the estimated signal attributes is for the center of the time window.

Event 1 -- Teleseismic earthquake (Hindu Kush). This event, shown in Fig. 7.2.1, has a very high SNR and is dominated by relatively low frequency energy. The signal has an emergent onset and it starts at 9.2 s on the given time scale. The length of the sliding time window was 2 s and the analyzed frequencies are from 0.5 to 5.0 Hz. The QL-values rise as soon as the window moves into the signal and stay close to 1.0 well into the signal. Only for the velocity estimation do we find significant differences for the three models. The estimates for the layered models are quite stable and close to the expected velocity for an event at this distance (13.9 km/s). In contrast, the halfspace models give estimates biased towards high velocity -- static corrections can offset part of the bias. Regarding azimuth estimation, both the single station and the array estimates are biased relative to the expected azimuth of 96^0 (about 10^0 for the array and 15^0 for single station).

Event 2 -- Local explosion (SE Norway). The window length is here 1 s and the analyzed frequency band is from 6 to 12 Hz. As seen from Fig. 7.2.2 the QL-values are also much lower for this event and in particular for the array where the signal correlation between stations is almost lost soon after the onset. For the three models a clear model dependency is seen in the velocity estimation for the single station. For the array it seems that the kinematic properties of the wavefield, i.e., phase shift between identical components at different stations, serves to stabilize the velocity estimates. This effect is hardly seen for the teleseismic event where the low signal frequencies result in much smaller phase shifts between stations. For the later part of the signal (after 10.0 s), the velocities are very high both for the array and the single station. By vespagram analysis of all the vertical NORESS sensors, we also find high velocities in this time interval (9-10 km/s) although not as high as for the 3C processing.

Discussion

For the uniform halfspace model the transfer function is frequency dependent and our estimation method becomes similar to previous techniques, e.g., Esmersoy et al (1986). Although the inclusion of layered structures clearly improved the estimated velocities, we do not obtain a corresponding improvement of the quality parameter QL which measures how well the observed data fit our signal model. The reason for this seems to be that the layered models affect mainly the ratio of the radial to the vertical amplitudes, while phase differences between components remain small -- everywhere within 30 from that of the halfspace. From the given examples and from general experience with the method it is seen that analysis of high frequency signals is relatively less successful than for low fre-

quencies. An explanation here might be that the models used are not adequate at high frequencies -- being derived from Rg waves at periods from 0.7 to 1.7 s -- and/or that lateral variations are highly significant.

In conclusion, we have here demonstrated the importance of incorporating the crustal transfer in 3C analysis methods to ensure accurate estimates of P-wave slowness -- the technique will be extended to analysis of SV and SH waves.

E.S. Husebye
B.O. Ruud, Oslo University
D.E. Lokshtanov, Norsk Hydro

References

Cassidy, F., A. Christoffersson, E.S. Husebye and B.O. Ruud (1990): Robust and reliable techniques for epicenter location using time and slowness observations, *Bull. Seism. Soc. Am.*, 80, 140-149.

Christoffersson, A., E.S. Husebye and S.F. Ingate (1988): Wavefield decomposition using ML probabilities in modelling single site 3-component records, *Geophys. J.*, 93, 197-213.

Esmersoy, C., V. Cormier and M.N. Toksöz (1985): Three-component array processing, in: *The VELA Program: A Twenty-five year review of basic research*, ed. A.U. Kerr, DARPA, Washington D.C., 565-578.

Husebye, E.S. and B.O. Ruud (1989): Array seismology -- Past, present and future developments, in: *Observatory Seismology*, ed. J.J. Liteheiser, Berkeley Univ. Press, Berkeley, California, 123-153.

Kennett, B.L.N. (1991): The removal of free surface interactions from three-component seismograms, *Geophys. J. Int.*, 104, 153-163.

Lokshtanov, D.E. and A.V. Trusov (1988): Determination of crustal velocity structure between the NARS-s stations, *Comput. Seism.*, 22, 153-160, Allerton Press.

Lokshtanov, D.E., B.O. Ruud and E.S. Husebye (1991a): The upper crust low velocity layer: a Rayleigh (Rg) phase velocity study from SE Norway, *Terra Nova*, 3, 49-56.

Lokshtanov, D.E., B.O. Ruud and E.S. Husebye (1991b): The crustal transfer function in seismic 3-component slowness estimation, Geophys. Res. Lett., 18, 1393-1396.

Roberts, R.G. and A. Christoffersson (1990): Decomposition of complex single-station three-component seismograms, *Geophys. J. Int.*, 103, 57-74.

Roberts, R.G., A. Christoffersson and F. Cassidy (1989): Real time event detection, phase identification and source location estimation using single station three component data, *Geophys. J.R. Astr. Soc.*, 471-480.

Ruud, B.O. and E.S. Husebye (1991): A new three-component station detector and automatic single station bulletin production, *Bull. Seism. Soc. Am.* in press.

Ruud, B.O., E.S. Husebye, S.F. Ingate and A. Christoffersson (1988): Event location at any distance using seismic data from a single three-component station, *Bull. Seism. Soc. Am.*, 78, 308-325.

	Model	P-vel. (km/s)	S-vel. (km/s)	Density (g/cm^3)	Thickness (km)
1	1-layer	5.10	2.95	2.60	0.92
	halfspace	6.14	3.55	2.70	∞
2	2-layer	4.93	2.85	2.60	0.5
		5.40	3.12	2.60	0.5
	halfspace	6.12	3.54	2.70	∞
3	halfspace	5.9	3.14	2.60	∞

Table 7.2.1. The crustal models used in analysis. Model 1 and 2 are based on Rayleigh (Rg) dispersion analysis as reported by Lokshtanov et al (1991).

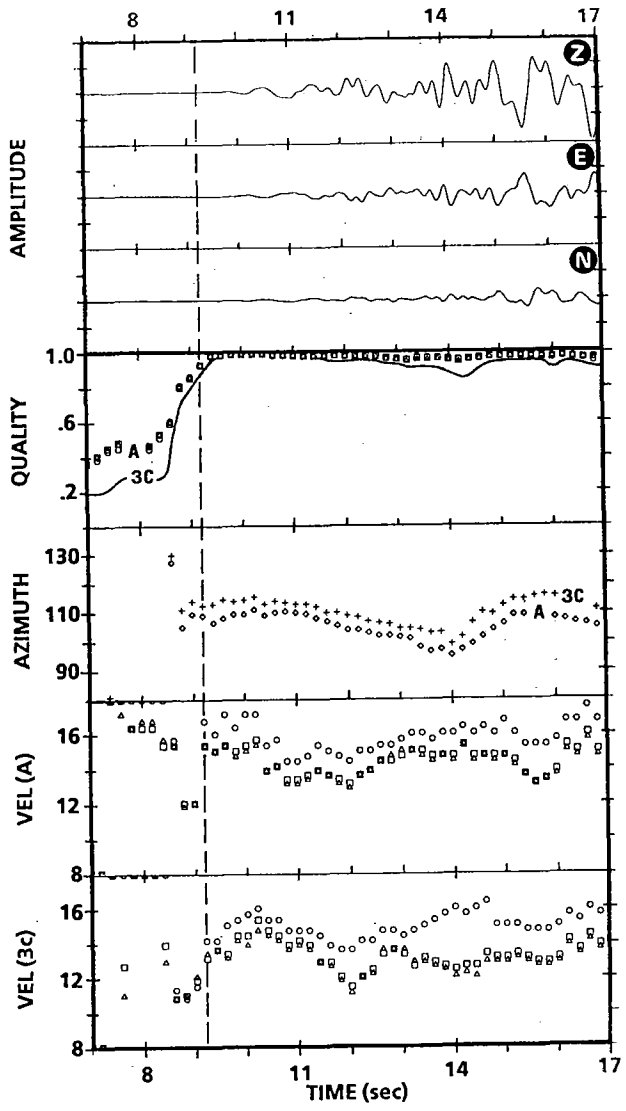

Fig. 7.2.1. Analysis results for Event 1 (Earthquake, Hindu Kush, July 29, 1985, origin time 07:54:44.5, backazimuth 95.7, distance 44.2). Processing parameters are given in text. From top and down the figure shows 3C seismograms (Z,E,N), quality parameter, azimuth, apparent velocity for the array of four 3C stations and apparent velocity for the single central 3C station. For quality and velocity the results for the three models are given with different symbols: circle (O) for halfspace, triangle (Δ) for one-layer and square (□) for the two-layer model. The model independent azimuth estimates are shown with plus (+) for single station and diamond (◊) for the 3C array. For quality the results for single 3C and 3C array are shown in the same diagram and are identified with "3C" and "A" respectively.

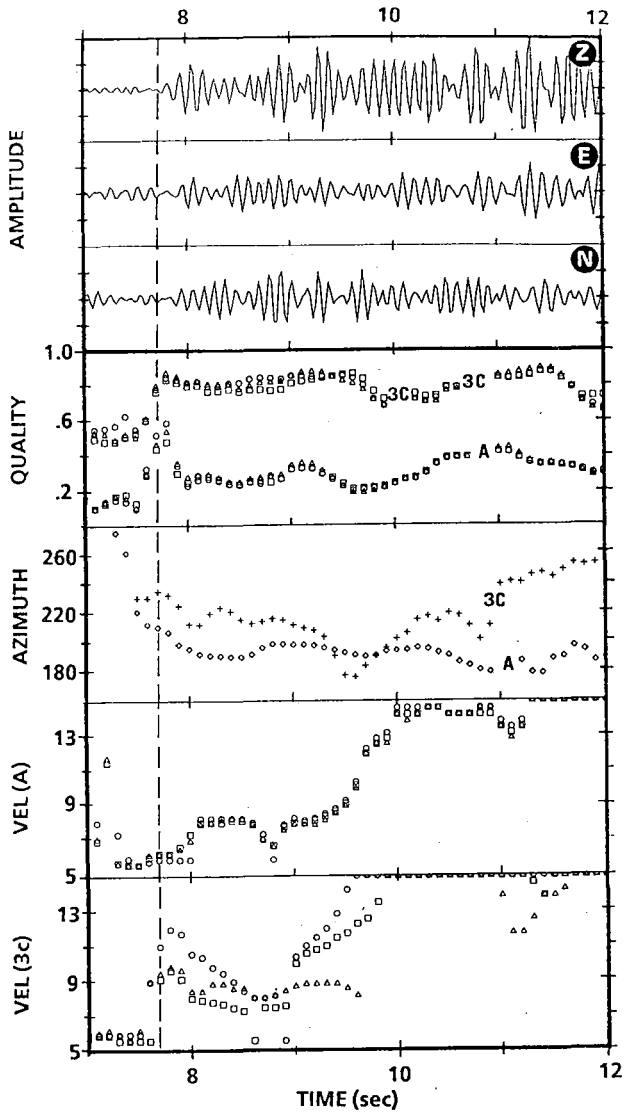

Fig. 7.2.2. Analysis results for Event 2 (Local explosion SE Norway, July 19, 1989, origin time approx. 11:17:50). Processing parameters are given in text. Figure layout and symbols as for Fig. 7.2.1.

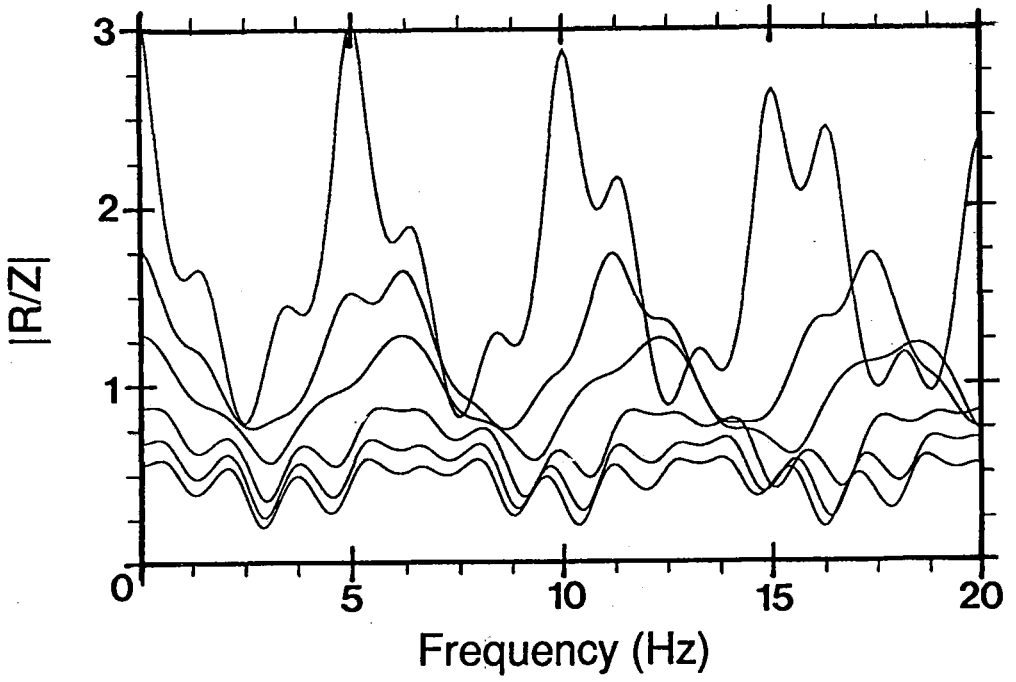

Fig. 7.2.3. Computed radial-to-vertical component amplitude ratio as a function of frequency for the one-layer over halfspace model in Table 7.2.1. Counted from the top of the six curves are for apparent velocities of 6, 7, 8 10, 12 and 14 km/s respectively. The corresponding phase shifts between components are within 30 from that of a halfspace model for all frequencies.The strong frequency dependence of the amplitude ratio illustrates the need for correcting velocity estimates for the effect of upper crustal layering.

7.3 On-line detection using adaptive statistically optimal algorithms

Background

In a series of reports (Pisarenko et al, 1987; Kushnir et al, 1989, 1990, 1991), the use of adaptive optimal group filtering (AOGF) for the wideband estimation of seismic signals has been investigated. The method includes autoregressive adaptation to the current noise matrix power spectrum and yields improved noise suppression compared to conventional beamforming, especially at low frequencies where noise power and coherency is highest.

The processes have been implemented in the NORSAR Event Processor (EP) program Package (Fyen, 1989; Kushnir et al, 1991), and comprise adaptive group filtering (AOGF), optimal detection (OD) and optimal onset time estimation (OE).

The main advantage of this signal estimation technique is that it retains an undisturbed signal waveform over a wide frequency band (0.2-5.0 Hz), allowing us to detect and identify signals at frequencies where the noise coherency and power are the greatest. Moreover, when the final decision is to be made on whether the estimated signal is from an earthquake or explosion source, it is important to have a wide-band undisturbed estimate of the signals for discrimination.

The conventional beamforming as an estimator of the signal is together with bandpass filtering a simple and quick process which allows us to detect most interesting signals. However, due to high noise coherence for small arrays, this estimate of the signal will be distorted.

The scope of this report is to analyze the AOGF and OD for the purpose of using the methods in online processing, i.e., continuous processing of all incoming data for a small aperture array like NORESS and ARCESS.

To use AOGF we must do autoregressive adaptation to the noise using a certain time window and a given apparent velocity and azimuth.

We therefore need to investigate how often we need to adapt to the noise and determine how many different aiming points in slowness space we need to be able to detect the signals. Moreover, since the optimal detector (OD) is very sensitive, the threshold to use for acceptable false alarm rates must be carefully considered.

Automatic Regional Array Processing

The current on-line detection system uses the STA/LTA detector on conventional bandpass filtered array beams. A large number of different slownesses are used, combined with a number of bandpass filters. The array beams are formed using combinations of sub-geometries of the array.

Considerable gain in noise suppression is obtained by utilizing the negative correlation of the noise wavefield at certain frequencies and inter-sensor distances (Mykkeltveit et al, 1990).

Although the conventional beamforming, filtering and STA/LTA detector scheme work very well, requiring small computer power, there are a few problems that make it reasonable to evaluate the more costly statistical optimal algorithms (SOA) as an alternative online process tool.

1. The STA/LTA detector thresholds and bandpass filters are fixed, so contrary to SOA, it may not take into account the temporary variations in noise coherency and spectrum.
2. As shown by Fyen (1986) and Mykkeltveit et al (1990), the conventional beamforming provides less than $\sqrt{N}$ noise suppression for frequencies below 1 Hz. Therefore the conventional beam detector is used for frequencies only above 1 Hz.
3. The statistical assumptions for the STA/LTA detector to be optimal are not satisfied, which may lead to excessive false alarms and missed detections. The AOGF and OD are based on noise characteristics that better describe the real situation.

We shall here discuss separately the implementation of two algorithms: adaptive statistically optimal group filter (AOGF), here also referred to as adaptive beamformer (AB), and statistically optimal scalar detector (OD), having in mind that the two will be combined as a two-step detector system.

Time consumption for the detector based on AOGF. Broad band AB deployment.

The AOGF procedure consists of two steps: adaptation and filtering. Adaptation is the most time consuming and is not realizable in real time (without changing to a recursive adaptive beamformer).

To compute the covariance matrix function and the vector of filter coefficients now takes approximately 5 minutes for 2 minutes of broadband (40 Hz sampling rate) 25-channel data. On the other hand AOGF filtering is rather fast and takes approximately the same time as filtering with Butterworth bandpass filters.

Since the procedure is broken into two individual steps, the adaptation may be performed in parallel to the AOGF, i.e., one process may do noise adaptation (generate the filter) and report this into a data base that may be used by the filter process. So the AOGF processing depends only on how often the parameters of the group filter are to be changed.

In Kushnir et al (1990), it was shown that high noise suppression of AOGF without readaptation remains during at least 40 minutes. On Fig. 7.3.1 the result is shown of AOGF noise suppression without readaptation for 50 hours. Each curve depicted there is the ratio of noise powers P(average channel)/P(AOGF) and P(beam)/P(AOGF). By beam, we mean the conventional array beam - unfiltered.

In this noise study 90 different noise time intervals, each of 2 minute length, were selected by scanning the detection list and requiring that the noise interval started at least 6 minutes after any detection, and at least 6 minutes before any detection.

Adaptation was performed for the 2 minutes in the beginning of this total time interval with the following parameters: frequency band 0.2-1.5 Hz, resampling factor 4, azimuth 334 degrees, velocity 24 km/sec. Subsequently, AOGF filtering was done for these 90 intervals of noise.

Note that the resampling factor 4 means resampling from 40 to 10 Hz, i.e., the adaptation is here done for the frequency range 0.2 - 1.5 Hz, but the output AOGF and conventional beam represent the full frequency range up to the Nyquist frequency (5 Hz).

From Fig. 7.3.1 it is seen that, without readaptation, we get more than 40 times (16 dB) noise suppression compared to an average of single channels.

Some drops in the noise suppression seen on the figure may be related to incoming signals not reported in the detection bulletin, or problems with finding a 'clean' noise interval.

The similar curves were obtained for ARCESS noise with noise adaptation to the frequency bands 0 - 4.5 Hz and 0.2 - 1.5 Hz (Fig. 7.3.2 and 7.3.3).

From the figures it is seen that noise suppression by AOGF is not so stable as for NORESS but nevertheless high noise suppression of more than 16 dB is consistently achieved for more than 6 hours after adaptation.

The stability of AOGF noise suppression in time may be explained by the fact that the adaptation is done in the lower frequency bands where noise power fluctuations are smallest (Fyen, 1990).

Let us consider now the possibilities of constructing a small array detector system consisting of several adaptive beams steered at certain azimuths and velocities. Such a system will be analogous to the on-line NORESS detector system.

The main question here is: what is the minimum number of AB providing adequate detectability while still allowing real-time or routine processing.

To try to answer this question, an experiment was performed with simulating events of different SNR - signal to noise ratio. A strong regional event with Pn parameters: azimuth 193, velocity 8.2, frequency band 2.5-4.5 Hz, SNR 148, was selected. This event was treated as a signal without noise, and then scaled down and added to arbitrary NORESS noise. Figures 7.3.4 and 7.3.5 show the results. The 5 curves in each figure correspond 'events' of 5 different SNR as function of slowness of the AOGF beam. For each chosen azimuth and velocity, adaptation was done for 120 seconds of preceding pure noise, followed by filtering of the signal segment by AOGF (i.e., forming an AOGF beam). The curves show SNR for the AOGF beam (SNROGF) and the corresponding single channel A0 maximum SNR for each different scale of the signal. SNR was estimated by the ratio of STA of the 2 first seconds of the signal and average STA of 40 sec of pure noise.

From the figures we see that we get highest SNR of the AOGF at the correct azimuth, whereas SNR is nearly constant for velocities above 6 km/sec. Looking at the shape of the SNR curve for azimuth, we see for azimuth range 150 - 225 degrees, the SNR varies by a factor of two.

Allowing a predefined beam set to have a worst case missteering loss of 3 dB, we may infer that 8 different azimuths and two velocities may be enough to produce high detectability for all azimuths and velocities. That is, 16 noise adaptations has to be performed at regular intervals separated up to 6 hours. This will be an acceptable load for most systems.

Frequency dependence of noise suppression for AOGF and standard beams. Low frequency AOGF deployment.

The current NORESS detector system was designed mainly for the detection of local and regional events, having its best performance in the high frequency band (>2 Hz). But as it was shown by Ringdal (1990), it is very effective also for the detection and reporting of teleseismic signals.

Most of the teleseismic events detected at NORESS are from the Eurasian continent having the best properties of propagation at high frequencies (1.5 - 4 Hz). But for teleseismic signals coming from other directions, energy at these frequencies attenuate much more strongly. As a result, much of the teleseismic information is masked by low frequency noise and this reduces the detectability of the current operational system.

We shall try to show that complementing the current detector system with SOA may improve the detectability also for teleseismic distances. Let us compare noise suppression by AOGF and standard beams in different frequency bands reflected in Table 7.3.1. By a standard beam we mean one of the conventional beams used in NORESS/ARCESS online system. Such a standard beam is defined by array sub-configuration, velocity and azimuth. Sub-configurations are denoted in such a way that, e.g., A0AC, means the center instrument A0, plus the A-ring and C-ring.

The table comprises STA values evaluated on pure NORESS noise using AOGF and standard beam traces filtered in the most important frequency bands, that is, the AOGF as the result of the group filtering is additionally filtered with the same bandpass filters as the standard beams. The AOGF was based on noise adaptation in the frequency band 0-16 Hz. As STA is an estimate of the power, the table is also indicative of the absolute level of noise suppression.

For AOGF, the 25 vertical NORESS channels (A0ABCD configuration) were used. Noise adaptation was performed using a 100-second noise segment preceding the 40 seconds of data used for beams and AOGF filtering. For these teleseismic AOGF and standard beams, infinite velocity and zero azimuth was used.

From the table it is seen that:

1. In all of the listed frequency bands, the resulting noise power of AOGF is lower than the standard beams, i.e., better noise suppression is obtained.

2. The best standard beam configurations were A0D for 0.3-1.0 Hz and 0.5-1.5 Hz, and A0CD for 1.5-5.0 Hz and 5-16 Hz.
3. Compared to the A0D beam, broadband AOGF has 10 dB better suppression in the 0.3-1.0 Hz and 6 dB improvement in the 0.5-1.5 Hz frequency bands.
4. In the highest frequency band the AOGF and A0CD have comparable noise suppression results.
5. As the highcut frequency of the lowpass prefiltering in the noise adaptation (lowpass 16 Hz in the first part of the table) decreases, the STA power of AOGF also decreases, that is, noise suppression improves.

For a lowpass (lp) 1.5 Hz filter, the AOGF shows approximately 6 dB smaller STA value for the 0.3-1.0 Hz and 0.5-1.5 Hz bands, as opposed to adaptation with lp 16 Hz. In the band 0.2-0.6 Hz, comprising a considerable part of the noise power, the AOGF is suppressed 19 dB compared to A0D.

Hence, the best teleseismic performance of AOGF is achieved by prefiltering the data with a low pass filter 1.5 Hz

Comparison of optimal detector and STA/LTA detectability

We will here present some preliminary results concerning application of the one-dimensional statistically optimal detector, i.e., the so-called ESTDET algorithm (Kushnir et al, 1991). This algorithm is based on optimal accounting of noise features. Compared to the ordinary STA/LTA algorithm, this algorithm not only takes into account amplitude level, but also variations of the spectrum content.

The procedure has two steps: The first is adaptation on a time segment of pure noise. As a result we get an estimate of whitening filter coefficients. The second step is filtering using the coefficients computed at the previous step and computation of Chi-square statistic in a moving window.

To examine the performance of ESTDET as a function of SNR, we have chosen a NORESS recording of a regional event in Sweden, i.e., the same event used for Fig. 7.3.4.

The event was detected with relatively high SNR by standard beam N055 (configuration A0BCD, frequency band 2.5-4.5 Hz). Again we used the procedure of superposing this signal onto pure NORESS noise with different scaling.

Fig. 7.3.6 shows the display of the bandpass filtered beam N055, the STA for this beam, and ESTDET (XISQT1 Chi-square statistics from ESTDET process) for this original signal. The lower part of the figure shows the same three processes when the signal is scaled down by a factor 80 in amplitude and added to a noise trace.

The advantage of ESTDET over STA for the latter case is obvious.

The next experiment was to obtain ESTDET statistics with varying noise scale factors for the simulated data.

The ESTDET statistic was computed for the AOGF beam and for the standard beam. Signal-to-noise ratio was estimated by the ratio of ESTDET for the 3 first seconds of P-wave and 40 seconds of preceding pure noise, i.e. Xi-square values are averaged for the noise segment to get a signal-to-noise ratio comparable to STA/LTA. For the standard beam, the STA was used.

Fig. 7.3.7 shows the results. The upper curve is the ratio of ESTDET statistic maxima on signal and noise. The curve is computed for unfiltered AOGF data. The bottom curve is the corresponding ratio for the STA algorithm (SNR) on standard beam N055. This ratio estimates STA/LTA. The middle curve is similar to the upper one, but additionally band-pass filtered in the frequency band 2.5-4.5 Hz.

Comparing upper and bottom curves, it is seen that the ESTDET SNR is better than that of the STA/LTA algorithm, especially for the unfiltered AOGF beam. For example, for noise scale equal to 100, SNR for STA is 2 and for ESTDET is 50-60.

To examine ESTDET false alarms we have chosen from two days bulletin all noise intervals of at least 2 minutes length and selected 2 minutes segments from each. The total amount of noise is about 3 hours.

Fig. 7.3.8 shows the number of ESTDET values exceeding a given threshold, as a function of threshold. For low thresholds it is very large, but it decreases with increasing of the threshold value. Only one exceedance is detected for a threshold larger than 500. Let us compare it with the maximum values of ESTDET on the signal+noise (Fig. 7.3.9) computed for different noise scales. It is seen that value 500 corresponds to a noise scale of 85 or STA/LTA value around 2 which is lower than the conventionally used threshold.

So, we may suppose that if the threshold for ESTDET is equal to, say, 550, it is possible to detect a weak regional P-wave, STA/LTA=2, with a low probability of false alarms during several hours of processing.

From these preliminary results we may draw the following conclusions:

1. AOGF is computed after adaptation to the noise. This process is time consuming, but it is shown that high noise suppression may be obtained using only one noise adaptation for several hours of data processing.
2. It has been shown that for a NORESS-type array adaptation to the noise for about 8 different azimuths and two velocities, is sufficient to obtain adequate beam coverage for regional P phases.
3. The main advantage of AOGF is to be expected for low frequency teleseismic signals, where we have both good detectability and a broadband undisturbed estimate of the signal.

4. The ESTDET detector is much more sensitive to the detection of seismic phases compared to conventional STA/LTA due to optimal accounting to noise spectrum variations.
5. Due to higher sensitivity the ESTDET process may be used for the detection and timing of much weaker seismic phases than detected now.

V. Pinsky, MITPAN Institute, Moscow
S. Tsvang, MITPAN Institute, Moscow
J. Fyen

References

Fyen, J., (1989): Event processor program package. *Semiannual Technical Summary*, NORSAR Sci. Rep. 2-88/89, Kjeller, July 1989.

Fyen, J., (1986): NORESS noise spectral studies - beam suppression. *Semiannual Technical* Summary, NORSAR Sci. Rep. 1-86/87, Kjeller, November 1986.

Fyen, J., (1990): Diurnal and seasonal variations in the microseismic noise level observed at the NORESS array. *Physics of the Earth and Planetary Interiors*, 63: 252-268.

Kushnir, A.F., V.I. Pinsky and J. Fyen (1989): Statistically optimal event detection using small array data. *Semiannual Technical Summary*, NORSAR Sci. Rep. 1-89/90, Kjeller, December 1989.

Kushnir, A.F., V.I. Pinsky, S. Tsvang, J. Fyen, S. Mykkeltveit and F. Ringdal (1990): Optimal group filtering and noise attenuation for the NORESS and ARCESS array. *Semiannual Technical Summary*, NORSAR Sci. Rep. 1-90/91, Kjeller, November 1990.

Kushnir, A.F., J. Fyen and T. Kværna (1991): Multichannel statistical data processing algorithms in the framework of the NORSAR event processing program package. *Semiannual Technical Summary*, NORSAR Sci. Rep. 2-90/91, Kjeller, May 1991.

Kushnir, A.F., V.M. Lapshin, V.I. Pinsky and J. Fyen (1990): Statistical optimal event detection using small array data. *Bull. Seism. Soc. A*m., Vol. 80, No. 6, pp. 1934-1950, December 1990.

Mykkeltveit, S., J. Fyen, F. Ringdal and T. Kværna (1990): Spatial characteristics of the NORESS noise field and implications for array detection processing. *Physics of the Earth and Planetary Interiors*, 63: 277-283.

Pisarenko, V.F, A.F. Kushnir and I.V. Savin (1987): Statistical adaptive algorithms for estimations of onset moments of seismic phases. *Phys. Earth Planet. Inter.*, 47, 4-10.

Ringdal, F. (1990): Teleseismic event detection using the NORESS array, with special reference to low-yield Semipalatinsk explosions. *Bull. Seism. Soc. A*m., Vol. 80, No. 6, pp. 2127-2142, December 1990.

Adaptation lp 16 Hz

Filter band	AOGF	A0ABCD	A0BC	A0D	A0CD	A0AB	A0
0.3 - 1.0 Hz	0.035	0.150	0.188	0.105	0.131	0.206	0.207
0.5 - 1.5 Hz	0.044	0.142	0.192	0.085	0.114	0.219	0.226
1.5 - 5.0 Hz	0.018	0.038	0.062	0.032	0.022	0.093	0.113
5.0 - 16.0 Hz	0.005	0.0056	0.0076	0.065	0.0071	0.0094	0.027
Unfiltered	0.05	0.174	0.225	0.157	0.145	0.256	0.271

Adaptation lp 4.5 factor 4

0.3 - 1.0 Hz	0.023
0.5 - 1.5 Hz	0.029
1.5 - 5.0 Hz	0.016
Unfiltered	0.034

Adaptation lp 1.5 factor 4

0.2 - 0.6 Hz	0.011	0.090	0.139
0.3 - 1. Hz	0.019		
0.5 - 1.5 Hz	0.023		
Unfiltered	0.025		

Table 7.3.1. Comparison of AOGF noise suppression in different frequency bands.Case study of NORESS noise segment start 1991-140:00.05.00.004. The table shows STA power values (normalized with factor 1000) for AOGF and different standard beams. AOGF adaptation using velocity 99999, azimuth 0.0, lowpass 16 Hz prefilter and 100 seconds noise. Data are not resampled (resample factor 1). STA power values on the following 40 seconds. Before STA, traces are butterworth bandpass filtered in the given filter bands. A0BC, etc., show which sub-configuration that is used. Additional values are computed for AOGF using lowpass 4.5 and 1.5 Hz and resampling factor 4. (Resample from 40 to 10 Hz).

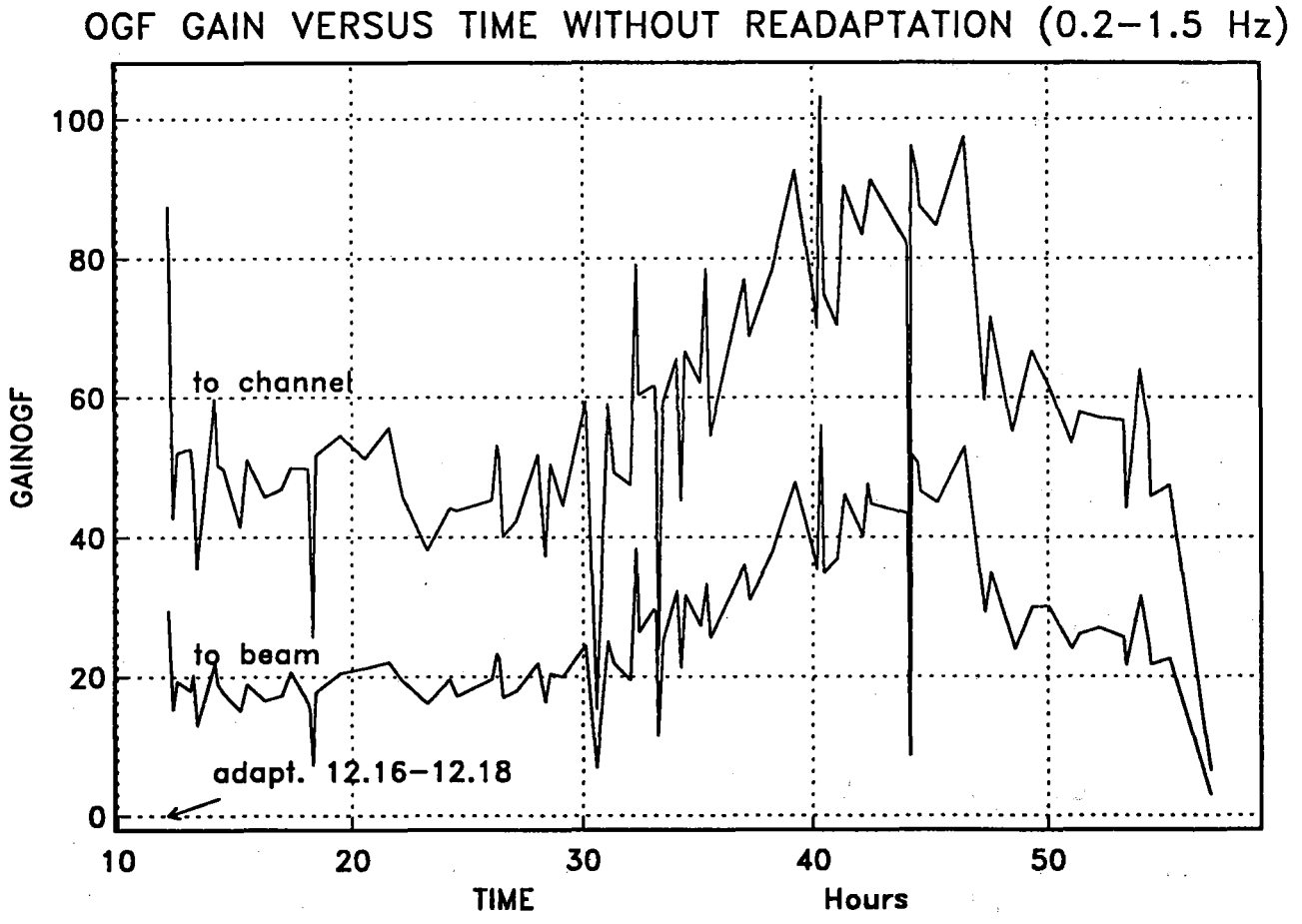

Fig. 7.3.1. AOGF gain versus time without readaptation on pure NORESS noise selected from bulletin. OGFGAIN is the ratio of noise powers on 2-minute noise intervals. Start time 1991-176:12. Adaptation interval 1991-176:12.16 - 12.18. Data frequency band 0.2-1.5 Hz. Adaptation velocity 24 km/sec, azimuth 334 degrees.

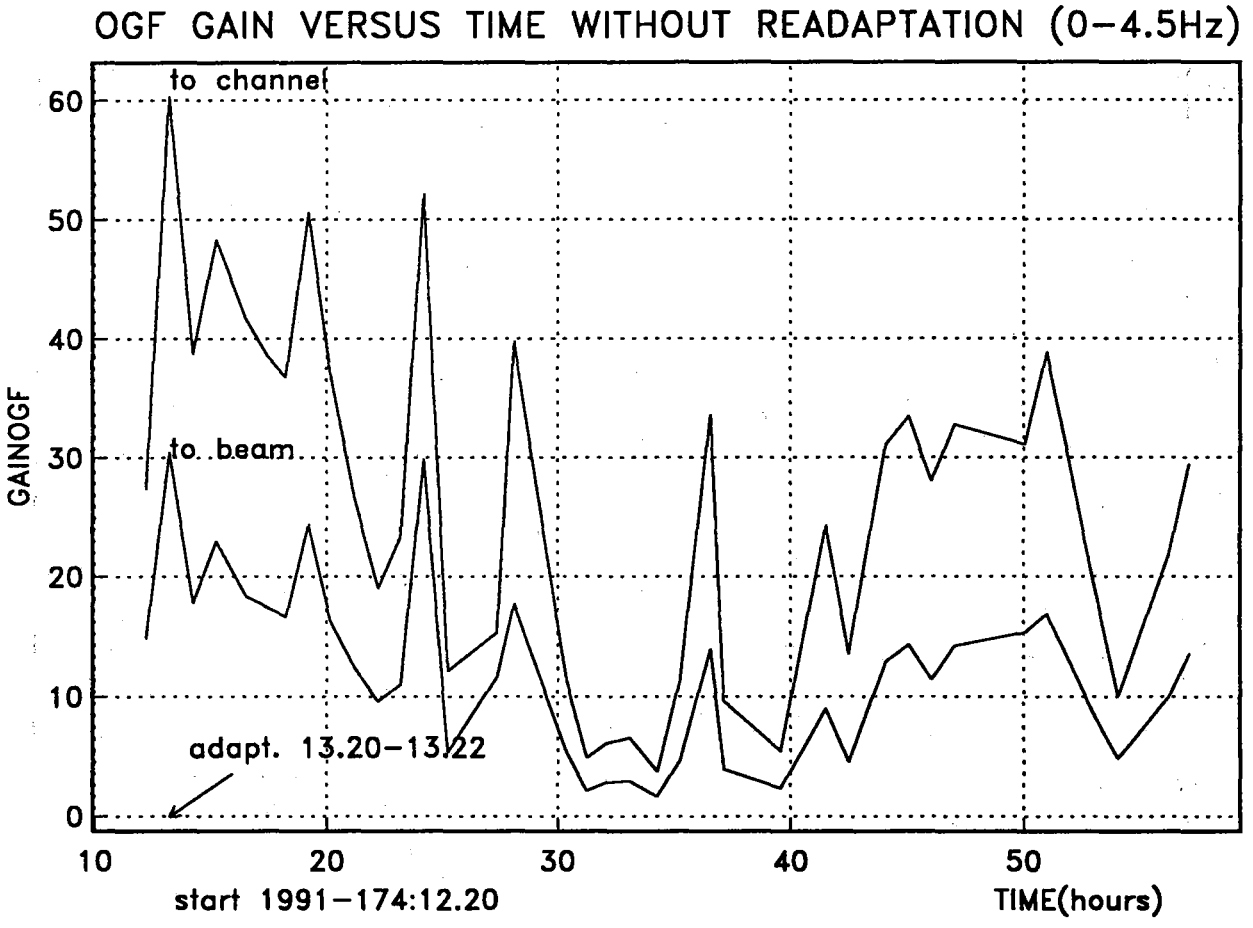

Fig. 7.3.2. AOGF gain versus time without readaptation on pure ARCESS noise selected from bulletin. OGFGAIN is the ratio of noise powers on 2-minute noise intervals. Start time 1991-174:12.20 Adaptation interval 1991-176:13.20 - 13.22. Data frequency band 0-4.5 Hz. Adaptation velocity 10 km/sec, azimuth 193 degrees.

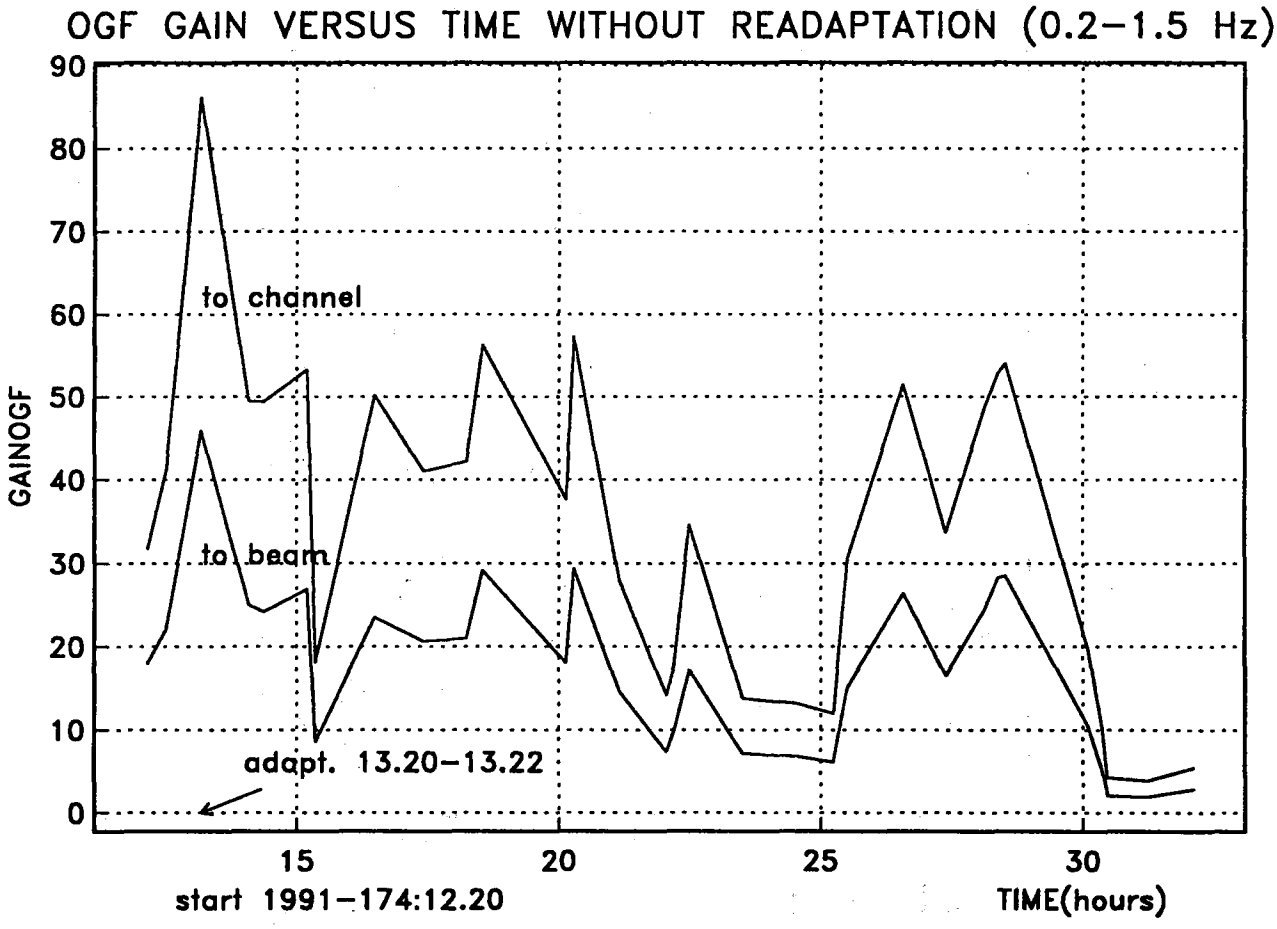

Fig. 7.3.3. AOGF gain versus time without readaptation on pure ARCESS noise selected from bulletin. OGFGAIN is the ratio of noise powers on 2-minute noise intervals. Start time 1991-174:12.20 Adaptation interval 1991-176:13.20 - 13.22. Data frequency band 0.2-1.5 Hz. Adaptation velocity 10 km/sec, azimuth 193 degrees.

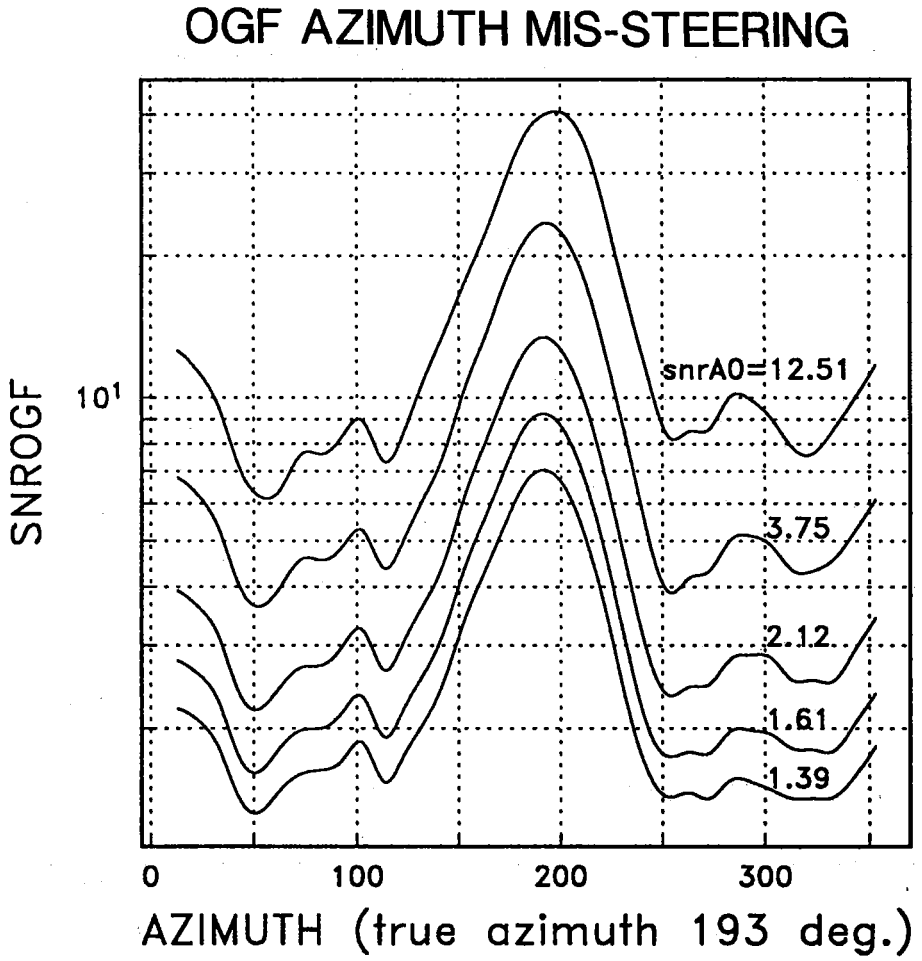

Fig. 7.3.4. AOGF azimuth missteering on regional event NORESS P-wave with different scaling of added noise. Signal parameters: start 1991-086:05.18.46, velocity 8.2 km/sec azimuth 193 degrees, freq. 3.35 Hz. Noise start 1991-140:00.05. OAGF adaptation on 100 seconds of pure noise with velocity 8.2 km/sec, frequency band: 0-4.5 Hz, and different azimuths. Filtering on 50 seconds of signal + noise. SNROGF= (average STA on 2 sec. of P-wave)/(average STA on 40 sec. of noise)

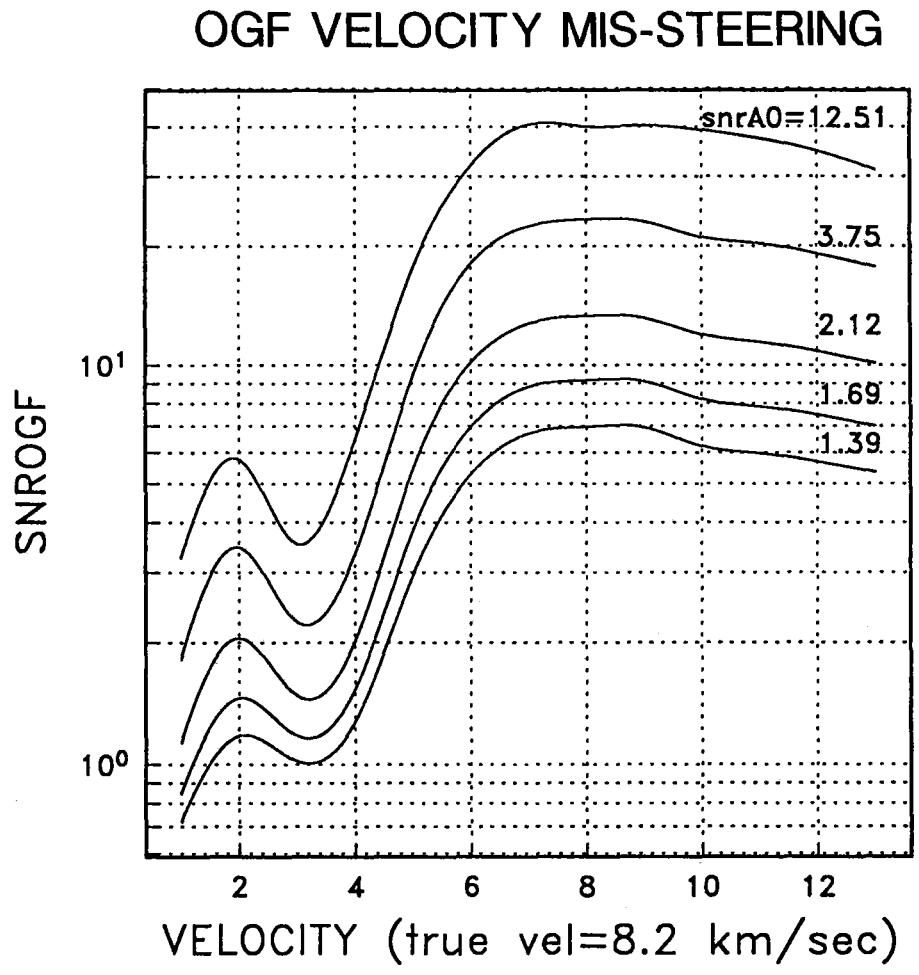

Fig. 7.3.5. AOGF velocity missteering on regional event NORESS P-wave with different scaling of added noise. Signal parameters: start 1991-086:05.18.46, velocity 8.2 km/sec azimuth 193 degrees, freq. 3.35 Hz. Noise start 1991-140:00.05. OAGF adaptation on 100 seconds of pure noise with azimuth 193 degrees, frequency band: 0-4.5 Hz and different velocities. Filtering on 50 seconds of signal + noise. SNROGF= (average STA on 2 sec. of P-wave)/(average STA on 40 sec. of noise)

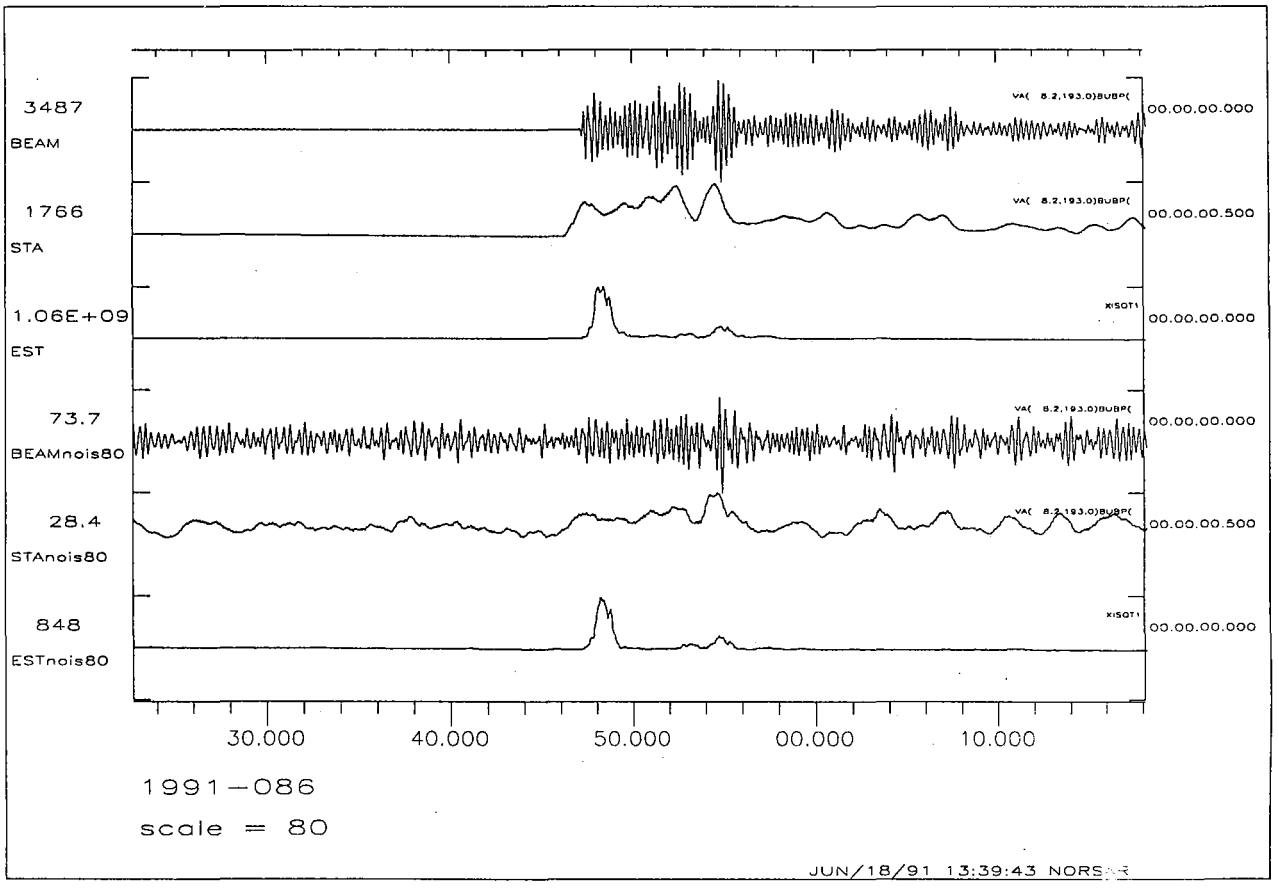

Fig. 7.3.6. STA for ESTDET and standard beam n055 for regional event. Signal parameters: start 1991-086:05.18.46, velocity 8.2 km/sec azimuth 193 degrees, freq. 3.35 Hz. Noise start 1991-140:00.05. Traces: 1. standard bean (SB), fr.band 2.5-4.5 Hz; 2. STA on SB; 3. ESTDET on SB; 4. SB + noise,scale=80; 5.,6. STA and ESTDET on SB + noise.

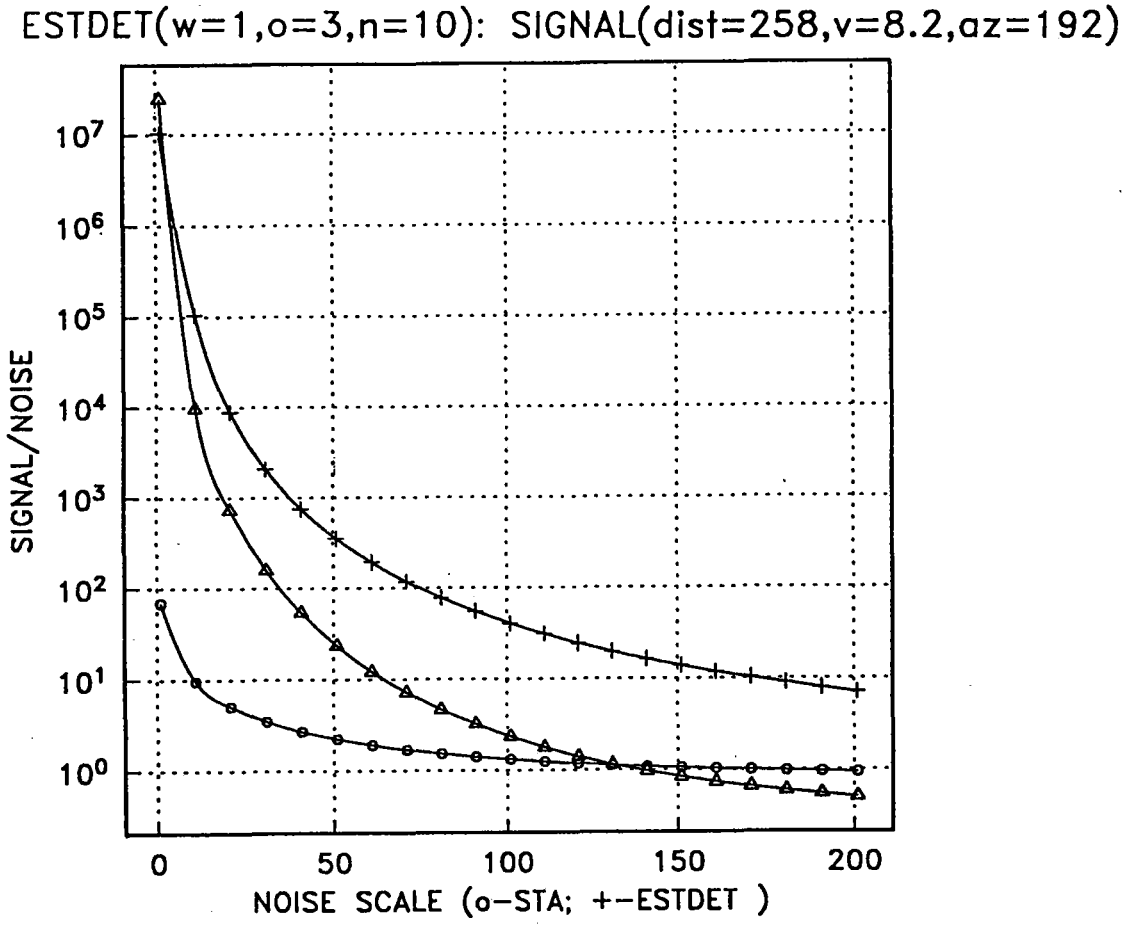

Fig. 7.3.7. Comparison of ESTDET and STA/LTA on the regional P-phase + noise for the different noise scales. ESTDET parameters: (w=1,o=3,n=10).

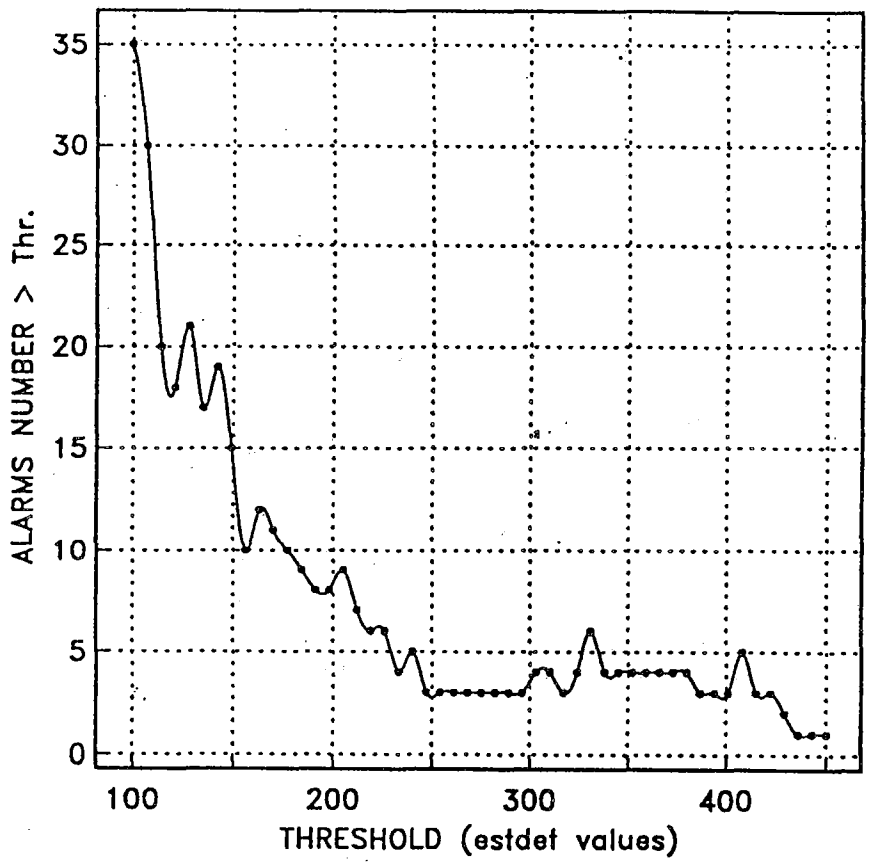

Fig. 7.3.8. Number of ESTDET false alarms versus threshold for 3 hours of NORESS noise taken from 48 operational hours.

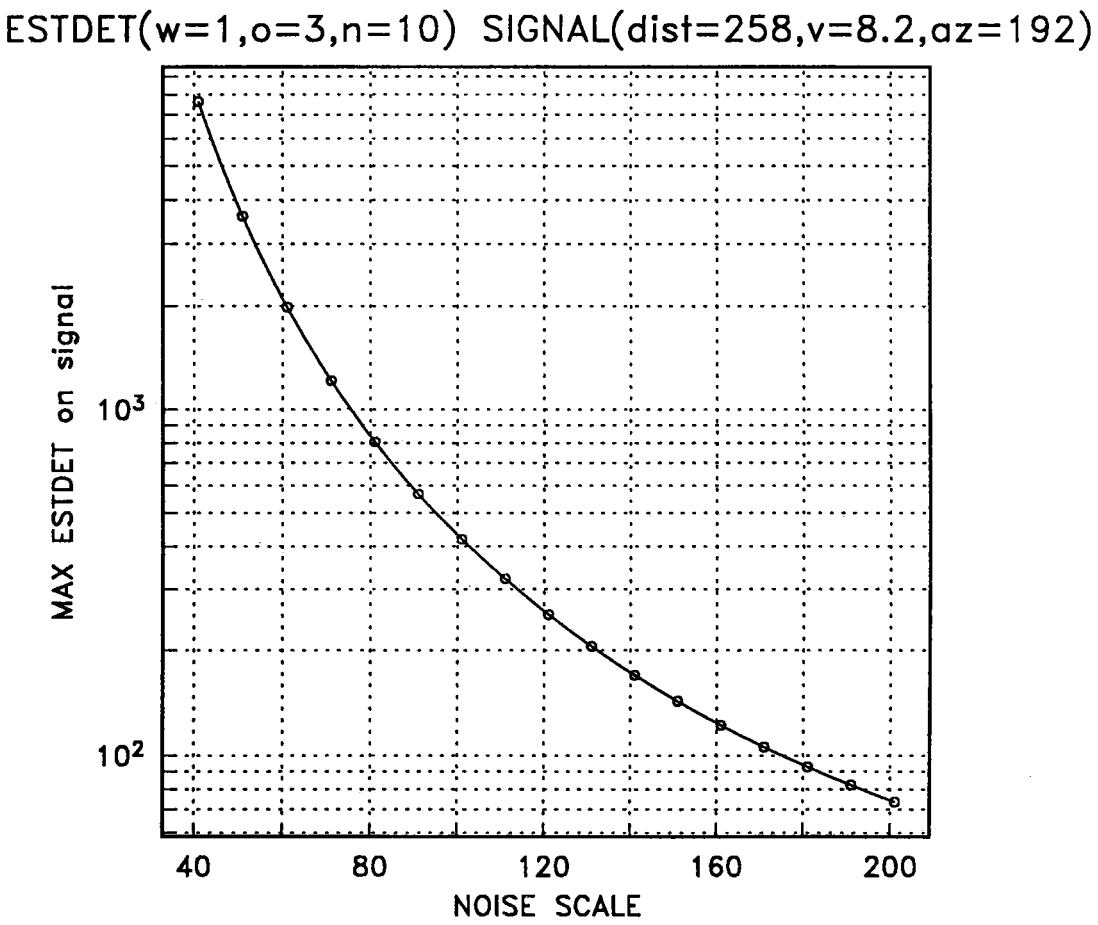

Fig. 7.3.9. Maximum values of estdet on regional P-phase + noise versus noise scale.

7.4 Extensions of the Northern Europe Regional Array Network -- a new three-component station at Apatity, USSR, and a planned array at Spitsbergen

The Northern Europe Regional Array Network currently comprises the high-frequency arrays NORESS and ARCESS in Norway, FINESA in Finland and GERESS in Germany, as well as the two three-component stations KSP and SFP in Poland. The locations of these stations are shown in Fig. 7.4.1 Data from all of these installations are transmitted continuously and in real time to the NORSAR Data Processing Center at Kjeller, Norway, where the data are processed jointly by the Intelligent Monitoring System (IMS). Current prospects for extending this network and, if possible, integrating new data sources into IMS, are described in this contribution.

The establishment of the FINESA array in Finland was made possible through joint efforts between NORSAR and the University of Helsinki, based on a bilateral cooperative agreement. A similar arrangement has recently been made with the Kola Science Center of the USSR Academy of Sciences, and as first result of this cooperation, a high-quality three-component station was installed by NORSAR personnel in Apatity (see Fig. 7.4.1) in June 1991. The following paragraph gives a description of the system installed in Apatity and contains material related to analysis of data from this new station.

According to current plans, a 9-element array with a 1-kilometer aperture will be installed on the island of Spitsbergen in the Arctic (see Fig. 7.4.1) in the summer of 1992. A short description of these plans are given in this contribution.

A new 3-component station at Apatity, USSR

In mid-June 1991, a high-quality three-component station was installed in Apatity, on the Kola Peninsula of the USSR. The station was installed and is operated under an agreement on scientific cooperation within seismology between the Kola Science Center of the USSR Academy of Sciences and NORSAR.

The three-component station installed in Apatity comprises S-13 seismometers, a Nanometrics RD3 digitizing/synchronization/multiplexing unit, an Omega clock and a PC-based system for data acquisition, analysis and archiving. The amplitude response of the system is shown in Fig. 7.4.2. The PC system has a 25 MHz 386 processor, 4 Mbyte RAM, a 300 Mbyte ESDI disk, and a cartridge tape drive. The system was installed in the basement of the building of the Seismological Laboratory of the Kola Science Center, in the town of Apatity. The S-13 seismometers were placed on the same pad as the seismometers of the analog APA station (established in 1956). Data are recorded continuously on magnetic disk in Apatity and copied to cartridge tapes, which are sent to NORSAR. An archive of continuous data from the new station in Apatity is thus maintained both at Apatity and at NORSAR.

Analysis of data recorded at the new Apatity station -- noise levels

Fig. 7.4.3a shows six noise spectra for the new Apatity station. All noise samples are taken during daytime (2 pm to 5 pm local time), with the exception of the sample corresponding to the dashed curve, which is taken around midnight, local time. The trend of the curves strongly indicates cultural origin for the noise above 2 Hz. Also, one must keep in mind that the station is located within the town of Apatity, which has approximately 100,000 inhabitants. The very heavy mining activities in the nearby (20 km) Khibiny Massif is supposedly also contributing to the noise level. A distinct and consistent peak at 4 Hz indicates a localized source. This 4 Hz wave can be clearly seen in the noise preceding the onset in the recording of the shot in Mine II in Fig. 7.4.5. All spectra except one also exhibit a pronounced peak at 2.5 Hz. The origin of these peaks in the noise spectra are as yet unknown. There is an indication of a slightly lower noise level above 7-8 Hz at nighttime.

Compared to the NORESS noise model (superimposed on Fig. 7.4.3a), the noise level at the new Apatity station stands out as being very high above 2 Hz. For lower frequencies, the noise levels at NORESS and Apatity are similar. This is also to be expected on the basis of usual assumptions about noise generating mechanisms for frequencies below 2 Hz.

On 12 June, prior to installing the station at the Seismological Laboratory in Apatity, the entire system was deployed for an hour at a location approximately 15 km to the west of Apatity (denoted PROF in Fig. 7.4.4). This is a candidate location for a possible future deployment of a small array in Apatity. While the noise level is still high relative to the NORESS noise model, the level is clearly lower than in the town of Apatity, as can be seen by comparing Figs. 7.4.3a and 7.4.3b.

Analysis of data recorded at the new Apatity station -- P-wave signals

The map of Fig. 7.4.4 shows the location of the new Apatity station and the nearby mining area of the Khibiny Massif. The lateral extent of the mining area is approximately 15 km, and there is information available that allows the assignment of each individual explosion since early 1991 to one of the five subareas indicated in Fig. 7.4.4. Fig. 7.4.5 shows three-component records for the new Apatity station for five such explosions, one from each of the five mines. Detailed information on these shots is given in Table 7.4.1. From Fig. 7.4.5, it is clearly seen that there is a large variation among the shots with respect to amplitude and frequency content of P, S and Rg waves, and this variation cannot be explained by differences in epicentral distance and shot size alone. Hence, other factors like propagation path effects and specific conditions pertaining to the individual shots are important. For example, information on shot geometry and ripple firing delay times is not currently available.

As a check on the performance and integrity of the new three-component Apatity station, we used the data for the five shots in Fig. 7.4.5 to derive the apparent arrival azimuth for the P wave onset using the broad band slowness estimation technique of Kværna and Doornbos (1986). The results are given in Table 7.4.1, along with the true azimuths, which

are given in terms of intervals, due to the spatial extent of each of the five mines. The calculations were made for four different frequency bands, as shown in the table. The length of the time windows used were 1.0 s for the 8-16 Hz band, 1.5 s for the 5-10 Hz and 3-5 Hz bands, and 2.0 s for the 1-3 Hz band. The start time for all windows was 0.1 s prior to the P arrival time. The table shows reasonable figures with an average deviation of 5.5 degrees from the midpoint of the interval for the true azimuth, when disregarding the low SNR event from mine II. We take this result to indicate that the new Apatity station performs well from a technical point of view.

As a further illustration of the new data now available from Apatity, recordings at Apatity, ARCESS and FINESA of a probable earthquake approximately 200 km due south of Apatity are shown in Fig. 7.4.6. The bulletin of the University of Helsinki, Finland, gives an epicenter of 65.71°N, 33.24°E, based on altogether 41 readings of P and S phases. The magnitude is M_L 3.7 and the depth is estimated at 8.8 km (standard deviation 4.5 km) in the Helsinki bulletin. The arrival azimuths of the first P wave at the new Apatity station were estimated as was done for the five mining shots, and results are also given in Table 7.4.1. Again, the results are reasonable, with an average deviation from the true azimuth of about 6 degrees. A feature of special interest in Fig. 7.4.6 is the Rg wave seen in the Apatity and FINESA data. Especially surprising is the presence of an Rg phase at FINESA, at a distance of 593 km. The strong Rg waves also point toward a shallow-focus event, and maybe shallower than 8.8 km, as given in the Helsinki bulletin.

We think that the new data now available from Apatity will prove to be very valuable. It is of special interest that we are now able to obtain near-field recordings of the mining shots in the Khibiny Massif. All of these shots are well recorded at ARCESS (distance 480 km), and the majority of the larger ones also at FINESA (distance 780 km) and NORESS (distance 1315 km). Plans including a computer-to-computer link between NORSAR and the Kola Science Center and possible deployment of additional stations are now being discussed.

Plans for a small-aperture array at Spitsbergen

Companies taking part in oil exploration and production on the Norwegian Continental Shelf have earlier sponsored the establishment of a network of seismic stations onshore northern Norway. As a further development of this network, NORSAR will establish, under the sponsorship of the same oil companies, a small-aperture array near Longyearbyen on the island of Spitsbergen during the summer of 1992.

A site survey was conducted in August 1991. A suitable location was found approximately 20 km from Longyearbyen, which is the largest Norwegian settlement and also administrative center on the island. The plan is to install a 9-element 1-kilometer aperture array of vertical sensors. The array will have two concentric rings with 3 and 5 elements, respectively, plus one sensor at the center. The rocks at the site are of Cretaceous age, covered by thin moraine of variable depth. The sensors will be placed in boreholes, drilled either to the Cretaceous rock or to a depth where stable permafrost conditions are obtained (depths of the order of 6 meters are considered to be sufficient in this regard). All necessary permissions to deploy the array have been granted by the appropriate authorities.

The site survey included noise measurements at the selected site. A noise spectrum is shown in Fig. 7.4.7. Even if the noise level is seen to be higher than the average noise level at NORESS, we consider the noise level at the Spitsbergen site to be quite satisfactory for an array installation. For example, there are no specific peaks in the spectrum. There is mining activity in the area, with mines located at distances between 10 and 20 km from the site.

The system to be established at Spitsbergen will have an on-site recording capability only. We do, however, consider that the data from this new array would be of great value to the IMS. This requires continuous transmission via satellite of data from Spitsbergen to Kjeller. The annual lease of such a link is estimated at approximately USD 30,000.

S. Mykkeltveit **A. Dahle** **J. Fyen** **T. Kværna**
P.W. Larsen **R. Paulsen** **F. Ringdal**
E.O. Kremenetskaya, Kola Science Center

References

Fyen, J. (1990): Diurnal and seasonal variations in the microseismic noise level observed at the NORESS array. *Phys. Earth Planet. Inter.*, 63, 252-268.

Kværna, T. and D.J. Doornbos (1986): An integrated approach to slowness analysis with arrays and three-component stations, *Semiannual Tech. Summ., 1 October 1985 - 31 March 1986,* NORSAR Sci. Rep. No. 2-85/86, Kjeller, Norway.

Epicenter	Shot size (tons)	P wave arrival time	True azimuth (deg)	Estimated P-wave arrival azimuth (deg) 1-3 Hz	3-5 Hz	5-10 Hz	8-16 Hz
Mine I	120	216/12.49.55.8	36-46	47.1	38.5	44.6	37.0
Mine II	35	259/12.19.27.1	46-53	(55.3)	(99.5)	(78.9)	(34.0)
Mine III	94	187/19.24.01.9	55-60	58.5	57.6	68.2	71.7
Mine IV	430	207/12.31.00.3	60-66	69.2	61.6	74.2	63.7
Mine V	392	193/10.21.22.1	68-74	72.4	64.5	60.1	64.8
65.71°N,33.24°E	-	236/10.57.01.2	180.2	174.3	182.8	185.5	189.4

Table 7.4.1. Apparent arrival azimuths at the new 3-component station at Apatity, as determined from broad band slowness estimation using the method of Kværna and Doornbos (1986). The epicentral information on the earthquake at the bottom of the table is from the Helsinki bulletin. The SNR for the event from Mine II is very low in all frequency bands and the estimated arrival azimuths are given in parenthesis.

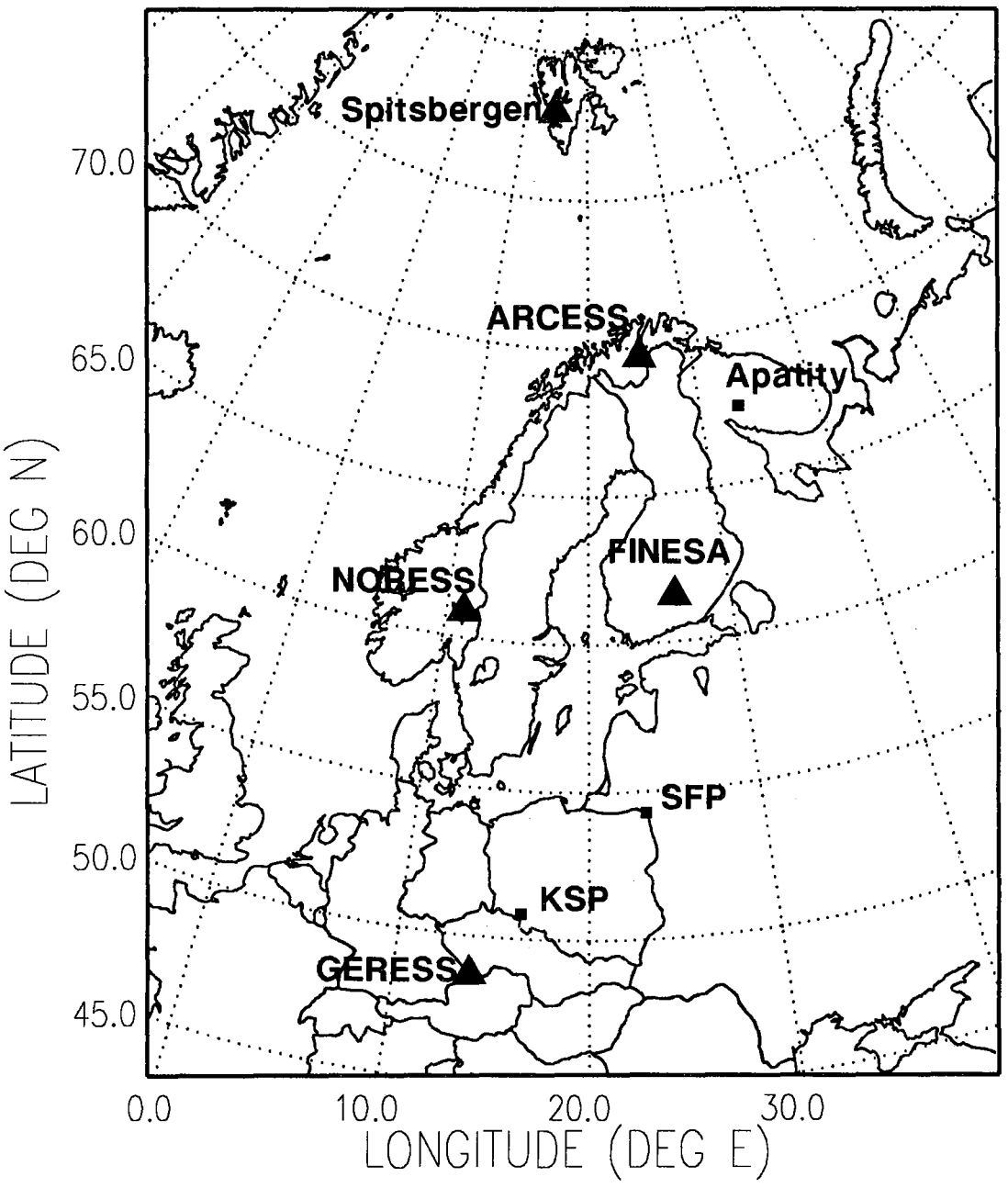

Fig. 7.4.1. The map shows the existing stations of the Northern Europe Regional Array Network as well as the location of the two new stations at Apatity and Spitsbergen, dealt with in this contribution.

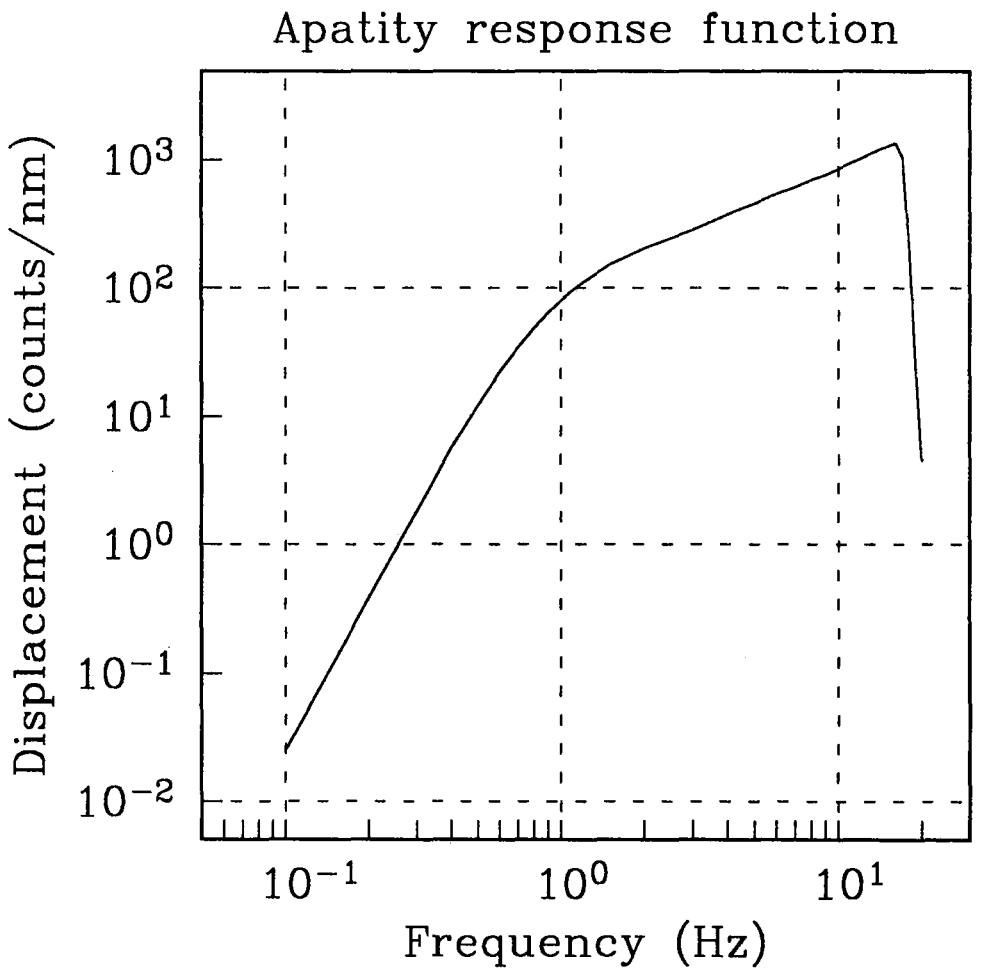

Fig. 7.4.2. Amplitude (displacement) response function for the system installed in Apatity in June 1991.

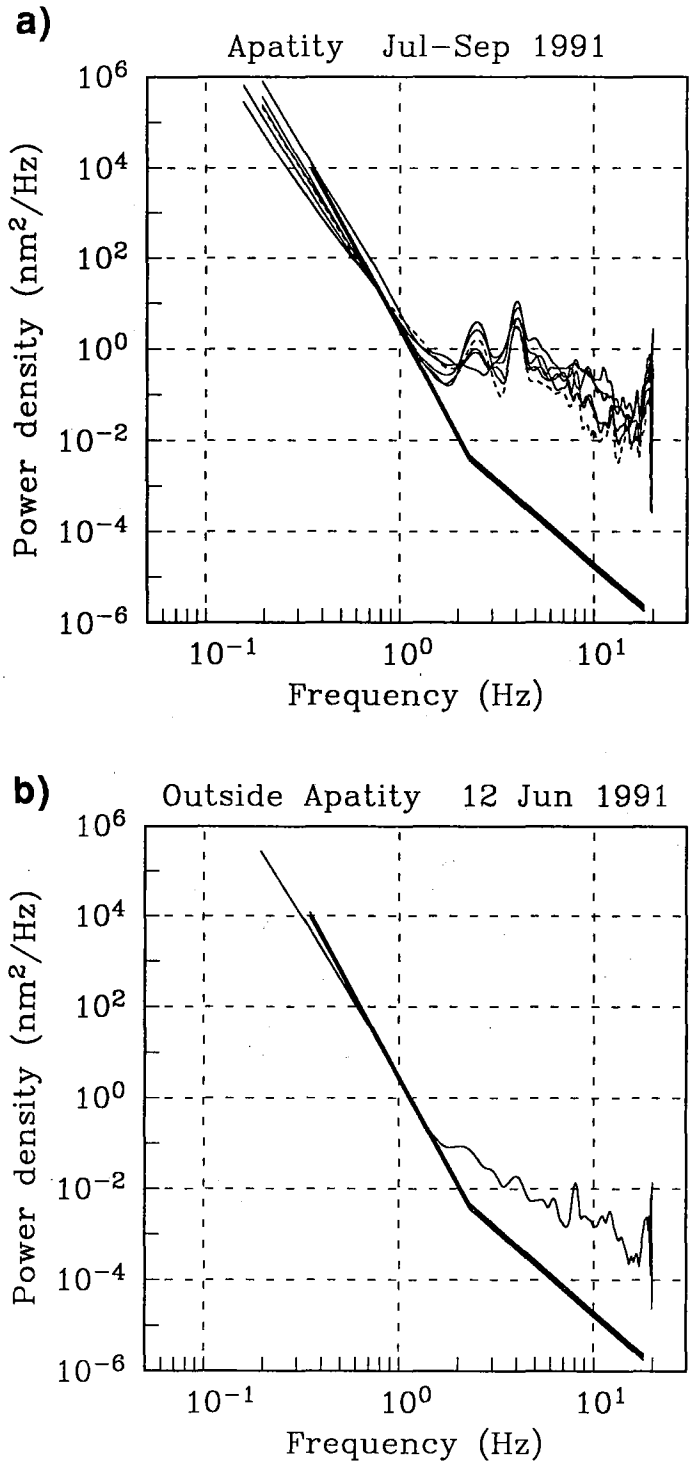

Fig. 7.4.3. a) (top): Six noise spectra for the new Apatity station. b) (bottom): Noise spectrum from the location outside Apatity, denoted PROF in Fig. 7.4.4. The solid line in each of the figures denotes the NORESS noise model of Fyen (1990). All spectra were estimated from partly overlapping 5-second windows, using the indirect covariance method (see Fyen, 1990). The total length of each noise sample was approximately 1 minute.

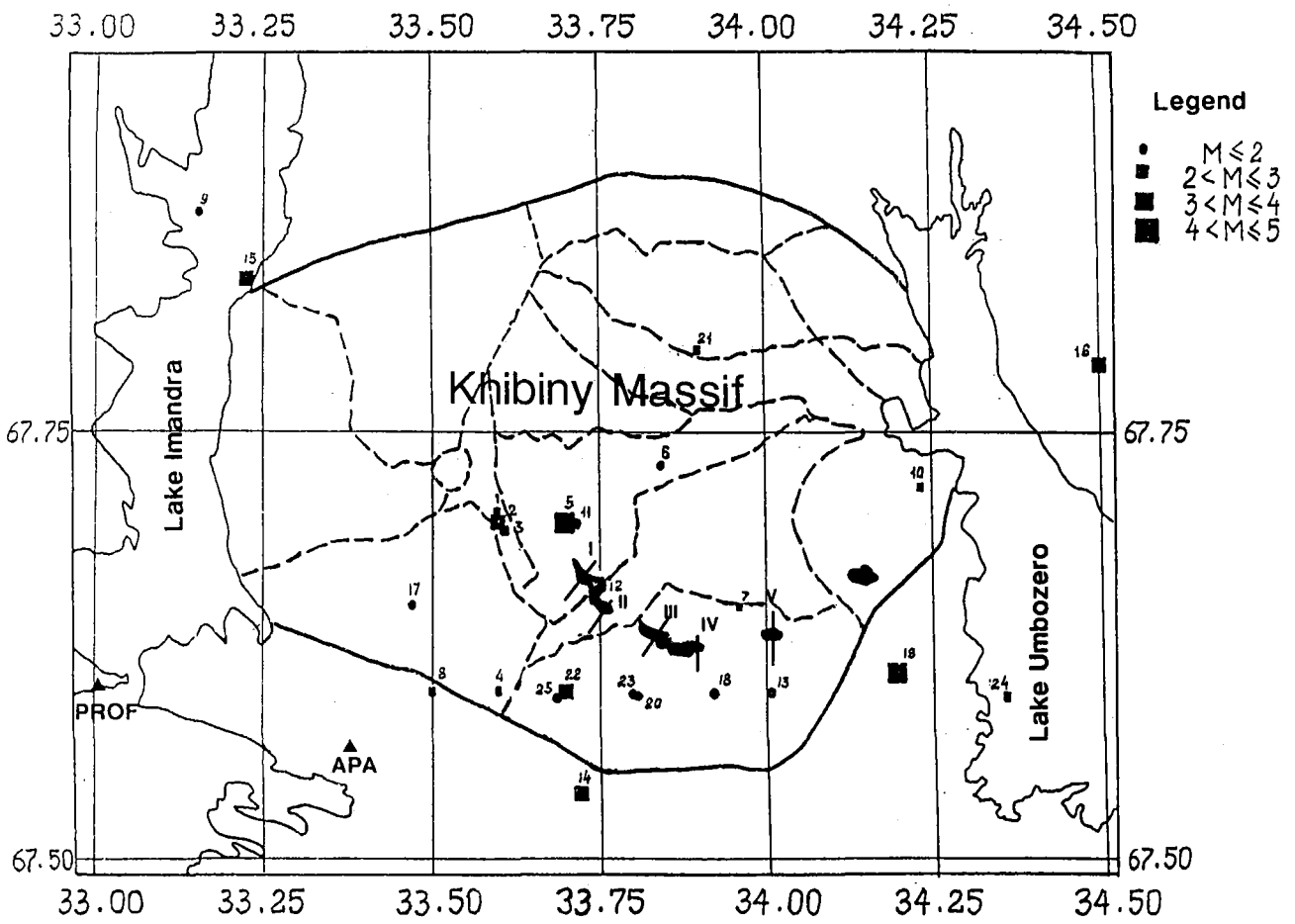

Fig. 7.4.4. Map of the Apatity area, showing the location of the new Apatity station and also the candidate site PROF for a future small array. Also shown is the mining area of the Khibiny Massif, and the division into five (denoted I - V) separate subareas where explosions are currently taking place. Locations for 25 mining induced earthquakes (magnitude range 2-5) are also shown (see also section 7.7, this volume.).

Mine I

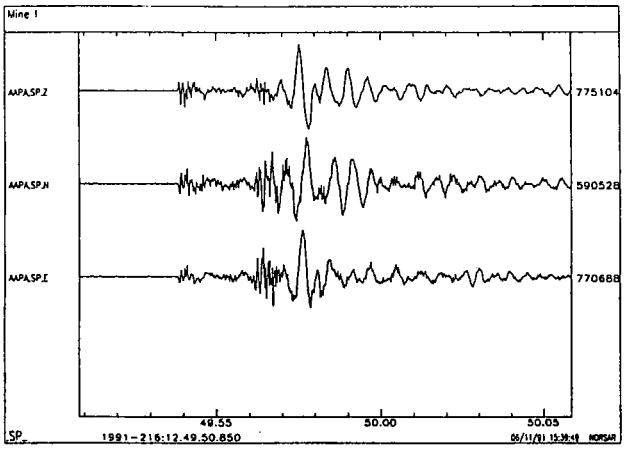

Mine II

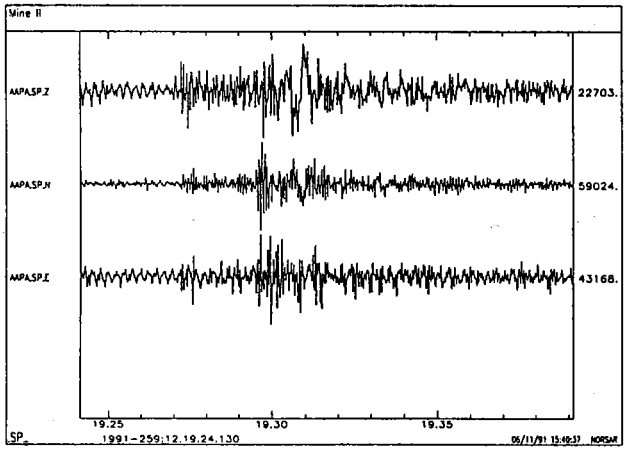

Mine III

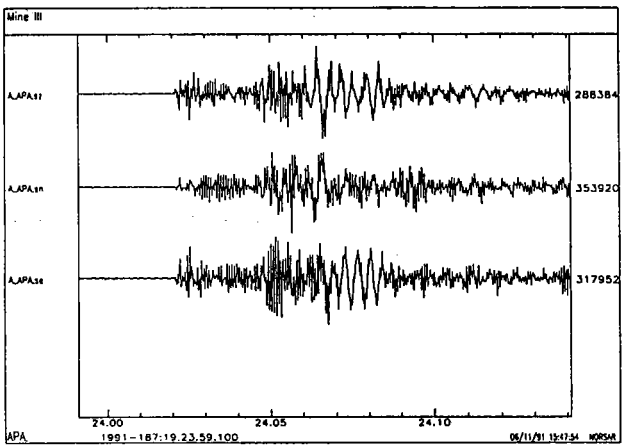

Mine IV

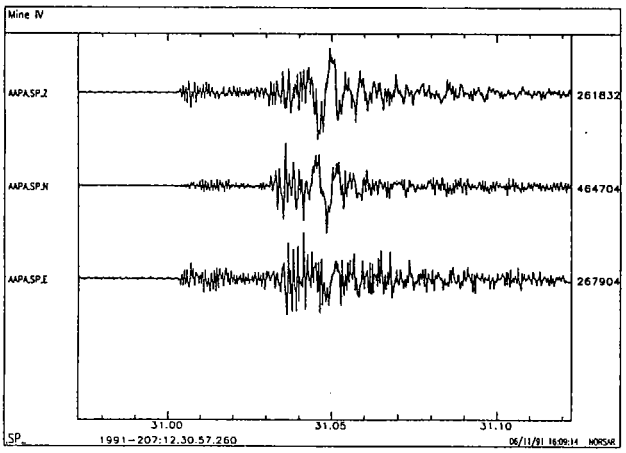

Mine V

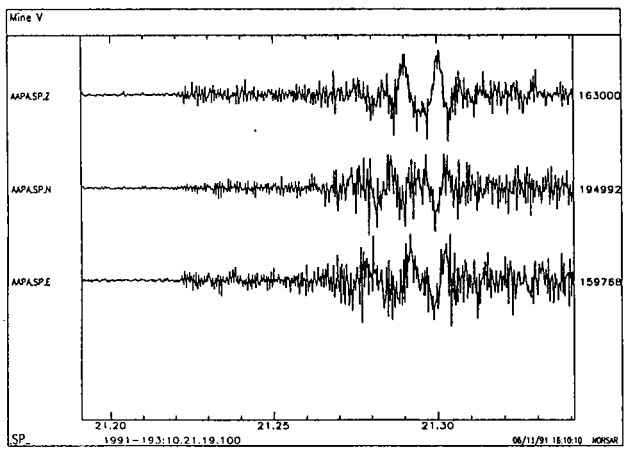

Fig. 7.4.5. Apatity three-component data for five mining shots, one from each of the mines I - V in Fig. 7.4.4.

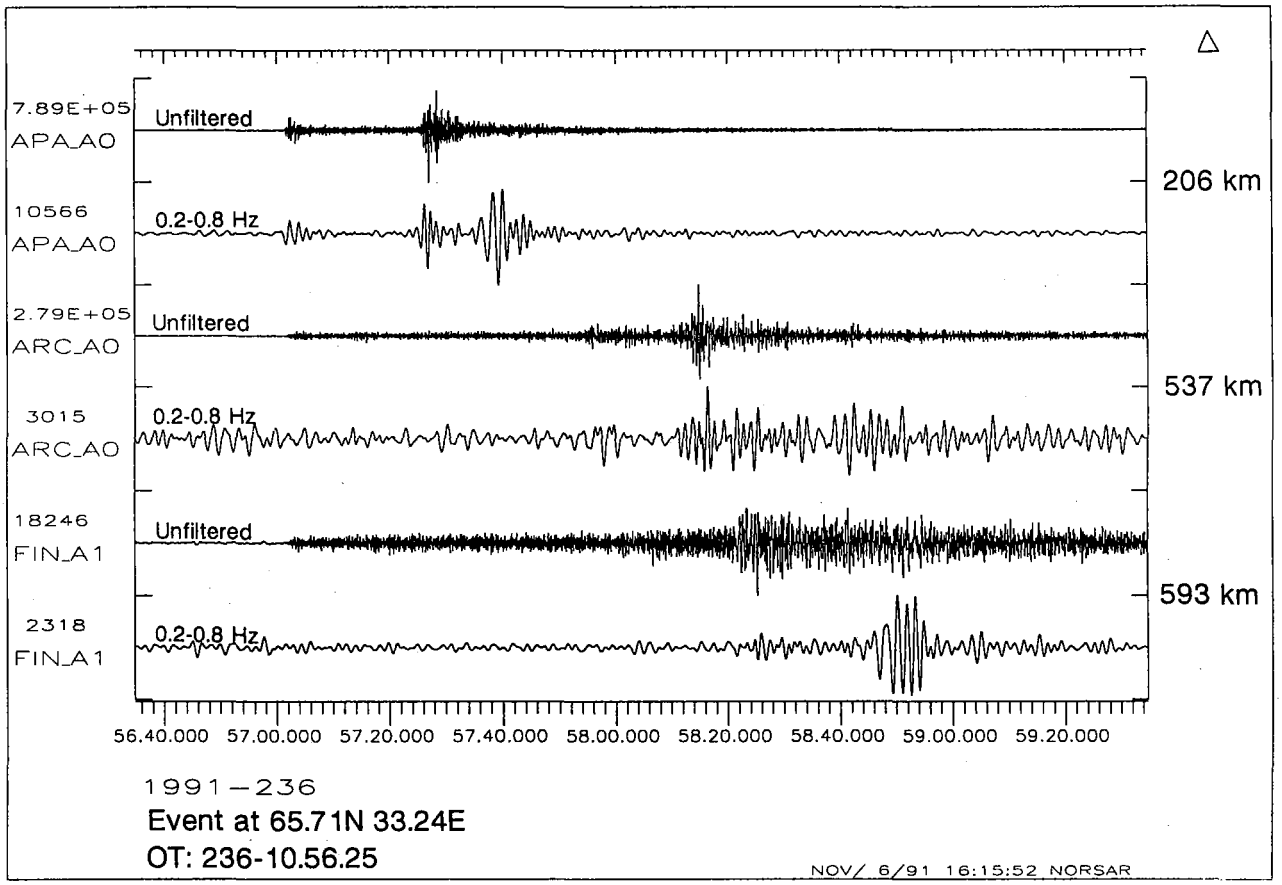

Fig. 7.4.6. Apatity, ARCESS and FINESA single vertical component recordings for a presumed earthquake 200 km south of Apatity. For each station, the plot shows unfiltered data, and data filtered in the band 0.2-0.8 Hz. Note the presence of an Rg phase at FINESA at a distance of nearly 600 km. The time axis refers to the Apatity station on top; ARCESS and FINESA data are aligned with respect to the P onset.

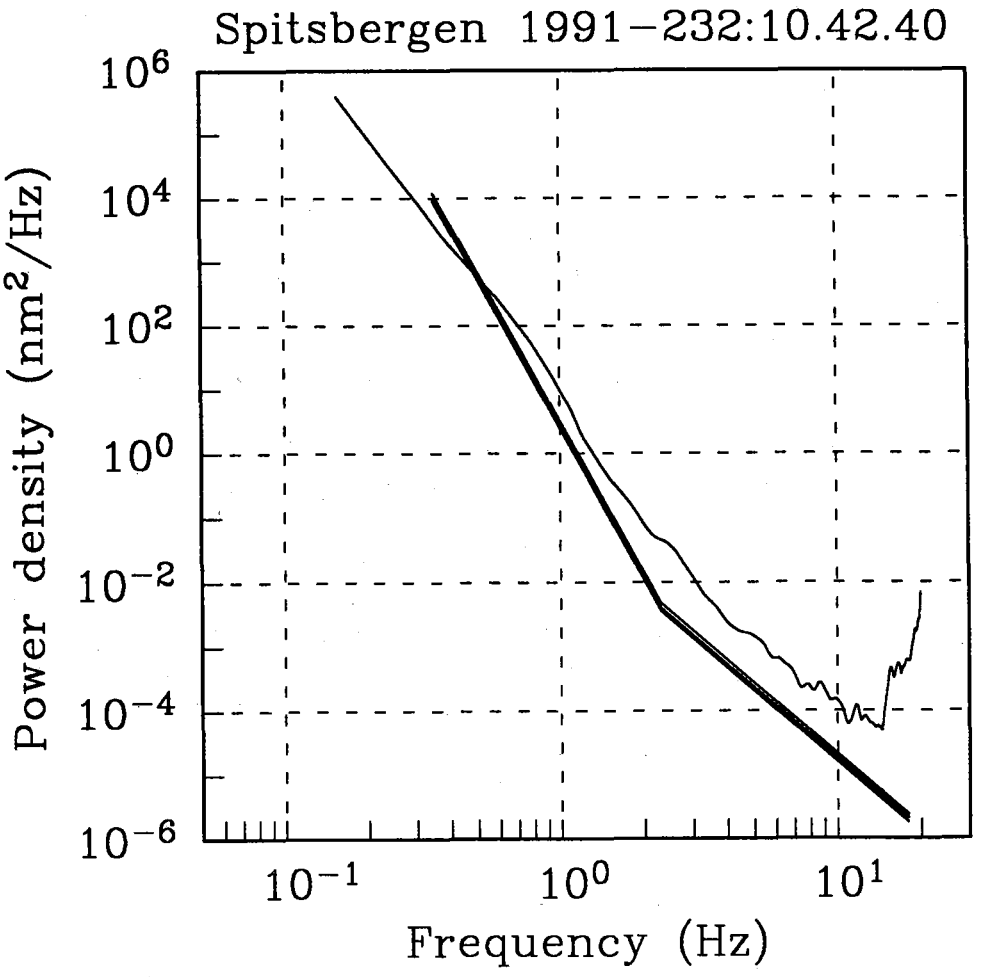

Fig. 7.4.7. Noise spectrum taken at the site for the new small-aperture array to be installed on Spitsbergen in 1992. The solid line denotes the NORESS noise model of Fyen (1990). The spectrum was estimated in the same way as the spectra of Fig. 7.4.3.

7.5 Initial testing of mixed event separation using a statistically optimal adaptive algorithm.

Introduction

The network of the three Fennoscandian regional arrays, ARCESS, FINESA and NORESS, has shown an excellent capability to monitor the seismic activity at the Soviet test site at Novaya Zemlya. In a previous report (Kværna and Ringdal, 1990), we demonstrated the application of the threshold monitoring (TM) technique to obtain continuous estimates of the largest size of events that might go undetected by the monitoring network. This study showed that during normal noise conditions, it was possible to monitor the Novaya Zemlya test site in this way down to m_b 2.5 more than 99% of the time.

However, during intervals of increased seismic amplitude levels at the arrays, e.g., caused by the arrivals of signals from strong earthquakes, the monitoring capability may deteriorate significantly, as shown in Fig. 7.5.1. For the day analyzed in Fig. 7.5.1, a maximum network threshold of 3.8 occurred because of arrivals from a strong earthquake at Hindu Kush (m_b = 6.0). This implies that an event of magnitude 3.8 in theory could have occurred at Novaya Zemlya at that time without exceeding the network threshold.

To improve the monitoring capability during such intervals of increased magnitude thresholds, we have started to evaluate the potential of a statistically optimal processing scheme (Kushnir and Lapshin, 1984) for suppressing the effect of interfering coherent arrivals. The method, denoted adaptive optimal group filtering (AOGF), has earlier been applied for extraction of signals from background noise (Kushnir et al., 1990). Compared to conventional beamforming at NORESS and ARCESS, AOGF has demonstrated a capability to provide significant SNR gains over a wide frequency band (0.2-5.0 Hz). The largest gain (12-18 dB more than conventional beamforming) is obtained at low frequencies where the method utilizes the very coherent nature of the noise. But even for the frequency band from 2 to 4 Hz, AOGF provides a typical SNR gain of the order of 6 to 8 dB compared to the conventional beam.

Theoretical background for adaptation to interfering events

In the study of Kushnir et al. (1990), a pure noise interval preceding the signal was selected for adaptation. Exploiting the stationarity of the background noise field, the interval containing the signal was subsequently processed by the AOGF method using the parameters obtained during the adaptation.

This procedure is, however, *not* relevant when we want to extract a hypothetical signal hidden somewhere in the coda of another signal. In this case, we do *not* know *if* or *when* the hypothetical event occurred, and do only have information on the slowness and azimuth of the hypothetical signal. For AOGF to be applicable to our new purpose, the adaptation needs to be successful even if the adaptation interval contains the wave we want to extract.

We will in the following show theoretically that the AOGF method has the desired property:

The AOGF method is based on an optimal Wiener group filter (OGF) with frequency response:

$$\vec{g}(f) = (g_1(f), \ldots, g_m(f)) \tag{1}$$

where m is the number of array sensors.

The OGF has the characteristics of effectively suppressing the coherent part of the noise field while keeping the signature of the wanted plane wave undistorted. The filter $\vec{g}(f)$ transforms the input array data $\vec{x}_t = (x_{1t}, \ldots, x_{mt})^T$ (where T denotes the transpose) into a scalar trace y_t. $y_t = \vec{g}_t * \vec{x}_t$ where * denotes convolution, and $y(f) = \vec{g}(f) \cdot \vec{x}(f)$, where $y(f)$, $\vec{g}(f)$ and $\vec{x}(f)$ are the Fourier transforms of y_t, $\vec{g}_t$ and $\vec{x}_t$.

It is well known that $\vec{g}(f)$ has the form:

$$\vec{g}(f) = \frac{\vec{h}^{\dagger}(f) \cdot F_n^{-1}(f)}{\vec{h}^{\dagger}(f) \cdot F_n^{-1}(f) \cdot \vec{h}(f)} \tag{2}$$

where $F_n(f)$ is the power spectral density matrix of the noise $\vec{n}_t = (n_{1t}, \ldots, n_{mt})^T$. $\vec{h}(f) = (h_1(f), \ldots, h_m(f))^T$, where $h_k(f) = e^{-2\pi f T_k}$ and T_k is the time delay at the k^{th} sensor for the plane wave to be extracted from the background noise field. $\dagger$ denotes the Hermitian conjugate.

If we are adapting to a pure noise interval, the matrix $F_n^{-1}(f)$ is estimated by a special procedure. From a computational and statistical point of view,a good way to estimate the large size matrix $F_n^{-1}(f)$ is to use autoregressive modelling of the noise field $\vec{n}_t$. The new filter

$$\vec{g}(f) = \frac{\vec{h}^{\dagger}(f) \cdot \hat{F}_n^{-1}(f)}{\vec{h}^{\dagger}(f) \cdot \hat{F}_n^{-1}(f) \cdot \vec{h}(f)} \tag{3}$$

is referred to as the adaptive optimal group filter (AOGF) where $\hat{F}_n^{-1}(f)$ is the autoregressive estimate of $F_n^{-1}(f)$.

If the adaptation interval contains a mixture of the signal and pure noise, i.e., $\vec{x}_t = \vec{s}_t + \vec{n}_t$, we cannot estimate $F_n^{-1}(f)$ but only the spectral density matrix $F_x^{-1}(f)$ of the mixture. Let us consider the group filter

$$\vec{d}(f) = \frac{\vec{h}^{\dagger}(f) \cdot F_x^{-1}(f)}{\vec{h}^{\dagger}(f) \cdot F_x^{-1}(f) \cdot \vec{h}(f)} \tag{4}$$

where

$$F_x(f) = E\{[\vec{n}(f) + \vec{h}(f) z(f) e^{-2\pi i f T_0}] [\vec{n}(f) + \vec{h}(f) z(f) e^{-2\pi i f T_0}]^{\dagger}\}$$

$$= F_n(f) + \vec{h}(f) \vec{h}^{\dagger}(f) \cdot p(f)$$

and $z(f)$ is the Fourier transform of the signal waveform, T_0 is the travel-time to the reference sensor of the array, $p(f)$ is the power spectral density of the signal waveform and E denotes statistical expectation.

Using a formula of Bartlett (1951) for matrix inversion, we can write:

$$F_x^{-1}(f) = F_n^{-1}(f) - F_n^{-1}(f) \vec{h}(f) \vec{h}^{\dagger}(f) F_x^{-1}(f) p(f) \left[1 + \vec{h}^{\dagger}(f) F_x^{-1}(f) \vec{h}(f)\right]^{-1} \tag{5}$$

Substituting (5) into (4) yields:

$$\vec{d}(f) = \frac{\vec{h}^{\dagger}(f) \cdot F_n^{-1}(f)}{\vec{h}^{\dagger}(f) \cdot F_n^{-1}(f) \cdot \vec{h}(f)} \cdot \frac{I\left[1 - \vec{h}^{\dagger}(f) F_n^{-1}(f) \vec{h}(f) \cdot C\right]}{\left[1 - \vec{h}^{\dagger}(f) F_n^{-1}(f) \vec{h}(f) \cdot C\right]} = \vec{g}(f) \tag{6}$$

where I is the identity matrix and $C = p(f) \cdot \left[1 + \vec{h}^{\dagger}(f) F_n^{-1}(f) \vec{h}(f)\right]^{-1}$.

Equation (6) shows that in theory, AOGF will work even if the adaptation interval contains the plane wave we want to extract.

Processing of synthetic mixtures

The main problem arising when attempting to utilize the derived theoretical property of AOGF in data processing practice, is to estimate $F_x^{-1}(f)$ with sufficient accuracy using a mixture of signal and noise records. Autoregressive modelling in principle gives us such an opportunity. This will be shown in some experiments with simulated array data.

Using the geometry of the NORESS array, we have synthesized a mixture of a transient plane wave and a stationary coherent noise field with some added white noise. The slowness vector of the modelled transient is identical to that of a P-wave originating at the Novaya Zemlya test site. With relevance to the problem case outlined in the introduction, the slowness vector of the stationary coherent noise field corresponds to that of a P-wave from an event in the Hindu Kush region. Using the current implementation of the AOGF method, a successful signal extraction is shown in Fig. 7.5. 2. The conventional beam shown on the top trace did not reveal the signal, whereas the signal clearly stands out on the AOGF filtered trace shown in the middle. For comparison, a single array sensor is shown at the bottom. This experiment shows that the current AOGF implementation is

capable of extracting a simple signal from a simple noise field, even if adaptation is made to the data containing the signal we want to extract.

Experiments with NORESS data with a real Novaya Zemlya signal superimposed in the coda of a real Hindu Kush event did not give the desirable result with the current implementation of the AOGF method. This can be explained by the specific features of the software, which has been designed for on-line implementation, as shown by Kushnir et al. (1990). In this program, adaptation is made after steering the array to the chosen direction, resulting in synchronized signal waveforms when data contain the signal we want to extract. Our working hypothesis is that this creates a problem for the multichannel autoregressive estimation procedure, in particular if the background noise has rather complex spatial features like an earthquake coda.

An additional experiment indicates that if we introduce the appropriate changes to the AOGF implementation (by doing all computations in the frequency domain without steering of the array sensors), a successful signal extraction can be achieved, even in the case when the adaptation interval contains a real seismic signal superimposed in the coda of another seismic event.

The experiment, simulating the frequency domain version of AOGF by use of the current AOGF software, consisted of the following steps:

1. A synthetic mixture was created by superimposing down-scaled records of the Novaya Zemlya explosion of 24 October 1990 in the coda of a real Hindu Kush event (event 1 of Table 7.5.1). The SNR between the Novaya Zemlya and the Hindu Kush signals was approximately 1.
2. Adaptation to this data was made without introducing time delays (steering with infinite apparent velocity), thus avoiding synchronized waveforms.
3. A new synthetic mixture was created by superimposing a transient plane wave with infinite apparent velocity and the waveform of the Novaya Zemlya explosion in the coda of the Hindu Kush event. In this case the SNR was only 0.25.
4. This data was then AOGF filtered with the parameters obtained during the previous adaptation.

The result is given in Fig. 7.5.3, indicating the successful extraction of the signal.

This procedure is similar to what will be done by the new frequency-domain implementation of AOGF, thus indicating that the theoretical property outlined in the preceding section, may also be valid in practice.

Adaptation to a neighboring event

We have also investigated the possibility of using two neighboring events in the AOGF processing, using one event for adaptation, and subsequently AOGF filtering the other event (which may contain another signal) with the parameters obtained during the adaptation to the first event.

Two strong Hindu Hush earthquakes with an epicentral difference of approximately 100 km were chosen for this experiment (see Table 7.5.1). The first 20 seconds of the two P-wavetrains recorded at NORESS are shown in Fig. 7.5.4, and the spectra of the first 10 seconds are given in Fig. 7.5.5. Note that the spectra show very similar characteristics.

The results of this test are summarized in the spectra of Fig. 7.5.6. The upper curve shows the spectrum of a conventional beam steered with a slowness vector corresponding to a P-wave from the Novaya Zemlya test site, using NORESS data for Hindu Kush event no. 1 (see Table 7.5.1). The spectrum shown by the solid line below, corresponds to the AOGF beam steered to Novaya Zemlya of Hindu Kush event no. 1, using Hindu Kush event no. 2 for adaptation; and the spectrum shown by the dashed line, corresponds to the AOGF beam steered to Novaya Zemlya of Hindu Kush event no. 1, using the same event (no. 1) for adaptation.

Comparing the spectra suggests that for frequencies below 1 Hz, the AOGF method can suppress the effect of interfering events much better than conventional beamforming, when a neighboring event has been used for adaptation. For higher frequencies, the improvement is also significant. The spectrum shown by the dashed line, indicate that more improvement can be obtained if the same event is used for adaptation.

To visualize the effect of using a neighboring event for adaptation, we superimposed records of the down-scaled Novaya Zemlya explosion in the coda of Hindu Kush event no. 1. As in Fig. 7.5.3, the SNR was 0.25. The results from AOGF filtering this mixture signal with the adaptation parameters retrieved from Hindu Kush event no. 2., are shown in the middle trace of Fig. 7.5.7. As expected, due to signal loss during the plane-wave beam-forming, the amplitude of the Novaya Zemlya signal is reduced with comparison to the amplitude of Fig. 7.5.3. Also indicated by the spectra of Fig. 7.5.6, the amplitude of the Hindu Kush event is not as effectively suppressed as in the case of Fig. 7.5.3, but we are still able to identify the Novaya Zemlya arrival on the AOGF beam.

To further compare the relative performance between the conventional and the AOGF beams, we bandpass filtered the traces of Fig. 7.5.7 in the frequency band providing the largest SNR (i.e., 1.5-3.5 Hz). The results are shown in Fig. 7.5.8. The only difference from Fig. 7.5.7, is that instead of using all sensors of the NORESS array when forming the conventional beam, we used a sub-geometry consisting of A0Z, the C-ring and the D-ring (17 sensors). In the frequency band 1.5-3.5 Hz, this sub-geometry will provide the best SNR improvement, at least when comparing to background noise conditions (Kværna, 1989). The result shows that when using a neighboring event for adaptation, the AOGF beam provides better SNR than the optimum conventional beam (optimum = best sub-geometry and best filter band).

Discussion

The results presented above suggest that application of the AOGF method has a potential for significantly improving the signal-to-noise ratios of seismic events occurring in the coda of large earthquakes. This is important, e.g., for improving the threshold monitoring capability during periods of increased magnitude thresholds. The experiments with the

Hindu Kush events recorded at NORESS indicate that with the appropriate changes to the AOGF software (by implementing the frequency domain version), a significant threshold magnitude reduction may be achieved for each phase considered.

Applying the software currently available, using adaptation to a neighboring event, we have the capability of some reduction of the magnitude thresholds.

The continuation of this research will consist of carefully testing the frequency-domain version of AOGF, and special emphasis will be devoted to ensuring the undistorting feature of AOGF on the signal we want to extract from the background coda. In addition, practical problems related to the use of AOGF in the threshold monitoring algorithm will be investigated.

Tormod Kværna
Alex Kushnir, MITPAN Institute, Moscow, USSR

References

Bartlett, M.S. (1951): In inverse matrix adjustment, arising in discriminant analysis, *Ann. Math. Stat.*, Vol. 2, No. 1

Kushnir, A.F., J. Fyen and T. Kværna (1990): Multichannel statistical data processing algorithms in the framework of the NORSAR event processing program package, *Semiannual Tech. Summary, 1 Oct 1990 - 31 Mar 1991*, NORSAR Sci. Rep. 2-90/91, NORSAR, Kjeller, Norway.

Kushnir, A. F. and V. M. Lapshin (1984): Optimal processing of the signals received by a group of spatially distributed sensors, in *Computational Seismology*, Allerton Press, Inc., Vol 17, 163-174.

Kværna, T (1989): On exploitation of small-aperture NORESS type arrays for enhanced P-wave detectability, *Bull. Seism. Soc. Am.* 79, 888-900.

Kværna, T. and F. Ringdal (1990): Continuous threshold monitoring of the Novaya Zemlya test site, *Semiannual Tech. Summary, 1 Apr - 30 Sep 1990*, NORSAR Sci. Rep. 1-90/91, NORSAR, Kjeller, Norway.

Event no.	Year	Day	Mon	Or.time	Lat	Lon	Depth	m_b
1	1990	25	Oct	04.53.59.9	35.121N	70.486E	114	6.0
2	1990	15	May	14.25.20.6	36.043N	70.428E	113	5.9

Table 7.5.1. PDE locations of the Hindu Kush events.

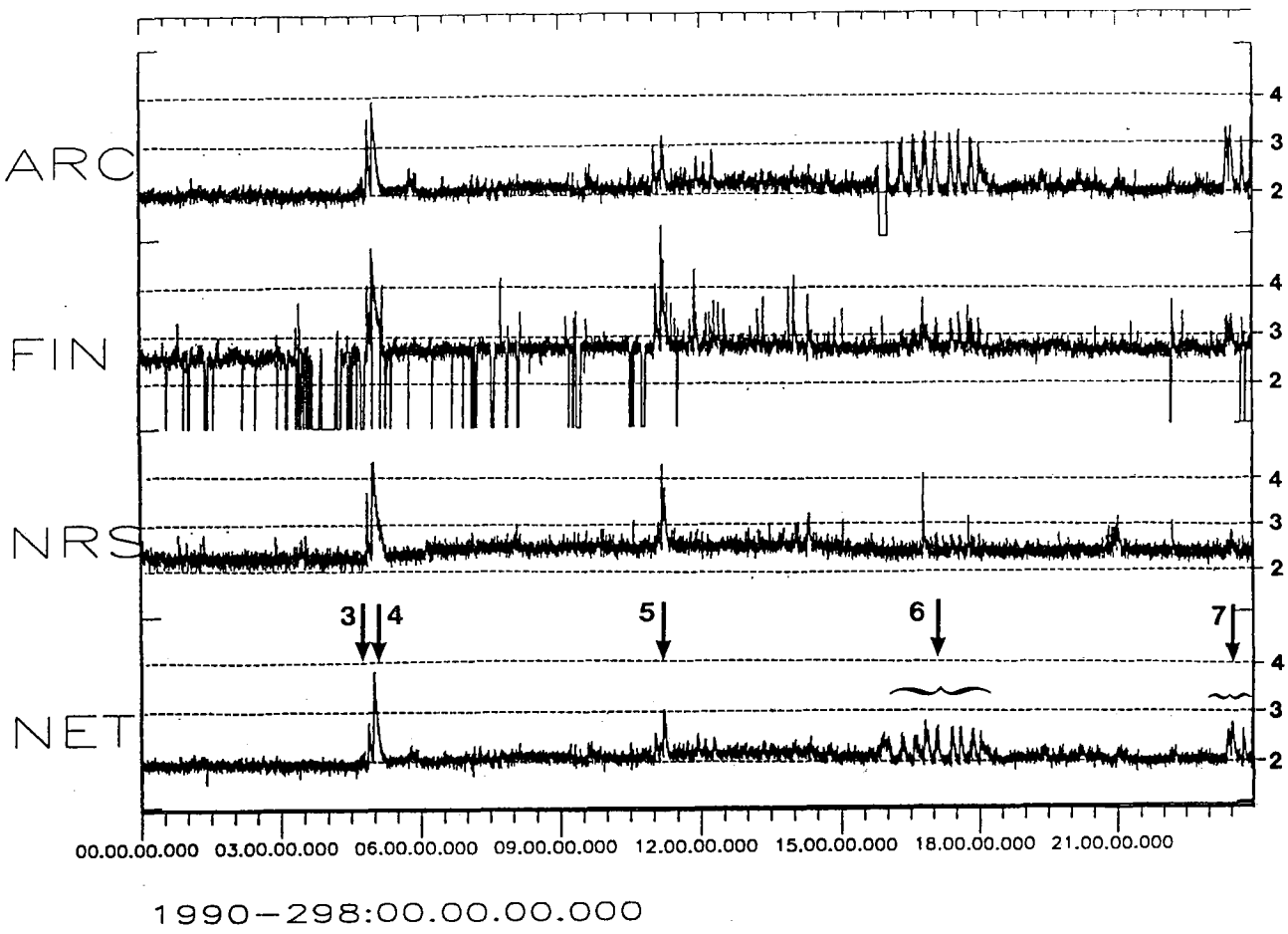

Fig. 7.5.1. Threshold monitoring of the Novaya Zemlya test site for day 298(25 October 1990). The top three traces represent thresholds (upper 90 per cent magnitude limits) obtained from each of the three arrays (ARCESS, FINESA, NORESS), whereas the bottom trace shows the combined network thresholds. The FINESA array had several short outages this day, but this caused no particular problems in terms of network threshold capacity.

Notes:

3. An earthquake (m_b = 4.5) near Jan Mayen. The corresponding network threshold peak for Novaya Zemlya is m_b = 2.8.
4. A teleseismic earthquake (m_b = 6.0) at Hindu Kush. The relatively strong P-wave train caused a peak threshold of m_b = 3.8 for monitoring Novaya Zemlya.
5. A teleseismic earthquake (m_b = 5.9) at Mindanao, Philippine Islands. Corresponding threshold is m_b = 3.0.

6.-7. A sequence of seismic events (presumably underwater explosions) near Murmansk, Kola Peninsula. The network threshold for monitoring Novaya Zemlya is about m_b = 2.5 to 2.8 at the times of these events.

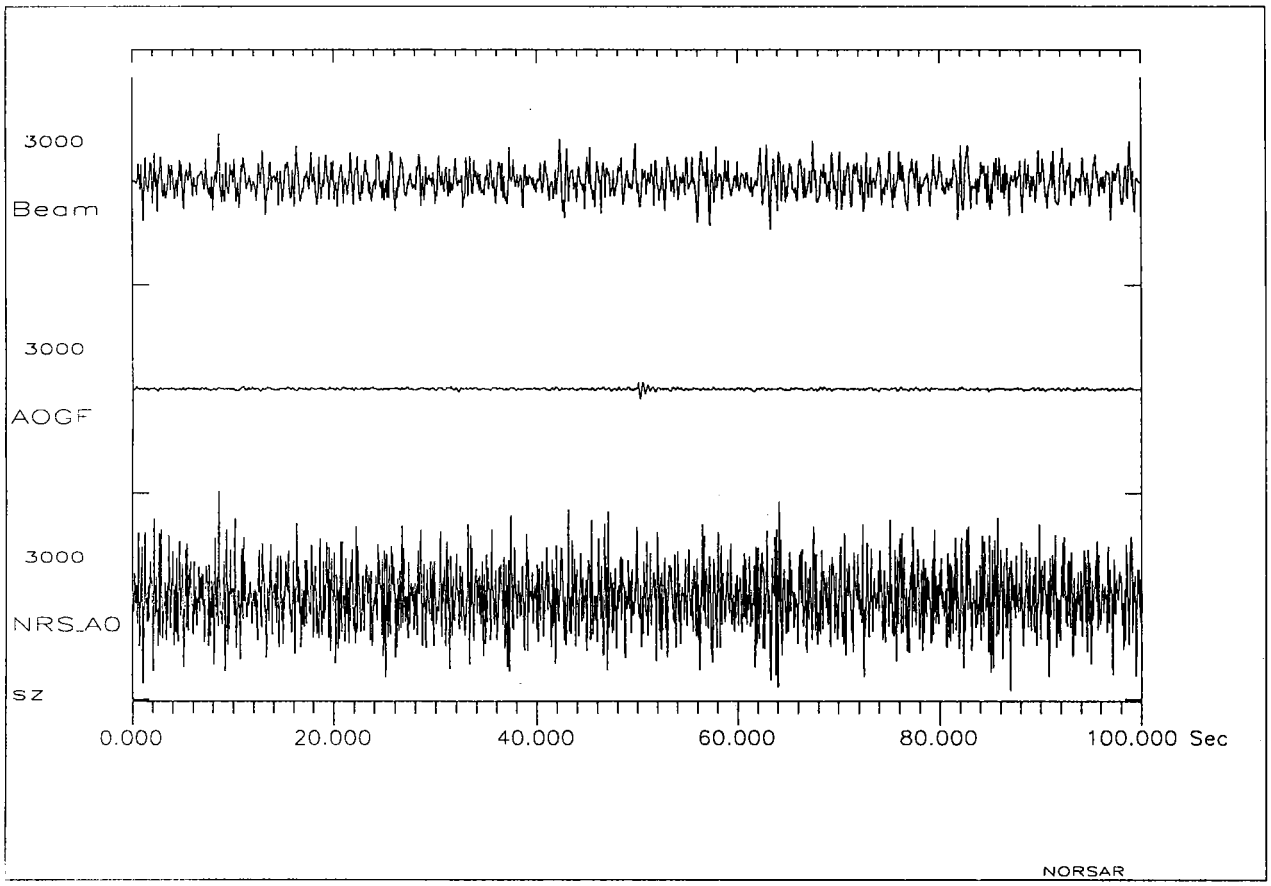

Fig. 7.5.2. Synthetic processing example.
A synthetic signal has been created by adding three components as follows:

1) A stationary, coherent noise field (Hindu Kush direction, P velocity).
2) A stationary, incoherent "white noise" field.
3) A transient, coherent signal (Novaya Zemlya direction, P velocity).

The top trace shows the conventional beam steered to Novaya Zemlya.
The middle trace shows the AOGF beam steered to Novaya Zemlya.
The bottom trace shows the single sensor A0Z.

Note that the signal is clearly visible on the AOGF trace, but not on the other two.

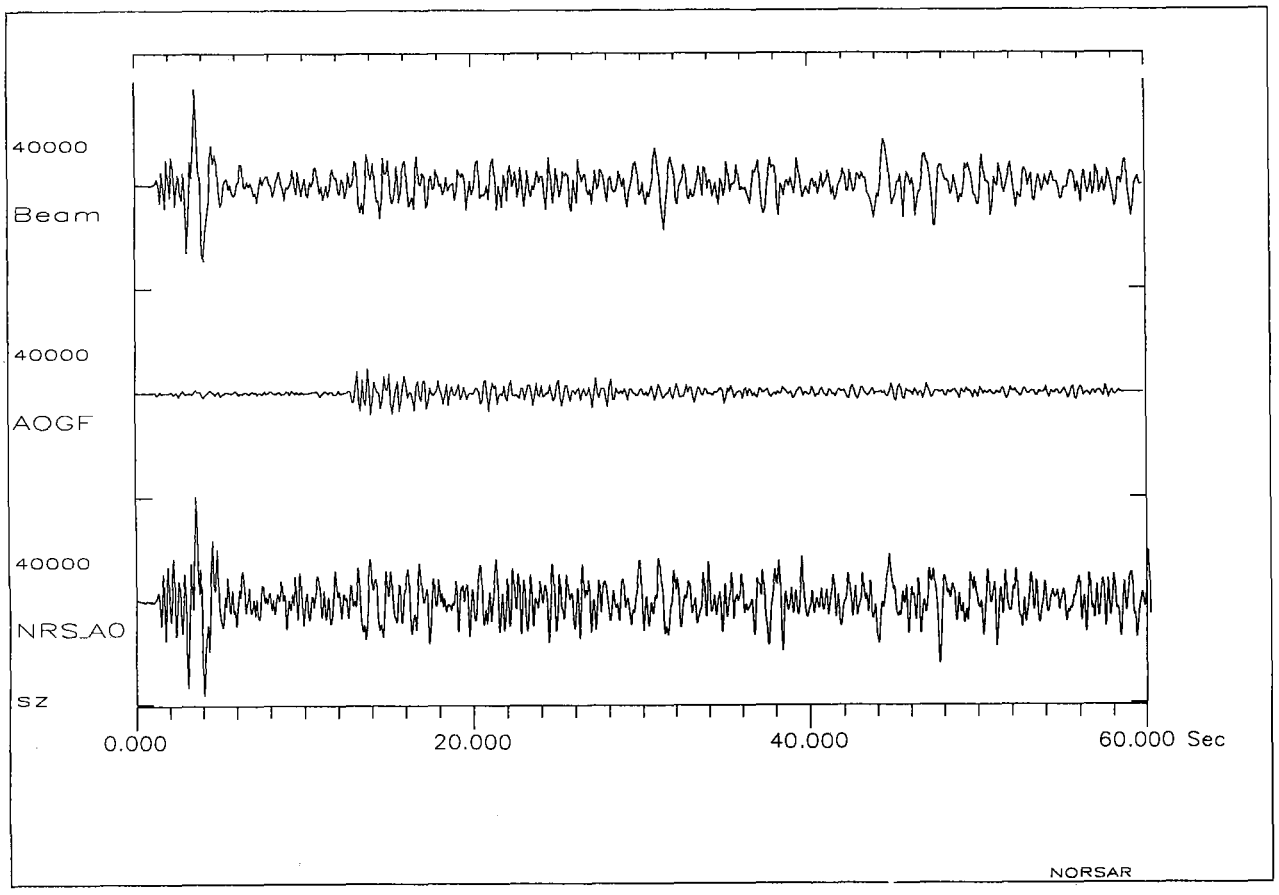

Fig. 7.5.3. Synthetic processing example, illustrating that with the appropriate changes to the AOGF program, we may have the possibility of extracting a real seismic signal from an earthquake coda, even if the adaptation interval containing the signal we want to extract.

The experiment, simulating the frequency domain implementation of AOGF, consisted of the following steps:

1) A synthetic mixture was created by superimposing down-scaled records of the Novaya Zemlya explosion of 24 October 1990 in the coda of a real Hindu Kush event (event 1 of Table 7.5.1). The SNR between the Novaya Zemlya and the Hindu Kush signals was approximately 1.

2) Adaptation to this data was made without introducing time delays (steering with infinite apparent velocity), thus avoiding synchronized waveforms.

3) A new synthetic mixture was created by superimposing a transient plane wave with infinite apparent velocity and the waveform of the Novaya Zemlya explosion in the coda of the Hindu Kush event. In this case the SNR was only 0.25.

4) This data was then AOGF filtered with the parameters obtained during the previous adaptation.

The top trace shows the conventional beam steered with infinite apparent velocity.
The middle trace shows the AOGF beam steered with infinite apparent velocity.
The bottom trace shows the single sensor A0Z.

Note that the signal is clearly visible on the AOGF trace, but not on the other two.

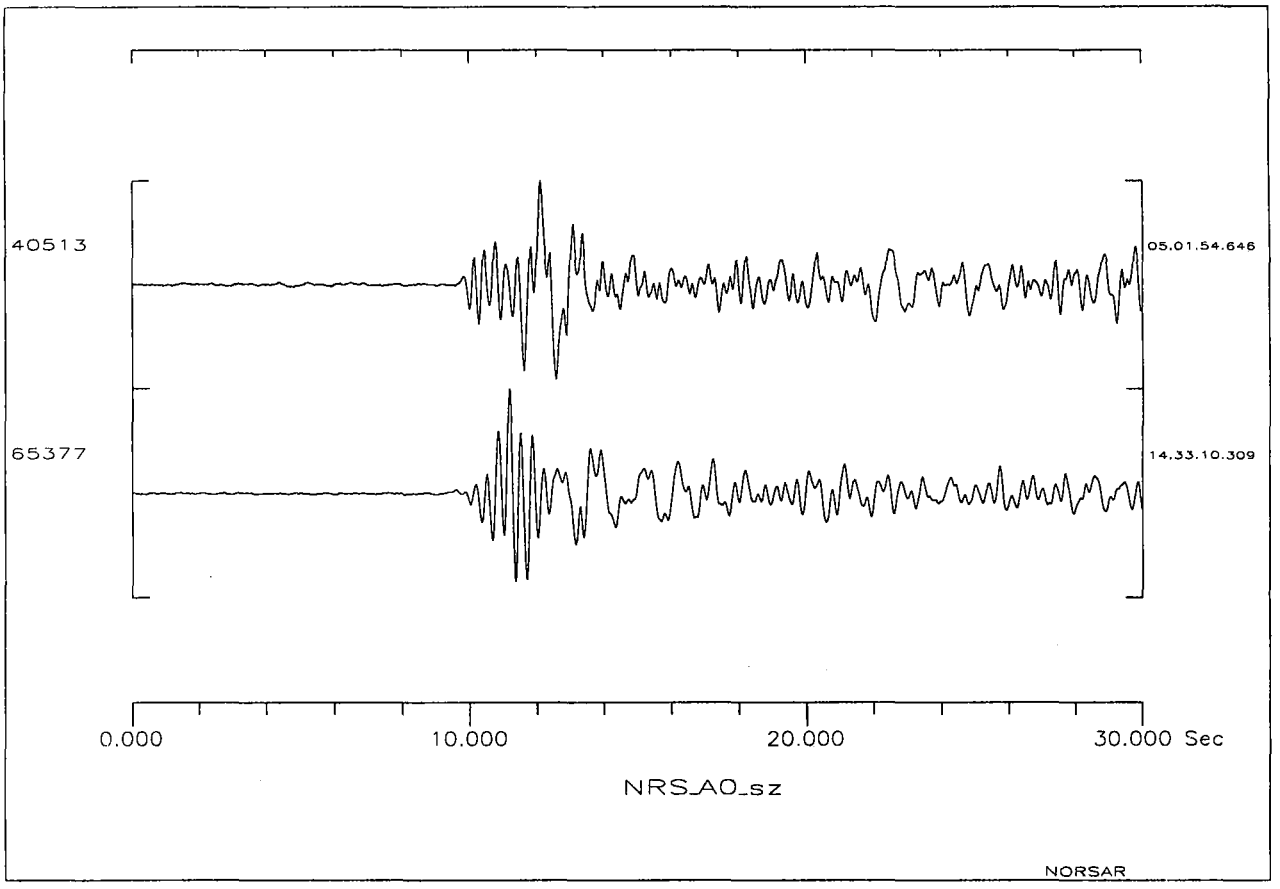

Fig. 7.5.4. NORESS recordings (instrument A0Z) of the two Hindu Kush events described in Table 7.5.1. Event no. 1 is shown in the upper trace, and event no. 2 in the lower.

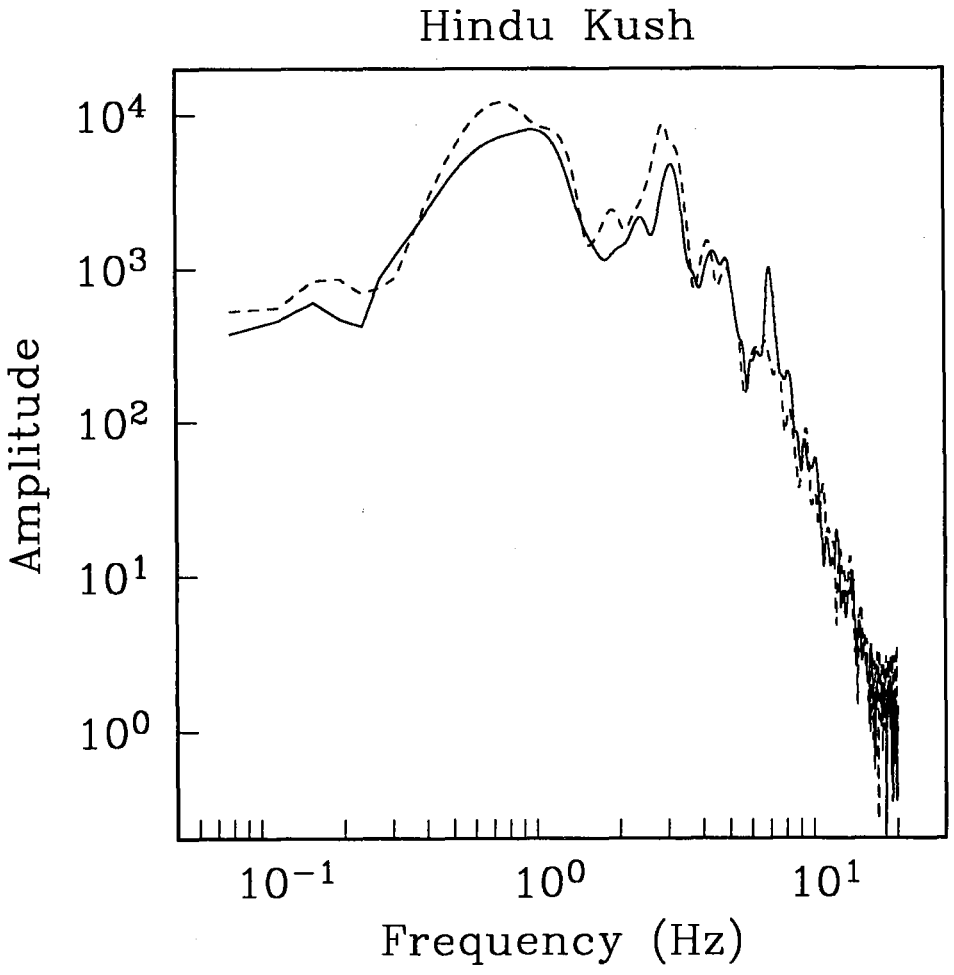

Fig. 7.5.5. P-wave spectra of NORESS recordings of the two Hindu Kush events described in Table 7.5.1. Solid line: Event no. 1. Dashed line: Event no. 2. Both spectra were estimated using 10 seconds of data.

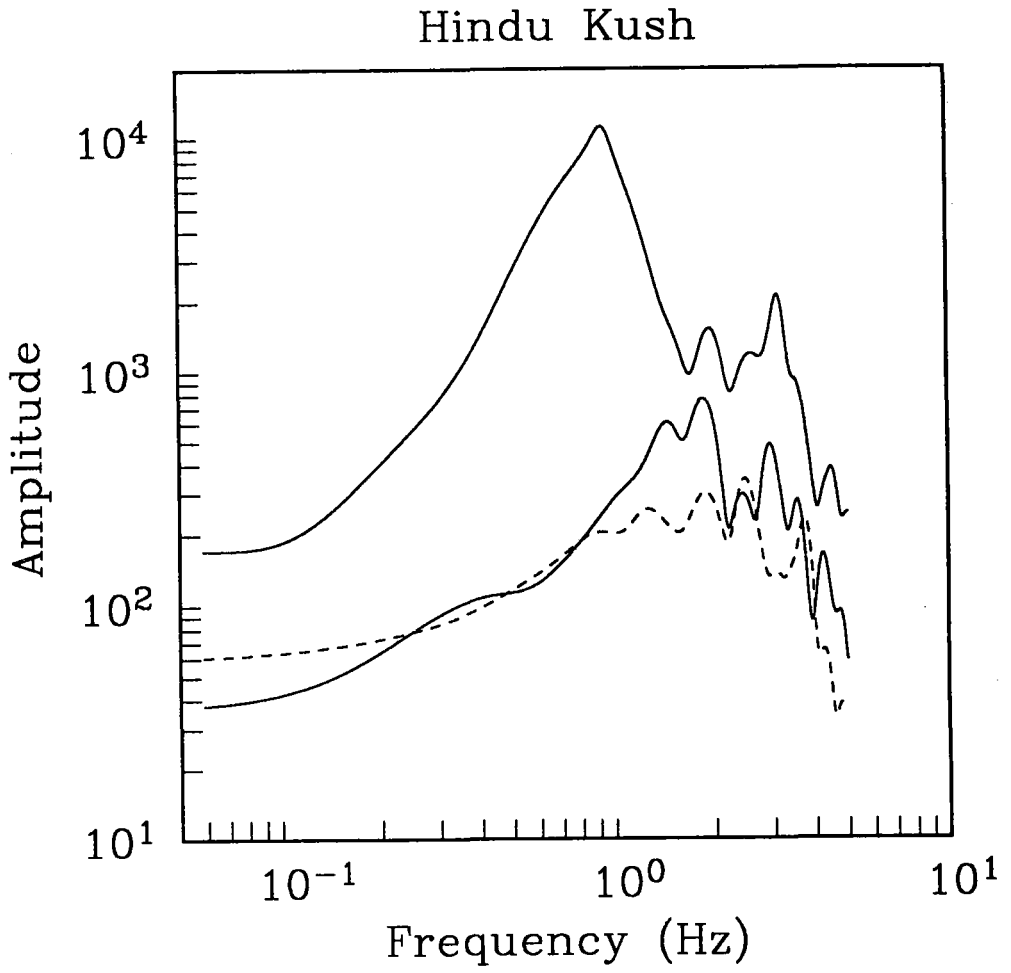

Fig. 7.5.6. After processing Hindu Kush event no. 1 with different techniques, we computed P-wave amplitude spectra of the first 10 seconds of the signal. The upper spectrum results from conventional beamforming using the Novaya Zemlya P-wave steering delays. The lower solid line spectrum results from AOGF filtering with Novaya Zemlya P-wave steering delays using Hindu Kush event no. 2 for adaptation. The dashed line spectrum results from AOGF filtering with Novaya Zemlya P-wave steering delays using the same event (no. 1) for adaptation.

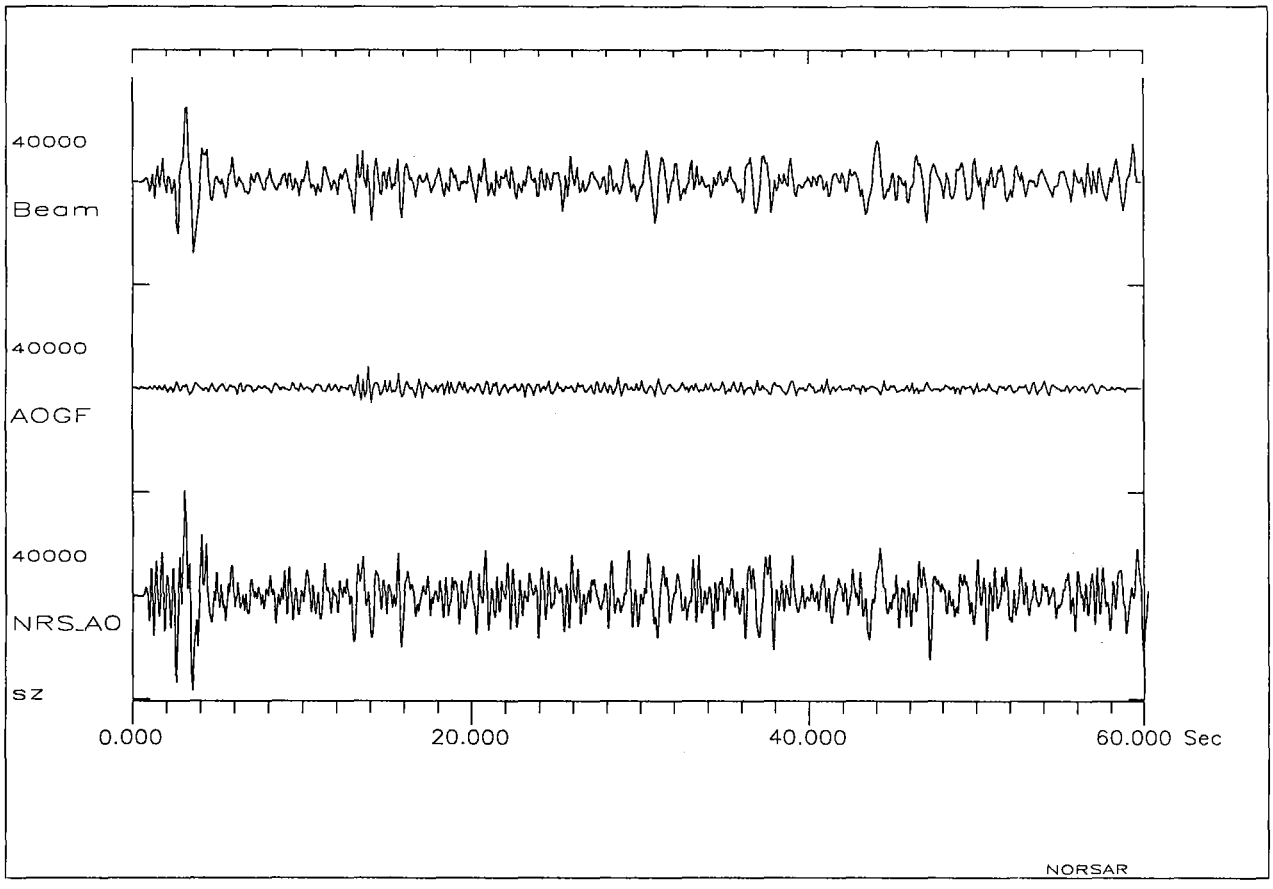

Fig. 7.5.7. Results after processing the mixture of Hindu Kush event no. 1 and the down-scaled Novaya Zemlya signal. Single channel SNR ~ 0.25. The lower trace shows a single NORESS sensor, the top trace is a conventional beam steered to Novaya Zemlya, whereas the middle trace is the AOGF output using Hindu Kush event no. 2 for adaptation.

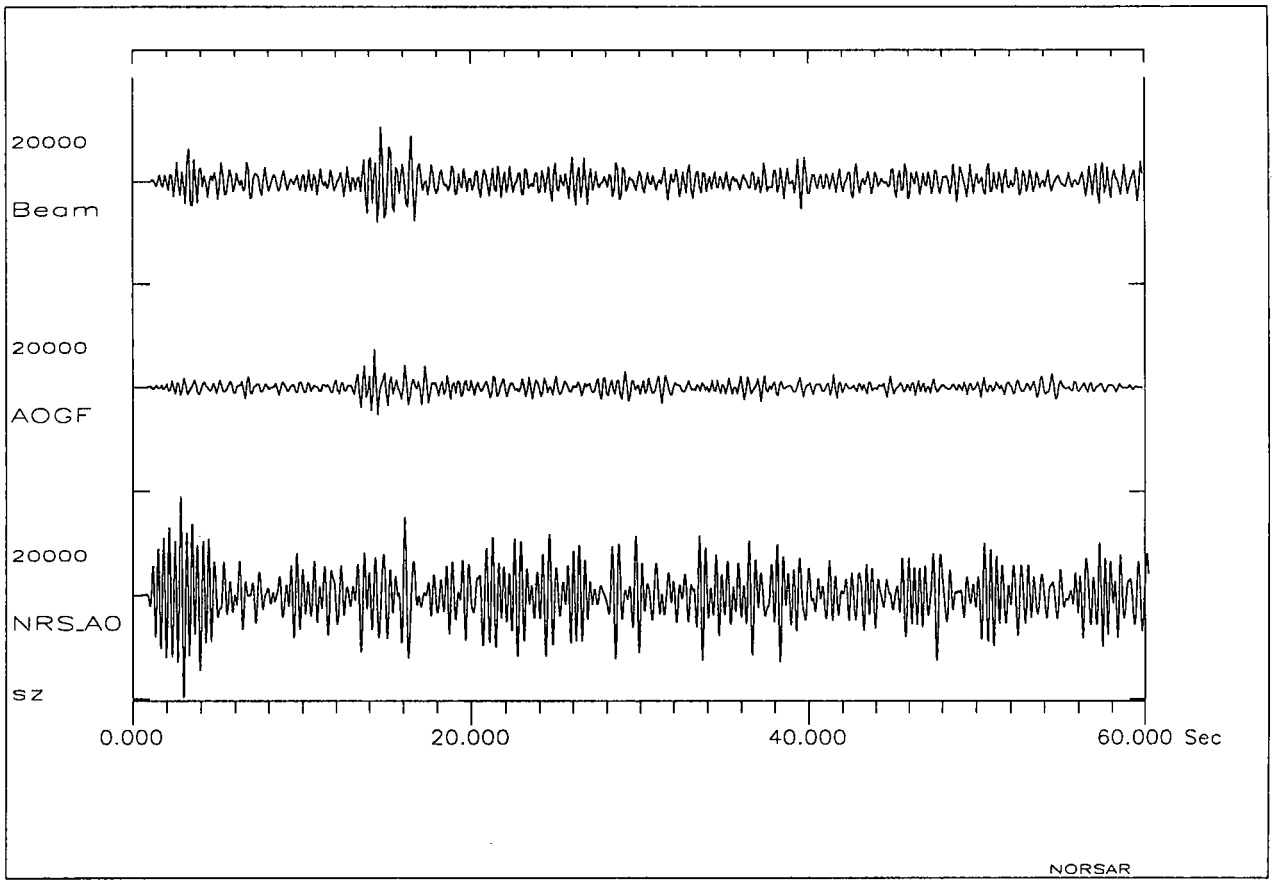

Fig. 7.5.8. Results from bandpass filtering the data of Fig. 7.5.7 in the passband 1.5-3.5 Hz. The only difference from Fig. 7.5.7, is that instead of using all sensors of the NORESS array when forming the conventional beam, we used a sub-geometry consisting of A0Z, the C-ring and the D-ring (17 sensors). Note that even under these optimum conditions for conventional beamforming, the AOGF beam provide the best SNR.

7.6 Regional detection performance during GSETT-2: Initial results for the Fennoscandian array network

Introduction

During the period 22 April to 9 June 1991, the Conference on Disarmament's Group of Scientific Experts carried out the main phase of its Second Technical Test (GSETT-2). A total of 34 countries participated in this test, providing seismic data for 42 consecutive data days from 60 stations distributed around the globe (Fig. 7.6.1). Data were recorded and processed at National Data Centers, and results as well as waveform segments were transmitted to four experimental International Data Centers (EIDCs) for further analysis. Results of these analyses were summarized in event bulletins, which were transmitted back to participants from the EIDCs.

An important aspect of the performance evaluation of GSETT-2 is the completeness and quality of the final event bulletin (FEB). This seismological output is closely linked to the actual spatial distribution of seismic stations. For GSETT-2, a very heterogeneous global coverage yielded large regional variations in detection threshold. About one half of the participating stations were situated in and around Europe, consequently a large number of small events were detected, mainly quarry blasts and rock bursts of magnitude 1 to 4. On the other hand, in many areas of the globe where the station distribution was very sparse, only larger earthquakes were detected.

In this paper a preliminary assessment is made of the detection capability during GSETT-2 for Fennoscandia and NW Russia. This is the region that had maybe the best instrumental coverage during the experiment. In particular the regional arrays deployed in this area made significant contributions.

Our results for this region represent in a sense the "best" regional performance during GSETT-2. It is in no way representative for the performance on a global or more extended regional scale. However, it does serve to illustrate the potential capabilities of a monitoring network, assuming that an adequate density and number of high quality, sensitive array stations are deployed.

Method

The method used for detectability estimation has been described by Ringdal (1975), and is briefly summarized as follows:

1. A reference system, independent of the system to be evaluated, is used. Event lists and magnitudes from this reference system are compiled.
2. For each reference event, a comparison is made to see if the system to be evaluated has detected the event.
3. Based on the number of detections/no detections at each magnitude, a maximum likelihood approach is made to estimate a "detection curve" of the form

$$G(m;\mu,\sigma) = \int_{-\infty}^{m} \frac{1}{\sqrt{2\pi}\sigma} e^{\frac{(x-\mu)^2}{2\sigma^2}} dx \quad (1)$$

Here $G(m;\mu,\sigma)$ denotes the incremental probability of detection, given event magnitude m. The detection curve is completely characterized by the parameters μ and σ. The 50 and 90 per cent incremental detection thresholds (μ_{50} and μ_{90}) become:

$$\mu_{50} = \mu \quad (2)$$

$$\mu_{90} = \mu + 1.29 \cdot \sigma \quad (3)$$

It should be noted that while the method assumes that the reference network provides independent event estimates, it is not necessary to have a complete event catalogue in any given magnitude range. Thus the reference events actually selected are assumed to be randomly sampled from the total number of events available, much in the same way as opinion survey polls attempt to address randomly selected subsets of the population. The resulting detectability estimates will be representative for the region considered only to the extent that the reference event set is representative.

Reference network

The reference data base for this study has been the catalogue of seismic events in northern Europe regularly compiled by the Seismological Institute, University of Helsinki.

The stations used in compiling this catalogue are in almost all cases comprised of the Finnish seismic network single stations. For all practical purposes, the compilation is independent of the regional arrays in Fennoscandia (NORESS, ARCESS, FINESA). The magnitudes quoted in the bulletin are likewise derived independently of the regional arrays, and comprise either duration magnitudes (in most cases) or local magnitudes. These magnitudes are fairly consistent with magnitudes calculated by the Intelligent Monitoring System, while their relationship to teleseismic m_b estimates is at present not well established.

For the month of May 1991, upon which this analysis is based, the reference catalogue contained 321 seismic events in the region bounded by 58°-70°N, 20°-40°E, of which 108 had an assigned magnitude in the range 1.7-2.9.

Results

The initial results from the detectability study are presented in Figs. 7.6.2-7.6.4. Each figure is based upon analyst comparison of the reference events with bulletin reports according to different reporting criteria:

a) One-array detection:

In Fig. 7.6.2, an event is considered detected if it was reported with 2 phases (P and S; or P and Lg) by at least one of the three regional arrays (NORESS, ARCESS, FINESA). In terms of GSETT-2 final event bulletins, this means that the event would either be located as a multi-station event, or listed as an NDC-reported event. We note that the 50 % threshold is close to 1.7, and the 90 % threshold is 2.3 in this case.

b) Two-array detection:

In Fig. 7.6.3, the detection requirement is 2 phases (P and S; or P and Lg) from one array and at least one confirming phase from another array. This added requirement has the effect of increasing the 50 % threshold to 2.1, and the 90 % threshold to 2.4.

c) GSETT-2 reported events:

In Fig. 7.6.4, the GSETT-2 reported events, located by at least one IDC, are shown. (We have not counted as detected events those events whose definition depended upon reportings from the Finnish network stations KAF and VAF, since these two stations were part of the reference network.) The resulting thresholds are similar to those displayed in Fig. 7.6.3 (the two-array case).

Conclusions

The regional evaluation of detection results from GSETT-2 presented here shows that in a region with dense coverage of high-quality array stations as in Fennoscandia, it is possible to detect seismic events at very low magnitudes.

The 90 per cent threshold of around magnitude 2.5 found in this study must of course be considered with the appropriate caution: thus it refers to a regional magnitude scale that currently is not well calibrated in terms of global magnitude. Also, in other geological environments, the wave propagation and array noise suppression characteristics may be different. Therefore, it is not known to which extent such results would be possible to duplicate in other parts of the world.

Further work should be undertaken to evaluate the GSETT-2 detection performance in other regions, in order to gain experience for future studies. It will also be necessary to study event location performance, and evaluate how the detection capability varies as a function of different requirements with regard to event location accuracy.

F. Ringdal

References

Ringdal, F. (1975): On the estimation of seismic detection thresholds, Bull. Seism. Soc. Am., 65, 1631-1642.

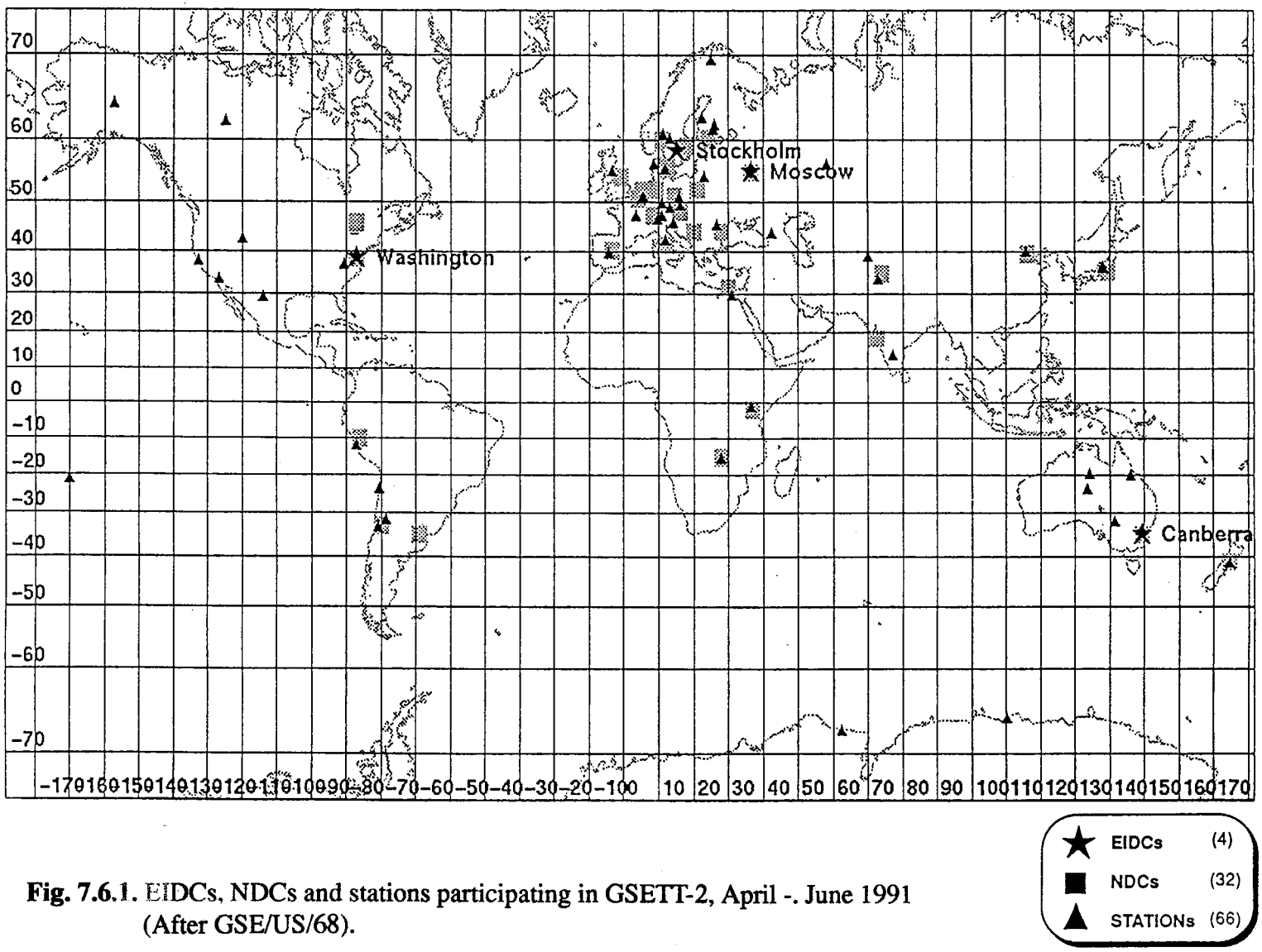

Fig. 7.6.1. EIDCs, NDCs and stations participating in GSETT-2, April -. June 1991 (After GSE/US/68).

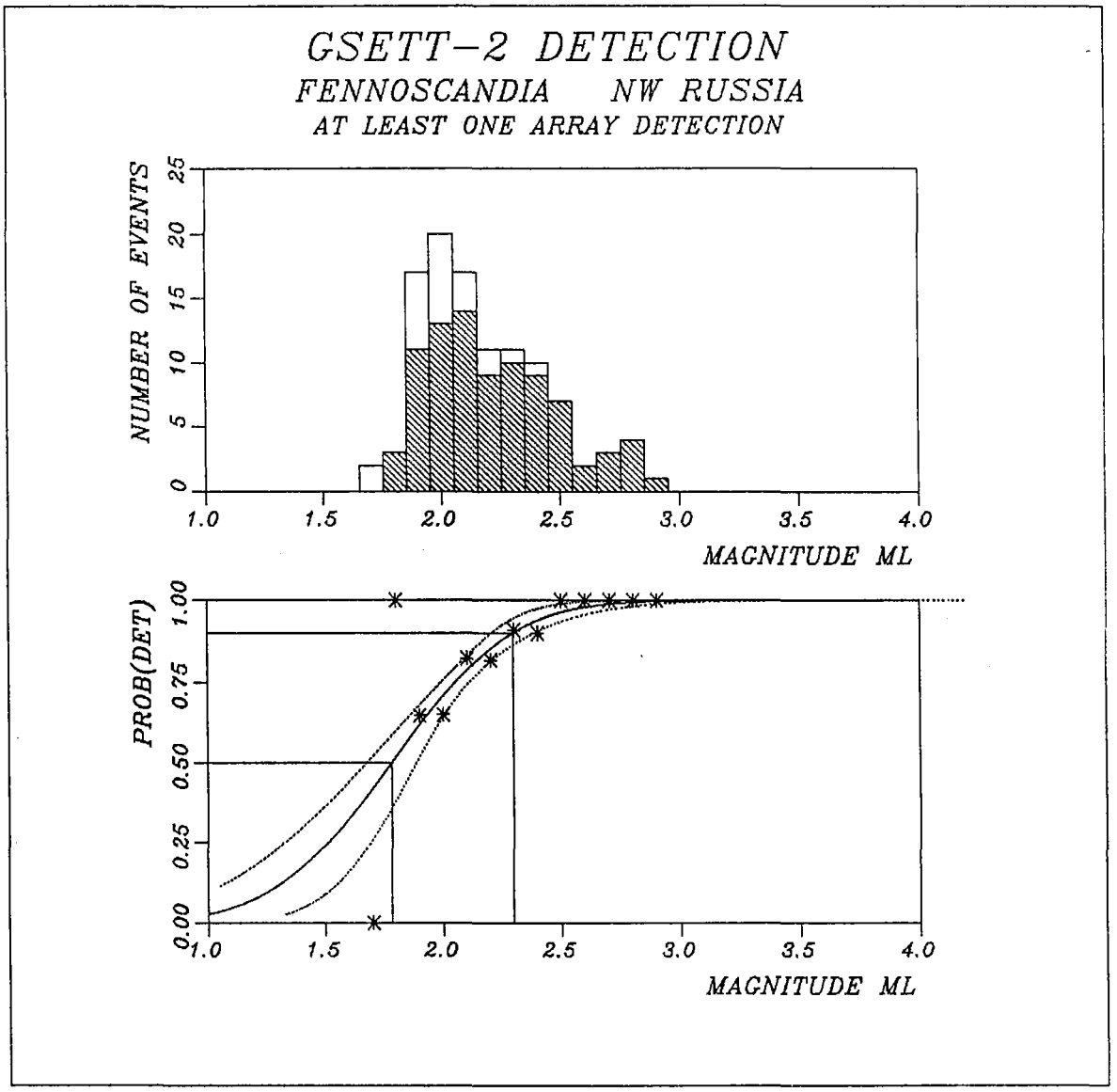

Fig. 7.6.2. Maximum likelihood detectability estimation for Fennoscandia-NW Russia using the Univ. of Helsinki bulletin as a reference. The upper half shows the reference event set and the number of events actually detected for each magnitude. The lower half shows the maximum likelihood detectability curve and its confidence limits. The actual percentage of detected events at each magnitude is also shown. This figure is based upon a one-array detection requirement.

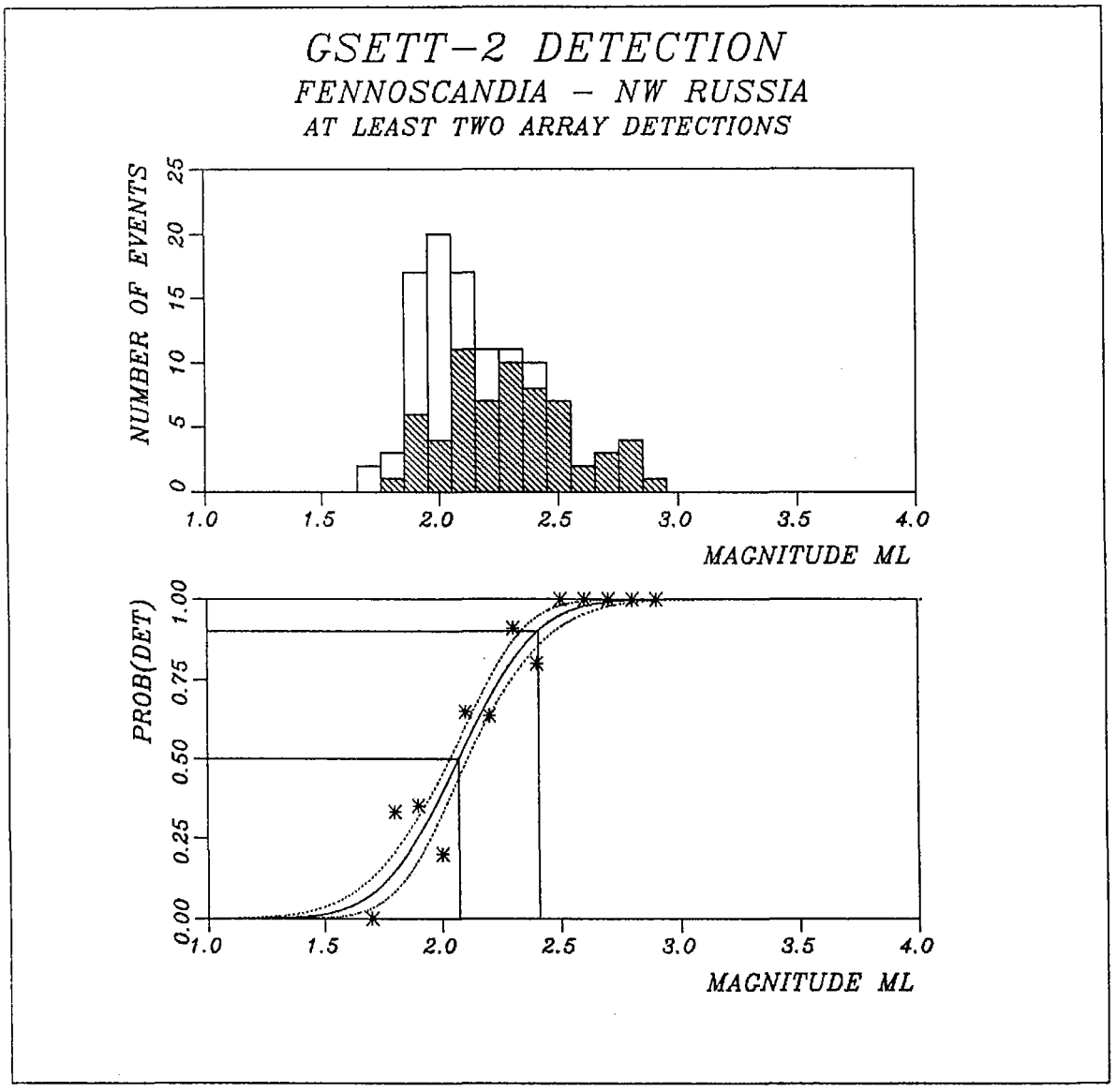

Fig. 7.6.3. Maximum likelihood detectability estimation for Fennoscandia-NW Russia using the Univ. of Helsinki bulletin as a reference. The upper half shows the reference event set and the number of events actually detected for each magnitude. The lower half shows the maximum likelihood detectability curve and its confidence limits. The actual percentage of detected events at each magnitude is also shown. This figure is based upon a two-array detection requirement.

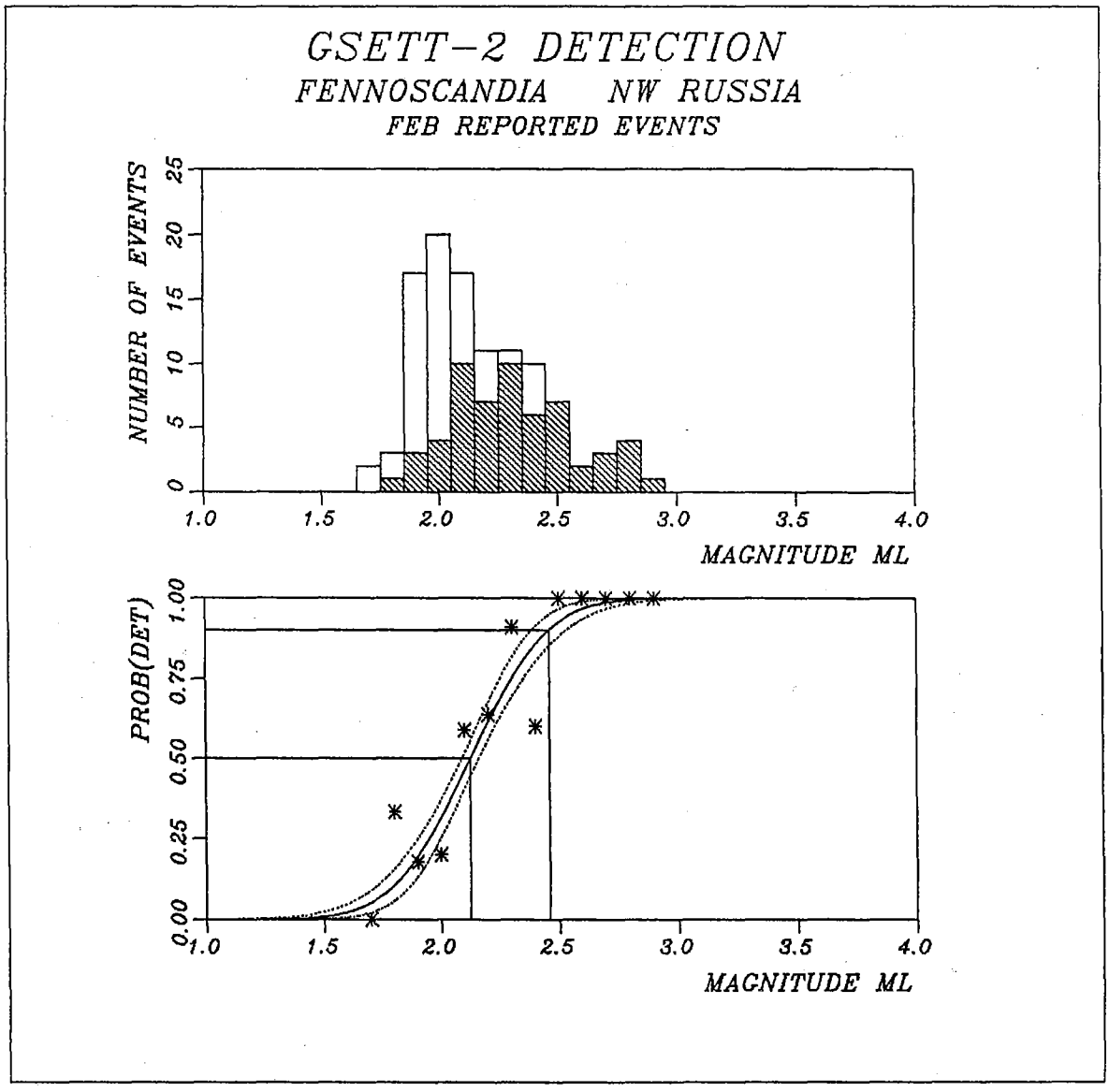

Fig. 7.6.4. Maximum likelihood detectability estimation for Fennoscandia-NW Russia using the Univ. of Helsinki bulletin as a reference. The upper half shows the reference event set and the number of events actually detected for each magnitude. The lower half shows the maximum likelihood detectability curve and its confidence limits. The actual percentage of detected events at each magnitude is also shown. This figure is based upon FEB reported events as discussed in the text.

7.7 Contemporary seismicity of the NW part of the USSR

Introduction

The regional seismic network of the Kola Science Centre began to be established in 1982. Today, 7 seismic stations are used to monitor the seismic activity of the Barents Sea and the NW part of the USSR. The station list is shown in Table 7.7.1. All stations are equipped with short-period seismometers with photo sensitive analog recording, and paper speed 60 mm/min. A three-component digitally recording station has recently (June 1991) been installed in Apatity. For better location of seismic events in the Barents Sea platform, data from the seismic station KHE in Franz Josef Land (80.37°N, 58.03°E) are used, even though this station is not part of the network.

Strong earthquakes are known from as far back as the 17th century for the eastern Baltic Shield (T. Ahjos and H. Korhonen, 1984), and before the seismic networks in this region were installed, it was suggested that only large earthquakes could take place here, because the crust of the rigid ancient shield was believed not to be able to produce many small earthquakes (e.g., Panasenko, 1969). Now this opinion has been revised.

The contemporary seismicity in northern Europe is shown in Fig. 7.7.1. Most of the earthquakes shown are for the past 30-year period, but some historical epicenters are also included, dating back as far as the year 1542. The earthquake activity is characterized by small and moderate size earthquakes. The largest earthquake in the Baltic Shield in recent years was the m_L = 5.2 event of 20 May 1967, located at 66.6°N, 33.7°E (Meyer and Ahjos, 1985). It was felt with MSK intensity VII in Karelia, and generated a small tsunami in the White Sea.

The main seismic zones of the Kola Peninsula are seen more clearly when considering only the time interval 1986 to 1991. They comprise the Kola-Finnmark zone and the Khibiny Massif (Fig. 7.7.2).

The Kola-Finnmark zone

Information about the seismicity of the Kola-Finnmark zone was known already from 1772 when an earthquake with maximum intensity VI took place near Murmansk (68.7°, 33.3°E). The largest earthquake known in the Kola-Finnmark zone (Kola Peninsula) during this century occurred on 10 April 1981 (68.8°N, 36.0°E). The magnitude estimated for this event ranges from 4.5 M_L (Upp) to 4.7 m_b (ISC). The 1981 earthquake had two shocks about 10 seconds apart and was felt with intensity V at Murmansk.

During 1986-1990 some tens of events were registered from the Kola-Finnmark zone. One of the larger of these was the earthquake that occurred on 16 June 1990 (69.14°N, 35.15°E) with M_L = 4.0, which was felt with intensity IV at Murmansk.

The seismicity of the Murmansk-Finnmark zone is largely confined to intersections of faults separating the Murmansk Block from the South Barents Sea platform, i.e., the so-called Karpinsky lineament, and to NS-trending faults which are clearly discerned from

Landsat imagery (Fig. 7.7.3). Fig. 7.7.4 presents a fragment of the neotectonic framework for these earthquakes.

The Khibiny Massif

In the last several years there has been a great increase of induced seismicity in the Khibiny Massif. This began to manifest itself after large volumes of rocks had been extracted from a high-stress environment. Fig. 7.7.5 demonstrates the position of the five main mines of the Khibiny Massif (a) and allows a comparison of the quantity of rock removal with the number of Khibiny earthquakes per year (b).

Exploration of the Khibiny apatite deposits was started in 1929. At the present time the production is more than 50 mill. tons per year. The first earthquake on record in the Khibiny area occurred on 23 September 1948 and was felt with intensity IV in populated areas.

The largest earthquake in Khibiny took place on 16 April 1989 (M_L = 4.2). This event was felt with intensity VIII in the upper levels of the Kirovsk mine and caused considerable destruction. The maximum measured displacement was 15-20 cm and it occurred along a fault striking at 125-135^o and dipping at 30-35^o NE. This displacement was traced along the surface for 1200 m and observed to a depth of at least 220 m.

The earthquake was felt with intensity V-VI in the Kirovsk area, and it was followed by several hundred aftershocks during the next two months. The earthquake on 16 April 1989 occurred simultaneously with a 240 ton explosion in one of the Kirovsk mines. It thus appears that the explosion triggered the earthquake. Supporting this assertion is the observation of analogous events at the Kirovsk mine on 29 August 1982, when an earthquake with maximum intensity VI took place at the same time as a large explosion. A similar pair of events occurred on 28 March 1991.

The location of mines and earthquakes relative to each other is shown in Fig. 7.7.6.

NE Archangelsk and Novaya Zemlya

The seismic station Amderma (AMD) began operation in 1983 (see Fig. 7.7.7). The station was established to study seismic activity of the Barents Sea Platform. The first investigations identified two zones of weak seismic activity in the NE Archangelsk region (Assinovskaya, 1989). The shaded area in Fig. 7.7.7 shows the seismic zone to the southeast of Amderma. No definite information exists about the nature of the events recorded in this region, but neotectonic conditions are consistent with this zone being seismically active.

A seismically active zone has also been found on Novaya Zemlya. Of particular interest is the earthquake on 1 August 1986 with m_b = 4.6 near the south coast of the Matochkin Shar strait. The location of this event is shown in Fig. 7.7.8 together with the system of lineaments and faults. There were at least four more earthquakes in this area, information about which has been included in Table 7.7.2.

In conclusion, we find that the seismicity of the NW part of the USSR is characterized by clustering of the most intense earthquakes at sites of intersections of NS and EW trending fault zones.

E.O. Kremenetskaya, Kola Science Centre, USSR

References

Ahjos, T. and H. Korhonen (1984): On a catalogue of historical earthquakes in Fennoscandian area. 24 pp.

Assinovskaya, B.A. and E.R. Acselevich (1989): Results of studies of seismicity in SE Barents Sea. **In:** *Geophysical Research of the Lithosphere of North European Part of the USSR.* Apatity, 41-48.

Meyer, K. and T. Ahjos (1985): Temporal variations of energy release by earthquakes in the Baltic Shield, *Geophysica,* 21, 51-64.

Panasenko, G.D. (1969): Seismic features of the north-east Baltic Shield, Nauka, Leningrad, 184 pp (in Russian).

Name	Coordinates	
APA	67.568N	33.388E
AMD	69.742N	61.655E
BRB	78.073N	14.240E
PLZ	67.400N	32.533E
PLQ	66.410N	32.750E
PLG	62.320N	36.930E
KEM	64.956N	34.635E

Table 7.7.1. List of seismic stations operated by the Kola Science Centre.

Date	Time	Coordinate		m_b
		N	E	
20.07.83	015941.7	73.2	56.3	-
31.01.86	110813.0	73.2	56.3	2.1
21.04.86	093753.9	73.2	56.3	3.2
01.08.86	135636.8	73.18	56.32	4.6
29.12.86	034407.4	-	-	3.0

Table 7.7.2. Recent earthquakes in Novaya Zemlya.

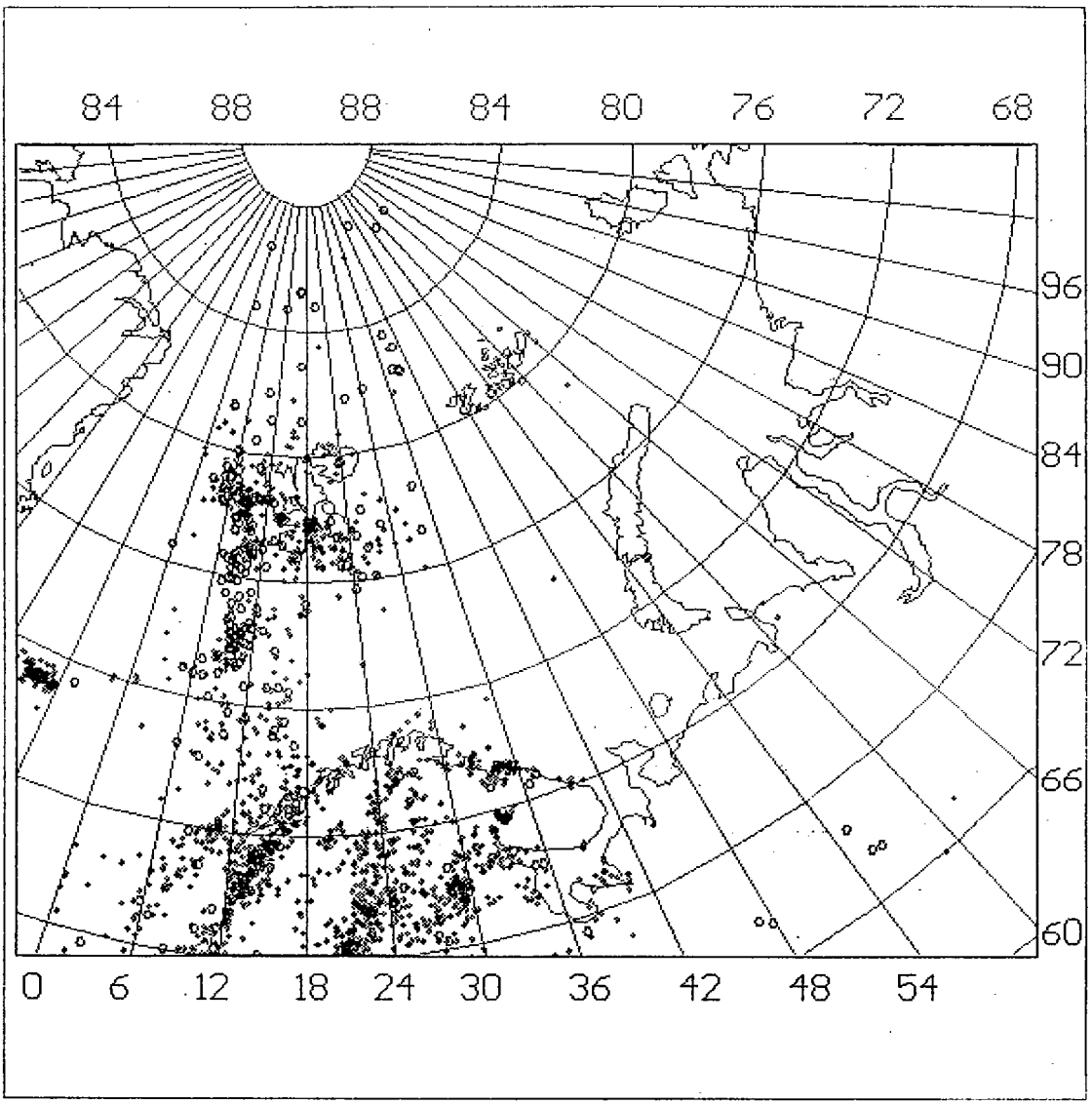

Fig. 7.7.1. Epicentral map of earthquakes in the European Arctic region. Most of the earthquakes shown are from the period 1960-1990, but some earlier events have been included.

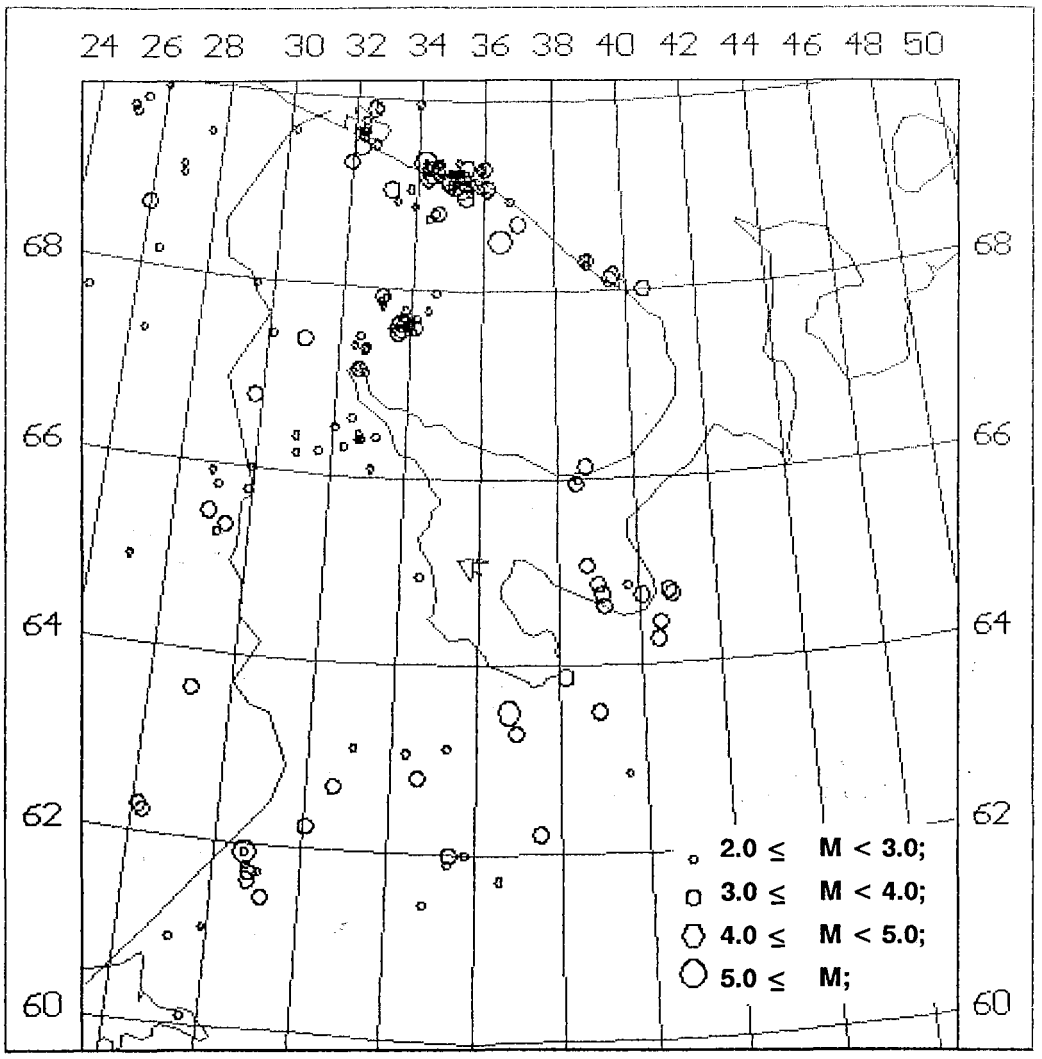

Fig. 7.7.2. Epicentral map of earthquakes of the eastern part of the Baltic Shield 1986-1991.

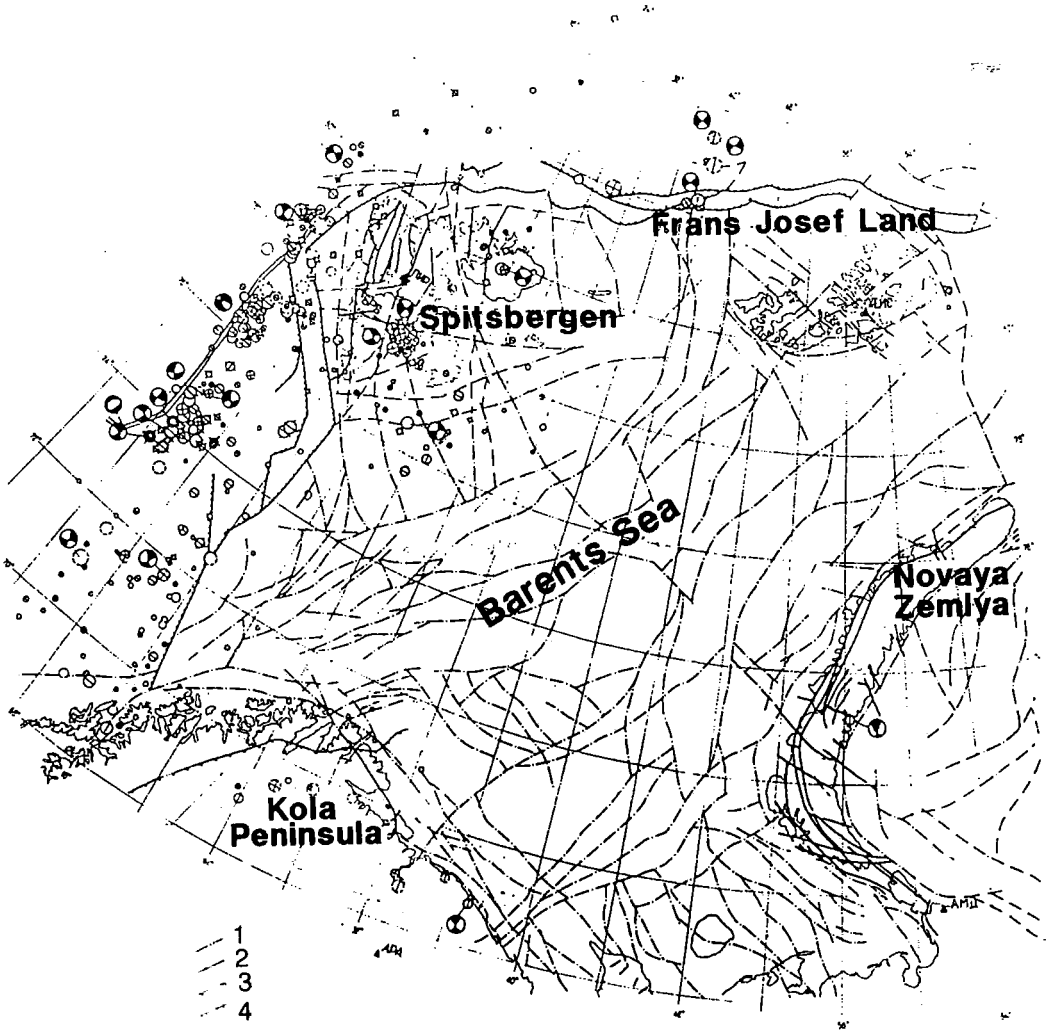

Fig. 7.7.3. Epicentral map of earthquakes of the Barents Sea with tectonic features:
1) faults from geophysical data; 2) faults from geological data; 3) thrusts; 4) dislocations.

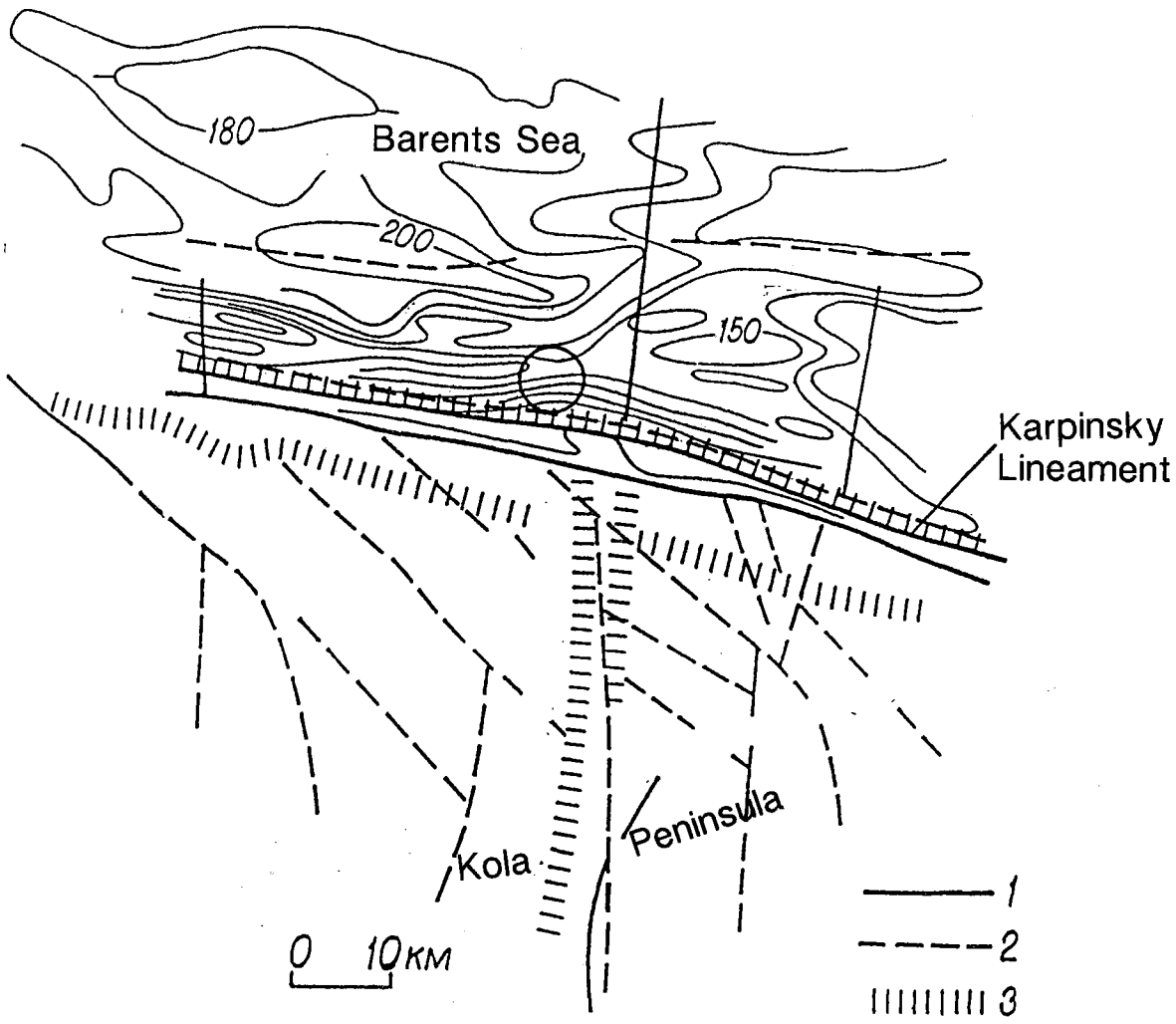

Fig. 7.7.4. Neotectonic framework for earthquakes of the Murmansk coast: 1) faults from geophysical data; 2) dislocations; 3) deep structures. The epicenter of the earthquake of 10 April 1981 discussed in the text is marked as a circle near the center of the map.

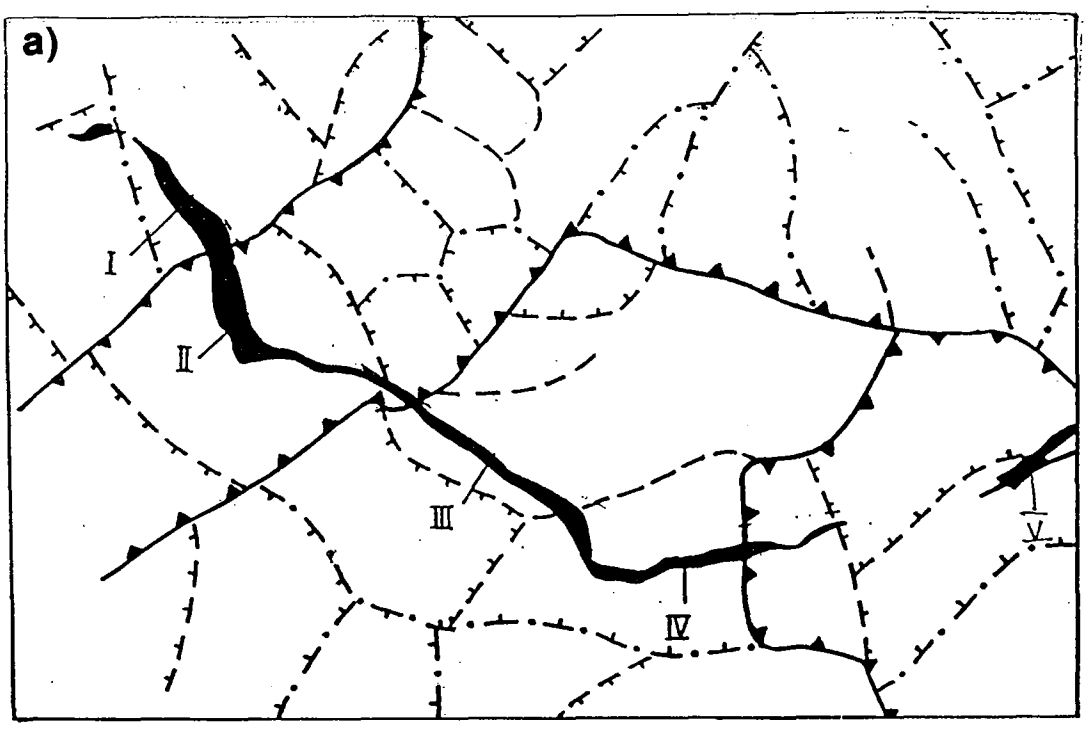

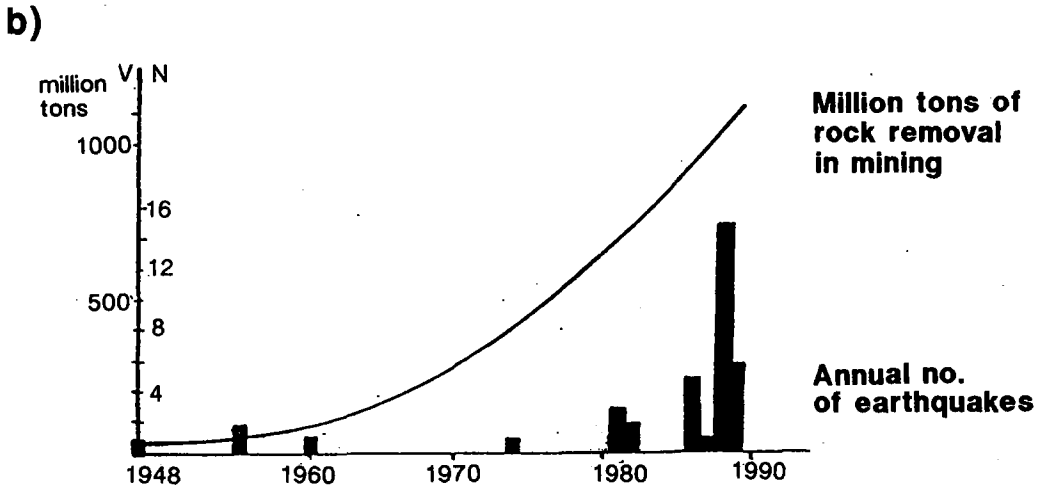

Fig. 7.7.5. a) The position of mines (I-V) in the Khibiny Massif together with fault structures. b) The relation between removed rock per year (1) and the number of earthquakes (2).

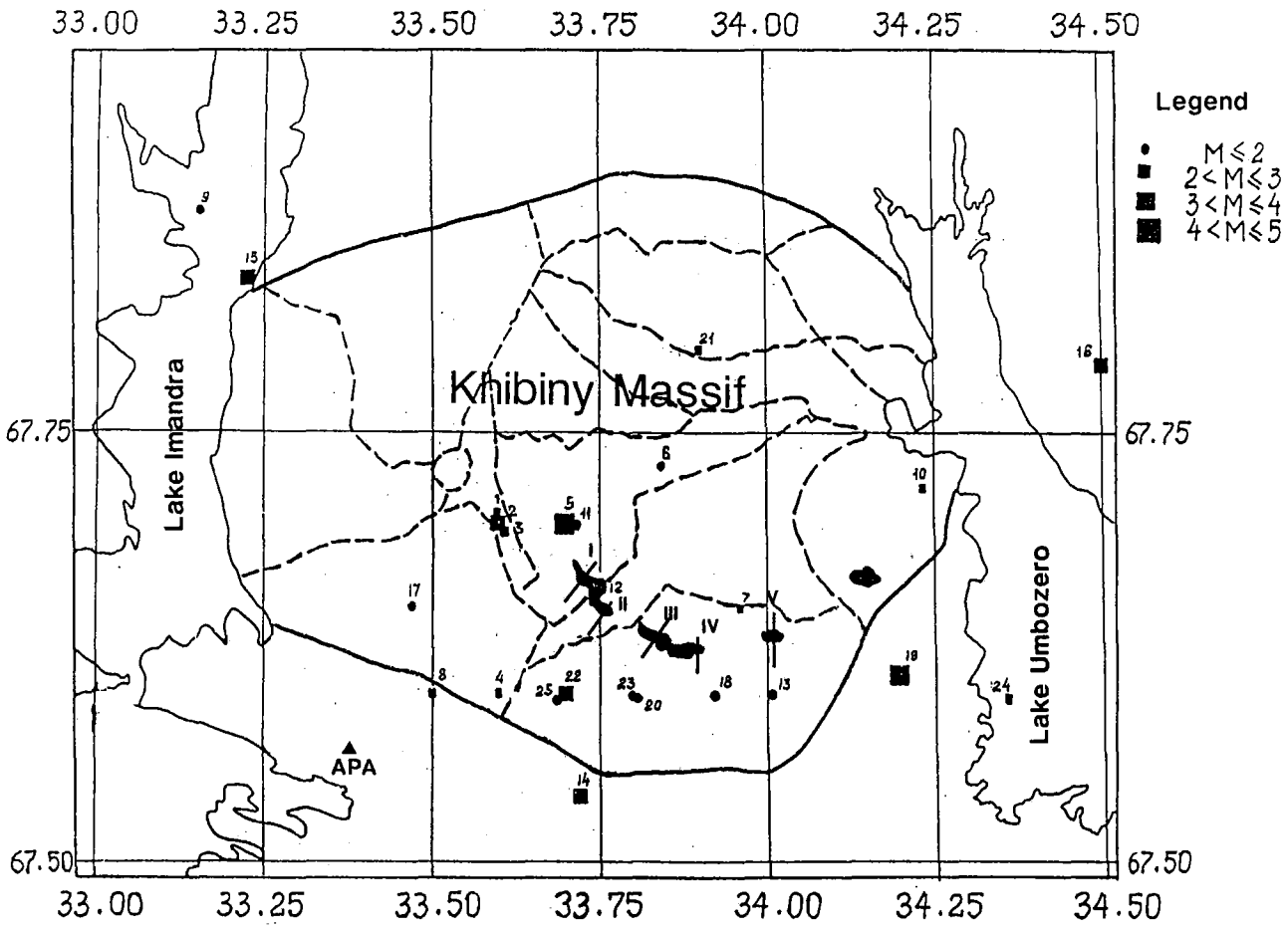

Fig. 7.7.6. Relative position of earthquakes and mines in the Khibiny Massif. The location of the Apatity seismic station (APA) is also shown. The mines (I-V) are shown in more detail in Fig. 7.7.5.

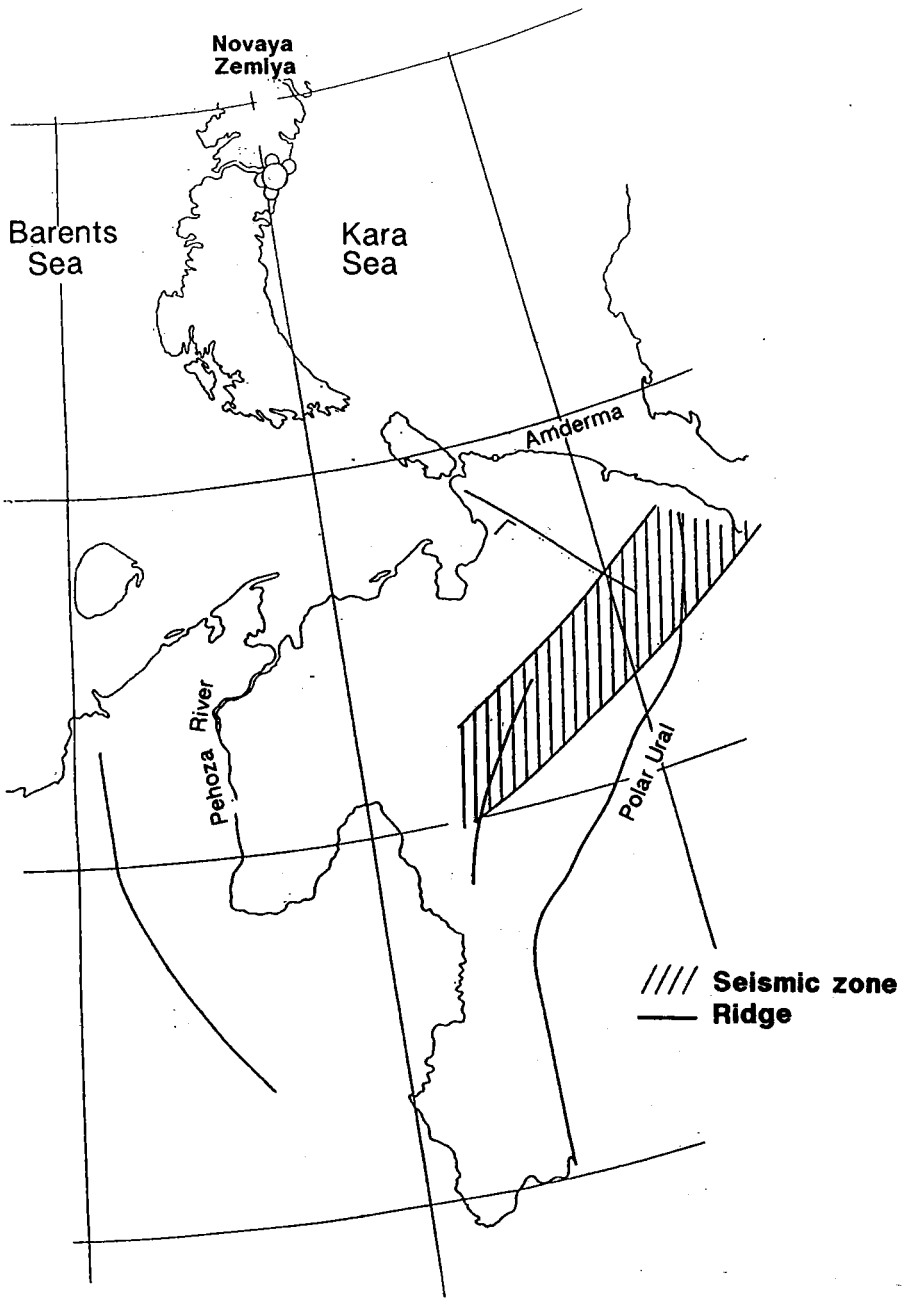

Fig. 7.7.7. The seismic zone southeast of Amderma. Epicenters of the Novaya Zemlya earthquakes (Table 7.7.2) are also shown.

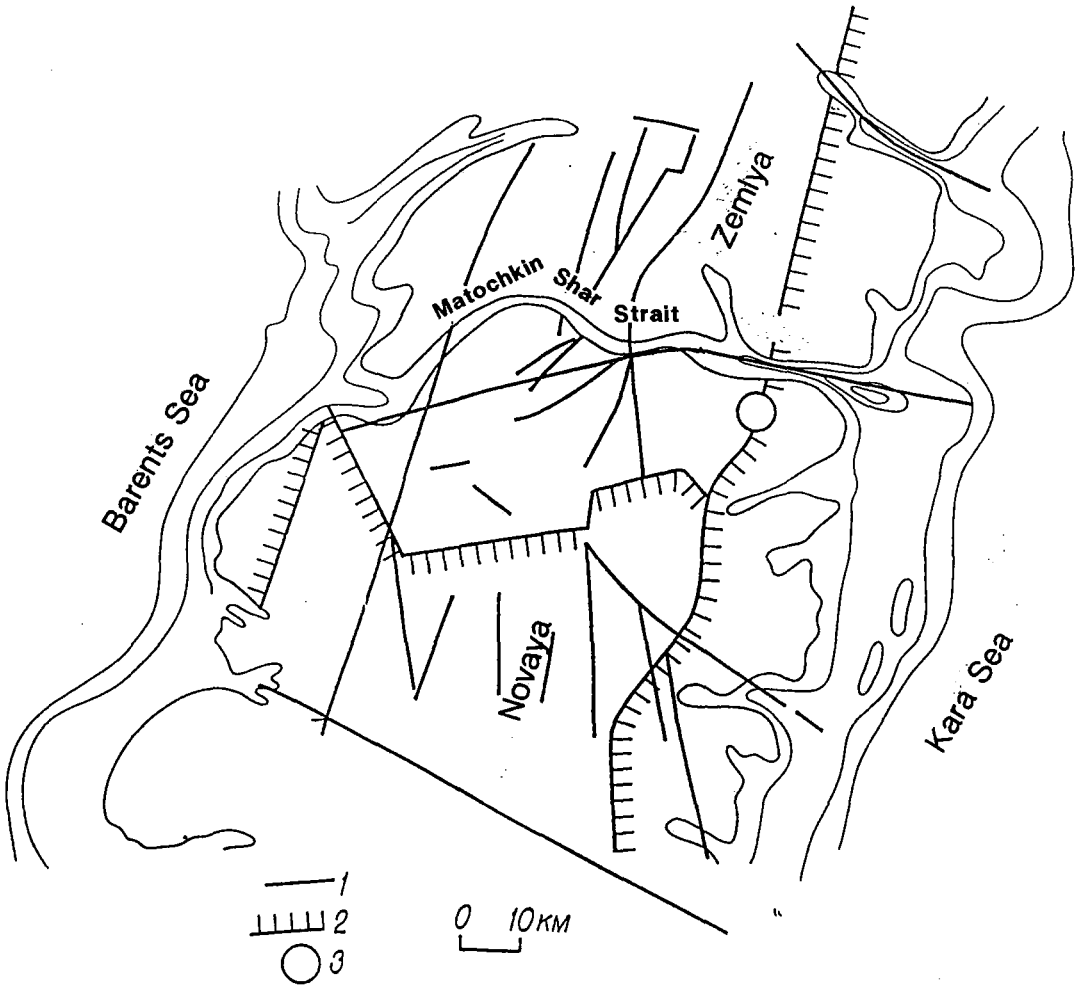

Fig. 7.7.8. The position of the earthquake of 01.08.86 with some neotectonic features: 1) faults; 2) boundaries of blocks; 3) epicenter.